K_{Ca} channels in breast cancer development, progression and response to endocrine and radiation therapy

Dissertation

der Mathematisch-Naturwissenschaftlichen Fakultät

der Eberhard Karls Universität Tübingen

zur Erlangung des Grades eines

Doktors der Naturwissenschaften

(Dr. rer. nat.)

vorgelegt von

Corinna Jasmin Mohr

aus Biberach a. d. Riß

Tübingen

2018

Gedruckt mit Genehmigung der Mathematisch-Naturwissenschaftlichen Fakultät der Eberhard Karls Universität Tübingen.

Tag der mündlichen Qualifikation:	14.12.2018
Dekan:	Prof. Dr. Wolfgang Rosenstiel
1. Berichterstatter:	Prof. Dr. Robert Lukowski
2. Berichterstatter:	Prof. Dr. Hiltrud Brauch

Table of contents

Illustration directory

List of tables

List of abbreviations

%	Percent
°C	Degrees Celsius
γH2AX	Histone 2A minor variant phosphorylated at serine 139
$[Ca^{2+}]_i$	Intracellular calcium ion concentration
°C	Degrees Celsius
µg	Microgram
µl	Microlitre
µM	Micromolar
µm	Micrometre
1-EBIO	1-Ethylbenzimidazolinone
AI	Aromatase inhibitor
AP	Alkaline phosphatase
AR	Androgen receptor
ATM	Ataxia telangiectasia mutated
ATP	Adenosine triphosphate
AUC	Area under the curve
bp	Base pairs
BCAC	Breast Cancer Association Consortium
BK	Big conductance for potassium
BRCA	*Breast cancer* gene
BSA	Bovine serum albumin
BW	Body weight
Ca^{2+}	Calcium ion
CaMK II	Calcium / calmodulin-dependent protein kinase II
CCS	Charcoal-stripped serum
CD45	Cluster of differentiation 45
cDNA	Complementary deoxyribonucleic acid
CHEK2	*Checkpoint kinase 2* gene
CI	Confidence interval
Cl^-	Chloride ion
cm^2	Square centimetre
CO_2	Carbon dioxide
COGS	Collaborative Gene-Environment Study
CR	Complete response
ctrl	Control
CYP	Cytochrome P450
d	Day
DAPI	4′,6-diamidino-2-phenylindole
DEPC	Diethyl pyrocarbonate
dH_2O	Deionised water
DM	Demethylation
DMSO	Dimethyl sulfoxide
DNA	Deoxyribonucleic acid
DNA-PK	Deoxyribonucleic acid-dependent protein kinase
dNTPs	deoxyribose nucleoside triphophates
DSB	Double-strand break
e.g.	Exempli gratia
E1	Oestrone

E2	17β-oestradiol
E3	Oestriol
E4	Oestetrol
EBF1	Early B-cell factor 1
EDTA	Ethylenediamine tetraacetic acid disodium salt dihydrate
EGFR	Epidermal growth factor receptor
eQTLs	Expression quantitative trait loci
ER	Oestrogen receptor
ERE	Oestrogen response element
FCS	Foetal calf serum
FPKM	Fragments per kilobase of transcript per million mapped reads
FSH	Follicle-stimulating hormone
FVB/N	Friend leukaemia virus B-susceptible
g	gram
GnRH	Gonadotropin-releasing hormone
GPER	G protein-coupled oestrogen receptor
Gy	Gray
h	Hour
H^+	Hydrogen ion
H_2O_2	Hydrogen peroxide
HER2	Human epidermal growth factor receptor 2
HPLC	High-performance liquid chromatography
HR	Hazard ratio
i.e.	Id est
i.p.	Intraperitoneal
IgG	Immunoglobulin G
IK	Intermediate conductance for potassium
Il	Interleukin
IR	Ionising radiation
K^+	Potassium ion
K_{Ca}	Calcium-activated potassium
kDa	Kilodalton
kg	kilogram
K_{ir}	Inward-rectifying potassium channels
KM plotter	Kaplan Meier plotter
KO	Knockout
K_V	Voltage-gated potassium
l	Litre
LH	Luteinising hormone
LRRC	Leucine-rich repeat-containing
M	Molar
MAF	Minor allele frequency
mg	milligram
Mg^{2+}	Magnesium ion
min	Minute
ml	Millilitre
mM	Millimolar
mm	millimetre
mm^2	Square millimetre
mm^3	Millimetres cubed
MMTV	Mouse mammary tumour virus

mV	Millivolt
MV	Megavolt
n	number
n.a.	Not available
n.d.	Not detectable
Na^+	Sodium ion
NDS	Normal donkey serum
ng	Nanogram
NGS	Normal goat serum
NHEJ	Non-homologous end joining
nM	Nanomolar
OR	Odds ratio
OS	Overall survival
p53	Tumour protein 53
PAM50	Prediction analysis of microarray
PBS	Phosphate buffered saline
PCR	Polymerase chain reaction
PFA	Paraformaldehyde
pmol	Picomolar
PR	Progesterone receptor
pS	Picosiemens
PyMT	Polyomavirus middle T antigen
qRT-PCR	Quantitative real-time polymerase chain reaction
rcf	Relative centrifugal force
RCK	Regulator of conductance for potassium
RFS	Relapse-free survival
RNA	Ribonucleic acid
ROS	Reactive oxygen species
rpm	Rounds per minute
RT	Reverse transcriptase
s	Second
s.c.	Subcutaneous
SEM	Standard error of the mean
SERM	Selective oestrogen receptor modulator
si*Gapdh*	*Gapdh* ribonucleic acid interference
si*GAPDH*	*GAPDH* ribonucleic acid interference
si*Lrrc26*	*Lrrc26* ribonucleic acid interference
si*LRRC26*	*LRRC26* ribonucleic acid interference
si*NT*	*Non-targeting* ribonucleic acid interference
siRNA	Ribonucleic acid interference
SK	Small conductance for potassium
Slack	Sequence like a calcium-activated potassium channel
SNP	Single nucleotide polymorphism
TAM	Tamoxifen
TBE buffer	Tris / Borate / Ethylenediamine tetraacetic acid disodium salt dihydrate buffer
TCGA	The Cancer Genome Atlas
TFS	Tumour-free survival
TM	Transmembrane
TNBC	Triple-negative breast cancer
TP53	*Tumour protein 53* gene

TRAM-34	Triarylmethane-34
v	Volume
WT	Wildtype
XRCC4	X-ray repair cross-complementing protein 4

1. Introduction

1.1 Breast cancer

1.1.1 Tumour aetiology and development

Breast cancer is the most frequent cancer and the second leading cause of cancer-related death in women[1]. Tumour cells derive from healthy body cells that have accumulated genetic and epigenetic changes during their life cycle. DNA mutations may derive from different sources such as oxidative damage, replication errors or the chromatin organisation. Loss of DNA repair genes and unsuccessful DNA repair further promote genome instability referring to a high frequency of mutations in different genes[2]. The inheritance of individual germ line mutations or a somatic mutation in a critical gene can act as a first hit that makes a cell susceptible to malignant growth during its lifetime. Inherited mutations predisposing for breast cancer include tumour suppressor genes such as *breast cancer 1* and *breast cancer 2* (*BRCA1* and *BRCA2*) as well as *checkpoint kinase 2* (*CHEK2)* and *tumour protein 53* (*TP53)* involved in cell cycle arrest, DNA repair or apoptosis. Due to the diploidy of the human genome, a first mutation leads to heterogeneous wildtype (WT) and mutant alleles. Further somatic mutations acquired in the homologous gene at a later time point can act as second hit. The consequence is loss of heterogeneity in certain gene clusters, which can result in malignancy[3,4]. Likewise, increased expression or activity of oncoproteins can contribute to carcinogenesis or promote characteristics of cancer cells[5].

Carcinogenesis of the breast gives rise to tumour cells with basal, basoluminal or luminal characteristics (figure 1.1). This is due to the morphological and functional variety of breast epithelial cells divided in the inner luminal, milk-secreting cell layer and the outer basal cell layer, whose contractility leads to milk ejection[6]. Breast cancer initially has been assigned according to histological morphology and grading. It is further classified based on the immunohistochemical expression status for oestrogen receptor (ER), progesterone receptor (PR) and human epidermal growth factor receptor 2 (HER2). Besides, defined intrinsic subtypes of breast cancer are involved in incidence, therapy response and survival[7-11]. Hormone receptor-positive tumours with luminal-enriched genes are divided in luminal A and luminal B subtypes, with the latter often associating with a positive HER2 status. Luminal breast cancers are additionally distinguished with regard to their Ki-67 index with low Ki-67 expression in luminal A and high in luminal B tumours, respectively. The most reliable Ki-67 cut-off to stratify patients is determined at 13.25% (section 1.1.5)[12-14].

Moreover, tumours with positive HER2 status but absent hormone receptor expression belong to the HER2-enriched breast cancer subtype[6]. Apocrine breast cancer is another rare

form of hormone-related breast tumours although no PR and an alternatively spliced and thereby truncated ER-36α are present. However, the most prominent characteristic of apocrine tumours is the positive androgen receptor (AR) status and many such tumours are enriched for HER2. The corresponding tumour cells show an apocrine phenotype with eosinophilic and granular cytoplasm as well as prominent nuclei and cell borders[15-18]. Generally, the AR is expressed in many breast tumours and thus cannot serve for subtype classification. Its expression levels correlate with HER2 amplification in ER-negative tumours. Besides, AR expression is a good prognostic marker in breast cancer and associates with more differentiated tumour cells. Nonetheless, a high AR to ER ratio can promote endocrine resistance via increased androgen-dependent growth during anti-oestrogen therapy[19,20].

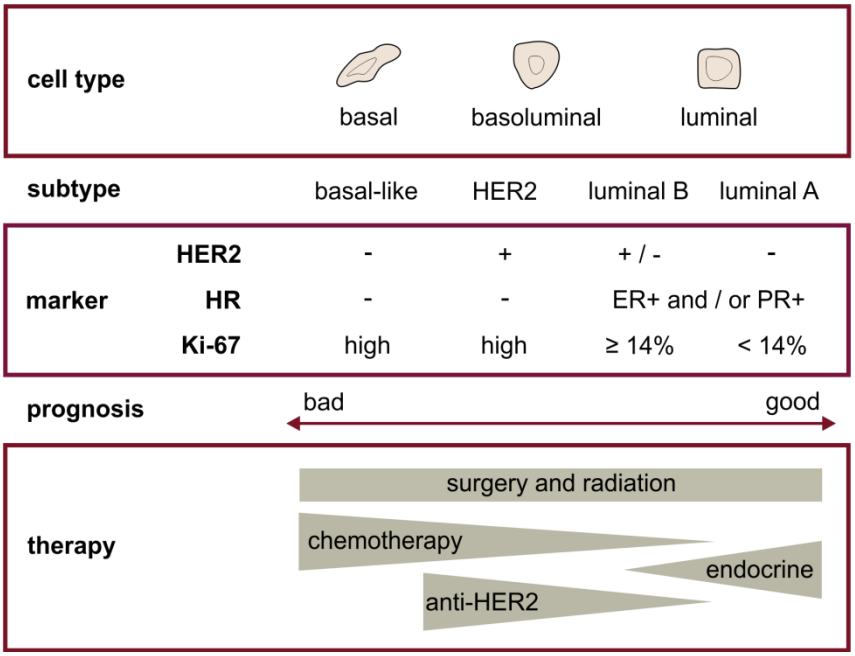

Figure 1.1: Classification and therapy of breast cancer
Different breast epithelial cell types give rise to morphologically distinguishable tumour phenotypes, which are further classified by different molecular properties. The latter, for example, are categorised by receptor expression and affect prognosis. Breast cancer subtype is also a major determinant of therapy[21,22]. Abbreviations: Human epidermal growth factor receptor 2, HER2; Hormone receptor, HR; Oestrogen receptor, ER; Progesterone receptor, PR.

Breast tumours lacking ER, PR and HER2 are histologically defined as triple-negative breast cancer (TNBC). The majority of these tumours can be stratified to the basal-like molecular subtype. Besides poor prognosis, their characteristic is a high expression of cytokeratins 5 and 6 as well as epidermal growth factor receptor (EGFR). Absence of these markers results in so-called “normal-like” tumours, as they share a similar profile to normal mammary stromal cells. In contrast to basal-like tumours, normal-like breast tumours have a much better prognosis and a bad response to neoadjuvant chemotherapy[23-25].

According to the intrinsic subtypes, a microarray-based assay of 50 classifier genes (PAM50) allows for reliable prognosis and predictions on therapy response[26]. In concordance with the intrinsic subtypes, analysis of copy number alterations in breast cancer delivers ten integrative clusters to be differentiated. These clusters were established by selection of the 1,000 genomic variants with highest impact on gene expression at their own genetic loci[27,28]. The ten groups are categorised in normal mammary gland (group I) and tumours with mesenchymal (group II), basal / myoepithelial (groups III - V), luminal (groups VI - VIII) or mixed (groups IX - X) characteristics[29].

1.1.2 Surgery and chemotherapy

Different therapeutic approaches are used to treat patients suffering from breast cancer. Surgery to remove the tumour can be conducted in a breast-conserving manner or by mastectomy. Sequential chemotherapy and radiotherapy are started soon after surgery with chemotherapy usually prior to radiotherapy. Additionally, neoadjuvant chemotherapy is considered with the aim of tumour size reduction before surgery[30,31]. In 1958, the first chemotherapy trial was initiated using an alkylating agent. Due to the observed reduction of breast cancer recurrence, this success was followed by poly-chemotherapy regimens and recommendations on the use of chemotherapy for the majority of breast cancer patients. Today, however, there is evidence that many patients receive chemotherapy without additional benefit[32]. It is known, for instance, that patients with low absolute mortality risk also receive a low benefit from chemotherapy. Therefore, chemotherapy in breast cancer is indicated when its benefit outweighs the side effects, namely for patients suffering from HER2-positive, triple-negative or high-risk luminal B breast cancer. Especially younger patients under 50 years of age seem to benefit from chemotherapy. Current evidence-based recommendations for first-line chemotherapy include the use of at least an anthracycline and a taxane for 18 to 24 weeks[31,33]. Tumour cytotoxicity from anthracyclines results from DNA intercalation and inhibition of topoisomerase II activity[34]. Antineoplastic agents from this class of drugs include doxorubicin, which exhibits sustained cardiotoxicity and its later developed and less cardiotoxic epimer epirubicin. With regard to the naturally occuring taxanes, their first approved representative paclitaxel prevents depolymerisation of the mitotic spindle and results in cell cycle arrest[32].

1.1.3 Radiotherapy

Radiotherapy of the surgical borders, the whole breast and axillary lymph nodes all show beneficial effects in the reduction of tumour recurrence and an increase in overall

survival[35,36]. In experimental setups, increasing doses of ionising radiation (IR) decrease single tumour cell survival, as measured by colony formation ability. In addition to the intrinsic radiosensitivity and reproductive ability of different cell types, plating efficiency and thus the fraction of cells that form colonies under specific growth conditions determine clonogenic survival after seeding of a cell suspension. In contrast to successful colony formation, irradiation can lead to the formation of giant cells. These are enlarged cells developed by growth while replication is inactivated. Furthermore, the formation of abortive colonies represent cells that divided several times before entry into mitosis-linked cell death, a process termed mitotic catastrophe[37,38].

IR causes DNA damage and thus stimulates DNA repair (figure 1.2). The high-energy particles used for IR induce direct damage at the helical backbone of the DNA by splitting chemical bonds. However, the major genetic damage is induced indirectly through the formation of reactive oxygen species (ROS). These are induced by the liberation of electrons through IR and thus the creation of highly reactive ions and ion pairs[39]. IR induces cell cycle arrest via tumour protein 53 (p53)[40] and causes delayed cell cycle progression and mitosis[41,42] attributable to cellular DNA repair processes. 1 Gy of IR causes approximately 1,000 single-strand breaks and 35 double-strand breaks (DSBs). Although DSBs are the minor DNA lesions following IR, they are central for IR-induced toxicity, as the majority of DSBs are repaired by error-prone non-homologous end joining (NHEJ) in mammals. DNA lesions are detected by the DNA damage response, which stimulates cell cycle checkpoints to determine cell fate resulting in DNA repair or cell death. Proteins involved in the DNA damage response protect the lesions from DNA decay and undesired DNA repair while allowing chromatin relaxation and thus access for DNA repair proteins. One such protein is ataxia telangiectasia mutated (ATM) that phosphorylates a variety of proteins including p53 and BRCA1 leading to the activation of cell cycle checkpoints and DNA repair. Another important target of ATM is the phosphorylation at serine 139 of the minor histone 2A.X variant (γH2AX)[43,44]. γH2AX is important for chromosomal stability, the recruitment of p53-binding protein 1 and BRCA1 and thus enables the assembly of DNA repair complexes at foci formed after exposure to IR[45,46]. For the initiation of NHEJ, the Ku complex forming as Ku70 / Ku80 heterodimer binds the DNA lesion. DNA-dependent protein kinase (DNA-PK) is recruited and phosphorylates different proteins such as the X-ray repair cross-complementing protein 4 (XRCC4), which is involved in the religation of DNA ends. In addition to NHEJ, DNA repair can be performed through homologous recombination in late S and G_2 phases of the cell cycle. Homologous recombination employs the homologous sequence on the sister chromatid as template for DNA repair via formation of a so-called holliday junction[44].

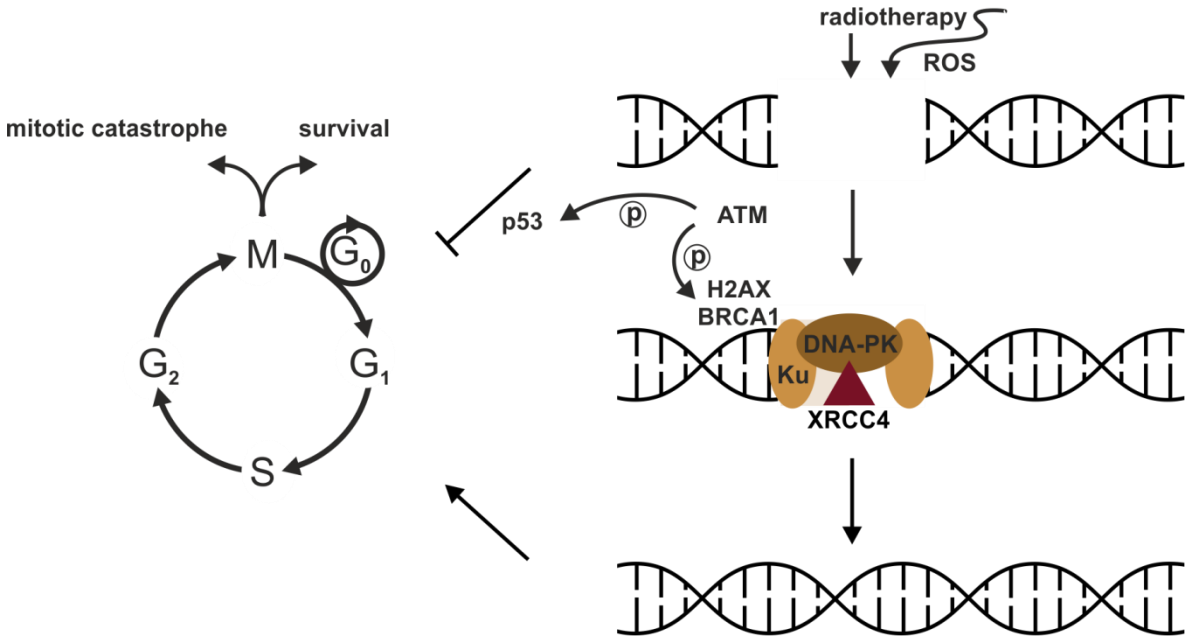

Figure 1.2: DNA damage and repair evoked by radiotherapy
Radiotherapy induces DSB formation either directly by breaking bonds in the helical backbone or indirectly by the formation of ROS. ATM via phosphorylation stimulates radiation-induced cell cycle arrest and activates the DNA repair machinery, i.e. NHEJ or homologous recombination. Successful DNA repair promotes cellular survival, whereas cell cycle progression despite critical DNA damage results in cell death mainly by mitotic catastrophe. Abbreviations used: Double-strand break, DSB; Reactive oxygen species, ROS; Ataxia telangiectasia mutated, ATM; Non-homologous end joining, NHEJ; Tumour protein 53, p53; Minor histone 2A.X variant, H2AX; Breast cancer 1 gene, BRCA1; DNA-dependent protein kinase, DNA-PK; X-ray repair cross complementing protein 4, XRCC4.

Conventional breast cancer radiotherapy regimes consist of a total dose of 50 Gy in 2 Gy fractions given for five consecutive days per week over a time period of 5 weeks[31]. In addition to these standard fractions used for external beam radiotherapy in patients, different treatment options have been tested to improve therapy outcome. The fractionation sensitivity is low for breast tumours, whereas it is high concerning late damage of normal tissue. Although fraction size is limited by the regenerative potential of healthy tissue affected by the irradiation process, different attempts to reduce the number of fractions have been made[47]. As a result, fewer fractions and thus so-called hypofractionation can be performed in a shorter time period showing at least the effectiveness as classic fractionation. Hypofractionation uses approximately 40 Gy in 15 to 16 fractions in 3 or up to 5 weeks depending on the individual breast cancer case[31,48-50]. Besides external beam radiotherapy, some patients may especially benefit from intraoperative radiotherapy[51,52] or brachytherapy[53]. Moreover, a radiation boost to the tumour bed after fractionated whole-breast irradiation can improve local control albeit increasing the risk of fibrosis. In particular in patients > 60 years of age, the radiation boost should be avoided, whereas it might be of value in younger patients[54,55]. Although the irradiation dose is delivered at specific loci such as the borders

after surgery where potentially remaining tumour cells are expected, radiotherapy can also induce acute and long-term adverse effects. These include nausea and emesis[56], as well as fatigue and breast pain[57]. Due to the usually applied external beam radiotherapy, skin alterations such as hyperpigmentation or fibrosis can occur[58]. Besides, incidental exposure of the heart increases the risk of ischaemic heart disease in an IR dose-dependent manner[59]. In rare events, radiotherapy can even cause the development of a second tumour[60]. As with other anti-cancer strategies, the benefit from irradiation generally outweighs the risk and impact of adverse effects.

1.1.4 Endocrine therapy

Oestrogens

The primary oestrogens are oestrone (E1), 17β-oestradiol (E2) and oestriol (E3). They are synthesised by the CYP19A1-representing aromatase enzyme, which uses C19 androgens as substrates (figure 1.3). Depending on their prosthetic groups, aromatase converts androstenedione, testosterone, 16-OH-androstenedione or foetal oestrogen in E1, E2, E3 or oestetrol (E4), respectively. In both males and females, aromatase expression occurs at tissue-specific rates with the gonads as the major source for sex hormones[61]. In pre-menopausal women, aromatase expression and thus oestrogen synthesis in the reproductive tract are regulated by the hypothalamic-pituitary-gonadal axis and its corresponding feedback systems. In this context, the hypothalamus represents the source for the secretion of gonadotropin-releasing hormone (GnRH), which binds its receptor at the pituitary. Pulsatile release of GnRH, for example, is evoked by ultradian rhythm and kisspeptin that is also produced in the hypothalamus[62]. GnRH stimulates the synthesis and secretion of follicle-stimulating hormone (FSH) and luteinising hormone (LH), the so-called gonadotropins, in the pituitary[63-65]. FSH binds its receptor, which stimulates the expression of aromatase in the granulosa cells of an ovarian follicle[66]. The hypothalamic-pituitary-gonadal axis has a major impact on the menstruation cycle. During menstruation, the endometrium is resolved in an inflammatory process. Comparably to a wound healing process, endometrium regeneration involves tissue formation, remodelling and angiogenesis. E2 is the main hormone to stimulate endometrial proliferation during the subsequent follicular phase. Aromatase expression and thus E2 synthesis predominantly occur in the granulosa cells of a developing follicle in the ovaries and, subsequently, in corpus luteum cells after ovulation. During the secretory phase following ovulation, the corpus luteum produces high amounts of progesterone, which induces endometrial differentiation. Regression of the corpus luteum in the late secretory phase degenerates the endometrium und thus initiates menstruation. In

women after menopause, adipose tissue becomes the main source for oestrogens[61,67] and oestrogens are further expressed in breast tissue, adrenal glands and hepatocytes[68].

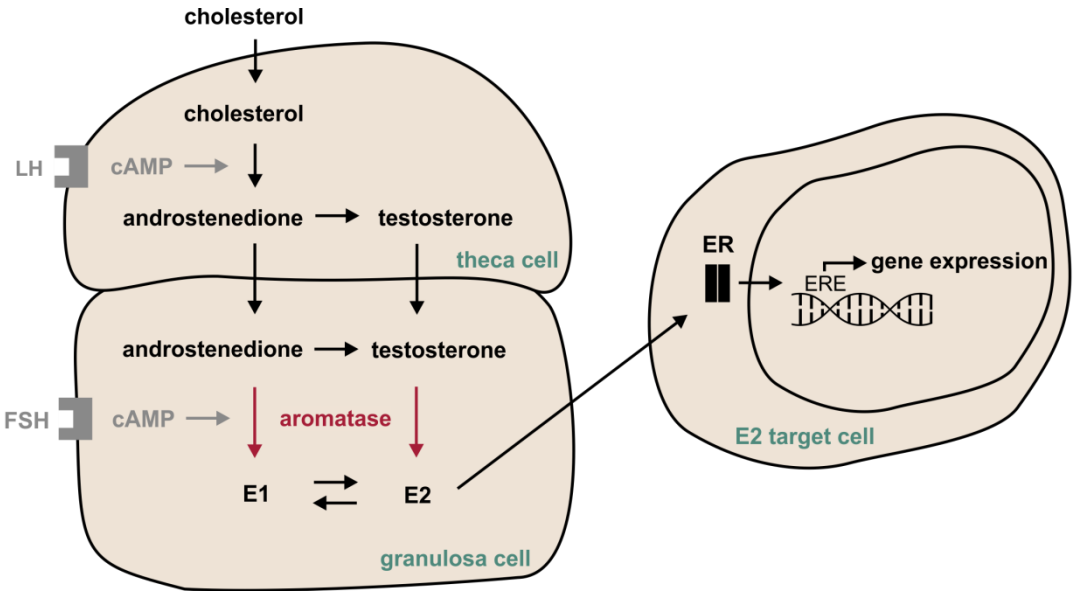

Figure 1.3: Oestrogen synthesis and activation of ER signalling
Oestrogens are synthesised mainly via the hypothalamic-pituitary-gonadal axis in pre-menopausal women. This involves the hypothalamus-induced production of the gonadotropins FSH and LH in the pituitary to stimulate oestrogen production in target theca and granulosa cells of a growing ovarian follicle. Aromatase converts C19 androgens into the respective oestrogens and is also expressed in further cell types, e.g. breast cells or adipocytes, and thus enables oestrogen synthesis also in post-menopausal women and men. E2 represents the most potent ER agonist and modulates the gene expression signature and thereby contributes to oncogenic events. Abbreviations: Follicle-stimulating hormone, FSH; Luteinising hormone, LH; Cyclic adenosine monophosphate, cAMP; Oestrone, E1; 17β-oestradiol, E2; Oestrogen receptor, ER; Oestrogen response element, ERE. Modified after Doshi et Agarwal, J Mildlife Health 2013[68] and Patel et al., Biol Reprod 2015[69].

E2 is the most potent female oestrogen binding with high affinity and specificity to its receptor[70]. The ER exists as homodimer or heterodimer of its α and β subunits. High expression of ER-α is found in uterus, ovary, breast, prostate, testis, epididymis and liver, whereas ER-β expression also is high in ovary, prostate and testis as well as in bone marrow and the brain. As common for members of the nuclear receptor family, the structure of the ER includes two transactivation domains, ligand and DNA binding domains and a hinge region for receptor dimerisation. ER-α and ER-β show sequence homologies of approximately 60% in the ligand binding domain and 95% in the DNA binding domain. Upon oestrogen binding to the ER, a conformational change is induced with subsequent chaperone dissociation and dimerisation. Translocation of the ER in the nucleus allows binding to oestrogen-response elements (EREs) in a variety of genes. In addition, protein-protein interactions with other transcription factors allow for indirect DNA binding. Additionally, non-genomic signalling via second messengers is described in many tissues. Even

ligand-independent activation through other signalling pathways such as their activation by phosphorylation is described for the ER[71-73].

With further regard to ER subunits, especially ER-α function is associated with breast cancer. The role of ER-β is not understood well, partly due to the existence of different ER-β isoforms. Besides the classic ER-α and ER-β isoforms, a G protein-coupled receptor responding to oestrogens (GPER) is described. In addition, two truncated ER-α splice variants of 46 kDa and 36 kDa exist that, together with the full-length 66 kDa ER-α protein, can translocate to the plasma membrane through palmitoylation to be associated with caveolin-1 allowing for rapid ER signalling[74]. Particularly in ER-positive breast tumours, ER signalling critically contributes to increased proliferation and decreased apoptosis[75]. In 1896 already, George T. Beatson postulated the importance of the ovaries for controlling proliferation of epithelial tissue. Especially pre-menopausal women, in whom tumour removal often had shown no improve, benefitted from mammary tumour regression after ovariectomy[76].

Moreover, E2 metabolism is supposed to possess carcinogenic properties. Phase I oxidative metabolism may lead to ROS formation and unstable adenine and guanine DNA base adducts. Besides, hormone levels can act as risk factors for breast cancer development: An increased breast cancer risk in post-menopausal women is associated with elevated blood levels of E2, androstenedione or testosterone. Another risk factor for breast cancer represents obesity, as it is associated with increased aromatase-mediated E2 production in adipose tissue. With regard to progesterone, its serum levels do not associate with post-menopausal breast cancer risk, but are irreversibly associated with the risk of breast cancer development in pre-menopausal women[75].

Anti-oestrogens

Due to the early observations on the contribution of oestrogens to the development of breast and other cancers, very high doses of synthetic oestrogens were initially applied to breast cancer patients in order to disturb oestrogen physiology. This approach turned out a first temporarily successful endocrine breast cancer therapy[77]. The pioneering drug to antagonise ER action in breast tumour cells is tamoxifen (TAM), although it was initially developed as potential contraceptive agent. In 1973, TAM marketing for breast cancer therapy started in the United Kingdom and it was approved by the Food and Drug Administration in 1977[78]. Together with other therapeutic advances, breast cancer mortality has declined continuously since the 1970s. TAM treatment for 5 years has resulted in increased disease-free survival after surgery in ER-positive, node-negative patients with invasive breast cancer. Endocrine therapy employed for additional 5 years further improves cancer recurrence and overall

survival (OS). In ductal carcinoma *in situ*, endocrine therapy generally shows a minor benefit and is employed cautiously. For the prevention of breast cancer in women at increased risk, prophylactic TAM administration may be further beneficial[79,80]. As selective ER modulator (SERM), TAM inhibits ER signalling in the breast while acting as agonist in other tissues such as bone or uterus. In addition to its grand success as effective anti-cancer therapeutic, TAM protects breast cancer patients from osteoporosis [71], but it may enhance thromboembolism[81] and increases the risk of endometrial cancer. However, the incidence of endometrial cancer development in breast cancer patients, even when treated with TAM, is very low[82].

The ER-inhibitory effects of TAM in the breast are attributable to its (Z) isomer (ICI-46474), which is simply referred to as TAM in this work[83,84]. With regard to its action, TAM is a pro-drug transformed into many metabolites by various cytochrome P450 (CYP) enzymes (figure 1.4). Amongst the direct conversion products of TAM are (Z)-4'-OH-TAM and TAM-N-oxide[85]. In different rat strains, application of TAM provokes liver tumours by the formation of hepatic DNA damaging adducts. These adducts do not accumulate with TAM administration over time and are also formed, to a lesser extent however, in the mouse liver. Mice do not develop such liver tumours upon TAM administration, which is probably due to metabolic differences and more rapid clearance of TAM as well as alterations in DNA repair. DNA adducts are especially formed via the TAM metabolite α-OH-TAM, which is the major route of TAM metabolism in rats, but not in humans. In the rat, TAM-provoked induction of liver cancer is the result of relative high α-hydroxylation combined with insufficient detoxification of the DNA[86,87]. The main conversion of TAM in human patients is N-demethylation (DM) primarily catalysed by CYP3A4 and CYP3A5. Thereby, DM-TAM reaches twofold higher plasma levels than the parent drug TAM. CYP2D6 activity turns DM-TAM into (Z)-4'-OH-DM-TAM or (Z)-endoxifen. (Z)-endoxifen together with (Z)-4-OH-TAM, which is directly metabolised from TAM by 4-hydroxylation through various CYP enzymes, represent the major active TAM metabolites. Both (Z)-4-OH-TAM and (Z)-endoxifen have a much higher ER binding affinity compared to TAM resulting in an increased anti-proliferative efficacy. Besides the corresponding (Z)-4-OH-TAM, (E)-4-OH-TAM exerts agonistic effects on the ER and may associate with TAM resistance. In this context, (E) and (Z) isomers of the TAM metabolites differ in their concentration, which is also influenced by the extent of glucuronation. Generally, (Z)-endoxifen reaches higher plasma concentrations compared to (Z)-4-OH-TAM. Therefore, (Z)-endoxifen is accepted the main effector of TAM therapy. Its concentration is strongly dependent on the CYP2D6 metaboliser status of the patient, which may determine success of TAM therapy[88-90].

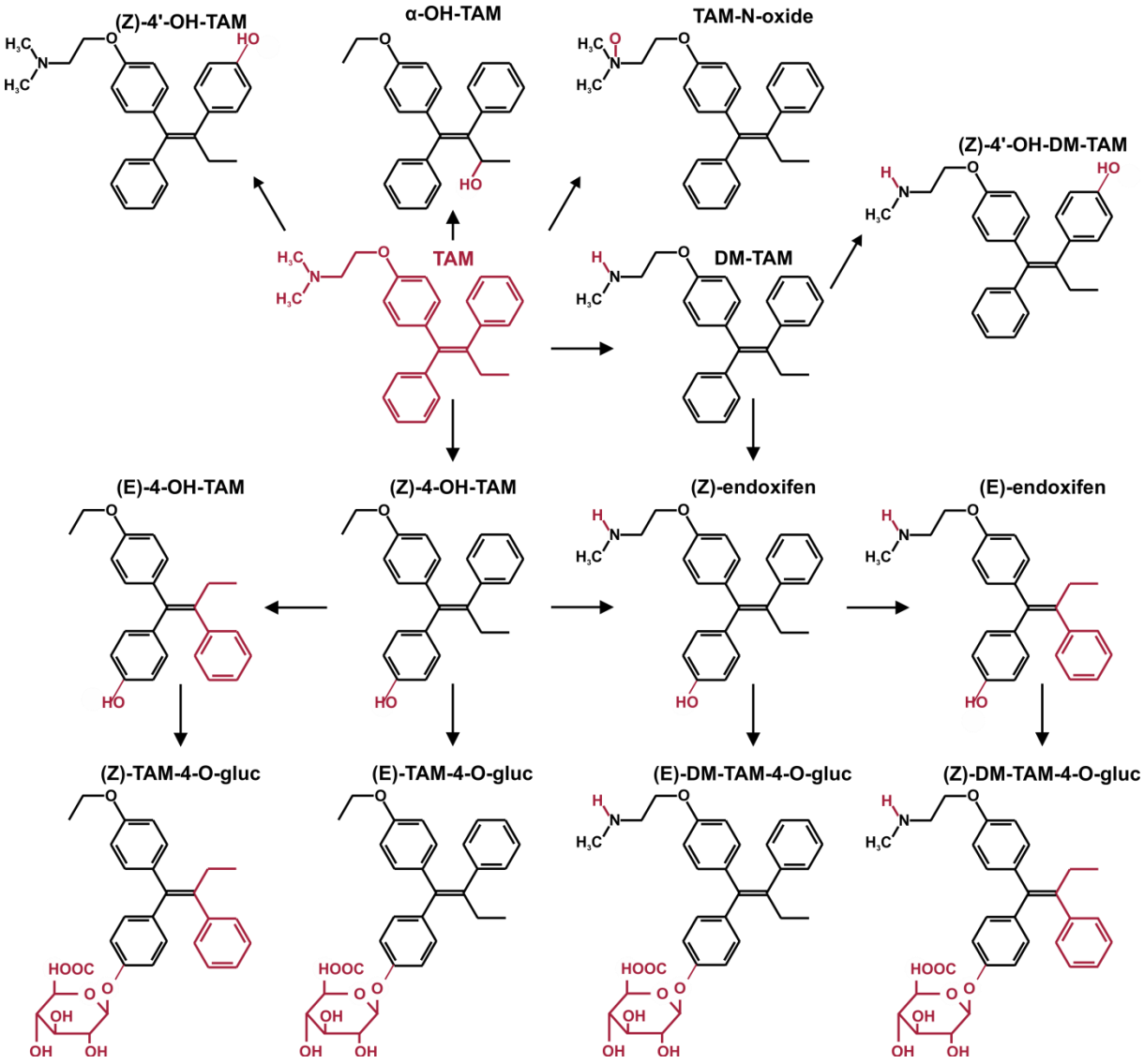

Figure 1.4: Metabolism of TAM
Tamoxifen (TAM) is a pro-drug extensively metabolised by phase I and II enzymes. Demethyl (DM)-TAM represents the main metabolic pathway in human patients and the ER antagonistic effects of TAM in the breast are primarily related to the (Z) isomers. The major active TAM metabolites to exert anti-tumour activity are (Z)-endoxifen and (Z)-4-OH-TAM (modified after Brauch et al., Clin Chem 2009 and Mürdter et al., CPT 2011).

In recent years, endocrine therapy in post-menopausal women has been recommended to include an aromatase inhibitor (AI) because of its superior effect and altered toxicity profile compared to TAM, which was investigated and confirmed in clinical trials. AIs include anastrozole, exemestane and letrozole. However, cardiovascular events[91,92] and bone fractions are more frequent under AI therapy. The latter is explained by their mode of action to reduce the formation of endogenous E2[80,93]. In pre-menopausal patients, an incomplete block of oestrogen synthesis provoked by AI application would induce gonadotropin release and thus stimulate aromatase to increase ovarian oestrogen synthesis. Therefore, AIs do not belong to the standard endocrine therapy in pre-menopausal women[71]. A switch to TAM after

prolonged AI therapy is possible, though. Accordingly, TAM pre-treated patients can switch to AI therapy when reaching menopause during endocrine therapy[80]. Exclusively in pre-menopausal patients, endogenous oestrogen levels can be depleted by the application of GnRH analogues. GnRH itself is secreted in a pulsatile manner and chronic administration of a GnRH analogue causes desensitisation of the GnRH receptor and thus diminished gonadotropin release resulting in decreased gonadal oestrogen synthesis[93].

Besides selective ER modulators and AIs, the selective ER degrader fulvestrant is in clinical practice since 2002 acting as a pure ER antagonist. It has shown at least the efficacy and tolerability as anastrozole in a first-line clinical trial. Initially, fulvestrant was introduced as second-line treatment after disease progression under TAM or AI therapy. Due to its positive evaluation, fulvestrant is also suggested as first-line therapeutic by now[31,94].

PR status

The PR consists of the isoforms A and B derived from two differential promoters within the PR gene and it is expressed as homodimer or heterodimer of these two isoforms. PR-A is a truncated version of PR-B and is more often over-expressed in breast cancer. Besides, a high PR-A to PR-B ratio is associated with a poorer prognosis and a decreased response to hormone therapy. However, the role of the PR in breast cancer is generally not understood well so far. Studies with anti-progestins such as mifepristone reveal decreased cell proliferation at low concentrations, but show the opposite effect with increasing doses. Due to the activation of PR transcription by ER-α signalling, PR expression may serve as indicator for ER-α function[74].

AR status

The AR is expressed in healthy tissues and in many breast tumours including most cases of ER-positive breast cancer, as described in section 1.1.1. Its presence can be associated with ameliorated prognosis and response to hormone therapy, plus its interaction with the ER modulates tumour progression. However, the role of the AR in breast cancer risk and progression generally depends on different factors such as tumour subtype and thus the presence of other steroid receptors[74,95].

HER2 status

The HER2-encoding *ERBB2* gene was simultaneously identified in several laboratories. HER2 consists of an extracellular domain, a transmembrane domain and an intracellular domain with tyrosine kinase activity. The frequent amplification of HER2 in breast cancer was

recognised and correlated with its impact on survival. In patients with HER2 amplification, relapse is more likely to occur and they have a shortened survival. Besides, the actual number of gene copies correlates with an exacerbated prognosis for the patient[6,96].

1.1.5 The Ki-67 proliferation marker in breast cancer

The Ki-67 antigen was identified at Kiel University in Germany representing clone number 67 on a 96-well plate tested for the development of a monoclonal antibody to detect proliferation. As proliferation marker, the Ki-67 protein can be detected during progression through the active phases of the cell cycle, whereas it is absent in G_0 phase quiescent cells. Ki-67 expression increases with cell cycle progression and reaches its maximum in mitosis. Herein, Ki-67 expression is highest in metaphase, whereas its levels are decreasing during anaphase and telophase.

Despite its established relevance as a marker for proliferation, physiological roles for the Ki-67 protein have remained elusive until recent years[97,98]. Moreover, its link to malignant cell proliferation is not without controversy. To provide an example, depletion of Ki-67 in HeLa cervical cancer and U2OS osteosarcoma cells has no effect on cell cycle kinetics[99]. In addition, Ki-67 absence has no impact on proliferation rates in DLD-1 colon and MCF-7 breast cancer cells although decreasing clonogenic growth[100]. Contrary to these results, Ki-67 depletion in several non-cancerous human cell lines diminishes RNAs known to peak at G_1/S transition and the entry of S phase. This effect is mediated by a functioning p21 cell cycle checkpoint induced by the reduced Ki-67 levels[101]. During mitosis, Ki-67 is known to be responsible for the maintenance of chromosome separation after nuclear disassembly as well as chromosome individualisation and condensation in the cytoplasm. It thus prevents the chromosomes from collapsing into a single chromatin mass and allows their motility. The Ki-67 protein has little secondary structure, it is highly positive charged and acts as surfactant at the phase boundary between chromosomes and cytoplasm. Furthermore, Ki-67 allows access of the spindle microtubules to the chromosomes and Ki-67 depletion prolongs mitosis[102]. The Ki-67 protein promotes the recruitment of protein phosphatase 1γ to anaphase chromosomes, which is a serine/threonine-specific phosphatase contributing to mitotic exit by resolving mitotic kinase activity. The γ subunit of the enzyme is thought to be important for chromatin decondensation. Phosphorylated Ki-67 is a substrate for protein phosphatase 1[103]. In addition, the p150 N-terminal domain of the chromatin assembly factor 1 interacts with histones leading to Ki-67 accumulation in the perichromosomal layer during mitosis, formation of Ki-67 foci at heterochromatic satellite repeats after cytokinesis and in early G_1 phase, as well as Ki-67 localisation to the perinuclear region during interphase[104].

With regard to breast cancer, Ki-67 staining distinguishes the luminal A molecular breast cancer subtype from luminal B tumours. In terms of 10-year relapse-free survival (RFS) in general and under TAM treatment, patients with luminal A breast tumours show highest survival, followed by luminal B tumour patients and least survival is observed in HER2-positive breast cancer[12,105]. The Ki-67 index, measured as the portion of Ki-67-positive cells within a tumour, is frequently higher in pre-menopausal compared to post-menopausal tumours and positively associates with nodal status, tumour grade, HER2 over-expression and negative ER or PR status. Regarding breast cancer survival, high Ki-67 expression is a prognostic factor for both shorter disease-free survival and overall survival outcome[106]. Besides, Ki-67 expression can be higher in distant metastatic lesions compared to the primary tumour. Therefore, metastatic breast cancer patients with high proliferation status might especially benefit from chemotherapy compared to other therapies[107]. Regarding ER-positive breast cancer patients with Ki-67 ≥ 14%, adjuvant docetaxel chemotherapy shows a tendency of prolonging disease-free survival and overall survival. Conversely, patients with ER-positive disease and a Ki-67 index < 14% have no such advantage from taxane treatment[108]. In a recent study, a Ki-67 cut-off at 20% identifies patients to benefit most from neoadjuvant chemotherapy[109]. Although Ki-67 may represent a promising marker for breast cancer classification as well as prognosis and prediction of therapy response, its clinical use is limited so far. Inter-laboratory differences in Ki-67 staining intensity and frequency of labelled nuclei challenge the reproducibility of a not-yet uniformed Ki-67 cut-off and thus highlights the need for standardisation of Ki-67 detection[110]. However, the International Ki-67 in Breast Cancer Working Group made an attempt for developing staining and scoring protocols in order to be able to compare Ki-67 results and which may prove valuable in the future[111,112].

1.1.6 Gene expression tests to personalise medicine

Different gene expression diagnostic tests based on breast cancer subtypes (section 1.1.1) are established for advanced tumour-specific treatment decisions and prognosis. As such, the MammaTyper® uses mRNA expression profiling of ER, PR, HER2 and Ki-67 from formalin-fixed and paraffin-embedded samples for molecular subtype classification of the tumour. This technique shows higher sensitivity and specificity compared to immunohistochemistry-based detection of theses markers and might serve as an amendment to routine diagnostics[113,114].

With regard to the PAM50 gene signature, the NanoString Prosigna™ assay detects mRNA levels for 46 of the original 50 PAM50 genes in formalin-fixed, paraffin-embedded tumour samples more precisely than polymerase chain reaction (PCR). Besides molecular subtype

classification, Prosigna™ determines a risk of recurrence score and predicts a tumour-specific benefit from endocrine therapy and chemotherapy[115]. Moreover, the MammaPrint® was developed as a gene expression profiling microarray that investigates the signature of 70 genes. From 25,000 genes tested in 98 tumour samples, these 70 genes represented the most accurate number of significant associates for disease outcome[116,117]. In one follow-up study, patients with early breast cancer and a high clinical risk were stratified by their genomic risk of breast cancer recurrence according to the test. 5-year distant metastasis-free survival was assessed in those patients with low genomic risk. Patients receiving chemotherapy only showed a random better outcome than patients without chemotherapy. Therefore, chemotherapy was proposed to be neglected in patients with low genomic risk despite their high clinical risk[118]. Initially, the Oncotype DX® test was designed for ER-positive and TAM-treated breast cancer with negative nodal status. It investigates mRNA expression of 16 cancer-related genes amended by 5 normalisation genes. A recurrence score to predict distant recurrence or even prospective mortality outcome can be calculated[119,120]. Independently from node status, it can predict whether a patient will benefit from chemotherapy prior to TAM[121,122]. As another test, the EndoPredict® investigates distant recurrence in early ER-positive, HER2-negative breast cancer patients treated with endocrine therapy. The EndoPredict® risk score investigates mRNA levels from eight cancer-related genes and three reference genes[123]. It is an independent prognostic marker after adjusting for ER and PR status, Ki-67 index, tumour size, grade, lymph node status and age also in node-positive breast cancer patients undergoing chemotherapy before endocrine therapy[124].

Several studies compared the gene expression tests described above, which vary in their methodology, use of gene signatures and inclusion of clinical parameters[125]. Dependent on the test, subtype classification, treatment recommendation and prognosis can differ[126]. As the tests have diverse approaches, none seems to be superior to another. However, the tests may provide different information with regard to individual patients[127]. For future directions, besides the analysis of the most frequently observed breast cancer predictors, the implementation of specific functional biomarkers may improve the value of such gene expression tests in terms of personalised medicine.

1.2 K^+ channels

Ion channels are membrane-spanning proteins that allow flux of different ions such as sodium (Na^+), potassium (K^+), calcium (Ca^{2+}) or chloride (Cl^-) through the cellular membranes[128]. K^+ channels constitute a big and topologically as well as functionally diverse group of ion channels. Their pore-forming α subunits are selective for K^+ ions and their gating

mechanisms switch between open and closed conformations. K^+ channels present with 2, 4, or 6 transmembrane (TM) segments. The members of the different groups are further divided in subtypes that interact with auxiliary subunits. Voltage-gated K^+ (K_V) channels, for example, belong to the 6 TM K^+ channels. Their voltage sensor is located in the S4 segment containing positively charged residues. K_V channels are activated by depolarising membrane potentials and therefore represent important contributors to cellular excitability and action potential duration. The group of 6 TM K^+ channels further comprises Ca^{2+}-activated K^+ (K_{Ca}) channels, whose members are activated by different concentrations of intracellular Ca^{2+} $[Ca^{2+}]_i$. Two-pore domain K^+ channels exist with 4 TM segments and sense the environmental conditions of a cell thereby contributing to background K^+ currents and the resting membrane potential. Besides, inward-rectifying K^+ (K_{ir}) channels pass K^+ ions more easily inward than out of the cell. K_{ir} channels are 2 TM proteins and contribute to the adjustment of the resting membrane potential of hyperpolarised cells. Due to their high structural and functional diversity, K^+ channels contribute to cardiac, neuronal and metabolic disorders and they also exert cancer-promoting activity[129,130].

Different types of K^+ channel members reportedly contribute to cancer cell characteristics such as proliferation, migration, angiogenesis and apoptosis. Cell volume generally is determined by the Cl^- gradient, but K^+ fluxes are required for counteracting the ionic imbalance. Thereby, spatially-confined cell volume changes by K^+ channels may support tumour or stroma cell migration, trigger apoptosis or cell division[131]. Generally, uncontrolled proliferation and thus tumour growth rely on aberrant progression through the cell cycle, which comprises a tightly controlled interaction of different cyclins and cyclin-dependent kinases. In contrast to a terminally differentiated or senescent cell, a transiently arrested cell can leave the resting G_0 phase upon mitogenic stimulation and thus enter G_1 phase. Retinoblastoma protein phosphorylation activates elongation factor 2 in order to induce genes involved in G_1/S transition and DNA synthesis, which is accomplished in S phase. After successful DNA replication, the cell progresses via G_2 phase into mitosis[132]. K^+ channels participate in the membrane potential changes observed throughout the cell cycle and during the corresponding phase transitions. Hyperpolarisation induced by K^+ efflux acts as driving force for Ca^{2+} entry into the cell[133]. Accordingly, MCF-7 breast tumour cells are hyperpolarised through G_0 and G_1 phases and during G_1/S transition, which is accompanied by increased K^+ permeability[134]. Moreover, aberrant expression or activity of many different K^+ channels is described for various tumour entities. In general, K^+ channels seem to modulate cancer driver genes and mutations to influence tumour progression. Moreover, K^+ channels are expressed in tumour and stroma cells, but their exact functions concerning tumour to stroma cell communication in complex situations are not known[135,136].

1.2.1 The K_{Ca} channel family

One important feature of K_{Ca} channels is their dependence on $[Ca^{2+}]_i$, which is a second messenger involved in many cellular processes. *Vice versa*, activation of K_{Ca} channels increases the driving force for Ca^{2+} influx to modify the induction and the response to Ca^{2+}-dependent signalling mechanisms within the tumour cell. One mechanism for the integration of Ca^{2+} signalling and K_{Ca} channel activity is the binding of calmodulin and down-stream activation of calmodulin-dependent kinases and calcineurin[137]. $[Ca^{2+}]_i$ in resting cells lies at 100 nM, but entry of Ca^{2+} across the plasma membrane or from intracellular stores, such as the endoplasmic reticulum, the golgi apparatus or lysosomes, can increase $[Ca^{2+}]_i$ to more than 1 µM. Ca^{2+} is needed for cell cycle progression and is also implicated in tumour cell proliferation. It is further important for immediate-early gene expression in early G_1 phase and for the initiation of G_1/S transition. Aberrant Ca^{2+}-dependent signalling is frequently observed in cancer. Ca^{2+} can modulate oncogenic signalling like retinoblastoma inactivation by phosphorylation through direct interaction with ras signalling. Besides, $[Ca^{2+}]_i$ oscillations are observed during G_1/S and G_2/M transitions. Ca^{2+} is also involved in signalling networks that control cellular survival and apoptosis. As an example, the flux of Ca^{2+} from the endoplasmic reticulum together with its accumulation in mitochondria is a potent cell death signal[138].

The K_{Ca} channel family includes big (BK), intermediate (IK) or small (SK) conductance channels of 100 to 300 pS, 20 to 80 pS or 5 to 20 pS, respectively[139-141]. SK1 - 3 channels and the IK channel open at low $[Ca^{2+}]_i$, whereas the BK channel primarily responds to voltage with $[Ca^{2+}]_i$ acting as amplifier[137]. So far, the oncogenic potential of BK channels is described in different tumours such as sarcoma or bone, brain, pancreas and breast cancer. The SK3 channel is known to be involved in breast cancer as well, but also in melanoma and gastrointestinal malignancies. In addition to breast cancer, functions of the IK channel in prostate, brain and gastrointestinal tumours as well as melanoma are reported[135].

1.3 The BK channel

1.3.1 Activation and structure of the BK channel pore-forming subunit

The BK channel is also known as $K_{Ca}1.1$, Slo1, or Maxi-K channel because of its high K^+ conductance[128]. Its gene, initially termed the *slo* gene, was discovered in drosophila melanogaster, in which mutation of the slowpoke locus abolishes BK channel-representing currents and immensely impairs flight ability[142]. Mouse and human homologues show more than 50% amino acid agreement compared to the drosophila slowpoke locus. By alternative splicing, multiple transcripts are generated from the BK channel-encoding *KCNMA1*

gene[143,144]. The BK channel protein derives from a single gene with 27 exons[128]. Different BK isoforms are known to be processed by alternative splicing, such as brain-specific isoforms[145] and the glioma BK[146], the mitochondrial BK[147], or by stress axis hormone regulation[148,149]. Splicing processes are observed at domain boundaries. Besides, constitutive exons, e.g. the pore-forming regions, are conserved between vertebrates and intervertebrates whereas this does not hold for alternatively spliced exons. [150].

BK channels (figure 1.5) present as tetramers of their pore-forming α subunits[151]. Although the BK channel belongs to the 6 TM proteins, it contains an additional S0 transmembrane segment that renders the N terminus to the extracellular side. Segments S0 - S4 function as voltage sensor. Besides, the BK channel possesses a large C terminus that forms a gating ring structure for the binding of Ca^{2+}. These Ca^{2+} sensors serve for the regulation of K^+ conductance and thus are named RCK1 and RCK2, the latter which contains the Ca^{2+} bowl holding high Ca^{2+} affinity[152-154]. Therefore, activation of BK channels by Ca^{2+} occurs at the C terminus[155]. Maximum activation of BK channels involves both voltage and Ca^{2+}. Nonetheless, the BK channel can be almost maximally activated by strong depolarisation alone[156]. Transition from closed to open state after sensing for voltage and Ca^{2+} is allosterically coupled. The BK channel can hereby occupy many different open and closed conformations and its activation by voltage and Ca^{2+} influence each other[157,158].

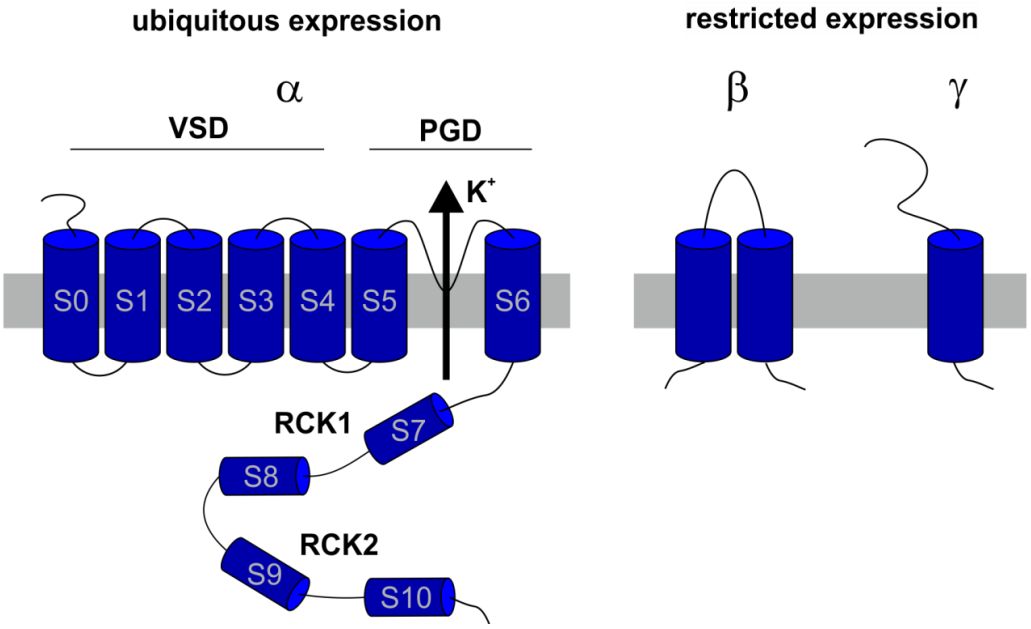

Figure 1.5: Structure of the BK channel complex
The BK channel consists as complex of its pore-forming α subunit that interacts in a cell- and tissue-specific manner with auxiliary β and γ subunits in order to modify its activity. BK-α is a 6 TM protein with an additional S0 segment, whose activity depends on voltage and $[Ca^{2+}]_i$. In contrast, BK-β and BK-γ subunits are proteins with 2 and 1 TM segments. Abbreviations: Voltage sensor domain, VSD; Pore-gate domain, PGD; Regulator of K^+ conductance, RCK.

1.3.2 Modification of BK channel activity by its auxiliary subunits

Despite the ubiquitous expression of the BK-α pore-forming subunit, BK channels have tissue-specific electrophysiological properties. Besides, the expression of BK-β and BK-γ accessory subunits and posttranslational modifications as well as alternative splicing of the BK-α subunit gene allow for increased diversity. However, BK channel half-activation voltage requires membrane potentials > 100 mV in the absence of $[Ca^{2+}]_i$. Alternatively, the half-maximal effective Ca^{2+} concentration needed is ≥ 10 µM at resting conditions. Thus, the BK channel would hardly be active in non-excitable cells with a membrane potential ≤ -40 mV and $[Ca^{2+}]_i$ ≤ 100 nM[159].

In this context, the first BK-α-modulating subunit was identified in bovine smooth muscle of the trachea and showed high affinity for the BK channel blocker charybdotoxin[160]. The subunit was termed BK-β1 and its knockout (KO) in mice decreased BK channel Ca^{2+} sensitivity while increasing blood pressure[161]. Sequence alignment of BK-β1 further allowed for the identification of BK-β2, four differentially spliced BK-β3 variants as well as BK-β4. The BK-β family members have a sequence similarity of 21 - 43% and present as membrane proteins with 2 TM domains (figure 1.5). The different BK-β subunits are expressed in a tissue-dependent manner. BK-β1 is found especially in smooth muscle but very weakly in brain and other tissues, whereas BK-β2 gene expression is highest in ovary and weak in many other tissues. BK-β3 expression is prominent in testis and additionally, it shows very little expression in other non-neuronal tissues. In contrast, BK-β4 is strongly expressed in all neuronal tissues. Half-activation voltages of the BK channel at a 1 µM concentration of free Ca^{2+} are shifted by -26 mV and -51 mV for BK-β1 and BK-β2, respectively. These shifts towards more negative membrane potentials for activation are increased at higher concentrations of free Ca^{2+}. For BK-β4, the free Ca^{2+} concentration determines to which direction half-activation voltage is shifted. Co-expression of a particular BK-β3 variant with BK-α may determine its influence on BK channel activation albeit it seems the shift induced by BK-β3 stays in the physiological range without affecting BK channel activation[162,163]. Concerning BK channel inhibition, the presence of the BK-β4 extracellular loop irreversibly renders the BK channel complex resistant to charybdotoxin and iberiotoxin binding and action[164].

As the first member of a new class of BK channel subunits, high abundance of BK-γ1 was detected by a cDNA library screen in breast and prostate cancer cell lines. In contrast to the cancer cell lines tested, the non-tumourigenic MCF-10A epithelial cell line was negative for BK-γ1. Besides, BK-γ1 was identified in 26 out of 33 tested human breast tumour samples, but was also expressed in other cancers[165]. In LNCaP prostate cancer cells, the BK-γ1

subunit shifts the voltage dependence of BK channel activation to more negative potentials in a Ca^{2+}-independent manner[159,166]. Regarding BK channel openers, BK-γ1 prevents BK activation by mallotoxin, but only has a small impact on the NS-1619 compound. Both substances open the BK channel by inducing a hyperpolarising shift[167,168]. Regarding the stoichiometry of γ1 to α, BK-γ1 opens the channel in an all-or-none fashion. In other words, there is no intermediate shift observed at low γ1 to α ratios, a finding that is in clear contrast to the mode of BK channel activation in the presence of BK-β subunits[169].

Four of these BK-γ subunits have been described in the past few years. They belong to the group of leucine-rich repeat-containing (LRRC) proteins and were identified as 35 kDa proteins named LRRC26 (BK-γ1), LRRC52 (BK-γ2), LRRC55 (BK-γ3), and LRRC38 (BK-γ4)[170]. As first described for BK-γ1, the γ subunits possess an amino-terminal signal peptide that is cleaved in the mature protein allowing for extracellular localisation of the following large LRR domain. The BK-γ subunits further present as single-span transmembrane proteins with a short intracellular C terminus[159]. Therefore, the BK-γ subunits differ structurally from the previously described BK-β subunits (figure 1.5). However, BK-β and -γ subunits share significant amino acid sequence identity of 30 to 40%. With regard to the modulation of BK channel activity, the BK-γ subunits induce a negative shift of BK-α half maximal activation of about 140, 100, 50, and 20 mV for BK-γ1-4, respectively. With regard to terminology, the BK-γ1-4 subunits are sorted in a descending manner according to their impact on BK channel activation[170]. In addition, BK-γ subunits can be further distinguished by their tissue-specific expression pattern. The BK-γ1 subunit, for example, is detected in secretory epithelial cells such as lacrimal, parotid and submandibular glands as well as in the lactating mammary gland[171]. The BK-γ2 subunit is highly expressed in testis and skeletal muscle, albeit it is found in other tissues such as placenta and some glands to a much lower extent as well. In contrast, BK-γ3 expression is restricted to the nervous system. The BK-γ4 subunit is abundant in skeletal muscle, adrenal gland and thymus, but it is also found in the nervous system[170].

1.3.3 Pharmacological BK channel blockade

As described for other ion channels, BK´s unitary conductance is reduced in the presence of extracellular and intracellular protons other than K^+. Intracellular proton block depends on proton concentration, voltage and the intracellular K^+ concentration. Intracellular H^+, for instance, competitively inhibits the BK channel. Under physiological conditions, however, this block can be neglected[172,173]. Further, BK channel activity is antagonised by the broad K^+ channel inhibitor tetraethylammonium[151]. For the group of peptide toxins, charybdotoxin

was the first available potent BK blocker although interacting with SK and K_V channels as well. In contrast, BK channel inhibition by iberiotoxin was found to be specific[174]. Interestingly, charybdotoxin binding to the BK channel can be prohibited in the presence of other non-peptide BK channel inhibitors, or enhanced as with the fungal toxin paxilline[175]. More recent experimental approaches utilise paxilline for BK channel inhibition. Paxilline efficiently and specifically blocks the BK at low nanomolar concentrations by stabilisation of the closed state while lacking effects on open BK channels. Onset and recovery of the BK channel block by paxilline is in the range of minutes in electrophysiological attempts, depending on the washout[176,177]. Paxilline was isolated as tremorgenic agent and its effect is dependent on the presence of the BK-β4 subunit, whose co-expression with BK-α was tested next to BK-β1[178].

1.3.4 Role of the BK channel complex in cancer

The contribution of BK channels to tumour cell proliferation is described for different tumour entities including prostate[166,179], cervix and ovarian cancer[180,181]. BK channel activity is also found in glioblastoma[182,183], in which a glioma-specific and pro-proliferative BK splice variant is expressed[146,184], and in the aggressive and therapy-resistant glioblastoma stem-like cells[185]. Besides, BK channels seem to enhance migration of glioma cells, which links different levels of BK activity and status to the response to radiation therapy[186].

With regard to breast cancer, *KCNMA1* gene amplification can be found, which is associated with high tumour grade and stage, proliferation and a poor prognosis[187]. Besides, *KCNMA1* gene expression is higher in metastasising human breast cancer cells and especially those from brain metastases, which also reveal higher BK channel-mediated migration and invasiveness[188,189]. An early study determined a possible role for the BK channel in MCF-7 cell proliferation indicating that cell cycle-dependent BK channel expression is peaking in late G_1 phase, although BK channel blockade had no significant impact on tumour cell proliferation. Apparently, serum-containing proteins or other compounds had an impact on BK or the effect of BK inhibitors on the channel[190]. Later studies from the same group revealed G_0/G_1 cell cycle accumulation as well as reduced cyclin D1 and cyclin-dependent kinase 4 expression levels resulting in a suppression of proliferation in MCF-7 cells after BK channel mRNA knockdown. In contrast, BK channel depletion in the non-cancerous MCF-10A normal breast cell line did not alter the behaviour of these cells. Further, functional co-localisation of the BK channel and the second messenger inositol 1,4,5-trisphosphate in cholesterol-rich domains such as lipid rafts was observed in MCF-7 cells. In this context, adenosine triphosphate (ATP) application to the MCF-7 cells induced Ca^{2+} release from

intracellular stores via type 3 inositol 1,4,5-trisphosphate receptors leading to BK channel activation and hyperpolarisation[191].

Proliferation-stimulating effects of BK are also dependent on the cholesterol content of the plasma membrane and the localisation of the channel to caveolin-1-enriched lipid rafts in melanoma. Accordingly, BK release from these lipid rafts by cholesterol depletion of the plasma membrane augments channel activity[192]. With regard to further membrane-associated proteins, HER2 signalling activates the glioma BK channel with involvement of changes in $[Ca^{2+}]_i$[193]. In contrast, the HER2 status has not generally proven an indicator for the proliferation response to the BK channel inhibitor iberiotoxin tested in three different breast cancer cell lines[194]. In addition, BK channel activation by a broad range of molecules is shown for different tumour types, such as somatostatin in pituitary tumour cells[195] or prostaglandin E_2 in osteosarcoma[196]. Moreover, stromal cell-derived factor 1-α induces pituitary adenocarcinoma cell proliferation[197] and glioblastoma cell migration[186] by BK channel activation.

1.3.5 Interaction of anti-/hormones with the BK channel

Cis unsaturated fatty acids are described for their potential to activate BK channels without change in the fluidity of the cellular membrane, whereas the respective trans isoforms show no effect[198]. Moreover, E2 by endothelium-dependent mechanisms, but also by targeting the smooth muscle cell BK channel may promote vasodilation[199,200]. Along these lines, the activation of smooth muscle BK channel complexes by E2 requires the BK-β1 subunit, whereas the E2 stereoisomer 17α-oestradiol has only modest effects on BK channel activation. In addition, E2-mediated BK activation stimulates MCF-7 breast cancer cell proliferation and that can be mimicked with E2 bound to bovine serum albumin (BSA), to prohibit E2 from membrane penetration and thus activation of the intracellularly-located ER[201,202]. A stoichiometry of at least two BK-β1 subunits per BK channel was calculated to be necessary to mediate BK channel activation by E2, as shown in human embryonic kidney cells[203].

Interestingly, BK-modulating effects of anti-hormones have also been reported. This was first described for TAM and its membrane-impermeable form ethylbromide TAM by inducing an increased channel open probability in the presence of BK-β1 in smooth muscle cells[204,205]. The mechanism was confirmed by studies in human embryonic kidney cells transfected with an expression construct containing BK-α and BK-β1. Here, the channel gating effects were dependent on the TAM concentration with a half-maximal effective concentration of 0.2 µM[206]. The BK channel-stimulating effects of TAM are confirmed in MCF-7 cells, in which

BK activation promotes cell proliferation[207]. Besides TAM, the pure anti-oestrogen fulvestrant also activates smooth muscle BK channels in a non-genomic manner. In contrast, fulvestrant administration to coronary endothelial cells decreases the BK channel current in a concentration-dependent mode. These opposing effects may be attributed to cell type and the BK-β and BK-γ subunit profile, which have not been studied in this report. Yet others observed lower BK channel activity at higher µM concentrations of fulvestrant in smooth muscle as well[208,209].

So far, the available evidence indicates that the intensively studied BK-β1 subunit is involved in BK channel activation by E2 and anti-hormones. BK-β1 and E2 interaction sites are different from the sites of protein-protein interaction between BK-β1 and BK-α. In comparison to K_V channels and other K_{Ca} channels, BK channels have an additional S0 segment (mentioned in section 1.3.1) that locates the N terminus to the extracellular side. This S0 segment is necessary for BK channel function[210,211]. As shown for BK-β1 and -β4, the interaction of BK-α with these auxiliary subunits is closely related to the S0 segment[212,213]. Moreover, it is established that the assembly of different BK channel subunits orchestrate steroid hormone sensitivity of the channel. As an example provided in human embryonic kidney cells, BK-β2 mediates BK channel activation by the stress-related adrenal androgen dehydroepiandrosterone and to a minor extent by corticosterone, E2 and testosterone. In comparison, the BK-β4 subunit mediates BK´s response to corticosterone, but also other sex and stress steroids. However, the steroid precursor cholesterol does not significantly affect BK channel activation via BK-β2, BK-β4 or BK-α alone[214]. Whether and which other BK-β or the newer BK-γ subunits would mimic or modulate these effects in other settings is not described in detail and thus needs further elucidation. To conclude, an ambivalent either anti-proliferative effect via the ER or pro-proliferative effect via BK channel activation may be observed for TAM therapy and at least partly also for the administration of fulvestrant with regard to breast cancer.

Besides modulation of BK channel activity, reports from different groups suggest a modulation of BK channel expression after E2 administration. This may, at least in part, be attributable to the presence of ERs. In smooth muscle cells, an E2-mediated increase of BK channel activity can be further augmented by enhanced ER-α expression, but is abrogated after ER-α knockdown[215]. In experiments using a GnRH-secreting neuronal cell line treated with E2 for 3 d, ER-β but not ER-α knockdown decreases the BK-representing K^+ current. Moreover, E2 treatment increases BK-α and BK-β4 mRNAs, but not those of BK-β1 or BK-β2 expressed in the particular cell line as well[216]. Work in the mouse N2a and the human SK-N-SH neuroblastoma cell lines reveals an E2-mediated increase of mRNA

expression for all BK channel subunits investigated. The effects were dependent on ER-β but not ER-α expression. Additionally, BK-α expression levels positively associate with E2 concentrations administered[217]. In a rat *in vivo* study, the influence of ovariectomy and E2 replacement on BK-α expression was further analysed. Protein but not mRNA levels were 1.5 fold higher in ovariectomised compared to sham-operated Sprague-Dawley rats. Similarly, E2 replacement after ovariectomy restored BK-α levels, whereas no effects on other BK channel subunits were observed[218].

Rapid actions induced by the interaction of different growth factors with the BK channel are well established today. For most work, oestrogens exert a BK channel-stimulatory effect, but some few articles describe an inhibitory mode of oestrogen action on BK channels or even BK channel downregulation by oestrogens. These opposing effects seem independent from oestrogen dose, but may depend on the cell type investigated. Besides BK, other K^+ channels like K_v channels, but also Ca^{2+} channels, Na^+ channels such as the sequence like a Ca^{2+}-activated K^+ channel (Slack), Cl^- channels as well as ligand-gated channels respond to hormones by activation[219-221].

1.3.6 BK channel-mediated tumour cell migration and survival after IR

Radiation-induced tumour cell migration involving Ca^{2+}/calmodulin-dependent protein kinase (CaMK) II and stromal cell-derived factor 1-α seem to require functional BK, whereas clonogenic survival after IR is not dependent on its presence. IR induces an increase in the open probability of BK channels without affecting the number of plasma membrane BK channels[186,222]. In contrast to these findings, studies in rat aortic smooth muscle cells reveal a decrease in *Kcnma1* and *Kcnmb1* mRNA expression levels induced by IR, as measured after 9 and 30 d. However, the major K^+ outward current in these cells can be attributed to the BK channel. As a consequence, a decrease in the K^+ outward current after IR as well as insensitivity to paxilline application were reported and the mechanism suggested involved protein kinase C[223,224].

1.4 The IK channel

1.4.1 Structure of the IK channel

The IK channel, named Gardos after its Hungarian discoverer, was detected in erythrocytes in 1958. It was described for the contribution to erythrocyte ion homeostasis by Ca^{2+}-dependent K^+ permeability[225]. In 1997, the *KCNN4* gene coding for the IK channel was

identified by sequence alignment[226,227]. Later, it was confirmed that IK and Gardos represent the same channel, which is also described as $K_{Ca}3.1$ or SK4 channel[228,229].

The IK channel pore-forming α subunits are proteins with 6 TM segments and a loop between S5 and S6 with four of the subunits forming the actual channel (figure 1.6). IK channels are insensitive to voltage, but they are activated by increasing levels of $[Ca^{2+}]_i$[129,137]. Ca^{2+}-mediated IK channel activation involves the constitutive binding of calmodulin to the cytosolic C terminus of each of the four pore-forming IK channel subunits. Free Ca^{2+} is tightly regulated in the cell and binding to its primary intracellular receptor calmodulin stimulates conformational rearrangement and gating with regard to the IK channel[230,231]. Generally, calmodulin is involved in pleiotropic physiological processes within the cell as evident by its many binding proteins to regulate protein (de)/phosphorylation in particular via CaMK and calcineurin, but also gene expression, proliferation and cytoskeleton dynamics[232,233]. Interestingly, signalling via the CaMK family leads to a feedback mechanism to stimulate IK channel expression[234].

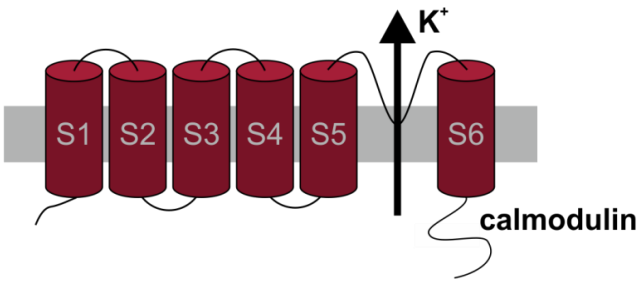

Figure 1.6: Structure of the IK channel
The IK channel forms as tetramer of its pore-forming α subunits, which are 6 TM-spanning proteins. Activation of the IK channel occurs by an increase in $[Ca^{2+}]_i$ and interaction with constitutively-bound calmodulin, which results in K^+ efflux and down-stream signalling events.

1.4.2 Pharmacological IK channel modulation

Pharmacological blockade of the IK channel can be achieved with the widely used clotrimazole. Its application results in reduced growth of lung and colon carcinoma as well as melanoma cell lines[226,235]. Due to the interaction of clotrimazole with CYP enzymes, its analogue triarylmethane-34 (TRAM-34) was developed to block the IK channel with higher potency and selectivity without significant CYP enzyme interaction[236]. However, more recent studies report some CYP enzyme interactions for TRAM-34, albeit with lower potency[237,238]. TRAM-34 has already proven efficient for blocking IK *in vivo* with a lack of toxicity in mice[236,239]. A potent and selective alternative to TRAM-34 is senicapoc. It was investigated in clinical trials and reached phase III for its therapeutic potency in sickle cell anaemia. Senicapoc is well tolerated and shows no dose-limiting toxicities. Further, it leads to

improved laboratory parameters such as an increased haematocrit and a reduction in circulating reticulocyte numbers and erythrocytes with high density in sickle cell disease. With regard to sickle cell-related painful crises, senicapoc failed to reduce the number of events compared to placebo, however[240-242]. In addition to IK inhibitors, various IK activators are available for experimental purposes with the frequently employed 1-Ethylbenzimidazolinone (1-EBIO)[243].

1.4.3 Roles of the IK channel in cancer

Increased IK channel expression and cancer-promoting characteristics are described for different tumour entities during the past years and as such, IK seems to be an important contributor to the proliferative behaviour of pancreatic carcinoma[244] and chronic lymphoblastic leukaemia cells[245]. In colon cancer cells, the IK channel-mediated proliferation is sensitive to TRAM-34, which induces a G_2/M arrest and phosphorylation of cyclin-dependent kinase 1[246]. Besides, IK expression promotes epithelial-mesenchymal transition and downregulation of E-cadherin, which is associated with cancer formation by loss of cell to cell interactions and cell polarity subsequently increasing invasiveness[247]. TRAM-34 treatment decreased the proliferation of hepatocellular carcinoma cells potentially by reducing the expression levels of ER-α and nuclear factor κ-light-chain-enhancer of activated B cells[248]. Additionally, an anti-apoptotic effect of IK channel activity is observed in head and neck squamous cell carcinoma cells[249]. The IK channel further contributes to growth and metastasis in angiosarcoma[250] and non-small cell lung carcinoma cells[251] and its high expression in clear cell renal carcinoma is an indicator for an elevated metastatic potential and a poor survival[252]. IK activity also stimulates migration of melanoma cells[253] and motility of glioblastoma-derived cancer stem cells[254]. Moreover, IK channels are upregulated in glioblastoma stem-like cells, which represent an extremely invasive and therapy-resistant subpopulation of glioblastoma cells[255]. With regard to gynaecological cancers and IK channel inhibition, endometrial cancer cells accumulate in G_0 and G_1 phases of the cell cycle[256,257] and cervix cancer cells proliferate less[258]. In addition, IK expression levels seem to be associated with ovarian cancer recurrence in patients[259].

In breast cancer, IK channel expression is regulated in a cell cycle-dependent manner with highest mRNA levels in late G_1 phase. IK activation by Ca^{2+} leads to hyperpolarisation of the cellular membrane potential, which in terms of an underlying mechanism may drive G_1/S transition and MCF-7 cell proliferation[260,261]. Accordingly, redistribution of cells through the division cycle after IK channel inhibition in other solid cancer cell lines leads to an increase in G_1 as well as a concomitant reduction of S and G_2/M. In addition, cell cycle regulators such as cyclin D and cyclin-dependent kinases 1 and 4 as well as retinoblastoma phosphorylation

are decreased while cyclin-dependent kinase inhibitor 1B expression levels are increased due to IK channel blockade. The G_1 arrest is accompanied by a decline in DNA synthesis[235,262]. Interestingly, prolactin, a lactation-causing hormone associated with breast cancer risk, stimulated MCF-7 cell proliferation in an IK-dependent manner[263]. In the triple-negative MDA-MB-231 breast cancer cell line, IK elicits pro-proliferative and anti-apoptotic responses as well as migration and epithelial-mesenchymal transition[264]. In breast cancer patients, IK channel expression correlates with tumour grade[265]. In addition, the *KCNN4* gene was identified as part of a neural progenitor-like stem cell signature found in basal breast cancer[266].

1.4.4 IK channel expression in stromal cell types

Regarding the important interaction between tumour cells and their surrounding stroma, it is interesting to note that IK channel expression has been identified in different stromal cell types (figure 1.7). Adipose tissue as a major endocrine organ, for example, is the main extra-gonadal oestrogen source, which is attributed to the expression of aromatase found in pre-adipocytes but not in mature adipocytes[267,268]. The IK channel is functionally expressed in pre-adipocytes and may contribute to their proliferative bahviours[269]. In line, the expression of IK channels in fibroblasts, which increases by stimulation with basic fibroblast growth factor, promotes proliferation while diminishing differentiation processes[270]. Fibroblast-derived factors as well as extracellular matrix that produces the structural framework, contribute to a range of tumour-related characteristics such as growth, metastasis and angiogenesis[271]. In this regard, it seems also worth mentioning that IK in synovial fibroblasts was shown to modulate the expression of interleukin (Il)-6 and Il-8, monocyte chemotactic protein 1 as well as matrix metalloproteinase-3[272]. So far, no direct link exists for a role of IK for tumour growth-related angiogenesis, which constitutes an important event in cancer progression. Nevertheless, the contribution of IK channels to endothelial cell proliferation is established with IK expression mediated by growth factors such as vascular endothelial growth factor[273].

The most prominent stroma cell type with regard to IK channel expression and function are cells of the immune system. IK expression is confirmed in T and B cells[274,275], natural killer cells[276], macrophages[277] as well as dendritic cells[278], granulocytes[279] and mast cells[280]. In tumour biology, paradoxically, immune cell infiltration enables tumour-promoting inflammation while tumour cell destruction due to immune recognition is avoided[281-283]. Cytokines released by tumour-associated macrophages are known to promote cancer progression and metastasis. Il-6 and Il-8 release as well as IK channel expression are elevated in tumour-associated macrophages when co-cultured with colorectal cancer cells. Thereby stimulated colorectal cancer invasiveness can be abolished by the IK inhibitor

TRAM-34[284]. In glioblastoma, anti-inflammatory and tumour-promoting microglia exhibit high IK channel expression. TRAM-34 administration polarises these brain-resident macrophages into pro-inflammatory anti-tumour microglia[285]. In addition, a pro-tumourigenic role of IK is also described for the regulation of natural killer cells[276]. Moreover, chronic lymphocytic leukaemia cells, which proliferate in lymphoid organs, show a high Ki-67 status associated with high IK expression. In contrast, most chronic lymphocytic leukaemia cells in the peripheral blood hold a cell cycle-arrested status and a low Ki-67 index as well as low levels of IK channel expression[245].

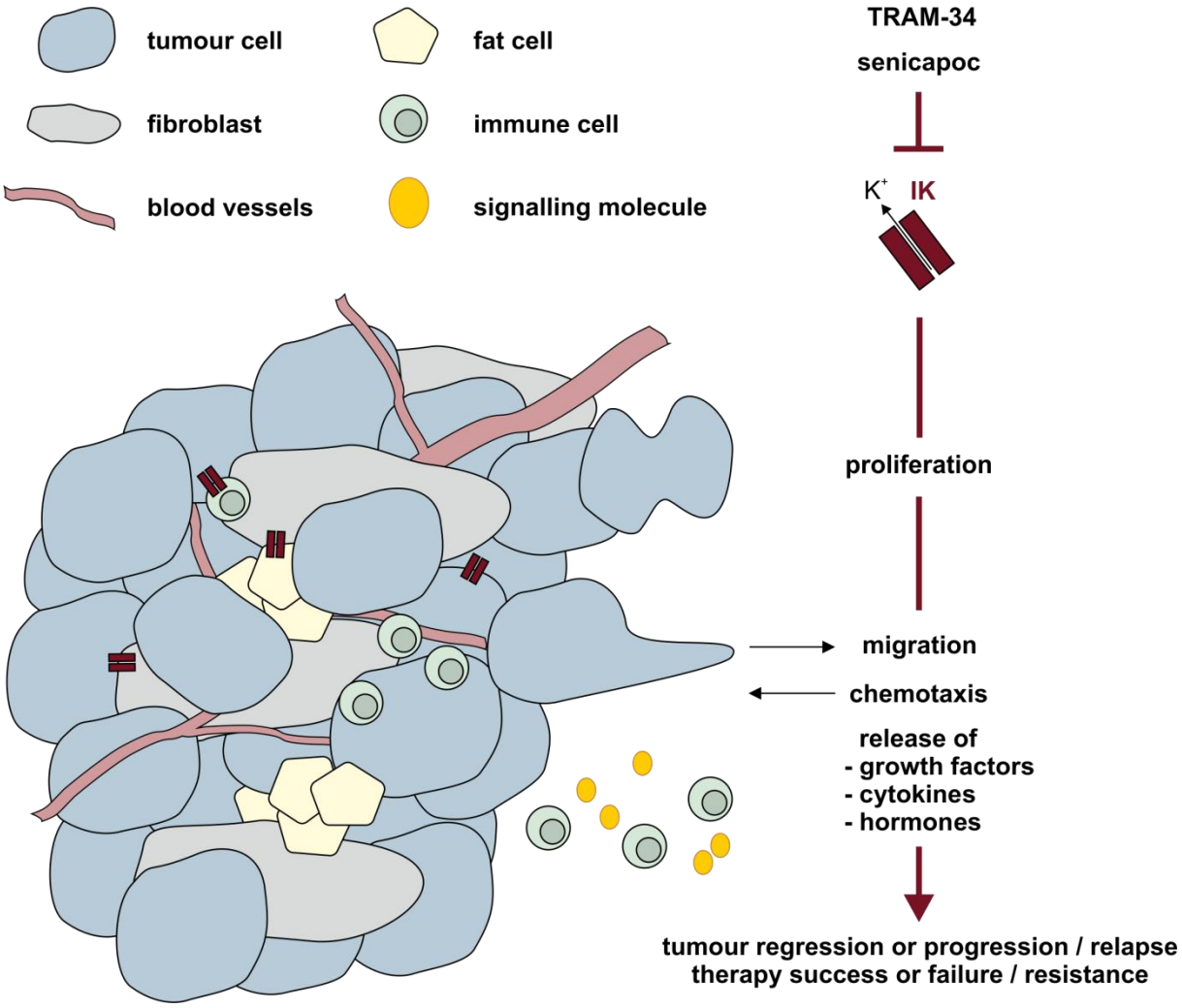

Figure 1.7: Role of the IK channel in tumour and stroma cell types
IK channel expression and activity is described for various cell types of different origin such as fibroblasts, cells from blood vessels, adipocytes and immune cells. The signalling network between IK-positive breast tumour cells and IK-positive cells contributing to the tumour microenvironment remains largely elusive. Modulation of IK channels in these different cells that constitute a tumour, for example by IK inhibition with TRAM-34 or senicapoc, may affect proliferation, migration and chemotaxis resulting in altered tumour progression and therapy response.

1.4.5 IK as modifier of radiation therapy

The response of various cancer cell lines to chemotherapeutic agents that interfere with DNA is modulated by the IK channel. In epidermoid cancer, for example, IK´s presence contributes to treatment sensitivity with the DNA crosslinking drug cisplatin. Interestingly, the observed reduction in cell viability induced by cisplatin treatment was counteracted with IK inhibition, whereas IK activation ameliorated the therapeutic effect of cisplatin. Accordingly, IK expression levels in cisplatin-resistant cancer cells are strongly decreased as compared to cisplatin-sensitive cancer cells[286]. Among other mechanisms, IK channels may contribute to cisplatin uptake as shown for colorectal cancer models[287]. Temozolomide, a DNA methylating drug, in combination with the IK inhibitor TRAM-34 exert synergistic effects in malignant glioma to reduce migration and invasion, clonogenic capability as well as proliferation while enhancing apoptotic cell death. These *in vitro* effects are confirmed in a glioma-bearing mouse model, in which in particular the combination of temozolomide plus TRAM-34, but also temozolomide or TRAM-34 alone, significantly reduces tumour volume by apoptosis[288]. Further electrophysiological studies indicate a direct interaction of temozolomide with the IK channel[289].

In addition to the DNA-interfering mode of action described for different chemotherapeutics, the primary effect of radiotherapy is the induction of DNA damage[290]. There is much evidence for IK channels to control different steps of the tumour cell response to radiotherapy. As such, IK activity is increased after irradiation in different cell lines, which is usually attributed to the IR-induced increase in $[Ca^{2+}]_i$[291,292]. ROS formation induced by irradiation reportedly provokes such $[Ca^{2+}]_i$ oscillations and thereby enhances IK channel activity[293]. Experimental irradiation of glioblastoma cells with five fractions of 2 Gy, a regimen comparable to the conventional fractionation scheme applied in glioma patients, upregulates IK mRNA expression and channel activity. In addition, repair processes after irradiation depend on energy needed for e.g. DNA decondensation. Tumour cells utilise glycolysis and thus especially consume glucose for fuelling, as first described by Otto Warburg[294,295]. In this context, K^+ efflux may provide the driving force for the uptake of glucose by tumour cells via Na^+-coupled glucose transporters[291]. In addition, IK channel inhibition disrupts the assembly of hexokinase II in the mitochondrial membrane, which is involved in glycolysis for the conversion of glucose to glucose-6-phosphate thereby contributing to ATP production[262]. As a possible consequence, TRAM-34 treatment increases residual γH2AX foci 24 h after irradiation and thus associates with a reduced DNA repair capacity of T98G glioblastoma cells[296]. Further, irradiation of these cells causes a G_2/M arrest, which relies on functional IK. In the absence of IK channels, cell cycle checkpoint dysfunction allows for entry of the cells into mitosis despite IR-provoked DNA damage and thus results in mitotic catastrophe[291]. In line, TRAM-34 treatment reduces clonogenic survival of glioblastoma cells after irradiation

with 2 Gy in a colony formation assay[296]. The radiosensitising effect after IK inhibition is also confirmed by the use of clotrimazole in U-87 MG glioblastoma cells[262].

2. Aims and objectives

Molecular classification and therapy progress have reduced mortality from breast cancer in the past decades. Due to the high breast cancer incidence in women, there is still need for new diagnostic markers, predictors and druggable targets[1]. Aberrant expression and activity of ion channels have been recognised for a range of cancer entities and different lines of evidence suggest BK and IK K^+ channels to associate with breast cancer[131,135]. Therefore, the overall goal of this work was to study endogenous BK and IK channels and their contribution to breast cancer development, disease progression as well as their utility for therapeutic interventions.

For this purpose, the spontaneous and allotransplant MMTV-PyMT$^{tg/+}$ WT, BK KO and IK KO mouse models were employed as well as *ex vivo* analyses in primary breast tumour cells derived thereof. Further, the clinical relevance of BK and IK in human breast cancer was tested by the impact of genetic variants on breast cancer development, mRNA expression status and effect on breast cancer survival together with *in vitro* proliferation experiments in human breast cancer cell lines.

With regard to the BK channel, it consists as a complex of its pore-forming α subunit together with auxiliary β and γ subunits, which are expressed in a tissue- and tumour cell-specific manner[229]. Hence, the project aimed at identifying the roles of these different BK channel subunits in breast cancer as well as their impact on the proliferative behaviour of the tumour cells. For the IK channel, such accessory subunits that modulate its pore-forming α subunit have not been identified. However, IK channel expression is high in various cell types that constitute the immune system[297]. Therefore, the potential tumour-modulatory role of IK in cells of the tumour microenvironment, in addition to breast tumour cell-specific IK channels, was of particular interest.

Finally, the putative interaction of BK and IK channels with established breast cancer therapies was studied *in vitro* and *in vivo*. BK channels may serve numerous cancer cell behaviours including the response to growth factors and anti-/hormones[207], hence breast cancer cell proliferation and tumour growth were assessed with regard to BK channel status. Based on the promising results for IK and BK as novel targets to overcome radioresistance in glioma, it is hypothesised that their status may also predict the response to radiotherapy in breast cancer cells and in breast cancer cell-derived transplant models[186,296].

3. Material

3.1 Equipment

Name	Article, Manufacturer
Analytical scales	BP 2100 S, Sartorius
	VWR-124, Sartorius
Animal scales	JOSHS MR1 (893), SSR-Produkt
Autoclave	VX-55, Systec
	VX-120, Systec
Calliper	30087-00, Fine Science Tools
Centrifuge	5415 D, Eppendorf
	5417 R, Eppendorf
	Multifuge X1R, Heraeus
Cryostat	Microm HM 560, Thermo Scientific
Electrophoresis chamber	MSMAXI, Biozym
Fluorescence microscope	BX51, Olympus
Freezer	Hera freeze, Heraeus
	Comfort, Liebherr
	FORMA 90 Series, Thermo Scientific
Freezing container	Mr. Frosty, Nalgene
Fridge	BluPerformance, Liebherr
Gel detection	BioDocAnalyze, Biometra
Heating block	Thermomixer compact, Eppendorf
Heating lamp	88258, Medisana
Heating pad	76084, TRIXIE
Histoscanner	Pannoramic Desk, 3DHISTECH
Ice machine	AF 103, Scotsman
Incubator	CB150, Binder
	APT.Line, Binder
	BBD 6220, Heraeus
Isoflurane vaporiser	19.1, Drägerwerk
Lab oven	FD 115, Binder
Linear accelerator 6 MV	SL15, Philips
Magnetic heating plate	IKAMAG RCT, IKA Labortechnik
	IKA-COMBIMAG RCT, IKA Labortechnik
Microscope	Wilovert S, Hund Wetzlar
	DM IL LED, Leica
	Axiovert 200M, Zeiss
Microwave	MW9675, Severin
Nanophotometer	P330, Implen
PCR cycler	CFX Connect, BioRad
	Mastercycler, Eppendorf
pH electrode	Blue Line, Schott
Pipettes	Research, Eppendorf

	Pipetman, Gilson
	Discovery Comfort, HTL
Pipettor	Pipetboy acu, Integra Biosciences
	Accu-jet pro, Brand
Power supply current / voltage	Standard Power Pack P25, Biometra
Tissue homogeniser	Ultra-Turrax T8, IKA Labortechnik
Security cabinet	2.12.925, Düperthal Sicherheitstechnik
	G90, Düperthal Sicherheitstechnik
Shaker	Duomax 1030, Heidolph
Sterile work bench	Herasafe, Heraeus
	Safe 2020, Thermo Scientific
Ultrapure water treatment plant	Biocel, Millipore
Vacuum pump	KNF Laborport, Neuberger
Vortexer	Vortex Genie 2, Bender & Hobein
Water bath	SW-20C, Julabo
	TW20, Julabo
xCELLigence	RTCA DP, ACEA Biosciences

3.2 Softwares and online tools

Software	Purpose of use	Manufacturer
Acrobat Reader	PDF reader	Adobe
AnalySIS 3.2	Fluorescence microscope	Olympus
Axio Vision Rel 4.8	Microscope	Zeiss
BioDocAnalyze	Gel detection	Biometra
CFX Manager	qRT-PCR	Bio-Rad
CorelDraw® Graphics Suite X8	Illustrations	Corel
GraphPad Prism 6	Statistics	GraphPad
ImageJ 1.42q	Cell counter	National Institutes of Health
Microsoft Office	Data, text	Microsoft
RTCA	xCELLigence	ACEA Biosciences
SigmaPlot 2001	Survival curve creator	Systat

Online tool	Purpose of use
BCAC	SNP data retrieval
BLAST	Sequence alignment
Ensembl	Gene information
Genevar	SNP-Protein interaction
HaploReg	SNP-Protein interaction
KM plotter	Survival plotter

NCBI	Literature search
	SNP information
Primer3	Primer design
SNAP	SNP linkage
SNiPA	SNP-Protein interaction
TCGA	mRNA expression analysis

3.3 General laboratory items and solutions

Product		Reference number	Manufacturer
Aluminium foil		2596.1	Carl Roth
Beaker glass	100 ml	2110624	Schott
Centrifuge tube	15 ml	430766	Corning
	50 ml	430291	Corning
		430897	Corning
Cryo tube	1.8 ml	368632	Thermo Scientific
DEPC-H_2O		T143	Carl Roth
dH_2O			Biocel, Millipore
Filter tip	10 µl	765288	Greiner Bio-One
	20 µl	774288	Greiner Bio-One
	200 µl	739288	Greiner Bio-One
	1,000 µl	740288	Greiner Bio-One
Glass bottle	500 ml	21801445	Schott
	2 l	21801635	Schott
PBS		14190169	Thermo Fisher
Reaction tube	0.2 ml	72.737	Sarstedt
	0.5 ml	0030124537	Eppendorf
	1.5 ml	72.706	Sarstedt
	2 ml	72.695.500	Sarstedt
Scalpel no. 21		02.001.30.021	Feather
Tip	10 µl	70.1116	Sarstedt
	200 µl	70.760.012	Sarstedt
	1,000 µl	70.762.010	Sarstedt
	2 ml	4486	Corning
	5 ml	4487	Corning
	10 ml	4488	Corning
	25 ml	4489	Corning
	50 ml	4490	Corning
Tissue wipes		05511	Carl Roth
Weighing pan	41 • 41 • 8 mm	1878.2	Carl Roth
	89 • 89 • 25 mm	1884.1	Carl Roth

Weighing paper	90 • 115 mm	MN226	Macherey-Nagel

3.4 Mouse lines and models

3.4.1 Mouse models

Mouse strain	Genetic nomenclature	Origin
FVB/N	FVB/NCrl	Charles River
MMTV-PyMT$^{tg/+}$	FVB/N-Tg(MMTV-PyVT)634Mul/J	The Jackson Laboratory
BK	Kcnma1^{tmRuth}/RuLu	Prof. Peter Ruth, University of Tübingen
IK	Kcnn4$^{tm1.1Jele}$/RuLu	Prof. Peter Ruth, University of Tübingen

3.4.2 Genotyping

Biopsy, DNA isolation and sequence amplification

Product	Reference number	Manufacturer
Ear clip pliers	73855000	Hauptner-Herberholz
Ear clips	73850100	Hauptner-Herberholz
Ear hole punch	3104605	Zoonlab
DMSO	D 8418	Sigma-Aldrich
Forceps mini straight	11200-12	Fine Science Tools
KAPA genotyping kit	07-KK5621-01	Peqlab

DNA isolation mix	
dH_2O	88 µl
1 U/µl KAPA Express Extract Enzyme	2 µl
10x KAPA Express Extract Buffer	10 µl

PCR mix	MMTV-PyMT	BK	IK
dH_2O	7.5 µl	9 µl	10.75 µl
2x KAPA2G Fast (HotStart) Genotyping Mix with dye	12.5 µl	12.5 µl	12.5 µl
Primer F1	1 µl	1 µl	0.5 µl
Primer R1	1 µl	1 µl	0.5 µl
Primer F2	1 µl	1 µl	0.5 µl
Primer R2	1 µl	-	-
DMSO	1 µl	0.5 µl	0.25 µl

Gel electrophoresis

Product	Reference number	Manufacturer
2-Log DNA Ladder	N3200S	New England Biolabs
Agarose	M3044.0500	Genaxxon
Boric acid	6943.3	Carl Roth
Bromphenol blue	15375	Serva
Ethidium bromide	E1510	Carl Roth
EDTA	8043.2	Carl Roth
Ficoll® 400	CN90.3	Carl Roth
Tris	5429.2	Carl Roth
Xylene cyanol	X4126	Sigma-Aldrich

0.5 M EDTA pH 8.0	
EDTA	186.1 g
dH_2O	add to 1,000 ml
→ pH adjustment with NaOH	

Xylene cyanol solution	
Xylene cyanol	100 mg
dH_2O	2 ml
→ ultrasound bath for 15 min	

10x TBE buffer	
Tris	108 g
Boric acid	55 g
0.5 M EDTA pH 8.0	40 ml
dH_2O	add to 1,000 ml
→ 1x TBE buffer: 1:10 dilution in dH_2O	

Bromphenol blue solution	
Bromphenol blue	110 mg
dH_2O	2 ml

6x gel loading dye	
Ficoll® 400	9 g
0.5 M EDTA pH 8.0	12 ml
10x TBE buffer	30 ml
dH_2O	add to 47 ml
Bromphenol blue solution	1.35 ml
Xylene cyanol solution	1.5 ml
→ mix ficoll® 400, EDTA, 10x TBE on a magnetic heating plate at 60°C for 1 h	
→ fill up to 47 ml with dH_2O	
→ add bromphenol blue solution and xylene cyanol solution	

Agarose gel	**2%**	**3%**
Agarose	6 g	9 g
Ethidium bromide	30 µl	30 µl
1x TBE buffer	300 ml	300 ml

2-Log DNA Ladder	
2-Log DNA Ladder	20 µl
6x gel loading dye	40 µl
dH_2O	180 µl

3.4.3 *In vivo* experiments

Instrument	Manufacturer
Cannula	Becton Dickinson
	Becton Dickinson
	Becton Dickinson
Clamp	Fine Science Tools
Forceps	Fine Science Tools
	Fine Science Tools
	Fine Science Tools
Halsted-mosquito haemostat	Fine Science Tools
Scissors	Fine Science Tools
	Fine Science Tools
Suture	Johnson & Johnson
	Johnson & Johnson
Syringe	Becton Dickinson
	Braun
Trocar	Innovative Research of America

Product	Reference number	Manufacturer
Ampuwa®	PZN 07610894	Fresenius Kabi
Bepanthen® eye and nose balm	PZN 01578681	Bayer
Capillary 1 mm diameter	612-2804	VWR
Rimadyl®	256692	Zoetis
Cotton swab	PZN 01525319	Dr. JUNGHANS
Drape sheet	2775021	Hartmann
Isoflurane	1214	CP Pharma
Ketamine	PZN 7538837	Inresa
Novaminsulfon	PZN 07387887	1A Pharma
NaCl solution	PZN 02159621	Fresenius Kabi
Octenisept®	PZN 04830483	Schülke & Mayr
0.5 mg/60 d placebo	SC-111	Innovative Research of America
0.5 mg/60 d TAM	SE-361	Innovative Research of America
5 mg/60 d placebo	SC-111	Innovative Research of America
5 mg/60 d TAM	SE-361	Innovative Research of America
0.3 ml K2E	16.444.100	Sarstedt
1.3 ml K3E	41.1395.005	Sarstedt
Xylazine	PZN 10124944	Bernburg
Petri dish	82.1473.001	Sarstedt

Anaesthesia	
Ketamine 50 mg/ml	2 ml
Xylazine 20 mg/ml	0.5 ml
NaCl solution 0.9%	7.5 ml
→ ketamine 100 mg/kg BW → xylazine 10 mg/kg BW	

Novaminsulfon solution	
Novaminsulfon (500 mg/ml)	1 ml
Ampuwa®	9 ml
→ 200 mg/kg BW	

Rimadyl solution	
Rimadyl® (50 mg/ml)	50 µl
NaCl solution 0.9%	950 µl
→ 5 mg/kg BW	

3.5 Cell culture

3.5.1 General material

Product		**Reference number**	**Manufacturer**
Cell dishes	patch-clamp	353001	Corning
	grid pattern	81166	ibidi
	55 cm²	430167	Corning
Cell flask	25 cm²	430639	Corning
	75 cm²	430641	Corning
	175 cm²	431080	Corning
Chamber slide	8-well PCA	94.6140.802	Sarstedt
	12-well glass	81201	ibidi
	8-well grid pattern	80826-G500	ibidi
Cell strainer 40 µm		431750	Corning
Collagenase D		11088866001	Roche
DMEM	+ phenol red	42430082	Thermo Fisher
	- phenol red	21063045	Thermo Fisher
DMSO Hybri-Max®		D2650	Sigma-Aldrich
Ethanol (100%)		32205	Sigma-Aldrich
Ethanol (99%)		ETO-5000-99-1	SAV Liquid Production
FCS		10270106	Thermo Fisher
Glass capillary		4522.1	Carl Roth
Haemocytometer		PDHC-N01	Merck Millipore
IMEM	+ phenol red	A1048901	Thermo Fisher
	- phenol red	A1048801	Thermo Fisher
L-15	+ phenol red	11415056	Thermo Fisher
	- phenol red	21083027	Thermo Fisher
Penicillin/streptomycin		15140122	Thermo Fisher
Sodium pyruvate		11360039	Thermo Fisher

10x trypsin	15400054	Thermo Fisher
6-well plate	353224	Corning

Collagenase medium	
Collagenase D	10 mg
IMEM + phenol red	10 ml

1x trypsin	
10x trypsin	1 ml
PBS	9 ml

Cell culture medium **Cell type**	**IMEM** **MMTV-PyMT**	**DMEM** **MCF-7**	**L-15** **MDA-MB-157, MDA-MB-453**
Medium	475 ml	500 ml	500 ml
Phenol red	+	+	+
FCS	25 ml	55 ml	55 ml
Penicillin/streptomycin	5 ml	5 ml	5 ml
100x sodium pyruvate	-	55 µl	-
→ for CCS medium, FCS is substituted with CCS			

Serum starvation medium **Cell type**	**IMEM** **MMTV-PyMT$^{tg/+}$**	**DMEM** **MCF-7**	**L-15** **MDA-MB-157, MDA-MB-453**
Medium	500 ml	500 ml	500 ml
Phenol red	-	-	-
Serum	-	-	-
Penicillin/streptomycin	5 ml	5 ml	5 ml
100x sodium pyruvate	-	55 µl	-

Cryo medium	
DMSO Hybri-Max®	20%
Cell culture medium	80%

3.5.2 Human breast cancer cell lines

Cell line	**Origin**
MCF-7	AG Prof. Dr. Brauch, IKP Stuttgart
MDA-MB-157	AG Prof. Dr. Brauch, IKP Stuttgart
MDA-MB-453	AG Prof. Dr. Brauch, IKP Stuttgart

3.5.3 *In vitro* assays

Product	**Reference number**	**Manufacturer**
Acetic acid	20104.298	VWR
dH_2O	3175.1	Carl Roth

Brilliant Blue R	B0149-25G	Sigma-Aldrich
CCS	-	AG Brauch, IKP Stuttgart
CIM plate 16	2801038	ACEA Biosciences
DharmaFECT 1	T-2001-02	Dharmacon
DharmaFECT 2	T-2002-02	Dharmacon
E2	E2758-250MG	Sigma-Aldrich
E2-BSA	E5630-5MG	Sigma-Aldrich
(Z)-endoxifen	-	AG Prof. Dr. Brauch, IKP Stuttgart
Formaldehyde 37%	104003	Merck
Fulvestrant	I4409-25MG	Sigma-Aldrich
Methanol	20847.307	VWR
(Z)-4-OH-TAM	H7904-5MG	Sigma-Aldrich
PBS tablets	003002	Thermo Fisher
Progesterone	P8783-1G	Sigma-Aldrich
5x siRNA buffer	B-002000-UB-100	Dharmacon
TAM	-	AG Prof. Dr. Brauch, IKP Stuttgart
Testosterone	T1500-1G	Sigma-Aldrich
TRAM-34	-	JProf. Dr. Pierre Koch, University of Tübingen

5 mM TRAM-34	
TRAM-34	17.242 mg
Ethanol (100%)	10 ml
→ 1 ml aliquots stored at -20°C	

PBS non-sterile	
PBS tablets	1
dH_2O	100 ml

3.7% formaldehyde	
37% formaldehyde	100 ml
PBS non-sterile	900 ml

70% ethanol	
Ethanol (99%)	700 ml
dH_2O	300 ml

0.05% Coomassie	
Acetic acid	37.5 ml
Brilliant blue R	0.25 g
Methanol	100 ml
dH_2O	362.5 ml
→ coomassie solution can be recycled for the next use	

Anti-/hormone stock	**Molecular weight**	**Stock concentration**	**Solvent**
E2	272.38 g/mol	1 mM	DMSO
E2-BSA	~ 30 mol E2/mol BSA (BSA 66,000 g/mol)	10 µM	PBS

(Z)-endoxifen	373.50 g/mol	1 mM	DMSO
Fulvestrant	606.77 g/mol	1 mM	DMSO
Progesterone	314.46 g/mol	1 mM	DMSO
(Z)-4-OHT	387.52 g/mol	1 mM	DMSO
TAM	371.52 g/mol	1 mM	DMSO
Testosterone	288.42 g/mol	1 mM	DMSO

Proliferation experiments

TRAM-34 dilution	**TRAM-34 stock**	**Ethanol (100%)**	**FCS medium**
10 µM	0.2% (5 mM)	-	99.8%
1 µM	10% (10 µM)	0.2%	89.8%
0.1 µM	10% (1 µM)	0.2%	89.8%
Ctrl	-	0.2%	99.8%

Hormone dilution	**Hormone stock**	**DMSO**		**CCS medium**
1,000 nM	0.1% (1 mM)	0.1%	E2-BSA	99.8%
		-	E2, progesterone, testosterone	99.9%
10 nM	1% (1,000 nM)	0.1%		98.9%
1 nM	10% (10 nM)	0.1%		89.9%
0.1 nM	10% (1 nM)	0.1%		89.9%
0.01 nM	10% (0.1 nM)	0.1%		89.9%
Ctrl	-	0.1%		99.9%

Anti-hormone dilution	**Anti-hormone stock**	**DMSO**	**CCS medium**
1,000 nM	0.1% (1 mM)	-	99.9%
100 nM	10% (1,000 nM)	0.1%	89.9%
10 nM	10% (100 nM)	0.1%	89.9%
1 nM	10% (10 nM)	0.1%	89.9%
Ctrl	-	0.1%	99.9%

Migration assay

TAM dilution	**TAM stock**	**DMSO**	**CCS medium**
1,000 nM	10.5 µl (1 mM)	-	add to 10.5 ml
10 nM	100 µl (1,000 nM)	10 µl	9.89 ml
Ctrl	-	10 µl	9.99 ml
→ each 25 cm² flask obtained 5 ml pre-incubation medium			

Chamber	TAM dilution	TAM stock	DMSO	CCS medium
Lower				
(160 µl 5% medium)	1,000 nM	1 µl (1 mM)	-	999 µl
	10 nM	15 µl (1,000 nM)	1.5 µl	1,483.5 µl
	ctrl	-	1.5 µl	1,498.5 µl
Upper				
(100 µl 5% medium)	2 µM	1 µl (1 mM)	-	499 µl
	20 nM	10 µl (2,000 nM)	2 µl	988 µl
	ctrl	-	2 µl	998 µl
Cell suspension				
(100 µl 0% medium)	all	-	-	100 µl/80,000 cells

Clonogenic survival experiments

TAM dilution	TAM stock	DMSO	CCS medium
100 µM	10% (1 mM)	-	90%
1 µM	1% (100 µM)	10%	89%
Ctrl	-	10%	90%
→ 50 µl of each dilution was added to 4,950 µl CCS medium in the 25 cm² flask			

TRAM-34 dilution	TRAM-34 stock	Ethanol	FCS medium
200 µM TRAM-34	4 µl (5 mM)	-	96 µl
10 µM TRAM-34	60 µl (200 µM)	-	1,140 µl
200 µM ethanol	-	4 µl (100%)	96 µl
Ctrl	-	60 µl (200 µM)	1,140 µl

γH2AX DNA damage experiments

TAM dilution	TAM stock	DMSO	CCS medium
11 µM	1.1% (1 mM)	-	98.9%
110 nM	1% (11 µM)	1.1%	97.9%
Ctrl	-	1.1%	98.9%
→ 20 µl of each dilution was added to 200 µl CCS medium in the 12-well chamber			

TRAM-34 dilution	TRAM-34 stock	Ethanol	FCS medium
200 µM TRAM-34	1 µl (5 mM)	-	24 µl
10 µM TRAM-34	15 µl (200 µM)	-	285 µl
200 µM ethanol	-	1 µl (100%)	24 µl
Ctrl	-	15 µl (200 µM)	285 µl

siRNA experiments

1x siRNA buffer	
5x siRNA buffer	20%
DEPC-H_2O	80%

20 µM siRNA stock	
1x siRNA buffer	250 µl
siRNA pellet	5 nmol
→ storage of 10 - 20 µl aliquots at -20°C	

3.6 RNA studies

Product	**Reference number**	**Manufacturer**
Chloroform	372978	Sigma-Aldrich
DNAse I recombinant	04716728001	Roche
Ethanol (100%)	32205	Sigma-Aldrich
iScript cDNA synthesis mix	1708891	Bio-Rad
Isopropanol	6752.3	Carl Roth
Low molecular weight DNA ladder	N3233S	New England Biolabs
Low Multiwell 96-well plate	MLL9601	Bio-Rad
Microseal 'B' adhesive seals	MSB1001	Bio-Rad
NucleoSpin® RNA isolation kit	740955.250	MACHEREY-NAGEL
peqGOLD RNA pure	30-1010-88	VWR
SsoAdvanced™ Universal SYBR® Green Supermix (2x)	1725274	Bio-Rad

RNA isolation 75% ethanol	
Ethanol 100%	75%
DEPC-H_2O	25%

cDNA synthesis mix	**+RT**	**-RT**
5x iScript	4 µl	4 µl
Reverse transcriptase	1 µl	-
DEPC-H_2O	10 µl	11 µl
RNA	5 µl	5 µl
→ DEPC-H_2O was replaced by RNA in siRNA experiments to employ 15 µl of RNA		

Primer	**DEPC-H_2O addition**	**Concentration**
Stock	according to manufacturer	100 pmol/µl
Dilution	98%	2 pmol/µl

qPCR mastermix	
SsoAdvanced™ Universal SYBR® Green Supermix (2x)	7.5 µl
Primers (2 pmol/µl)	2.25 µl
cDNA	3 µl

3.7 Histology

Product	Reference number	Manufacturer
ABC-AP kit	AK 5000	Vector laboratories
Ammonia solution (32%)	P093.2	Carl Roth
AP substrate	10279	Vector laboratories
Aquatex mounting medium	363123S	VWR
Blades for cryostat use	MX35	Thermo Scientific
Bouin´s solution (0.5%)	HT10132-1L	Sigma-Aldrich
Bovine serum albumin	8076.2	Carl Roth
Cover slip	LH26.1	Carl Roth
DePeX mounting medium	361254D	VWR
Ethanol (100%)	K928.4	Carl Roth
Eosin-G solution	X883.1	Carl Roth
Forceps	07.60.04	Medicon
	11009-13	Fine Science Tools
Glycine	3908.3	Carl Roth
Haematoxylin solution	X903.2	Carl Roth
Hydrogen peroxide (30%)	8070.4	Carl Roth
Hydrophobic barrier pen	H-4000	Vector Laboratories
Levamisole	SP-500	Vector Laboratories
L-Lysine x 1 H_2O	420751	Carl Roth
Nail varnish	01	Absolute pure, Essence
Neg-50™	6506	Thermo Fisher
Normal donkey serum	017-000-121	Dianova
Normal goat serum	S-1000	Linaris
Paraformaldehyde (PFA)	0335.2	Carl Roth
D-saccharose	4621.2	Carl Roth
Slides Superfrost	J1800AMNZ	Menzel
Staining system	TX88.1	Carl Roth
Toluene	7115.1	Carl Roth
Tris	5429.2	Carl Roth
TritonX100	3051.2	Carl Roth
Tween® 20	9127.1	Carl Roth
Vectashield	H-1200	Vector Laboratories

Immunoglobulins	Reference number	Manufacturer
AlexaFluor® 488 anti-CD45	103121	BioLegend
AlexaFluor® 488 rat IgG2bκ	400625	BioLegend
Alexa Fluor® 555 donkey anti-rabbit	A31572	Thermo Fisher
Alexa Fluor® 555 goat anti-mouse	A21127	Thermo Fisher
Biotinylated goat anti-rabbit	BA-1000	LINARIS
Anti-γH2AX (Ser139)	613402	BioLegend
Anti-ER-α (MC-20)	sc-542	Santa Cruz Biotechnology
Anti-Ki-67 (D3B5)	9129S	Cell Signaling Technology
Normal mouse IgG	NI03-100UG	Merck
Normal rabbit IgG	NI01-100UG	Merck

4% PFA	
PFA	20 g
PBS	500 ml
→ add PFA to PBS in a bottle together with a stirrer and solve at 60°C on a magnetic heating plate	
→ 2% PFA: 1:1 dilution of 4% PFA and PBS	

Sucrose solution	**D-saccharose / PBS**
5%	0.5 g/10 ml
10%	1 g/10 ml
20%	2 g/10 ml

Normal donkey serum (NDS)	
NDS	lyophilisate
dH_2O	10 ml
Final concentration	60 mg/ml = 100% serum
→ add dH_2O to NDS, 1 ml aliquots stored at -20°C	

0.3% TritonX100	
TritonX100	1.5 ml
PBS	add to 500 ml
→ storage at 4°C	
→ 0.1% TritonX100: 1:3 dilution of 0.3% TritonX100 in PBS	

Tissue blocking solution	
BSA	1 g
Glycine	0.2 g
Lysine	0.2 g
0.3% TritonX100 in PBS	add to 100 ml

→ 10 ml aliquots stored at -20°C
→ addition of NDS or NGS to final concentration of 10% blocking solution before use

100 mM Tris-HCl	
Tris	12.114 g
dH_2O	add to 1,000 ml
0.1% Tween® 20	
→ solve Tris in water	
→ adjust pH to 8.2 with HCl	
→ add Tween® 20	

1% H_2O_2	
30% H_2O_2	333 µl
PBS	10 ml

10% cell blocking solution	
NDS / NGS	10%
PBS	90%

0.001% Tween® 20	
Tween® 20	5 µl
PBS	500 ml
→ storage at 4°C	

ABC reagent	
Reagent A	1 drop
Reagent B	1 drop
PBS	5 ml

AP substrate	
Reagent 1	2 drops
Reagent 2	2 drops
Reagent 3	2 drops
Levamisole	2 drops
100 mM Tris-HCl	5 ml

4. Methods

4.1 Animal work

4.1.1 Mouse strains

FVB

The Friend leukaemia Virus B-susceptible (FVB/N) mouse strain was established at the National Institute of Health (United States of America) as an outbred colony of Swiss mice in 1933. It represents a widely-used mouse strain for transgenic analyses due to a high biological reproducibility, large litter sizes as well as prominent pronuclei detectable in fertilized eggs. Its proneness to cancer per se is emphasised by its terminology, but also according to chemically-induced skin tumours, mammary hyperplasia and tumours in different organs and especially the lungs[298-300]. In addition, FVB/N mice are known for their aggressive behaviour and their abnormal circadian rhythm with increased activity during the light cycle[301].

MMTV-PyMT$^{tg/+}$

For spontaneous breast tumour development, the MMTV-PyMT$^{tg/+}$ mouse model was studied. In this model, expression of the middle T antigen from polyomavirus (PyMT) is under the control of the mouse mammary tumour virus (MMTV) long terminal repeat[302]. MMTV itself is a weak oncogenic retrovirus to cause especially breast tumours in mice when transmitted by lactation through an infected mother. The use of MMTV to induce mammary tumours is thus limited. Its oncogenic function derives from insertional mutagenesis or transcription activation of oncogenes in close vicinity and includes the activation of developmental signalling pathways such as Wnt[303-305]. Activation of the MMTV promoter relies on steroid hormone binding to the hormone response element region found in the long terminal repeat[306-308]. Yet, it is not fully elucidated whether MMTV is able to induce breast cancer in humans[309]. The murine polyomavirus can stimulate carcinogenesis in different cell types thereby leading to the formation of a variety of tumours. Polyomavirus replication and infection is suggested to depend on cell proliferation, as mammary gland, skin and bone are majorly prone in adult mice. Three oncoproteins with big, middle and small size, respectively, were initially extracted from tumour-bearing animals. All three promote virus replication and cellular transformation with middle T antigen representing the most important contributor to tumourigenesis. It interacts with different signalling pathways such as mitogen-activated protein kinase and phosphatidylinositol 3-kinase[310,311]. MMTV-PyMT$^{tg/+}$ malignancy is characterised by ER and PR expression in early stages and a decline or absence towards late carcinoma. In contrast, HER2 expression together with the cyclin D1 cell cycle marker

increases with disease progression[312]. MMTV-PyMT$^{tg/+}$ tumour latency is strain-specific with an aggressive mode in FVB/N mice showing an early tumour onset at approximately 53 d of age[302,313,314]. In this work, MMTV-PyMT$^{tg/+}$ mice with the respective BK or IK KO, as described below, were assessed in comparison to litter-matched MMTV-PyMT$^{tg/+}$ mice with WT status for BK and IK.

BK KO

Mice lacking the pore exon that also encodes a part of the S6 of BK-α subunit (BK KO) were available from earlier studies[315]. Both, a model for constitutive (L1) as well as a Cre recombinase-mediated conditional (L2) BK KO were initially established on a hybrid 129/Sv x C57Bl/6 background[316]. Through repeated mating, backcrossing of the BK L2 allele on FVB/N background was achieved within this work (supplement 9.1).

IK KO

A constitutive IK KO mouse strain was generated previously. IK KO mice were bred and maintained on the hybrid 129/Sv x C57Bl/6 background[317] and backcrossed to the FVB/N background to generate a breast cancer-pone model utilising the MMTV-PyMT$^{tg/+}$ mouse strain[315].

4.1.2 Animal housing and breeding

All animal experiments were approved by the local Ethics Committee for Animal Research at the Regierungspräsidium Tübingen. The mice were kept in an open specific-pathogen-free animal house with a 12 h light/dark cycle and access to water and food *ad libitum*. Mice were housed, depending on their weight, in groups of 2 - 3 animals in makrolon type II cages or up to 8 animals in makrolon type III cages. For backcrossing the BK L2 allele-carrying mouse strain to the FVB/N background, one female was kept in a makrolon type II cage together with one male, which was removed before the delivery of pubs after approximately 21 d of pregnancy. For all other breeding schemes, two females were kept in a cage together with one male. The male mouse was either permanently kept in the breeding cage or it was removed before the delivery of pubs in order to avoid immediate further breeding. In general, mice selected for breeding were at least four weeks (females) and up to one year (males) old. Pubs were separated from their mothers according to gender at an age of 21 d.

4.1.3 Mouse labelling and genotyping

Identification of the BK L2 allele during backcrossing occurred through ear clipping whereas all other mice were marked according to a common ear punch scheme (figure 4.1). For the latter, each mouse got up to three punches including one round punch serving as biopsy for genotyping. Other punches were half-round in order to limit the trauma area. Biopsy tissue from ear-clipped mice was obtained from approximately 1 mm of tail that was cut with scissors. The biopsies were collected in 1.5 ml tubes and stored at 4°C overnight or at -20°C for several days.

Genotyping of all biopsies was carried out with the KAPA genotyping kit. For DNA isolation, a mastermix was prepared with 2 µl of 1 U/µl KAPA express extract enzyme, 10 µl 10x KAPA express extract buffer and 88 µl dH_2O per sample. The tissues were lysed on a thermomixer at 75°C and 500 rounds per minute (rpm) for 10 min. Afterwards, the KAPA express extract enzyme was heat-inactivated at 95°C and 500 rpm for 5 min. In the next step, DNA was amplified by preparation of a mastermix (section 3.4.2 and supplement 9.1) with the KAPA2G fast genotyping mix containing DNA polymerase, deoxyribose nucleoside triphosphates (dNTPs), $MgCl_2$, buffer, stabilisers and two inert dyes that served for loading in the subsequent gel electrophoresis. At 94°C, the DNA polymerase was heat-activated (hot start) for 3 min. Then, 30 amplification cycles were run each starting with 94°C for 30 s to separate the DNA in single strands. Annealing temperature for MMTV-PyMT$^{tg/+}$ genotyping was 64°C for 30 s, for BK genotyping 54°C for 30 s, and for IK genotyping 58°C for 15 s. Elongation took place at 72°C carried out for 30 s in MMTV-PyMT$^{tg/+}$ and BK samples and for 15 s in IK samples. After termination of the last cycle, elongation was prolonged for another 5 min at 72°C before the peltier element of the thermocycler cooled down to a holding temperature of 10°C.

By the use of gel electrophoresis, the amplified DNA sequences were separated according to their size. For the preparation of a 2% agarose gel, 6 g agarose and 300 ml TBE buffer were heated in a 500 ml glass bottle in the microwave until the agarose was completely solved. The gel was cooled down on a magnetic heating plate with a stirrer before 30 µl ethidium bromide was added. The gel was poured in a gel chamber prepared with combs and further cooled down until it was solid. The combs were removed and 12 µl 2-Log DNA ladder in loading dye or 25 µl per sample were loaded into the wells. The DNA was run on the gel at 80 mV for approximately 15 min until the samples were completely moved out of the wells. Then, the gel was run at 120 mV for about 1 h. Finally, the gel was placed under ultraviolet light to detect the DNA bands. In comparison with the known band sizes of the 2-Log DNA ladder, bands of expected base pair (bp) length could be confirmed in the samples and thus mouse genotype was determined: 556 bp and 200 bp for PyMT$^{tg/+}$, BK L1,

WT and L2 showed 132, 466 and 577 bp, respectively, whereas IK WT and L1 presented with 264 and 507 bp (figure 4.1).

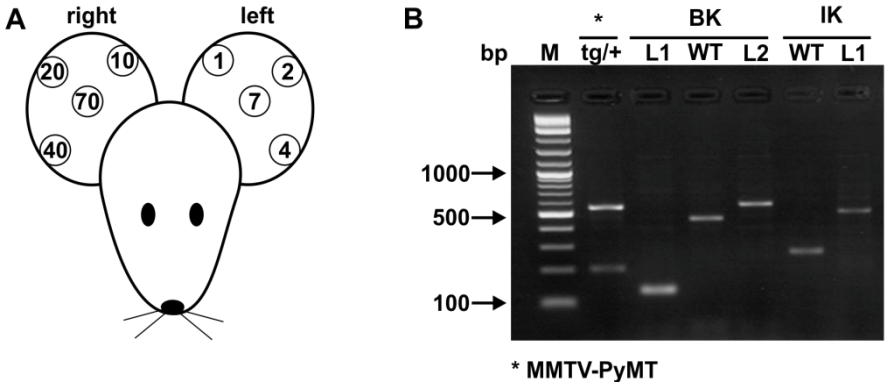

Figure 4.1: Ear punch scheme and a representative result of the genotyping assay
Biopsies for genotyping were obtained from ear, except for the BK L2 backcrossing where pubs were identified by ear clips in combination with tail tip biopsy. **(A)** The ear hole punch was used to mark each mouse with up to three punches. The first punch served as genotyping material, whereas following punches were made at the edges of the mouse ear to avoid additional trauma area. Accordingly, mice were identified with numbers between 1 and 100. **(B)** After DNA isolation and amplification, gel electrophoresis was run for genotyping. The different primer pairs used for genotyping (supplement 9.1) allowed amplification of gene-specific sequences. These sequences were separated via gel electrophoresis and the bands appearing allowed determining the genotype of the according mouse. The size of the respective bands were 556 bp and 200 bp for PyMT$^{tg/+}$; 132, 466 and 577 bp for BK L1, WT and BK L2; 264 and 507 bp for IK WT and L1. Negative controls for the PCR-based genotyping did not show bands (data not shown).

4.1.4 Spontaneous tumour development in MMTV-PyMT$^{tg/+}$ WT, BK KO and IK KO mice

Male MMTV-PyMT$^{tg/+}$ mice were imported from The Jackson Laboratory and were mated with female BK$^{L1/+}$ or IK$^{L1/+}$ ($K_{Ca}^{L1/+}$) mice. Male offspring with the MMTV-PyMT$^{tg/+}$ $K_{Ca}^{L1/+}$ genotype were again mated with female $K_{Ca}^{L1/+}$ mice to generate offspring used for experimental purposes (figure 4.2). Mice with IK KO or MMTV-PyMT$^{tg/+}$ genotype were born at the expected Mendelian ratio of 1:4. However, BK KO mice were born at a ratio of 1:7, which emphasises the importance of the BK channel in early developmental processes. BK- or IK-deficient tumour-developing female mice were utilised for experiments in comparison to the respective WT littermates (MMTV-PyMT$^{tg/+}$ $K_{Ca}^{+/+}$). Palpation of the breasts for potential tumour development started at an age of 6 weeks and was conducted once a week. Once established, tumour growth was monitored with a digital calliper until 15 mm diameter and BW was observed with animal scales twice a week.

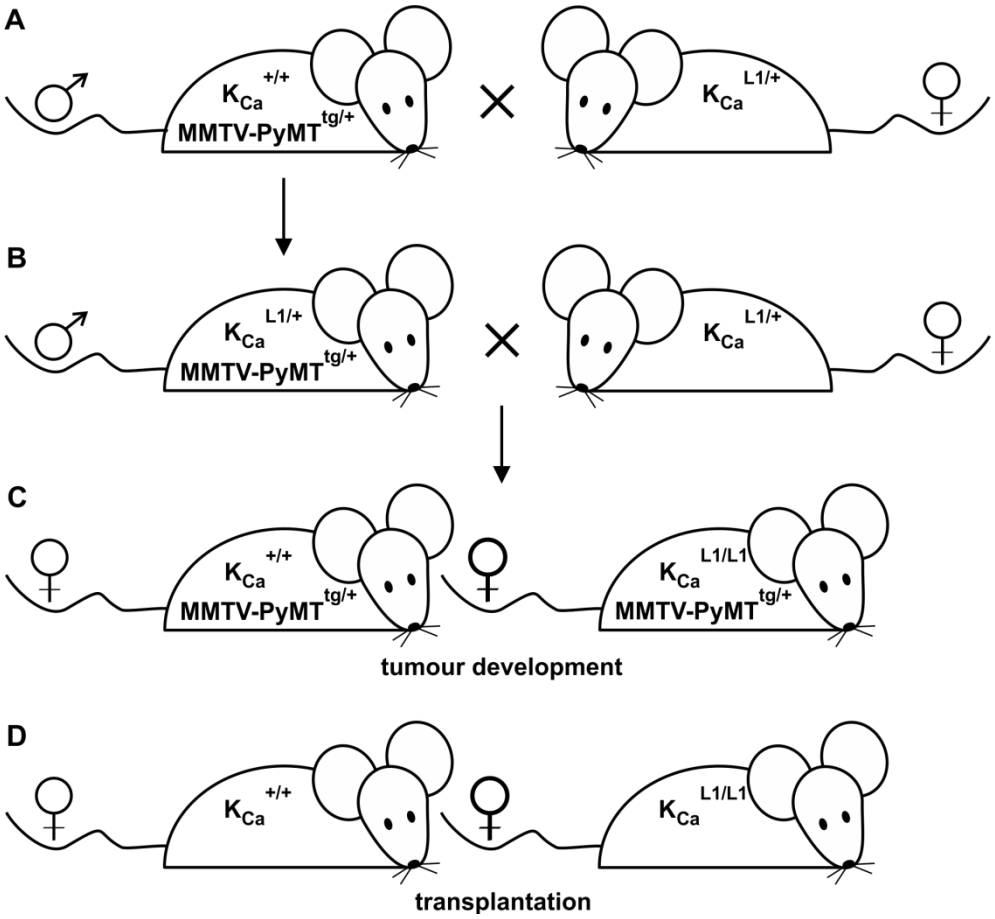

Figure 4.2: Breeding scheme of MMTV-PyMT$^{tg/+}$ WT and K_{Ca} KO mice
(A) Male MMTV-PyMT$^{tg/+}$ mice were mated with $K_{Ca}^{L1/+}$ female mice. **(B)** These crossings produced male offspring carrying MMTV-PyMT$^{tg/+}$ x $K_{Ca}^{L1/+}$, which were mated again with $K_{Ca}^{L1/+}$ females. **(C+D)** Female MMTV-PyMT$^{tg/+}$ x $K_{Ca}^{+/+}$ and MMTV-PyMT$^{tg/+}$ x $K_{Ca}^{L1/L1}$ offspring were used for subsequent analyses, **(C)** i.e. spontaneous tumour development. Tumour cell cultures derived from these spontaneous tumour-developing MMTV-PyMT$^{tg/+}$ mice of the various genotypes were characterised *in vitro* (see 4.2) and used for **(D)** allotransplantations in $K_{Ca}^{+/+}$ or $K_{Ca}^{L1/L1}$ mice.

4.1.5 Allotransplantation of MMTV-PyMT$^{tg/+}$ WT, BK KO and IK KO cells

An orthotopic allotransplant model was established for investigating the growth of MMTV-PyMT$^{tg/+}$ WT, BK KO and IK KO cells in female FVB/N recipients. In order to investigate a putative environmental influence on tumour development and growth in the BK KO or IK KO model, these mice were transplanted with MMTV-PyMT$^{tg/+}$ WT cells. In general, recipient mice were 12 week old at the time point of tumour cell inoculation. For endocrine (section 4.1.6) and radiation (section 4.1.7) therapy, FVB/N mice were purchased from Charles River Laboratories at an age of 11 weeks to allow for a one week recovery from their travel before the start of surgical interventions.

MMTV-PyMT$^{tg/+}$ WT, BK KO or IK KO cells were inoculated in the fourth right mammary gland. The tumour cells were obtained from the spontaneous tumour-developing

MMTV-PyMT$^{tg/+}$ WT, BK KO or IK KO mice and were maintained in culture for 6 to 12 passages before transplantation, as described in section 4.2.2. Cells were detached from the bottom of 75 cm² cell flasks with trypsin. A solution of 10^6 cells in 50 µl PBS was prepared in 1.8 ml cryo tubes. For tumour cell transplantations, each mouse was anaesthetised with 100 µg/g BW of ketamine and 10 µg/g BW of xylazine by intraperitoneal (i.p.) injection using a 27G cannula. Then, recipient mice were placed on the back at a heating pad and treated with bepanthen® eye and noise balm for prohibition of eye drying during surgery. After disinfection with 70% ethanol, the fur between the fourth mammary gland and the ventral midline was carefully removed with a scalpel. Afterwards, the mouse was covered with a drape sheet leaving out the operation area. An approximate 10 mm caudocranial cut between the nipple and the ventral midline permitted access to the transplantation site. The mammary fat pad was gently lifted up and fixed with a halsted-mosquito haemostat. The cell suspension was pipetted up and down three times using a 200 µl pipette and then taken up in a 1 ml syringe attached to a 30G cannula. 10^6 cells were injected as 50 µl suspension in PBS into the fat pad of the 4th mammary gland. Finally, the mammary fat pad was retracted and the wound was closed with a 6-0 suture in three stiches and disinfected with octenisept®. For post-operative pain relief, the mouse obtained a subcutaneous (s.c.) injection with 200 µg/g BW of novaminsulfon and was set back in the cage warmed with a heating lamp for the first 2 h after surgery. Palpation of tumour development and measurement of tumour size with a digital calliper started one week after surgery and was conducted three times a week. In order to assess the role of BK and IK in breast cancer cells for tumour formation and growth *in vivo*, MMTV-PyMT$^{tg/+}$ WT, BK KO and IK KO mice were monitored until tumours were grown to a size of 15 mm diameter.

4.1.6 Ovariectomy and TAM pellet implantation

To test for the influence of BK channels in endocrine therapy, tumour progression in response to TAM was investigated. For this purpose, MMTV-PyMT$^{tg/+}$ WT or BK KO cells were orthotopically transplanted in FVB/N mice, as described in section 4.1.5, and grown to a volume of approximately 62.5 mm³. Then, the ovaries were removed to avoided disturbances by natural menstrual cycle-induced changes of endogenous E2 levels. This allowed standardised experimental conditions and was of further clinical relevance due to the post-menopausal state of the majority of breast cancer patients. One week after ovariectomy, a TAM or placebo pellet was implanted. TAM therapy lasted for the maximum pellet release time of 60 d or until abortion criteria were reached (table 4.1). In a first set of experiments, 0.5 and 5 mg per 60 d releasing TAM pellets were used in order to get an impression of the blood accumulation of TAM and its major metabolites in the murine organism. These mice

were not allotransplanted with tumour cells, but blood was collected at the 7, 14 and 21 d time points after pellet implantation.

For ovariectomy, mice were anaesthetised with a 0.9% NaCl solution containing 100 µg/g BW ketamine and 10 µg/g BW xylazine by i.p. injection with a 27G cannula. Bepanthen® eye balm was applied on the open eyes. For post-operative pain management, 5 mg/kg BW rimadyl® in 0.9% NaCl solution was administered by s.c. injection. The operation area was disinfected with 70% ethanol and a scalpel was used to shave a 1.5 cm^2 area at the central back. Then, the operation area was disinfected with octenisept® and a drape sheet covered the mouse except for the operation area. The skin was gently stretched with forceps and a cut of approximately 10 mm was made with scissors along the dorsal midline and separated from the underlying peritoneum by dull preparation. Each 5 mm laterally of the midline, another cut was gently made to access the abdomen and each respective ovary via the dorsal route. Carefully, the ovary-enveloping fat tissue was lifted with forceps. The ovary was identified and ligated from the uterus with a 7-0 silk suture. Then, the ovary including the associated fat tissue was cut and removed before the uterus was put back into the abdomen. The skin was closed with a 6-0 suture in three stiches and disinfected with octenisept®. Another 5 mg/kg BW rimadyl® in 0.9% NaCl solution was administered by s.c. injection. Post-operatively, the mouse was warmed with a heating lamp during the first 2 h post operation. On the day after surgery, the mouse received another 5 mg/kg BW rimadyl® in 0.9% NaCl solution by s.c. injection for pain relief [318].

To study the response of the BK-negative or -positive tumours to TAM therapy, a 3 mm-sized TAM or placebo pellet was used. It continuously released the active substance over a time period of 60 d and thereby avoided stress by otherwise repeated handling of the animal. The right lateral side of the neck was chosen as implantation site due to maximum space availability between skin and muscle. For pellet implantation, the mouse was anaesthetised as described previously. The skin was lifted and a trocar was used to insert the pellet approximately 2 cm apart via a small puncture. A 6-0 suture closed the skin in two stiches. In the end, the area was disinfected with octenisept®. Blood collection for measurement of TAM and metabolite levels was conducted with alternating collections from the right and left eyes 7, 14 and 21 d after pellet implantation. For this purpose, the mouse was shortly anaesthetised with isoflurane. Jugular veins were stowed by gripping the neck of the animal with one hand. With a carefully rotating move, a capillary was gently pressed against the retrobulbary vein plexus with the other hand. At each time point, approximately 100 µl blood was collected with a pipette using a 200 µl filter tip and transferred in a microvette. The blood volume withdrawn was substituted with isotonic NaCl solution previously warmed to body temperature. The microvette was centrifuged at 2,000 rcf for 5 min. Plasma was collected in

0.5 ml tubes and stored at -20°C until analysed in cooperation with Dr. Thomas Mürdter (AG Prof. Dr. Brauch, IKP Stuttgart) via HPLC. Levels of TAM and its main metabolites were measured in comparison to a patient standard, which determined the lower level of quantification.

For growth experiments of MMTV-PyMT$^{tg/+}$ WT and BK KO tumours under TAM therapy, the selected endpoint was an eightfold-increased tumour volume as compared to the size of the tumour on the day of pellet implantation.

4.1.7 Fractionated radiotherapy of MMTV-PyMT$^{tg/+}$ WT or IK KO tumours *in vivo*

MMTV-PyMT$^{tg/+}$ WT or IK KO cell-transplanted mice (section 4.1.5) were subjected to a radiotherapy regime starting at a tumour volume of approximately 62.5 mm^3. The aim of this approach was to assess potential BK- and IK-dependent effects on radiation dose-dependent tumour regression and regrowth after radiotherapy. Tumour growth was monitored until the tumour reached an eightfold higher tumour volume, which is equivalent to duplication of diameter, compared to the first day of irradiation. Irradiation occurred under isoflurane anaesthesia, as shown in figure 4.3. For this purpose, a 2.5% isoflurane-oxygen mixture was introduced in a transparent plastic box, in which the mice were put beforehand. Once the mice were anaesthetised, the inhalative anaesthesia was connected to the irradiation desk and the mice were moved to the irradiation device with the nose of each mouse directed to the isoflurane opening. The irradiation device had space to irradiate up to ten mice at once; irradiation groups in this work comprised 1 to 5 mice per procedure. The tumour was gently pulled aside and fixed with a plastic strap. The system was closed with a clear plastic upper shell and the isoflurane / oxygen mixture was reduced to 0.8%. In order to irradiate the tumour only, a lead block shielded the body of each mouse. In addition, a lead satellite with spare holes for the location of the tumour protected the animals during radiotherapy. Proper height and localisation of the mice for delivery of irradiation was checked with the help of a laser beam. The whole procedure took about 5 min. 0 Gy control tumour-carrying mice were also put under anaesthesia, but received no irradiation. Radiation of the tumours was carried out with a 6 MV photon linear accelerator[319,320]. The procedure was repeated daily for in total five consecutive days. In the weeks following irradiation, BW was observed twice a week and the tumour volume was measured three times a week until an eightfold increased tumour volume, according to the tumour volume at the start of radiotherapy, or other abortion criteria were reached.

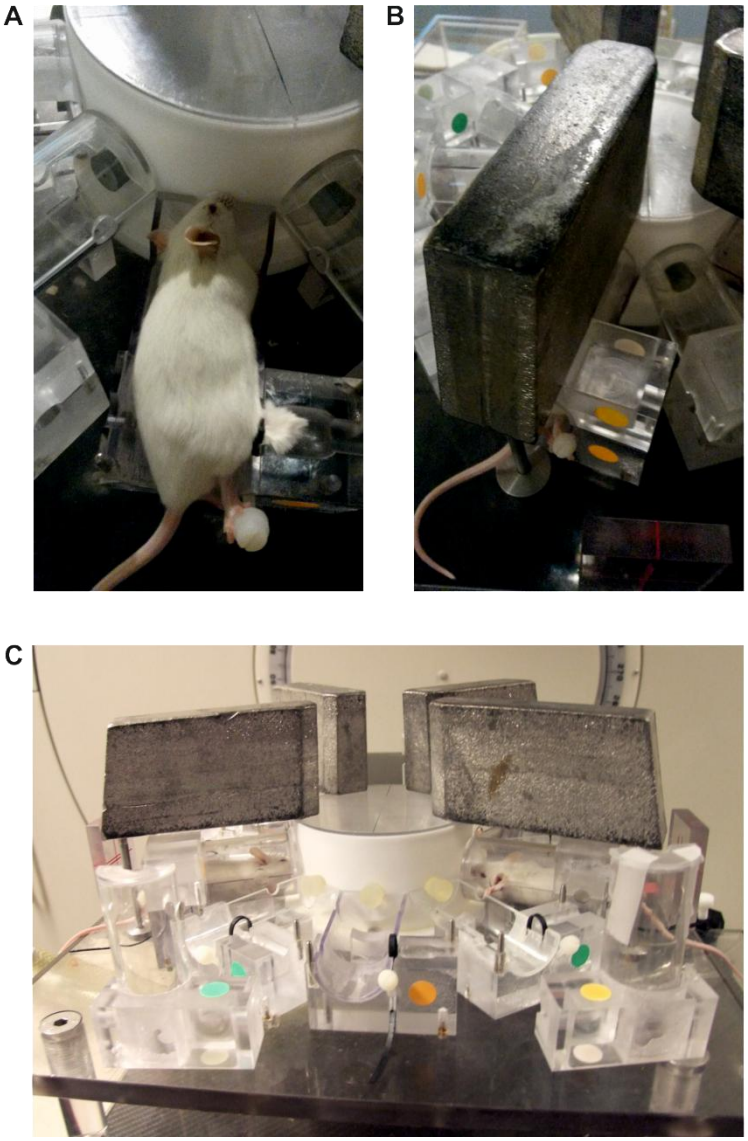

Figure 4.3: Radiation therapy setup and regime of mice with MMTV-PyMT$^{tg/+}$ WT and IK KO tumours
Mice received radiotherapy at a target tumour volume of 62.5 mm³. Irradiation was applied for five consecutive days at different dosage, which occurred under isoflurane anaesthesia. **(A + B)** For the delivery of IR, anaesthetised mice were placed in the mouse irradiation device and shielded with lead blocks. **(C)** The irradiation device was located under the linear accelerator containing an additional lead satellite with spare holes (not shown) for IR delivery.

4.1.8 Health monitoring, scarification and organ isolation

Tumour size measured in two dimensions with a digital calliper was translated into tumour volume with the following formula: (length • width²) / 2. For the various tumour models and treatment groups, different end points were set, as described in sections 4.1.4 - 4.1.7, respectively. Besides, general abortion criteria included in the score sheet (table 4.1) served for keeping mice in good general conditions during the experiments. If a mouse scored 8 or

more in sum, it had to be sacrificed. For this purpose, mice were weighed twice a week and regularly checked for their health condition.

Table 4.1: Abortion criteria for *in vivo* experiments
Experiments with tumour-bearing mice of both spontaneous and orthotopic transplant models were carried out with respect to the below-listed abortion criteria. Tumour size and appearance as well as shape, weight, behaviour, movement and respiration of each mouse were regularly controlled according to the score sheet.

Parameter	Measure	Score
Tumour size	≥ 13.5 mm diameter	4
	≥ 15 mm diameter	8
	≥ 1,350 mm^3	4
	≥ 1,650 mm^3	8
Tumour appearance	not ulcerated	0
	reddish	1
	subsided, almost ulcerated	4
	ulcerated / bloody	8
Animal shape	normal	0
	ruffled fur	2
	curved position	2
	emaciated, pale, subsided flanks	3
Animal weight*	decline of 5%	2
	decline of 10%	4
	decline of 15%	8
Animal behaviour	normal	0
	indifferent, isolated	2
	apathetic	4
	automutilation	8
Animal movement	normal	0
	careful, no climbing	2
	insecure	4
Animal respiration	increased frequency	2

* according to weight at experimental start and compared to weight of age-, gender- and strain-matched mice

For sacrification, CO_2 was added slowly to the cage of the animal until unconsciousness was followed by death of the mouse. This was verified by termination of breathing as well as eye lid and limb reflexes. Neck fracture was induced through pressure on the neck of the mouse and simultaneous tail stretching.

The sacrificed mouse was fixed on the back and the abdomen was opened with forceps and scissors. The following organs were collected from 3 months old FVB/N mice as mRNA and protein controls: Full brain, cerebellum, kidney, liver, ovary, testis, thymus, spleen and uterus. Tumour pieces from spontaneous tumour-bearing MMTV-$PyMT^{tg/+}$ WT, BK KO and IK KO mice were either stored at -80°C for mRNA or protein extractions or were fixed in 10 ml 4% PFA in PBS in a 15 ml centrifuge tube for subsequent analysis by

immunohistochemistry. Another tumour piece was used for the establishment of a primary tumour cell culture (section 4.2.1). From MMTV-PyMT$^{tg/+}$ WT, BK KO and IK KO tumour cell-transplanted mice, harvested tumours were used as RNA samples and for immunohistochemistry. In addition, metastasis was studied in the lungs, as this represents a frequent site of metastases in the MMTV-PyMT$^{tg/+}$ model. For this purpose, the right lung was incubated in Bouin´s solution for 3 d before the number of macroscopically visible metastases was counted. The left lung was fixed in 10 ml of 4% PFA in PBS in a 15 ml centrifuge tube for the detection of micrometastases by haematoxylin/eosin staining. Blood was collected by cardiac puncture with a 20G syringe after thorax opening with scissors. The blood was collected with a pipette, centrifuged for 10 min at 2,000 rcf, and stored at -80°C. For determination of TAM accumulation in the first 3 weeks after pellet implantation, blood was collected weekly (section 4.1.6). In addition, the uterus was extracted from all ± TAM pellet-implanted mice and weighed in order to assess the amount of endometrial hyperplasia, a well-known endocrine side effect of TAM.

4.2 Cell culture

4.2.1 Establishment of MMTV-PyMT$^{tg/+}$-derived primary cell cultures

Tumour pieces from MMTV-PyMT$^{tg/+}$ WT, BK KO and IK KO mice were used for the establishment of primary cell cultures. After isolation of the whole tumour and extraction of a large tumour piece, the latter was kept in a 50 ml tube filled with 10 ml cell culture medium. In the sterile hood, tumour and cell culture medium were transferred in a 55 cm² cell dish. Forceps and a scalpel were used to mince the tumour piece. The resulting smaller tumour pieces were transferred in a 15 ml tube containing 10 mg collagenase D in 10 ml IMEM. Digestion with collagenase took place in a 37°C water bath for 11 min with the tube inverted once every min. Then, tumour pieces were mechanically separated by pipetting up and down with a 10 ml first and then a 5 ml pipette each for several times. The tumour cell suspension and remaining tumour pieces were filtered through a 40 µm mesh size nylon cell strainer. The flow-through was centrifuged at 1,000 rpm for 5 min. After careful removal of the supernatant with a 10 ml pipette, the pellet was loosened by rubbing several times against the grids of the sterile hood. A 55 cm² cell dish was filled with 10 ml cell culture medium from which 1 ml was taken three times to resuspend the tumour cells and to transfer them in a 55 cm² cell dish. Tumour pieces remaining after collagenase digestion underwent a second collagenase digestion and were seeded in another 55 cm² cell dish after filtration and centrifugation. Tumour pieces that still remained after the procedure were used as explant culture in 10 ml cell culture medium in a 55 cm² cell dish. Medium was changed the following day before media changes started twice a week.

4.2.2 Cultivation and passage of tumour cells

Cell culture work was conducted in a sterile hood. Media, PBS and trypsin were pre-heated to 37°C in a water bath before use. Murine tumour cells were cultured in IMEM supplemented with 5% foetal calf serum (FCS) and 1% penicillin/streptomycin. Human MCF-7 cells were kept in 10% FCS and 1% penicillin/streptomycin-containing DMEM. MMTV-PyMT$^{tg/+}$ WT, BK KO and IK KO cells as well as MCF-7 cells were cultured in an incubator with 37°C, 95% humidity and 5% CO_2. Cultivation of MDA-MB-157 and MDA-MB-453 cells occurred in L-15 media supplemented with 10% FCS and 1% penicillin/streptomycin. These cells were kept in a 37°C incubator with 95% humidity and atmospheric air. Media was changed three times a week for MCF-7 and twice a week for all other breast tumour cell cultures.

Charcoal-stripped serum (CCS) was manufactured and supplied by Werner Schroth (AG Prof. Dr. Brauch, IKP Stuttgart). For the production of CCS from FCS, a 500 ml bottle of 37°C pre-heated FCS was supplemented with sulfatase for a final concentration of 2 U/ml sulfatase in FCS and incubated at 37°C for 2 h. In the meantime, 50 ml tubes were filled with 10 ml charcoal solution and centrifuged at 3,000 rpm for 10 min. The supernatant was aspirated. Half of the tubes were stored at 4°C and the other tubes were filled up to 50 ml with the sulfatase-treated FCS. The tubes were kept in a 56°C water bath for 30 min while gently shaking. Next, the tubes were cooled on ice for 5 - 10 min before a centrifugation step at 3,000 rpm for 15 min. Then, the supernatant was transferred to the charcoal-containing pellet stored at 4°C previously. Once again, the tubes were put in a 56°C water bath for 30 min and gently shook before cooling on ice and a centrifugation step at 3,000 rpm and 15 min. Finally, the supernatant was passed through a 0.2 µm filter and the CCS aliquots were stored at -20°C until further use.

4.2.3 Splitting and cryo conservation of tumour cells

During establishment of the primary murine tumour cell lines, purification was necessary by elimination of co-existing fibroblasts with trypsin. For this purpose, cells were washed twice with PBS and incubated in trypsin for 0.5 - 3 min at room temperature. The incubation time was dependent on the individual degree of cell culture adhesion to the cell flask or dish and was repetitively tested. As fibroblasts presented with lower adhesion to the cell flask compared to the tumour cells, continuous observation under the microscope and cautious tapping allowed the detachment of fibroblasts first while the tumour cells still adhered to the bottom of the cell flask. The fibroblast-containing trypsin solution was aspirated and the trypsin-induced cell detachment was stopped with cell culture media. After a wash with PBS, cells were supplied with cell culture media for further cultivation.

For cell harvesting, the cell monolayer was washed twice with PBS and incubated in trypsin in the incubator for 5 min. Then, cell detachment was enforced by tapping against the cell flask and it was confirmed with a glance through the microscope. The tumour cell-containing trypsin solution was washed to one corner of the flask with cell culture media and collected in a 15 ml or 50 ml centrifuge tube depending on the sample volume. Centrifugation at 1,000 rpm for 3 - 5 min resulted in the cell pellet placed at the bottom of the centrifuge tube. The supernatant was aspirated with a glass capillary before the cell pellet was separated mechanically and the tumour cells were resuspended in cell culture media. For further cultivation, tumour cells were passaged 1:2 for MDA-MB-157 cells, 1:3 for murine tumour cells and MDA-MB-453 cells as well as approximately 1:8 for MCF-7 cells. Counting of cells was performed by a disposable plastic haemocytometer loaded with 10 µl of the cell suspension. Within this chamber, the four quadrants at the outer corners were counted and the mean cell number was calculated. The mean represented the cell concentration in 0.1 µl cell suspension. Cells were cultured in different volumes according to the size of plates and dishes (table 4.2).

Table 4.2: Cell flask and dish sizes
Tumour cells were plated according to the number of available tumour cells after passaging and depending on the anticipated experimental procedure. Due to their different size, appropriate volumes of solutions were administered to flasks and dishes.

Flask or dish	Media [ml]	Trypsin [ml]
25 cm² cell flask	5	1
55 cm² cell dish	10	2
75 cm² cell flask	15	3
175 cm² cell flask	20	5

For cryo preservation, a cell suspension of 5 million cells in 0.5 ml cell culture medium was pipetted per 1.8 ml cryo tube. Then, 0.5 ml of 20% DMSO in cell culture medium was added to each cryo tube in order to avoid crystallising of water and thus harming of the cells during freezing and thawing. The cells were frozen at -80°C in a freezing container for the first 24 h. Isopropanol contained in the freezing container slowed down cooling to 1°C per min. For thawing of cells from cryo conservation at -80°C, a cryo tube was put in the 37°C water bath for 3 min. Then, the cell suspension was transferred in a 15 ml centrifugation tube with 9 ml cell culture medium. After centrifugation at 1,000 rpm for 3 min and supernatant removal, the cells were seeded in a 25 cm^2 flask. Medium was changed after 1 d.

4.2.4 *In vitro* tumour cell growth assays

Proliferation assays were performed upon serum starvation, which was carried out by two PBS washing steps before incubation of the cells in phenol red-free and serum-free cell culture medium. Starvation in phenol red-free medium was performed for 3 d in order to equalise experimental start conditions and to avoid a potential hormonal influence by phenol red with the anti-/hormone treatment[321,322]. At the end of serum starvation, cells were expected in G_0 and G_1 phases of the cell cycle[323,324].

Transfection with siRNA

The siRNA approach was used to study the role of BK-α and BK-γ1 subunits in MMTV-PyMT$^{tg/+}$-derived mouse tumour cells and in MDA-MB-453 human breast cancer cells. For resuspension of the siRNA in siRNA buffer, the tubes containing 5 nmol siRNA (supplement 9.1) were briefly centrifuged for collection of the siRNA as pellet at the bottom. 20 µM stock solutions were obtained by addition of 250 µl 1x siRNA buffer. After 30 min at a mixer, small volumes of 10 - 20 µl aliquots were stored at -20°C in order to avoid repeated freeze-thaw cycles. In all proliferation experiments conducted, cells were seeded and allowed to adhere overnight. Transfection occurred in two steps: First, 3 d transfection in cell culture medium without serum (serum starvation) followed by 3 d transfection in cell culture medium supplemented with FCS (serum restimulation). Serum starvation in the first 3 d prevented excessive growth and maintained controlled experimental conditions. For the transfection process, solutions of 100 nM siRNA in 0.2 µl transfection reagent per 100 µl media (DharmaFECT 1 for MMTV-PyMT$^{tg/+}$ WT and BK KO cells, DharmaFECT2 for MDA-MB-453 cells) achieved best transfection efficacies in combination with low toxicity (data not shown). Aliquots for the different siRNAs were thawed and measured as 1 µl samples with the nanophotometer. Here, a concentration of 13.3 ng/µl was equivalent to 1 µM siRNA. 5 µM siRNA was prepared as solution in 1x siRNA buffer and incubated for 5 min. In parallel, the transfection reagent was diluted in IMEM or L-15, respectively, and aliquoted in tubes according to the number of experimental conditions. After 5 min incubation, each siRNA solution was transferred to a pre-arranged tube with transfection reagent and incubated for 20 min. In between, cells were washed twice with PBS. For serum starvation, IMEM or L-15 medium was added to the tube containing siRNA and transfection reagent for concentrations of 100 nM siRNA in 0.2 µl transfection reagent per 100 µl media. For serum restimulation, IMEM or L-15 medium were supplemented with FCS for a final serum concentration of 5% for MMTV-PyMT$^{tg/+}$ cells and 10% for MDA-MB-453 cells. Then, the transfection medium was pipetted to the cells and incubated for 3 d. At the end of each experiment, mRNA was isolated to assess the amount of target gene depletion and thus guarantee successful knockdown. Due to the experimental design in small slides and plates,

only a low amount of mRNA was expected after isolation. In order to maximise the yield, the mRNA was isolated with the Machery-Nagel RNA isolation kit containing different column and centrifugation steps, which is further described in section 4.3.1.

Grid slides and dishes

For proliferation analysis of siRNA-treated cells, 8-well slides containing a grid pattern at the bottom to allow for cell tracking (figure 4.4 A) were utilised. A mastermix containing 10,000 MMTV-PyMT$^{tg/+}$ WT or BK KO cells per 300 µl IMEM (without phenol red) + 5% FCS, or 10,000 MDA-MB-453 cells per 300 µl L-15 (without phenol red) + 10% FCS was pipetted in duplicate in each well of the grid slide. After serum withdrawal in combination with siRNA transfection, a photo of the four centred quadrants of each well was taken with a 10x objective magnification at an inverted transmitted-light microscope. Then, the cells were transfected with siRNA in serum-containing medium. Photos were taken every 24 h for in total 72 h.

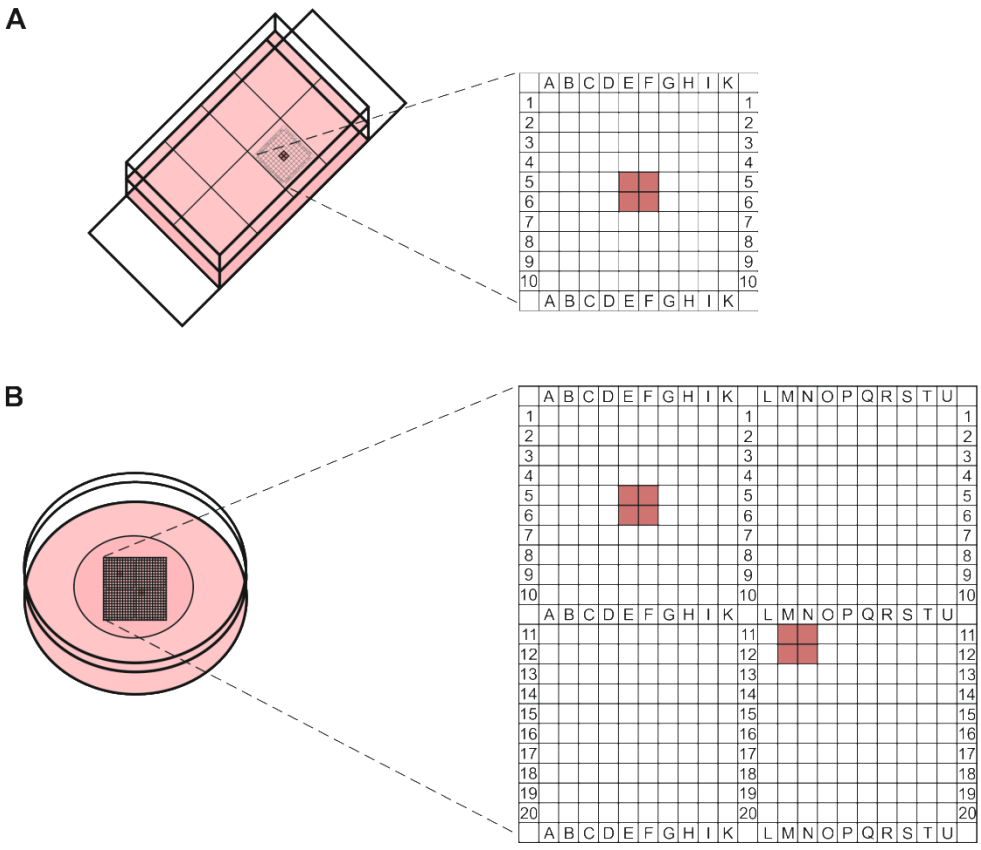

Figure 4.4: Slides and dishes with grid pattern for proliferation experiments
Tracking of tumour cells occurred in grid pattern-based **(A)** slides and **(B)** dishes. Using the 10x magnification of the microscope, four adjacent quadrants were photographed at 0 h and 72 h, as well as for 24 h and 48 h in selected experiments, for monitoring cell numbers by counting.

Investigations on tumour cell proliferation over a time frame of 72 h were performed in grid dishes (figure 4.4 B). 80,000 MMTV-PyMT$^{tg/+}$ WT, BK KO or IK KO cells, 30,000 MCF-7, 20,000 MDA-MB-157 or 80,000 MDA-MB-453 cells were seeded per dish and condition and were allowed to adhere for 24 h followed by serum starvation for 72 h. Before the end of serum starvation, selected grid areas of each dish were photographed with the microscope. Afterwards, re-stimulation occurred according to the treatment groups of the various experiments. For investigations of different TRAM-34 concentrations on the growth of MMTV-PyMT$^{tg/+}$ WT and IK KO cells, cells were monitored every 24 h for totally 72 h. In experiments investigating the role of selected anti-/hormones on proliferation, monitoring was restricted to 0 h and 72 h due to light sensitivity of the selected substances.

Ki-67 proliferation marker status

Genotype-specific differences in MMTV-PyMT$^{tg/+}$ WT, BK KO and IK KO tumour cell Ki-67 status were assessed by seeding 80,000, 50,000 or 30,000 cells of each genotype in 200 µl cell culture medium into the wells of 12-well chamber slides. After 24, 48 or 72 h, respectively, cells were fixed in 250 µl of 70% ethanol.

Ki-67 expression after serum and anti-/hormone treatment was conducted by seeding 50,000 MMTV-PyMT$^{tg/+}$ WT or BK KO cells, 10,000 MCF-7 cells, 10,000 MDA-MB-157 cells or 30,000 MDA-MB-453 cells in 400 µl cell culture medium per well of 8-well chamber slides. After 24 h of adhesion, cells were starved from serum in 400 µl media containing penicillin/streptomycin for 72 h, as described in section 4.2.3. Afterwards, the different wells were restimulated with selected concentrations of anti-/hormones in 400 µl CCS-containing cell culture media for 24 h. Finally, cells were fixed in 400 µl 70% ethanol.

Ki-67 immunofluorescence of siRNA-treated cells was carried out in 8-well chambers. For this purpose, cell suspensions of 20,000 MMTV-PyMT$^{tg/+}$ WT or BK KO cells per 400 µl IMEM (without phenol red) containing 5% FCS, or 20,000 MDA-MB-453 cells per 600 µl L-15 (without phenol red) with 10% FCS were prepared as mastermix and pipetted in the various wells of the chambers. As described in section 4.2.3., transfections in serum-free medium and restimulation in serum-containing media were conducted each for 72 h before the cells were fixed in 70% ethanol. Each experiment was prepared in duplicate, as one replicate served for RNA isolation and measurement of knockdown efficacy while the other replicate was used for anti-Ki-67 immunofluorescence.

From each genotype and treatment condition, four sections were taken with the fluorescence microscope in order to evaluate Ki-67 status. For this purpose, the numbers of nuclei and

Ki-67-positive cells in each section were counted and thus the fraction of Ki-67-positive cells was calculated.

4.2.5 Clonogenic survival assay after IR

The potential radiosensitising effect of BK and IK channels was investigated after seeding 5 ml cell suspensions of 600,000 MMTV-PyMT$^{tg/+}$ WT, BK KO or IK KO cells in 25 cm² cell flasks to allow for adherence and growth for 3 d. Then, the cells were irradiated in 2 Gy fractions in the various flasks using total radiation doses of 0, 2, 4 or 6 Gy. In order to investigate a potential modulation of survival after irradiation by co-treatment with 10 or 1,000 nM TAM, 600,000 WT or BK KO cells were seeded in 25 cm² cell flasks in 4.95 ml cell culture medium containing CCS instead of FCS. After 3 d of adhesion and growth in the flasks, the cells were treated with either 10 or 1,000 nM TAM or vehicle alone. Approximately 60 min later, the flasks were irradiated with 0 or 2 Gy.

In order to perform the delayed plating colony formation assays, cells were allowed to regenerate from irradiation for 24 h before detachment from the flask with trypsin. 3,500 cells were seeded in 3 ml cell culture medium per well of 6-well plates. Each experiment was conducted with six technical replicates. The 6-well plates were kept in an incubator for the following 14 d in order to allow surviving cells to form colonies containing at least 50 cells. Eventually, cell culture medium was removed from the 6-well plates. Cells were fixed with 2 ml 3.7% formaldehyde in PBS for 10 min. The formaldehyde solution was replaced with 70% ethanol for 10 min. Then, the ethanol solution was discarded as well and the wells were washed with dH_2O twice shortly. Afterwards, cells were stained with 0.05% coomassie solution for 10 min, depending on its freshness, until staining of the cells was macroscopically visible. The coomassie solution was recycled and the wells were washed again with dH_2O twice shortly. Then, the 6-well plates were air-dried and the colonies in each well could be counted by use of the 5x magnification of the microscope (figure 4.5).

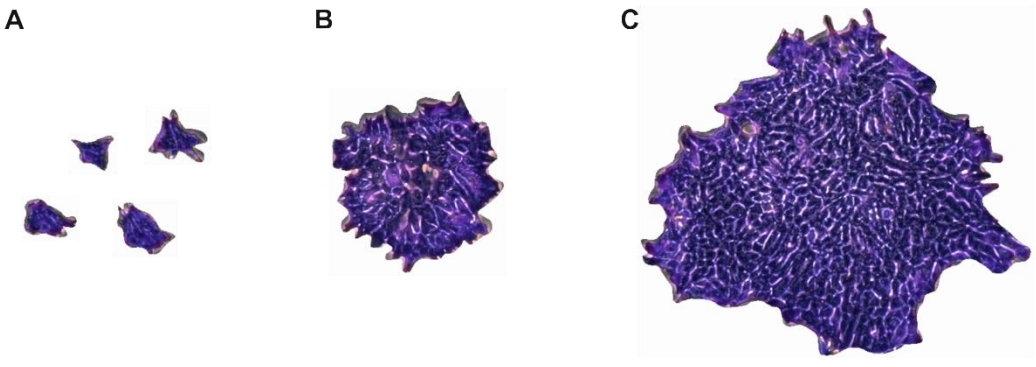

Figure 4.5: Colony formation after application of IR
Representative coomassie solution-stained colonies formed in 6-well plates 14 d after irradiation with 0, 2, 4, or 6 Gy. **(A)** After IR exposure, cells adhered to the 6-well plate but were growth-arrested and died by different mechanisms. **(B)** Cells undergoing mitotic catastrophe managed to accomplish several cell cycle divisions before the colony of cells stopped growing. **(C)** Successfully surviving cells formed colonies containing at least 50 cells.

4.2.6 DNA damage assessment by γH2AX status

Detection of DNA damage repair after irradiation was investigated by seeding 200 µl suspensions of 50,000 MMTV-PyMT$^{tg/+}$ WT, BK KO or IK KO cells in 12-well chambers to culture for 3 d. In an additional setup, the IK inhibitor TRAM-34 was employed in MMTV-PyMT$^{tg/+}$ WT cells where the cells were cultured in 190 µl cell culture medium and treated with 10 µl TRAM-34 or ethanol 1 h before IR. Irradiation was generally performed in 2 Gy fractions to final dosages of 0, 2, 4 and 6 Gy. To analyse the effect of 10 or 1,000 nM TAM treatment on γH2AX expression after irradiation, cells were grown in CCS-containing cell culture medium for 3 d. 1 h prior to irradiation with 0 or 2 Gy, cells were treated with either 10 or 1,000 nM TAM or its solvent. Four sections were taken for each genotype and treatment condition, from which γH2AX foci numbers per cell were determined.

4.2.7 xCELLigence-based tumour cell migration after TAM treatment

Metastases and in particular brain metastasis are the main cause of breast cancer mortality in patients[325-327]. At the same time, TAM is well accepted for its anti-proliferative but also anti-migrative properties in breast and other cancers[328-330]. Interestingly, several hints exist for a pro-migrative effect of TAM, which is independent from the nuclear ER, but seems to rely on non-genomic GPER signalling[331,332] that is also proposed to modulate BK channel activity[333,334]. Therefore, migration of MMTV-PyMT$^{tg/+}$ WT and BK KO cells was assessed with the xCELLigence system (figure 4.6) in the presence of 10 or 1,000 nM TAM. The CIM plates used for the assay were composed of an upper chamber with 16 wells for tumour cell application and a membrane with pores on its bottom. The upper chamber could be put on top of the lower chamber containing another corresponding 16 wells. Cells seeded in the upper chamber migrated to the lower chamber along a 2.5 - 5% CCS gradient through the microporous membrane below with microelectrodes sensing adhesion and thus impedance evoked by the cells.

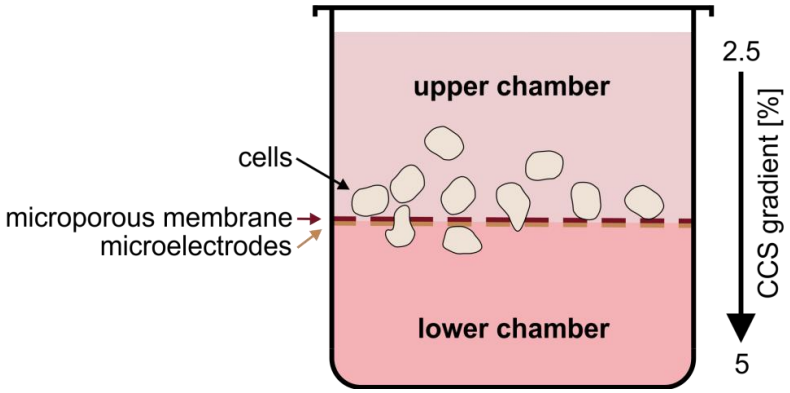

Figure 4.6: Migration assay in the xCELLigence system
An upper chamber and a lower chamber separated by a membrane with pores served as migration axis along a CCS gradient. MMTV-PyMT$^{tg/+}$ WT and BK KO cells were added in the upper chamber at a final concentration of 80,000 cells per 200 µl and migration was measured as impedance with the microelectrodes at the bottom of the pore membrane during 8 h after seeding.

For the experiment, 1.5 million MMTV-PyMT$^{tg/+}$ WT and BK KO cells were plated in cell culture medium in 25 cm^2 cell flasks overnight. The next day, cells were serum-starved for 72 h. Then, the cells were pre-incubated with TAM or vehicle in CCS-containing cell culture medium for 24 h. The lower chamber of the CIM plate was filled with 160 µl of 5% CCS-containing IMEM and TAM or vehicle. During this procedure, air bubbles were avoided, as they would disturb cell migration to the lower chamber. The upper chamber was prepared with 100 µl serum-free IMEM ± TAM in twice the concentration of the experimental setup. The plate was equilibrated in the incubator during preparation of the tumour cells. For this purpose, the MMTV-PyMT$^{tg/+}$ WT and BK KO cells were detached from their flasks with trypsin and counted. In this experiment, the trypsin reaction was not stopped with serum-containing cell culture medium but it was diluted in PBS in order to prevent serum-evoked migration effects. The cell suspension was centrifuged a second time and resuspended in IMEM to a concentration of 80,000 cells/100 µl. The CIM plate was calibrated before 100 µl cell suspension was added to the wells of the upper chamber for a total volume of 200 µl. After a time frame of 15 min to allow cells to settle down, the CIM plate was placed in the xCELLigence machine that was located in a separate incubator. The migration assay was run for 8 h because longer time periods would potentially disturb experimental outcomes due to changes in cell size and morphology after adhesion as well as increasing cell numbers because of proliferation. Electrode impedance served for measurement of migration and was recorded as cell index representing a dimensionless parameter. Cell index represented cell number and viability, morphology and adhesion degree[335].

4.3 RNA analytics

Tumour or organ pieces were dissected as described (section 4.1.8) and collected in 1.8 ml cryo tubes and frozen in dry ice followed by storage at -80°C until further analysis.

4.3.1 RNA isolation from tumour tissues and cells

RNA was extracted with peqGOLD RNAPure™ containing phenol and guanidinium thiocyanate. For RNA isolation from tissue samples, peqGOLD RNAPure™ was added to 2 ml tubes with 1 ml per 100 mg tissue or at least 500 µl was used for samples of lower weight. The samples were homogenised with an ultra-turrax and centrifuged at 12,000 rcf and 4°C for 10 min. For the isolation of RNA from cells in a 55 cm² cell dish, cells were washed twice with PBS. 1 ml peqGOLD RNAPure™ was added to the cells and pipetted up and down several times and transferred to a 1.5 ml tube. The samples were centrifuged at 13,000 rpm and 4°C for 10 min.

The supernatants were transferred to new 2 ml tubes for tissues and 1.5 ml tubes for cells. These tubes contained chloroform at 20% v/v as compared to the sample volume. After an immediate vortexing step, 5 min incubation followed on ice for tissues and at room temperature for cells. After centrifugation at 13,000 rpm and 4°C for 5 min, the upper phase was pipetted in a new 2 ml tube for tissues or 1.5 ml tube for cells. Isopropanol at 70% v/v as compared to the sample volume was added to the tube and incubated at 4°C overnight. The next day, samples were centrifuged at 13,000 rpm and 4°C for 10 min. Subsequently, two washing steps were carried out as follows: The supernatant was removed and 800 µl 75% ethanol was added to the samples before centrifugation at 13,000 rpm and 4°C for 5 min and the procedure was repeated once. Finally, the supernatant was removed and the tubes contained a pellet at the bottom to be dried for 20 - 30 min. 53 µl DEPC-H_2O was added to the tubes and mixed on a thermomixer at 500 rpm and 56°C for 10 min. During this time, the tubes were flipped every 2 min.

In order to use equal mRNA amounts for cDNA synthesis in the different experiments, mRNA concentration as well as impurities caused by DNA and protein in the sample were measured with a nanophotometer using 1 µl sample each for three measurements. Afterwards, traces of genomic DNA in the samples were digested by addition of 6 µl DEPC-H_2O and 5 µl DNAse followed by incubation on a thermomixer at 500 rpm and 37°C for 30min. The DNAse was heat-inactivated at 500 rpm at 80°C for 5 min. Finally, RNA concentrations were adjusted with DEPC-H_2O addition to 0.1 µg/µl. Samples were stored at -20°C until further use.

The experimental approaches using siRNA were conducted in a small format using lower cell numbers and sample sizes than necessary for the isolation of total or mRNA with the above-described protocol. Therefore, the Machery-Nagel RNA isolation kit (see section 3.6), an efficient, reproducible and high-yielding method for isolation of RNA was applied. For the kit-based RNA isolation, medium was removed from the cells and they were lysed with 2 µl β-mercaptoethanol in 200 µl RA1 buffer. Filtration through a NucleoSpin® filter placed in a 2 ml collection tube at 11,000 rcf for 1 min reduced viscosity and cleared the lysate. 350 µl of 70% ethanol was added to the lysate-containing collection tube and shortly vortexed. The lysate was loaded to a NucleoSpin® RNA column placed in a new 2 ml collection tube and centrifuged at 11,000 rcf for 30 s. The RNA was thus bound to the column. The column was placed in a new 2 ml collection tube and 350 µl membrane desalting buffer was added to the column. After centrifugation at 11,000 rcf for 1 min, the DNA was digested. The mastermix for DNA digestion contained 10 µl reconstituted rDNAse in 90 µl reaction buffer for rDNAse per sample. 95 µl of the mastermix was pipetted directly on the centre of the silica membrane, which was located at the bottom of the column, and incubated for 15 min. rDNAse was inactivated with 200 µl RAW2 buffer at 11,000 rcf for 30 s. Then, the column was placed in a new 2 ml collection tube. For washing, 600 µl ethanol-containing RA3 buffer was used for the next centrifugation step at 11,000 rcf for 30 s. The flow-through was discarded and the collection tube was placed back to the column. Another washing step with 250 µl RA3 buffer occurred at 11,000 rcf for 2 min in order to completely dry the membrane. Next, the column was placed into a 1.5 ml tube and the RNA was eluted with dH_2O, while volumes were adjusted according to experimental setups (section 4.2.4), at 11,000 rcf for 1 min.

4.3.2 Reverse transcriptase-based cDNA synthesis

The cDNA synthesis mix with reverse transcriptase (RT) was employed for each RNA sample to create a cDNA sample for further analysis. Volumes used are shown in table 4.3. The mastermix containing RT (+RT) was prepared of RT, DEPC-H_2O and the 5x iScript reaction mix containing dNTPs, oligo deoxythymidines and random hexamer primers as well as buffer components. For negative control, a mastermix without RT (-RT) was prepared with RT substituted by DEPC-H_2O. The mastermix was provided in a 0.5 ml tube and the eluted RNA was added. As RNA concentrations and volumes were lower in samples from siRNA experiments, the whole RNA yield per sample was used for cDNA synthesis. DEPC-H_2O was omitted except for its use as RT substitute, and the total volume of the cDNA mastermix was adjusted. In the thermal cycler, the lid was pre-heated to 105°C to avoid condensation. In a first step, samples were heated to 25°C for 5 min to allow for primer annealing. Then, reverse

transcription was conducted at 42°C for 30 min before the RT was heat-inactivated at 85°C for 5 min. After cooling down to 4°C, DEPC-H_2O was added for sample dilution.

Table 4.3: Composition of the cDNA synthesis mastermix
The cDNA synthesis mastermix constituted different amounts of RT, DEPC-H_2O and 5x iScript Reaction Mix as well as different amounts of RNA. After PCR termination, DEPC-H_2O was added to increase the amount of cDNA sample for subsequent conductance of quantitative real-time PCR (qRT-PCR). All listed volumes present in µl.

Approach	RT		DEPC-H_2O	5x iScript Reaction Mix	RNA	Final addition of DEPC-H_2O
Peggold	+	1	10	4	5	180
	-	-	5.5	2	2.5	90
Murine siRNA						
Grid slides	+	2	20	8	10	-
	-	-	5.5	2	2.5	-
Ki-67	+	2	-	8	30	70
	-	-	0.67	2.67	10	23.33
Human siRNA						
Grid slides	+	2.25	-	9	33.75	-
	-	-	0.75	3	11.25	-
Ki-67	+	2.25	-	9	33.75	-
	-	-	0.75	3	11.25	-

4.3.3 Primer design and qRT-PCR analysis of mRNA expression levels

For the design of target-specific primers, a preferably intron-spanning template sequence was identified. Therefore, the different coding isoforms of the target gene were compared for the target species on the ensemble website[336]. A sequence common for the isoforms of interest was selected (supplement 9.1) and introduced in the primer3.ut primer design website[337,338]. Criteria for primer selection were 80 - 120 bp length and 58 - 64°C melting temperature. After confirmation that the primer pairs were applicable to all coding isoforms, a blast search was conducted to proof target specificity and restriction to the gene of interest[339]. Primer lyophilisates were solved in DEPC-H_2O to a concentration of 100 pmol/µl.

Amplification of target sequences with qRT-PCR allowed conclusions on the relative target gene expression compared to *Actb*/*ACTB* encoding the murine/human β-actin, which was chosen as reference gene. A mastermix with 2.25 µl of each forward and reverse primers for the specific gene target as well as 7.5 µl SsoAdvanced™ Universal SYBR® Green Supermix (2x) was prepared. The SsoAdvanced™ Universal SYBR® Green Supermix (2x)

contained an antibody-mediated hot-start Sso7d-fusion polymerase, dNTPs, $MgCl_2$, stabilisers, enhancers, SYBR® Green I dye and passive reference dyes. 12 µl mastermix was pipetted in each of the scheduled wells of a 96-well plate before addition of 3 µl cDNA. For polymerase activation and DNA denaturation, the PCR machine was heated to 95°C for 2 min followed by 40 rounds of amplification: Each cycle started with cDNA denaturation at 95°C for 5 s. Then, annealing, extension and plate read occurred at 58°C for 20 s. After the last cycle, the machine hold 58°C for additional 5 s before it heated up to 95°C for separating the double strands of the last round. Finally, the melting curve was created and temperature dropped to 0.5°C.

After qRT-PCR, the correct product size of the amplified cDNA sequence was verified with a 3% agarose gel electrophoresis for establishment of new primer sequences. Due to the small band sizes expected in this assay, 12 µl of Low Molecular Weight DNA Ladder was used as reference. The samples were supplied with loading dye and a total amount of 15 µl was pipetted in each pocket of the gel. Gel electrophoresis and detection were conducted as described in section 4.1.3.

4.4 Histology

Whole tumours or organs were fixed in 15 ml tubes containing 10 ml 4% PFA for at least 3 h. Afterwards, PFA was discarded and the samples were washed twice with 10 ml PBS on a shaker for 5 min. The PBS was replaced with 10 ml of an increasing sucrose concentration gradient with 5% for 30 min, 10% overnight and 20% for 24 h, each prepared freshly in PBS. For sectioning, the samples were conserved in Neg-50™ frozen section medium in an aluminium foil pocket. All samples were kept at -80°C for at least 24 h and maintained on ice before cutting. Tissue blocks were generally cut to 10 µm sections, except for lungs that were cut to 30 µm sections. Temperatures of sample and cutting knife were -18°C and -21°C, respectively. In order to guarantee equal staining conditions across different genotypes and treatments, such samples were matched together on slides for direct comparison.

4.4.1 Fixation in Bouin´s solution for the detection of macrometastases

The right lung was incubated in Bouin´s solution for 3 d in order to visualise lung metastases macroscopically. Bouin´s solution contained 9% formaldehyde, 5% acetic acid and 0.9% picric acid. This led to fixation of the lung tissue and improved macroscopic detection and counting of metastases (figure 4.7).

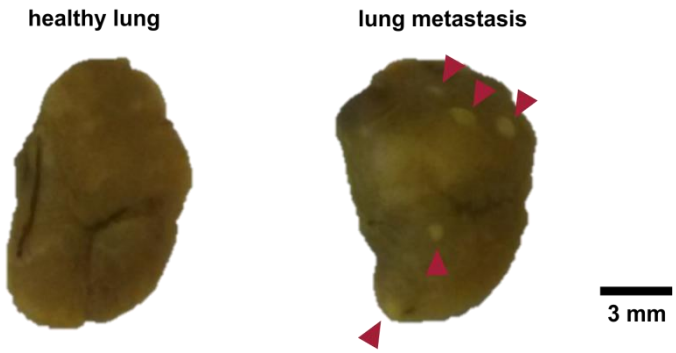

Figure 4.7: Representative fixation in Bouin´s solution for lung metastasis
Lungs of MMTV-PyMT$^{tg/+}$ WT and BK KO tumour-bearing mice were dissected and fixed in Bouin´s solution in order to detect macroscopically visible lung metastasis. Compared to healthy lungs (left), tumour metastases (right) presented as bright dots of smaller or larger size, respectively. In the example, these are highlighted by red arrows.

4.4.2 Haematoxylin/eosin staining for the detection of micrometastases

For the detection of micrometastases (figure 4.8), the left lung was dissected and sectioned, as described in section 4.1.9. Staining was performed in a glass tray with the slides positioned in an upright position. The slides were dehydrated and rehydrated in an ethanol gradient of 50, 70, 90, 100, 90, 70 and 50% each for 2 min. Three short washing steps in dH_2O were followed by haematoxylin staining for 5 s. Two further short washing steps were conducted in tap water. Next, the slides were incubated in 0.1% ammonia solution for 30 s before another 5 min washing step in tap water. Then, the slides were incubated in eosin-G solution for 10 min and were washed shortly for five times in tap water. Tap water was utilised for haematoxylin/eosin to induce intensive staining that was evoked by its ion content[340]. At the end, the sections were dehydrated with 80% ethanol for 2 min, followed by 100% ethanol for 3 min and toluene for 5 min. Finally, the slides were covered with a drop of DePeX and a glass cover slip.

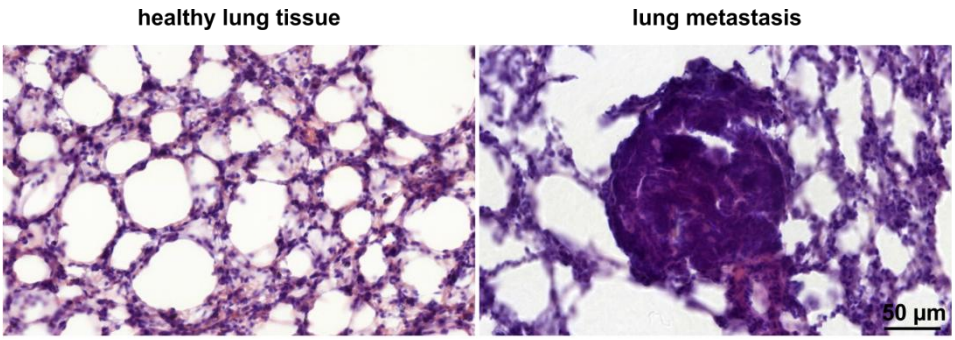

Figure 4.8: Representative haematoxylin/eosin staining of lung metastases
Lungs were dissected and processed as described (section 4.1.8) and finally stained with haematoxylin/eosin after scarification of MMTV-PyMT$^{tg/+}$ WT and BK KO tumour-bearing mice. Micrometastases were counted and compared between genotypes in the spontaneous and allotransplant breast cancer models (figure 5.1 and figure 5.4).

4.4.3 Anti-ER-α alkaline phosphatase staining

MMTV-PyMT$^{tg/+}$ WT, BK KO and IK KO sections and uterus sections (positive control) were encircled with a hydrophobic barrier pen and fixed in 4% PFA for 15 min. After a short wash and three washes for 5 min with PBS, the tissues were incubated in 1% H_2O_2 for 10 min. Consecutive washing steps of tissue sections were carried out as follows: Once shortly with PBS, 5 min with PBS, 5 min with 0.001% Tween® 20, 5 min with PBS. Alternatively, 170,000 MMTV-PyMT$^{tg/+}$ WT, BK KO and IK KO cells or 120,000 MCF-7 cells (positive control) were grown in 8-well chambers for 24 h followed by fixation in 2% PFA for 10 min, three washing steps with PBS and permeabilisation in 0.1% TritonX100 for 15 min. After fixation and permeabilisation, blocking of unspecific binding sites in tissue sections and cells occurred with 10% NGS in blocking solution (tissue) or PBS (cells) for 1 h. Then, the solutions were discarded and samples were incubated in 1.5% NGS in blocking solution (tissue) or PBS (cells) as negative control or amended with rabbit IgG or primary antibody at 4°C overnight (table 4.4). After washing, samples were incubated in the secondary antibody in 1.5% NGS in blocking solution (tissue) or PBS (cells) for 1 h in the dark. Samples were washed, incubated in 30 min pre-incubated ABC-AP reagent for 30 min in the dark, washed again and incubated in AP substrate solution for 10 min (tissue) or 8.5 min (cells) in the dark. The reaction was stopped once shortly and for 5 min in tap water (tissue) or by tap water followed by dH_2O before the plastic chamber was removed (cells). Finally, each slide was covered with aquatex permanent mounting medium and a cover slip.

4.4.4 Anti-Ki-67, anti-CD45 and anti-γH2AX immunofluorescence

Tissue sections were encircled with a hydrophobic barrier pen and cell experiments were prepared as described in sections 4.2.4 and 4.2.6. All anti-Ki-67 and anti-γH2AX stainings were fixed with 70% ice-cold ethanol for 10 min (tissue) or with 70% ethanol at -20°C for at least 10 min or up to several days (cells). In addition, cells to be stained against Ki-67 were permeabilised with TritonX100 for 15 min after washing and tissue sections for anti-CD45 immunofluorescence were incubated in 1% H_2O_2 for 10 min. Generally, cells for staining against γH2AX or Ki-67 underwent two or three short washing steps with PBS, respectively, whereas tissue sections were washed three times with PBS for 5 min. For background reduction in the anti-Ki-67 immunofluorescence of tissue sections, washing after incubation with the 1st and 2nd antibodies comprised 5 min in PBS, 5 min in 0.001% Tween® 20 and another 5 min in PBS. Following fixation, permeabilisation and washing of the different experimental setups, epitopes were blocked against unspecific binding with 10% NDS (anti-Ki-67, anti-CD45) or NGS (anti-γH2AX) normal serum in blocking solution (tissue) or PBS (cells) for 1 h. After removal of the respective solutions, samples were incubated in

1.5% normal serum in blocking solution (tissue) or PBS (cells) (negative control) amended by IgG or 1st antibody for 2 h (table 4.4). Washing of the samples was followed by incubation in the 2nd antibody in 1.5% normal serum in blocking solution (tissue) or PBS (cells) for 1 h, except for the anti-CD45 staining whose 1st antibody was directly tagged to the fluorophore. The washing procedure was repeated and, in cell experiments, the chamber was removed from the underlying slide. Nuclei were counter-stained and mounted with the DAPI-containing vectashield solution. The slides were covered with a cover slip and nail varnish avoided leakage of vectashield at the edges.

Table 4.4: Overview on stainings against ER-α, Ki-67, C45 and γH2AX
MMTV-PyMt$^{tg/+}$ WT, BK KO and IK KO tumour sections and primary cell cultures were employed for the staining approaches against, ER-α, Ki-67, CD45 and γH2AX. These stainings required different concentrations of primary antibody, IgG control and secondary antibody.

Staining	Sample	1st antibody	IgG	2nd antibody
anti-ER-α	**tissue**	1:150	1:75 normal rabbit IgG	1:200 biotinylated goat anti-rabbit
	cells	1:300	1:150 normal rabbit IgG	1:200 biotinylated goat anti-rabbit
anti-Ki-67	**tissue**	1:400	1:174 normal rabbit IgG	1:200 Alexa Fluor® 555 donkey anti-rabbit
	cells	1:1,000	1:435 normal rabbit IgG	1:800 Alexa Fluor® 555 donkey anti-rabbit
anti-CD45	**tissue**	1:200	1:200 AlexaFluor® 488 rat IgG2bκ	- -
anti-γH2AX	**cells**	1:500	1:100 normal mouse IgG	1:800 Alexa Fluor® 555 goat anti-mouse

4.5 In silico analyses

4.5.1 TCGA mRNA expression analyses and association with survival

The Cancer Genome Atlas (TCGA) (https://xena.ucsc.edu/welcome-to-ucsc-xena/) IlluminaHiSeq Breast cancer data set was used to investigate K_{Ca} mRNA expression in

n = 1,095 breast cancer biopsies in comparison to n = 113 biopsies derived from healthy parts of the breast[341]. Besides, stratification by age, PAM50 classification, ER/PR status, tumour stage or menopause was performed to investigate a potential bias of the data due to the influence of any of these factors. Besides, OS was investigated after stratification for *KCNMA1* or *KCNN4* mRNA expression levels.

4.5.2 KM plotter mRNA expression association with survival

The Kaplan Meier (KM) plotter (http://kmplot.com/analysis/) was employed to investigate the association of gene expression with survival. The breast cancer mRNA data set contained in total n = 3,955 samples for relapse-free survival, n = 1,747 for distant metastasis-free survival, n = 1,402 for overall survival, and n = 414 for post-progression survival. Numbers dropped with subtype analysis, e.g. ER / PR / HER2 status, and selection of a distinct patient cohort, i.e. untreated, endocrine therapy, chemotherapy[342]. For the analysis, samples were stratified according to high or low mRNA expression levels of the desired gene and the KM plotter analysed survival parameters. Investigations included K_{Ca} channel genes coding for different subunits as well as proteins binding to regions of selected single nucleotide polymorphisms (SNPs).

4.5.3 BCAC breast cancer risk analysis of genetic variants

K_{CA} SNP data collected in the Breast Cancer Association Consortium (BCAC), which forms part of the Collaborative Gene-Environment Study (COGS) focussing on breast as well as ovarian and prostate cancer, was received via an ongoing collaboration with Prof. Dr. Brauch (IKP, Stuttgart) for subsequent breast cancer risk analysis. The approximately 211,000 genetic variants were analysed on the iCOGS custom genotyping array from Illumina. These SNPs had been selected according to promising findings of previously published genome-wide and candidate gene association studies. With respect to the size of the human genome and the limited size of a gene array, imputation of SNPs in linkage disequilibrium to the measured SNPs on the iCOGS array and due to hereditary linkage multiplied the number of genetic variants to be investigated for risk and survival studies[343-345]. As an up-dated chip configured by Illumina and additionally covering lung and colon cancer, the OncoArray was developed to be used in further studies. It contains approximately 533,000 genetic variants[346,347].

In order to assess putative associations of K_{Ca} SNPs and breast cancer, the chromosomal location of each of the corresponding genes was checked in version GRCh37.p13 of the human genome assembly using NCBI PubMed gene search[348,349]. Risk data of the requested

chromosomal regions representing K_{Ca} channel genes was accessed from the BCAC. Ablebits Duplicate Remover was used for data processing in Excel. For each SNP found in the selected chromosomal regions, information regarding SNP number and position, reference and effect allele as well as p-value and odds ratio (OR) for the overall and the risk for ER-positive or ER-negative tumours were considered. Minor allele frequency (MAF) according to the 1,000 Genomes Project, variant type, i.e. SNP, deletion or insertion, and exonic or intronic location were extracted from the SNP database website[350]. With the SNAP online tool, pairwise linkage disequilibrium was calculated in the CEU European population panel[351,352]. HaploReg version 3 was employed for the detection of protein binding to the distinct SNP region, effects on regulatory motifs, and expression quantitative trait loci (eQTLs)[353]. Results were confirmed with the SNiPA[354] and Genevar[355] web-based tools. For each protein found to be associated with the SNP region of interest, its influence on breast cancer survival was investigated with the KM plotter. Besides, a literature search intended to get insight into putative functions of the protein in cancer and its potential interaction with the particular gene.

4.6 Statistics

Statistical analyses were carried out with GraphPad Prism for Windows version 6.01. Results are presented as means ± standard error of the mean (SEM). Significance threshold was set to $\alpha = 0.05$. Statistical significance between selected groups are highlighted with asterisks, number signs and section signs with */#/§ for $p < 0.05$, **/##/§§ for $p < 0.01$ or ***/###/§§§ for $p < 0.001$. Non-significant statistical outcomes and comparisons that were neglected for statistical consideration are not marked separately.

For the following experiments in the MMTV-PyMT$^{tg/+}$ model, a common MMTV-PyMT transgene-positive K_{Ca} WT served as control for both BK KO and IK KO experiments: Genotype-specific characterisation by K_{Ca} mRNA expression, ER and HER2 analysis and CD45 immune cell infiltration; Proliferation assessment regarding Ki-67 status and growth differences of orthotopically transplanted murine tumour cells; *in vitro* radiation experiments.

If not otherwise stated, all experiments were carried out at room temperature.

5. Results

5.1 The BK channel in breast cancer development and survival

Gene amplification and over-expression of the BK channel are frequently observed in cancers of the breast and also bone, brain, ovary and prostate. In MCF-7 breast tumour cells, BK channel expression occurs in a cell cycle-dependent manner and its inhibition in different human breast cancer cell lines results in a diminished proliferation response[190,356]. Besides, BK expression in human cancers positively correlates with high Ki-67 index and tumour stage[187].

5.1.1 BK channels in MMTV-PyMT$^{tg/+}$-positive spontaneous murine breast cancer

The impact of BK channel status on breast cancer development and survival was investigated in the spontaneous breast cancer-prone MMTV-PyMT$^{tg/+}$ model[302,311]. MMTV-PyMT$^{tg/+}$ WT and global BK KO mice were generated as described (section 4.1.4). In the BK KO genotype, hazard ratios (HR) were significantly lower for tumour-free survival (TFS) (figure 5.1 A) and OS (figure 5.1 B) with 0.35 (confidence interval (CI) 0.14 - 0.41) and 0.38 (CI 0.18 - 0.64), respectively. As TFS and OS were significantly prolonged in MMTV-PyMT$^{tg/+}$ BK KO mice compared to their WT littermates, it indicates that endogenous BK channels promote breast tumourigenesis and cancer progression. Tumour cell metastasis to the lungs after fixation in Bouin´s solution revealed no significant difference between genotypes (2.40 ± 1.17 macrometastases per WT lung and 4.75 ± 1.89 macrometastases per BK KO lung) (figure 5.1 C). However, haematoxylin/eosin staining of lung sections showed a significant higher number of micrometastases in MMTV-PyMT$^{tg/+}$ BK KO samples compared to WT samples (1.50 ± 0.47 micrometastases per WT lung and 9.50 ± 3.22 micrometastases per BK KO lung). Of note, lungs were isolated as soon as the experimental mice reached the pre-defined abortion criteria (section 4.1.8) and due to the significantly different OS also at different ages for both genotypes. In addition, BW prior to and during tumour progression was significantly lower in MMTV-PyMT$^{tg/+}$ BK KO mice than in MMTV-PyMT$^{tg/+}$ WT mice, which is in line with recent findings that BW gain depends on functional BK channels in adipocytes[357] (section 9.3).

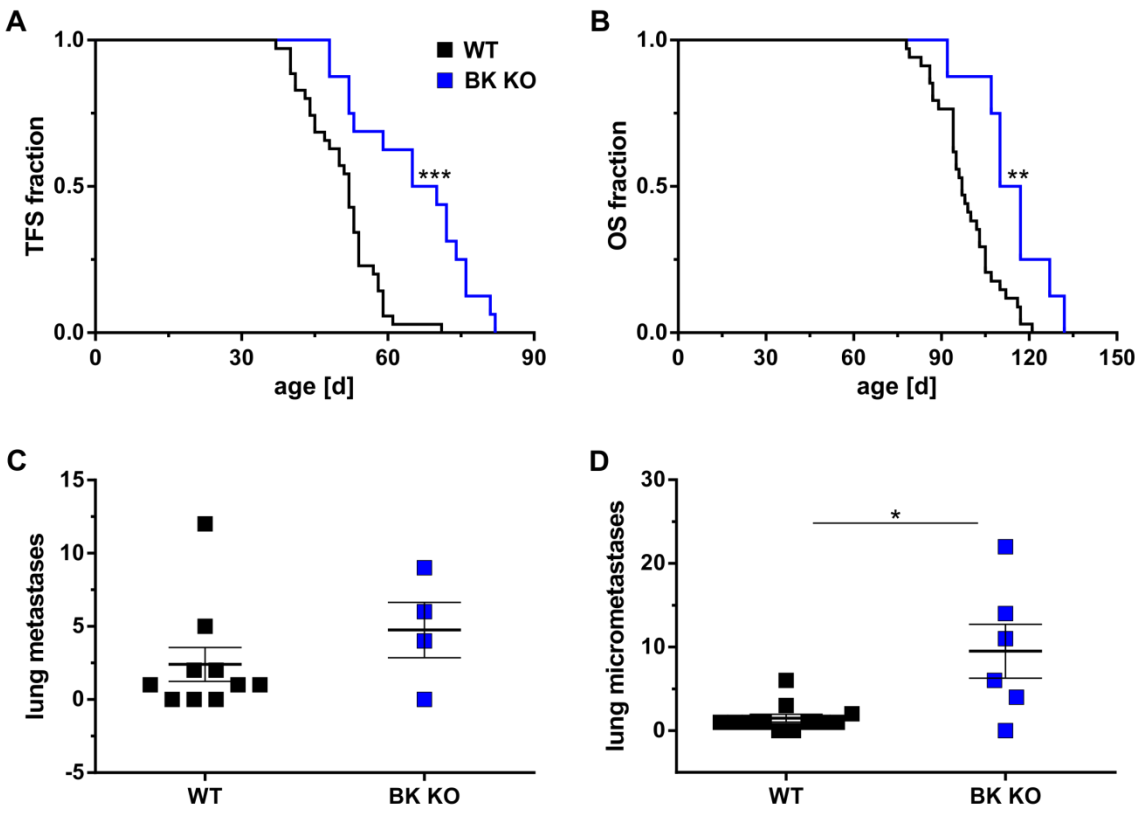

Figure 5.1: Spontaneous tumour development in MMTV-PyMT$^{tg/+}$ WT and BK KO mice
MMTV-PyMT$^{tg/+}$ BK KO mice and their WT littermates were studied for tumour onset and progression using Kaplan-Meier estimates. **(A)** TFS (n = 35 for WT, n = 16 for BK KO) and **(B)** OS (n = 34 for WT, n = 8 for BK KO) were significantly prolonged in log-rank tests of MMTV-PyMT$^{tg/+}$ mice lacking BK (TFS ***p = 0.0004 and OS **p = 0.009). **(C)** Macroscopic metastases were identified in the right lung preserved by Bouin´s fixative (n = 10 for WT and n = 4 for BK KO). The number of lung metastases did not differ significantly between genotypes (Mann-Whitney test). **(D)** To assess micrometastases in the left lung (n = 12 for WT and n = 6 for BK KO), tissue sections were stained with haematoxylin/eosin (M. Sc. thesis by Alice Dragoi). Results revealed a significant higher number of micrometastases in the BK KO compared to the WT genotype (Mann-Whitney test *p < 0.05). **(A - D)** Presented are means ± SEM. *Abbreviations:* Tumour-free survival, TFS; Overall survival, OS.

The MMTV-PyMT$^{tg/+}$ model is described to develop tumours with positive ER and HER2 status in mice. During the course of disease, HER2 expression is known to increase, whereas ER status seems to decline depending on the substrains generated by repetitive breeding of commercially available founders[312]. In order to investigate these widely-used breast tumour markers in the MMTV-PyMT$^{tg/+}$ model with regard to BK channel status, biopsies from both genotypes were assessed. *Esr1*, *Esr2* and *Erbb2* mRNA expression encoding ER-α, ER-β and HER2 were detectable in a qRT-PCR analysis, but this approach did not reveal any genotype-dependent differences (figure 5.2 A). In addition, ER-α protein expression could be detected in both MMTV-PyMT$^{tg/+}$ WT and BK KO tissues (figure 5.2 B), which was confirmed in primary cell cultures derived from these tumours (figures 5.2 C + D).

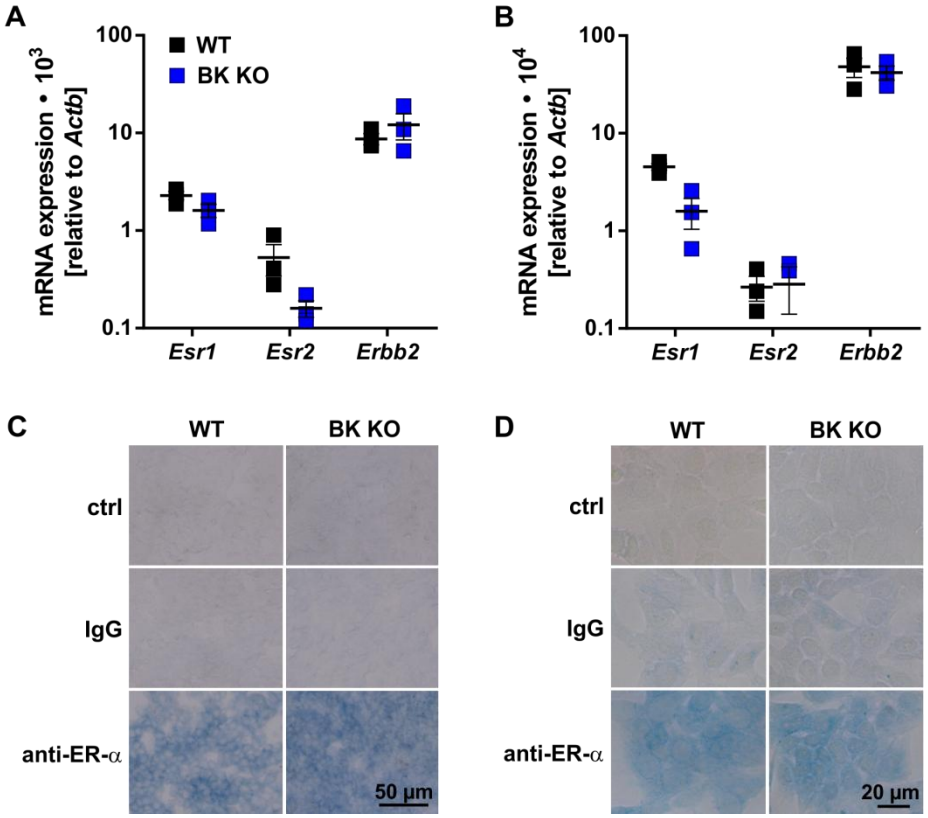

Figure 5.2: ER and HER2 expression in MMTV-PyMT$^{tg/+}$ WT and BK KO tumours and tumour-derived cells *in vitro*

(A) Expression of the ER-α, ER-β and HER2-encoding *Esr1*, *Esr2* and *Erbb2* mRNAs was measured with qRT-PCR and related to *Actb* mRNA expression coding for β-actin. Tissue samples and **(B)** cells derived from the MMTV-PyMT$^{tg/+}$ model expressed both *Esr1* and *Esr2* mRNAs and comparably higher levels of *Erbb2*. Tumour markers did not differ between genotypes albeit expression levels were higher in cells as compared to tissue samples. **(A + B)** Plotted are means ± SEM for n = 3 experiments, which were tested by two-way repeated measures ANOVA and Sidak´s test. **(C)** The positive ER-α status was confirmed at the protein level in tumour tissue and **(D)** cells derived from the MMTV-PyMT$^{tg/+}$ model.

With regard to tumour onset, the role of the immune system is to detect and degrade cells with foreign or aberrant structures, such as infective agents but also malignant cells. Therefore, only tumour cells that manage to avoid immune detection can establish as tumour. Even more, a modulated immune response induced by established tumours can promote their own growth and cancer progression[282]. For this purpose, immune cell infiltration was monitored in MMTV-PyMT$^{tg/+}$ WT and BK KO tumours and surrounding stroma by utilising the CD45 pan leukocyte marker. CD45 expression is a reliable marker found in all nucleated cells of the haematopoietic system and their precursors[358]. As an abundantly expressed glycoprotein with receptor type protein tyrosine phosphatase function in immune cells, CD45 is important for signalling and activation and thus proper immune cell actions[358-360]. CD45-positive cells were detected by immunofluorescence in MMTV-PyMT$^{tg/+}$ tumours of both genotypes with similar frequencies (11.9 ± 2.3 for WT and 8.3 ± 2.8 for BK KO) (figure

5.3 A). In the stroma, the presence of CD45-positive cells was higher in general; however, overall numbers were still comparable between genotypes (26.5 ± 2.7 for WT and 17.5 ± 9.3 for BK KO) (figure 5.3 B).

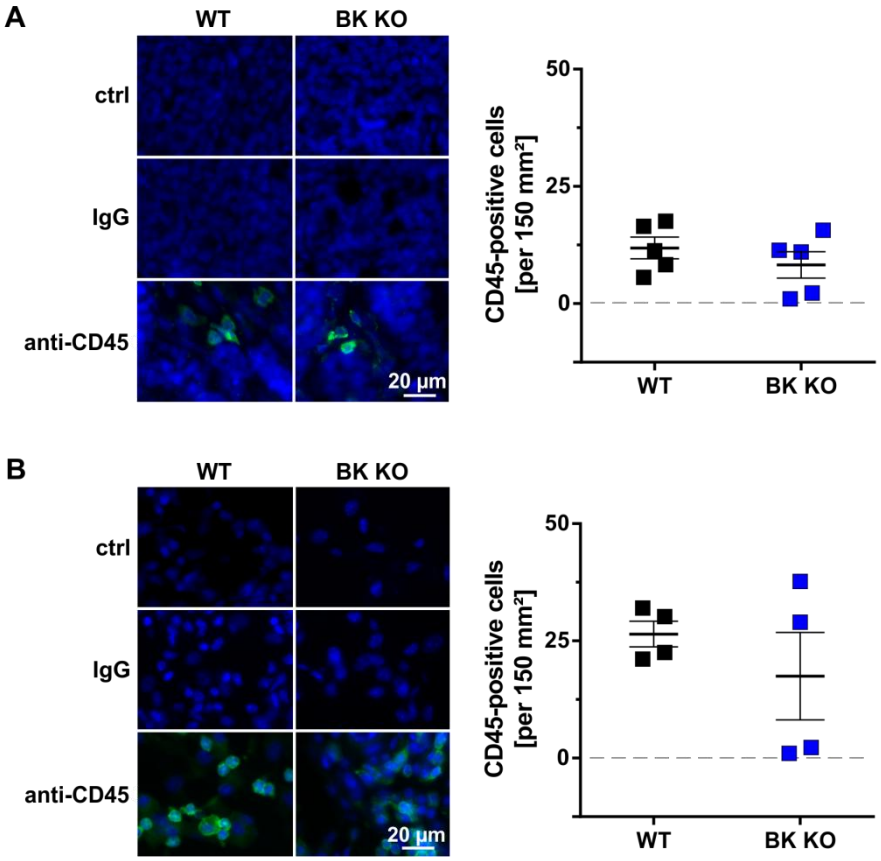

Figure 5.3: CD45-positive immune cell infiltration in MMTV-PyMT$^{tg/+}$ WT and BK KO tumours
Immune cells were detected by immunofluorescence using the CD45 pan leukocyte marker. CD45-positive cells occurred in BK-positive and -negative **(A)** tumour-surrounding stroma and to a minor extent **(B)** within the tumours with no differences between both genotypes, as calculated by unpaired t-test and Mann-Whitney test, respectively. Shown are means ± SEM for n = 5 experiments.

5.1.2 BK channels and tumour growth in MMTV-PyMT$^{tg/+}$ orthotopic breast cancer transplants

Tumour cells isolated from MMTV-PyMT$^{tg/+}$ WT and BK KO tumours were established as primary cell cultures, as described in section 4.2.1. In order to assess in how far a breast tumour-promoting role of the BK channel originates from the tumour tissue or the stroma, an orthotopic breast cancer transplant model was utilised (section 4.1.5). Herein, MMTV-PyMT$^{tg/+}$ WT cells were transplanted in WT and BK KO mice, and MMTV-PyMT$^{tg/+}$ BK KO cells were transplanted in WT mice. The recipient mice received the tumour cells at an age of 12 weeks in order to ensure transplantation in mature breasts (figure 5.4 A). Compared to TFS of MMTV-PyMT$^{tg/+}$ WT cell-transplanted WT mice (10.4 ± 1.5 d), TFS was increased with MMTV-PyMT$^{tg/+}$ BK KO cells transplanted in WT mice (22.9 ± 5.9 d,

HR = 0.35 (CI 0.06 - 0.63)) and it was decreased with MMTV-PyMT$^{tg/+}$ WT cells transplanted in BK KO mice (7.0 ± 0.5 d, HR = 2.48 (CI 1.88 - 19.06)) (figure 5.4 B). In contrast, OS did not differ between groups, but showed a tendency towards increased survival of MMTV-PyMT$^{tg/+}$ BK KO cells growing in WT recipients (62 ± 15 d), whereas OS of MMTV-PyMT$^{tg/+}$ WT cells transplanted into BK KO mice did not differ significantly (52 ± 3 d) compared to MMTV-PyMT$^{tg/+}$ WT cells grown in WT mice (52 ± 6 d) (figure 5.4 C). Moreover, tumour volume increase (figure 5.4 D) as well as macroscopic lung metastasis (0.33 ± 0.21, 0.43 ± 0.30 and 0.14 ± 0.14 metastases/lung for MMTV-PyMT$^{tg/+}$ WT cells in WT mice, MMTV-PyMT$^{tg/+}$ BK KO cells in WT mice and MMTV-PyMT$^{tg/+}$ WT cells in BK KO mice) were not altered between groups (figure 5.4 E).

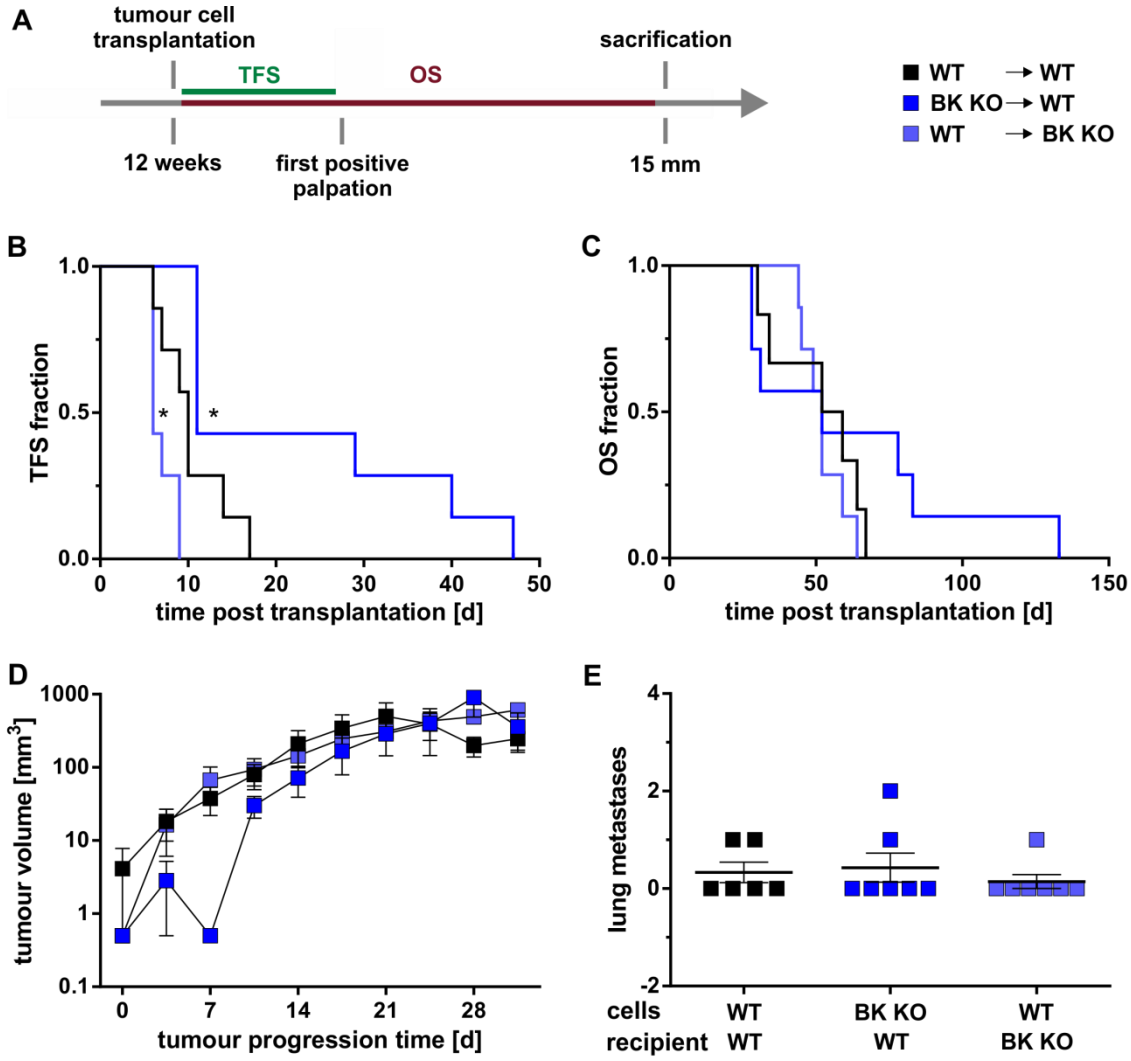

Figure 5.4: Tumour formation and progression after orthotopic allotransplantation of primary MMTV-PyMT$^{tg/+}$ WT and BK KO cells

Genotype-dependent differences in tumour formation and breast cancer progression were studied in WT and BK KO recipients receiving either MMTV-PyMT$^{tg/+}$ WT or BK KO cells as indicated. **(A)** Tumour cells of both genotypes were transplanted in the fourth right mammary gland of WT or BK KO mice. **(B)** Monitoring of tumour onset revealed a shorter log-rank tumour-free survival (TFS) fraction of MMTV-PyMT$^{tg/+}$ WT cells transplanted into BK KO mice and an increased log-rank TFS fraction after MMTV-PyMT$^{tg/+}$ BK KO cell transplantation into WT mice, as compared to the

transplantation of MMTV-PyMT$^{tg/+}$ WT cells into WT recipients. **(C)** Log-rank overall survival (OS) did not differ between test groups. **(D)** After the first palpation of a forming tumour, tumour growth was monitored three times a week with a digital calliper. This analysis did not reveal a significant difference in tumour volume increase between the test groups (two-way ANOVA with Tukey´s test). **(E)** Lung metastasis, as counted macroscopically after fixation in Bouin´s solution, was generally low and not different between groups (Kruskal-Wallis test with Dunn´s post hoc test). **(A - E)** n = 7 experiments were carried out with *p < 0.05. **(D + E)** show means ± SEM.

Haematoxylin/eosin-visualised micrometastases were not observed in the allotransplant model (data not shown). In addition, the infiltration and occurrence of CD45-positive cells in MMTV-PyMT$^{tg/+}$ WT tumours and their stroma were observed in the WT or BK KO recipient mice with no differences between genotypes (data not shown). qRT-PCR analysis for established tumour markers as well as K^+ channels related to BK showed increased *Esr1* and *Kcnmb4* mRNA levels in MMTV-PyMT$^{tg/+}$ BK KO compared to MMTV-PyMT$^{tg/+}$ WT tumours grown in WT mice (supplemental figure 9.4).

5.1.3 BK channel subunits in human breast cancer development and survival

Hence, it was hypothesised that the BK and its assembly with different of the β1-4 and γ1-4 subunits (section 1.3.2) may also represent a predictive marker for the development and survival of human breast cancer. With regard to the BK channel, the following SNPs were used from the BCAC iCOGS array (section 4.5.3) and imputation using linked SNPs: *KCNMA1* (n = 4,014), *KCNMB1* (n = 96), *KCNMB2* (n = 1,731), *KCNMB3* (n = 204), *KCNMB4* (n = 396), *LRRC26* (n = 6), *LRRC38* (n = 272), *LRRC52* (n = 131) and *LRRC55* (n = 51). As shown in figure 5.5, nine of these *KCNMB4* SNPs were the most interesting candidates to significantly associate with breast cancer increasing overall risk (OR 1.06) and in particular risk for developing an ER-positive tumour (OR 1.07), but not an ER-negative tumour. In this context, however, neither the *KCNMB4* nor any of the other BK channel-encoding genes contained an oestrogen response element (ERE) (data not shown). The MAFs of these SNPs in the population were 7 or 19% (figure 5.5 A)[347]. They were located in intron 1-2 and intron 2-3 of the *KCNMB4* gene found on chromosome 12[336,361] (figure 5.5 B). Except for rs66985177 that was independent from the other SNPs, linkage was 87 - 100% between all other SNPs (figure 5.5 C). Modelling protein binding (section 4.5.3) delivered no results for most SNPs except for CCAAT/Enhancer Binding Protein-β in rs61929945 (data not shown).

A

	SNP number	MAF	All		ER^+ BC		ER^- BC	
			OR	p	OR	p	OR	p
1	rs71454274	T = 0.07	1.06	4.6×10^{-5}	1.07	7.2×10^{-6}	1.04	0.14
2	rs61929945	A = 0.07	1.06	4.5×10^{-5}	1.07	7.2×10^{-6}	1.04	0.13
3	rs66985177	T = 0.07	1.06	4.5×10^{-5}	1.07	7.2×10^{-6}	1.04	0.13
4	rs17226248	C = 0.07	1.06	4.3×10^{-5}	1.07	6.9×10^{-6}	1.04	0.13
5	rs12423152	G = 0.19	1.06	1.6×10^{-5}	1.07	7.7×10^{-6}	1.06	0.02
6	rs36123350	T = 0.07	1.06	3.3×10^{-5}	1.07	8.8×10^{-6}	1.05	0.09
7	rs34501109	A = 0.07	1.06	3.3×10^{-5}	1.07	8.7×10^{-6}	1.05	0.09
8	rs7133295	T = 0.19	1.06	1.6×10^{-5}	1.07	7.4×10^{-6}	1.06	0.02
9	rs2870876	T = 0.19	1.06	8.7×10^{-6}	1.07	4.7×10^{-6}	1.06	0.02

B

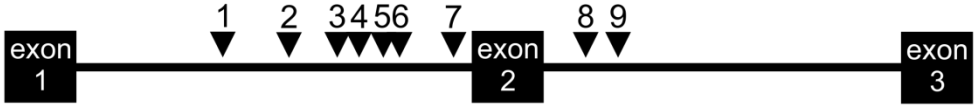

C

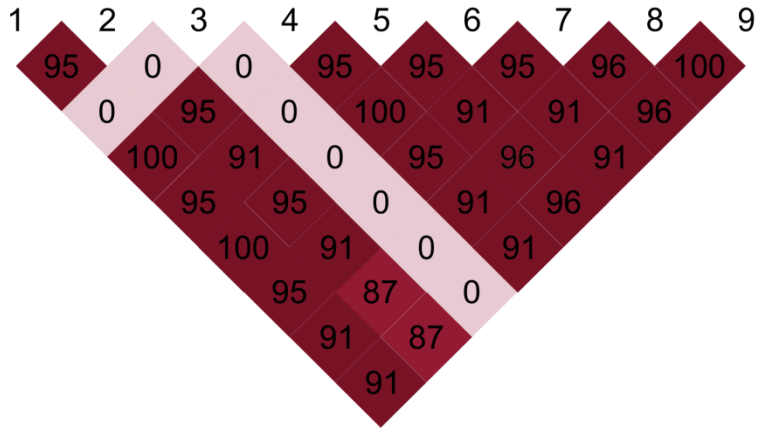

Figure 5.5: Association of *KCNMB4* SNPs with modified breast cancer risk in the BCAC dataset
Genetic variants located in genes that encode the different BK channel subunits were analysed for their association with breast cancer risk. Nine *KCNMB4* SNPS were most interesting for the modification of breast cancer risk due to their impact on ORs and low p-values. **(A)** These SNPs had MAFs of 7 or 19% in the population. All SNPs were found to increase breast cancer risk in general and particularly risk for the development of ER-positive tumours with ORs of 1.06 or 1.07, respectively[347]. **(B)** The SNPs were located in introns 1-2 and 2-3 of the *KCNMB4* gene. **(C)** Linkage analysis revealed linkage disequilibrium values of up to 100% between all SNPs, except for rs66985177 that showed no linkage to any of the other SNPs. *Abbreviations:* Minor allele frequency, MAF; Odds ratio, OR; Single nucleotide polymorphism, SNP.

In order to better elucidate a potential clinical importance of BK channel status, data derived from TCGA (section 4.5.1)[362] and the KM plotter (section 4.5.2)[363] were used to analyse the influence of *KCNMA1* mRNA expression levels on OS of breast cancer patients. Patients were stratified according to *KCNMA1* mRNA expression levels in tumour tissue. Strikingly, the two web tools showed opposing results: Low *KCNMA1* mRNA expression in TCGA with

HR = 6.89, whereas high *KCNMA1* mRNA expression in the KM plotter with HR = 0.58 served as an indicator for prolonged OS (figure 5.6 A + B).

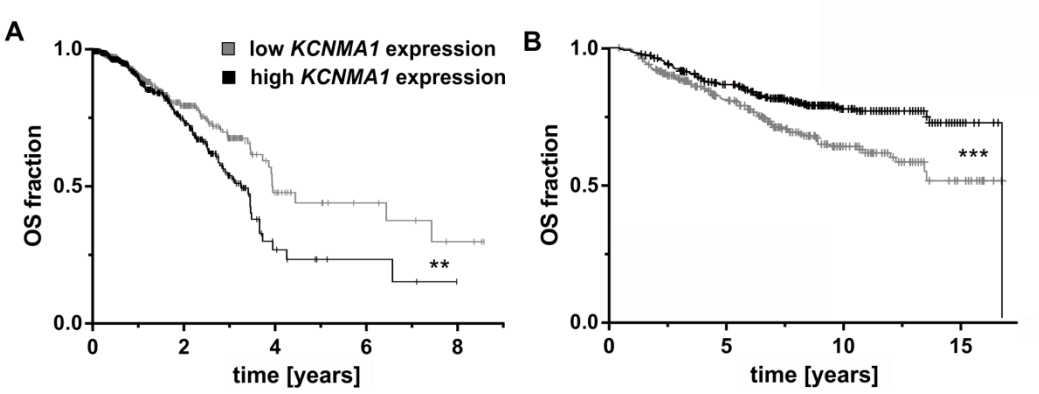

Figure 5.6: OS from breast cancer depends on *KCNMA1* mRNA expression levels

Overall survival (OS) time of patients suffering from breast cancer was analysed by stratification of the patients in two groups according to tumour *KCNMA1* expression levels. **(A)** TCGA estimator (n = 604 with high and n = 345 with low *KCNMA1* mRNA expression) revealed a significant prolonged survival of patients with low *KCNMA1* mRNA expression. **(B)** In contrast, the KM plotter dataset (n = 596 with high and n = 281 with low *KCNMA1* mRNA expression), which had a longer follow-up time, showed the contrary result. Here, high *KCNMA1* mRNA expression was in support of a prolonged OS time. Log-rank tests were performed with **$p < 0.01$ or ***$p < 0.001$.

5.1.4 Expression of BK channel subunits in normal and tumour breast tissue of human patients and cell lines

For a better understanding of tumour-specific roles for the different BK channel subunits described thus far, mRNA expression levels were assessed in healthy breast and breast tumour samples derived from TCGA (section 4.5.1). Gene expression analysis by TCGA had been performed by RNA sequencing to deliver the target genes in fragments as part of the whole, with sample frequencies depending on the length of the individual transcripts. Therefore, fragments per kilobase of transcript per million mapped reads (FPKM) were used as measure of mRNA expression, which considered the different transcript lengths of the target mRNAs[361,364].

Both healthy and tumour tissues included samples that expressed *KCNMA1*, *KCNMB1*, *KCNMB2*, *KCNMB3*, *KCNMB4*, *LRRC26* and *LRRC55* mRNA. *LRRC52* mRNA was absent in healthy and tumour tissues, whereas *LRRC38* mRNA was not available (n.a.). A significant downregulation of *KCNMB1* (statistical rank 13,090 in healthy and rank 9,838 in tumour tissue) and *KCNMB2* (rank 4,605 in healthy and rank 2,117 in tumour tissue) as well as a significant upregulation of *LRRC26* (rank 6,319 in healthy and rank 8,125 in tumour tissue)

was detected (figure 5.7). Therefore, the composition and the interplay of the BK-α pore-forming subunit and its auxiliary BK-β and BK-γ subunits may determine the overall oncogenic effect of the BK channel in breast cancer.

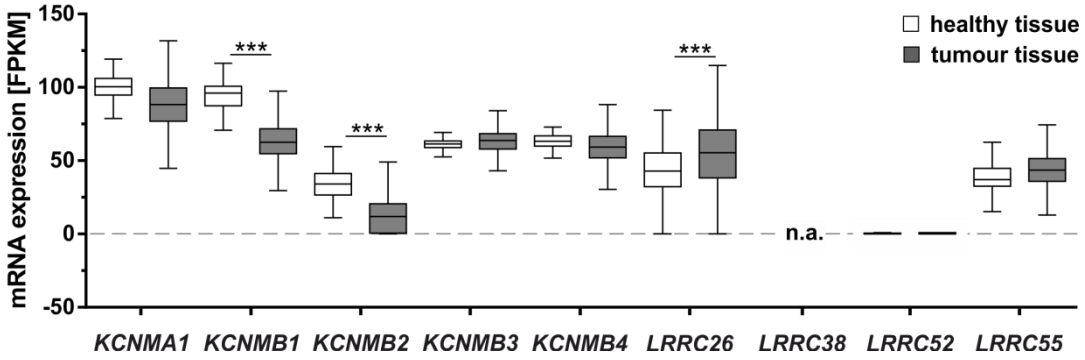

Figure 5.7: BK mRNA expression of normal and tumour breast tissue in TCGA
K_{Ca} mRNA expression levels were compared between breast cancer biopsies (n = 1,095) and biopsies obtained from healthy parts of the patient´s breasts (n = 113). Analysis of breast cancer samples and reference samples revealed decreased *KCNMB1* and *KCNMB2* as well as increased *LRRC26* mRNA expression levels in breast cancer samples compared to healthy samples. Data for *LRRC38* mRNA expression was not available (n.a.) and *LRRC52* mRNA was not expressed. mRNA expression levels obtained by quantitative sequencing, measured as fragments per kilobase of transcript per million mapped reads (FPKM), were not dependent on age, PAM50 classification, ER or PR status, tumour stage or menopausal status. Box plots show means ± SEM with ***p < 0.001 in Kruskal-Wallis test with Dunn´s post hoc analysis.

Besides *in silico* analyses, the K_{Ca} mRNA composition of 15 human normal breast and breast cancer cell lines with different ER, PR and HER2 status was experimentally investigated by Dr. Werner Schroth (AG Prof. Dr. Brauch, IKP Stuttgart) using TaqMan analysis in order to clarify the roles of these channels and their subunits in breast cancer. 11 out of 15 cell lines were positive for BK-α-encoding *KCNMA1* mRNA. Many of the cell lines also expressed *KCNMB3*, *KCNMB4* and *LRRC26* mRNAs, but also *KCNMB1*, *LRRC38*, *LRRC55* and *KCNN1-4* mRNAs were detected. None of the selected cell lines expressed *KCNMB2* mRNA, a subunit that is usually identified in pancreas, kidney, chromaffin cells and brain, nor the testis-specific *LRRC52*[170,365]. Interestingly, *KCNMA1* and *LRRC26* mRNA expression levels were highest in the MDA-MB-453 cell line. In comparison to BK, mRNA expression levels of SK1 - 4 were less prominent in the cell lines analysed (figure 5.8).

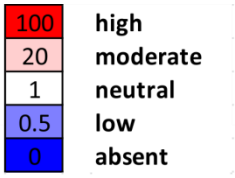

mRNA expression • 10^3 [relative to *GAPDH*]

	ER	PR	HER2	*KCNMA1*	*KCNMB1*	*KCNMB2*	*KCNMB3*	*KCNMB4*	*LRRC26*	*LRRC38*	*LRRC52*	*LRRC55*	*KCNN1*	*KCNN2*	*KCNN3*	*KCNN4*
MCF-10A	-	-	-	7	0.3	0	0	5	0	0	0	0	0	0	0	0
BT-20	-	-	-	14	0	0	0	7	2	1	0	0	3	0	1	1
Hs 578T	-	-	-	28	1	0	0	2	0	0	0	0	0	0	0	0
MDA-MB-157	-	-	-	0	0	0	0	0	0.4	0	0	0	0.3	3	0	0
MDA-MB-231	-	-	-	1	0	0	1	2	1	0	0	0	0	0	0	0
MDA-MB-468	-	-	-	1	1	0	3	4	1	0	0	0	0	0	0	0
MDA-MB-453	-	-	-	450	0	0	1	5	77	0	0	6	0	0	0	0
SK-BR-3	-	-	+	11	1	0	1	2	14	0	0	0	0	0	0.4	0.4
UACC-893	-	-	+	0	0	0	1	0	0.5	0	0	0	2	6	0	0
MDA-MB-134	+	-	-	0	0	0	0	0.3	0	0	0	0	0	2	0	0
MDA-MB-175	+	-	-	8	1	0	0	0	6	0	0	0	1	0	0	0
BT-474	+	+	+	5	0	0	1	0.4	19	0	0	0	0	0	0	0
MDA-MB-361	+	+	+	0	0	0	1	0	0	0	0	0	3	5	0	0
MCF-7	+	+	-	1	0	0	2	5	3	0	0	0	0	3	0	0
T-47D	+	+	-	19	0	0	7	61	12	0	0	0	0	1	0	0

Figure 5.8: K_{Ca} mRNA expression in human normal and tumour breast cell lines
The K_{Ca} expression profile was generated in 14 human breast cancer cell lines plus the non-tumourigenic MCF-10A epithelial cell line. The cell lines tested were chosen independently from their ER, PR and HER2 status. Most cell lines, including MCF-10A, expressed *KCNMA1* encoding BK-α. A majority was also positive for *KCNMB3*, *KCNMB4* and *LRRC26*, whereas *KCNMB1*, *LRRC38*, *LRRC55* as well as *KCNN1 - 4*. *KCNMB2* and *LRRC52* were less frequent or not detected in any of the breast cell lines. From the cell lines investigated, MDA-MB-453 turned out an interesting candidate for subsequent analyses due to its high *KCNMA1* and *LRRC26* mRNA expression levels. The well-studied MCF-7 cell line with its moderate *KCNMA1* and *LRRC26* mRNA levels as well as the MDA-MB-157 cell line, due to its positive *LRRC26* mRNA status while lacking *KCNMA1*, were further selected for further analysis (sections 5.2.2 and 5.2.3).

5.1.5 BK subunit mRNA profile of MMTV-PyMT$^{tg/+}$ tumour-derived tissue sections and cells

The expression of the different K_{Ca} channel members was also measured in the spontaneous MMTV-PyMT$^{tg/+}$ model. For both tissue sections (figure 5.9 A) and tumour cells (figure 5.9 B), BK-α-encoding *Kcnma1* mRNA was detected in the WT but not in the BK KO genotype. Furthermore, both MMTV-PyMT$^{tg/+}$ WT and BK KO samples expressed *Kcnmb1*, *Kcnmb4*, *Lrrc26*, *Kcnn1*, *Kcnn2* and *Kcnn4* coding for BK-β1, BK-β4, BK-γ1, SK1, SK2 and IK protein. In tumour cells, *Lrrc26* and *Kcnn4* (0.003 and 0.019 ± 0.001 for WT, 0.011 and 0.036 ± 0.001 for BK KO) were upregulated in the BK KO genotype (figure 5.9 B). In MMTV-PyMT$^{tg/+}$ WT and BK KO tissue sections, but not in breast tumour-derived cells maintained *in vitro*, *Kcnmb2* and *Kcnn3* mRNAs, coding for BK-β2 and SK3, were identified (figure 5.9 A).

Kcnmb3, *Lrrc38*, *Lrrc52* and *Lrrc55* mRNAs, encoding BK-β3, BK-γ4, BK-γ2 and BK-γ3, were not detected (n.d.) in tissues or cells.

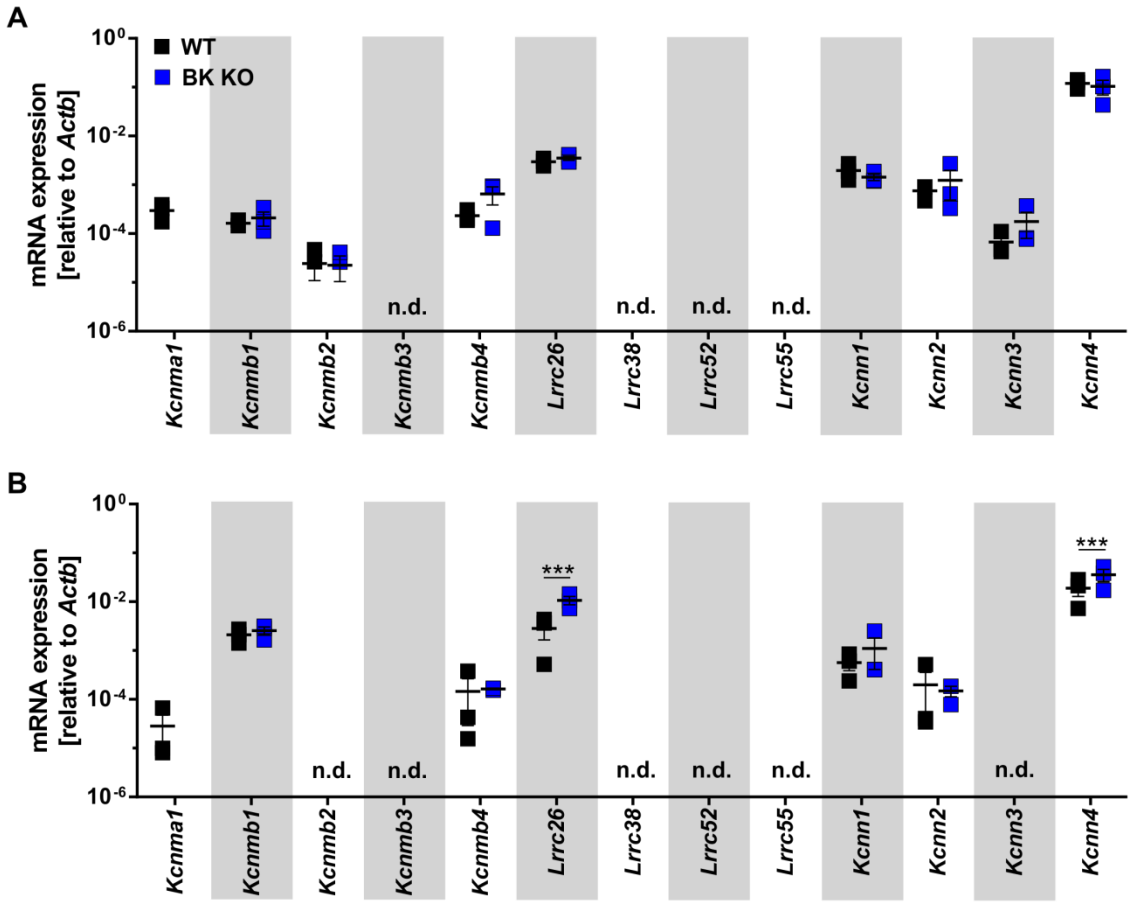

Figure 5.9: K_{Ca} mRNA expression in MMTV-PyMT$^{tg/+}$ WT and BK KO tissues and cells
K_{Ca} mRNA levels normalised to the amount of *Actb* mRNA were measured with qRT-PCR in MMTV-PyMT$^{tg/+}$ WT and BK KO samples. **(A)** *Kcnma1* mRNA was detectable in MMTV-PyMT$^{tg/+}$ WT but not in MMTV-PyMT$^{tg/+}$ BK KO tissue samples. With regard to the described BK-α accessory subunits, *Kcnmb1*, *Kcnmb2*, *Kcnmb4* and *Lrrc26* mRNAs, were measured. None of the other BK channel-encoding mRNAs, namely *Kcnmb3*, *Lrrc38*, *Lrrc52* and *Lrrc55*, were detected (n.d.). Further, both genotypes showed mRNA expression for all members that could be attributed to the SK family of channels, i.e. *Kcnn1*, *Kcnn2*, *Kcnn3* and *Kcnn4*. **(B)** MMTV-PyMT$^{tg/+}$ WT and BK KO cells showed a similar expression pattern when compared to tissues meaning *Kcnma1* mRNA was present in WT only, whereas *Kcnmb1*, *Kcnmb4*, *Lrrc26*, *Kcnn1*, *Kcnn2* as well as *Kcnn4* mRNAs were expressed in both genotypes. Besides, *Kcnmb3*, *Lrrc38*, *Lrrc52* and *Lrrc55* mRNAs were neither detectable in MMTV-PyMT$^{tg/+}$ cells. However, unlike tissue mRNA expression, *Kcnmb2* and *Kcnn3* mRNAs were not found in cells derived from the MMTV-PyMT$^{tg/+}$ mouse model. **(A + B)** Plotted are means ± SEM of n = 3 experiments with ***$p < 0.001$ in two-way repeated measures ANOVA and Sidak´s test.

5.1.6 BK-α and BK-γ1 control murine and human breast tumour cell proliferation

Proliferation status of tissue sections and cells derived from spontaneously developed MMTV-PyMT$^{tg/+}$ WT and BK KO tumours was assessed by Ki-67 (sections 4.2.4 and 4.4.4). In contrast to negative control (ctrl) and IgG isotype ctrl, MMTV-PyMT$^{tg/+}$ WT tissues stained

positive for Ki-67, whereas MMTV-PyMT$^{tg/+}$ BK KO tissues were much less abundant for Ki-67 (figure 5.10 A and supplemental figure 9.4). Moreover, the fraction of Ki-67-positive cells was higher in MMTV-PyMT$^{tg/+}$ WT (60.1 ± 5.1, 66.2 ± 6.0 or 74.3 ± 4.0%) than in MMTV-PyMT$^{tg/+}$ BK KO (39.2 ± 1.8, 42.3 ± 1.9 or 40.0 ± 2.8%) cells, when the tumour cells were restimulated with serum-containing media for 24, 48 or 72 h following 72 h of serum starvation (figure 5.10 B). Importantly, the BK KO genotype did not interfere with *Mki67* gene expression encoding Ki-67 in both MMTV-PyMT$^{tg/+}$ WT and BK KO tissues and cells (supplemental figure 9.5).

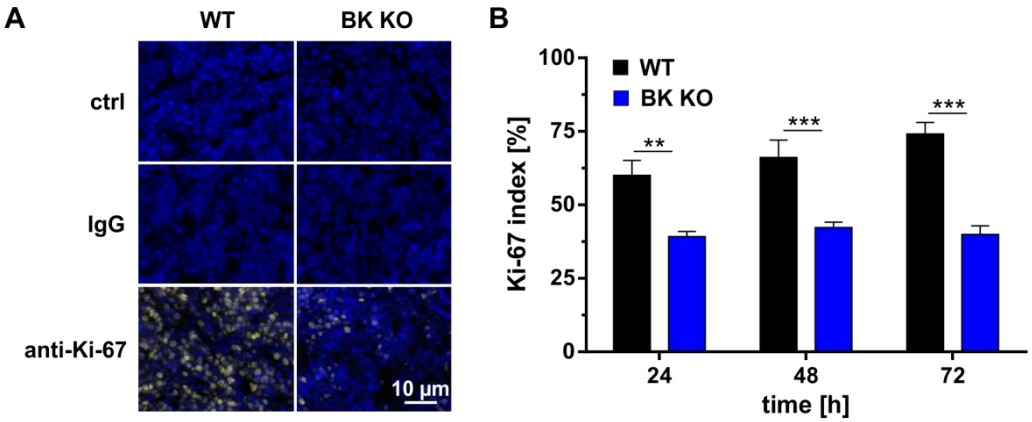

Figure 5.10: Ki-67 expression in MMTV-PyMT$^{tg/+}$ WT and BK KO tumours
Proliferation was assessed in tissue sections and cultured primary cells derived from MMTV-PyMT$^{tg/+}$ WT and BK KO tumours. **(A)** Ki-67-positive cells were more frequently detected in MMTV-PyMT$^{tg/+}$ WT in comparison to the BK-negative tumour tissue (n = 4). **(B)** The fraction of Ki-67-positive cells was studied in cultured MMTV-PyMT$^{tg/+}$ WT and BK KO cells after serum starvation for 72 h and restimulation with serum-containing medium for 24, 48 or 72 h, respectively. Again, absence of BK resulted in a decreased Ki-67-positive fraction as compared to MMTV-PyMT$^{tg/+}$ WT cells. Bar graphs show means ± SEM of n = 6 experiments with **p < 0.01 and ***p < 0.001 in a one-way ANOVA with Bonferroni correction.

In general, BK channel activity is strongly voltage-dependent and can be further increased by $[Ca^{2+}]_i$. Non-excitable cells such as epithelial-derived breast tumour cells possess only low negative membrane potentials[366,367]. However, accessory BK channel subunits and especially BK-γ1 can shift BK channel open probability towards more negative membrane potentials. The BK-γ1 subunit thus seemed an interesting candidate to study for its impact on tumour cell proliferation in the presence and absence of BK-α[170]. Therefore, *Lrrc26* coding for BK-γ1 was silenced with siRNA in MMTV-PyMT$^{tg/+}$ WT and BK KO cells (si*Lrrc26*). Knockdown efficacy (supplemental figure 9.6) and proliferation were studied and related to a *non-targeting* siRNA (si*NT*) ctrl. A possible effect of si*NT* treatment was assessed by parallel analysis of ctrl samples, which were treated as all other experimental groups except for the siRNA. To control for off-target effects of the knockdown, siRNA directed against

glyceraldehyde-3-phosphate dehydrogenase (si*Gapdh*) complemented the experimental setup (see section 4.2.4).

The relative proliferation rate of MMTV-PyMT$^{tg/+}$ WT and BK KO cells in the different treatment groups was monitored in grid slides 0, 24, 48 and 72 h after restimulation. si*NT* and ctrl conditions did not differ with respect to normalised proliferation rate within genotype. At 48 and 72 h, however, the relative proliferation rate was significantly lower in MMTV-PyMT$^{tg/+}$ BK KO ctrl (1.47 ± 0.19 and 2.10 ± 0.23 fold) and si*NT*-treated cells (1.46 ± 0.19 and 1.91 ± 0.12 fold) than in MMTV-PyMT$^{tg/+}$ WT si*NT*-treated cells (2.44 ± 0.45 and 3.87 ± 0.85 fold). The decreased proliferation rate evoked by BK-α genetic ablation confirms previous cell behaviour analyses in the MMTV-PyMT$^{tg/+}$ model[315]. The BK-α-dependent proliferation phenotype was mimicked by knockdown of *Lrrc26* in MMTV-PyMT$^{tg/+}$ WT cells at 48 and 72 h (1.30 ± 0.31 and 1.78 ± 0.39 fold, respectively) as compared to the si*NT*-treated condition. Importantly, the proliferation rate according to si*NT* or si*Lrrc26* treatment did not differ in the BK KO genotype suggesting that *Lrrc26* modulates cell division via BK-α (figure 5.11 A). Moreover, *Lrrc26* mRNA expression did not significantly differ between ctrl and si*NT* in both genotypes (data not shown). The proliferation effects observed in the grid slides could be confirmed with regard to Ki-67 status. Ki-67 index after si*NT* treatment did not significantly differ from ctrl in both genotypes (77.0 ± 2.3% for ctrl and 67.6 ± 3.5% for si*NT* in WT, 46.8 ± 2.7% for ctrl and 43.8 ± 4.3% for si*NT* in BK KO). Compared to MMTV-PyMT$^{tg/+}$ WT si*NT*, MMTV-PyMT$^{tg/+}$ BK KO ctrl and si*NT*-treated cells revealed a lower Ki-67 index. Importantly, the number of Ki-67-positive cells after si*Lrrc26* treatment in MMTV-PyMT$^{tg/+}$ WT cells was significantly decreased (46.0 ± 6.5%) compared to si*NT* treatment. Interestingly, the Ki-67 index in the WT and BK KO genotypes after si*Lrrc26* treatment did not significantly differ from each other and overall levels were comparable to MMTV-PyMT$^{tg/+}$ BK KO ctrl and si*NT* (figure 5.11 B). Potential off-target effects of *Lrrc26* knockdown on the expression levels of all other BK subunits known so far were analysed by qRT-PCR. Compared to the si*NT* group, *Kcnmb4* was significantly upregulated in si*Lrrc26*-treated MMTV-PyMT$^{tg/+}$ WT cells (2.38 ± 0.44 fold) while *Kcnmb1* mRNA expression was unaltered (1.15 ± 0.44 fold) (figure 5.11 C). With regard to the other BK channel subunits, namely *Kcnmb2*, *Kcnmb3*, *Lrrc38*, *Lrrc52* and *Lrrc55*, mRNA expression was not induced by any of the siRNA treatment conditions in both genotypes. Within genotype, *Lrrc26* mRNA expression was not significantly different in ctrl and si*NT*-treated MMTV-PyMT$^{tg/+}$ WT and BK KO cells (data not shown).

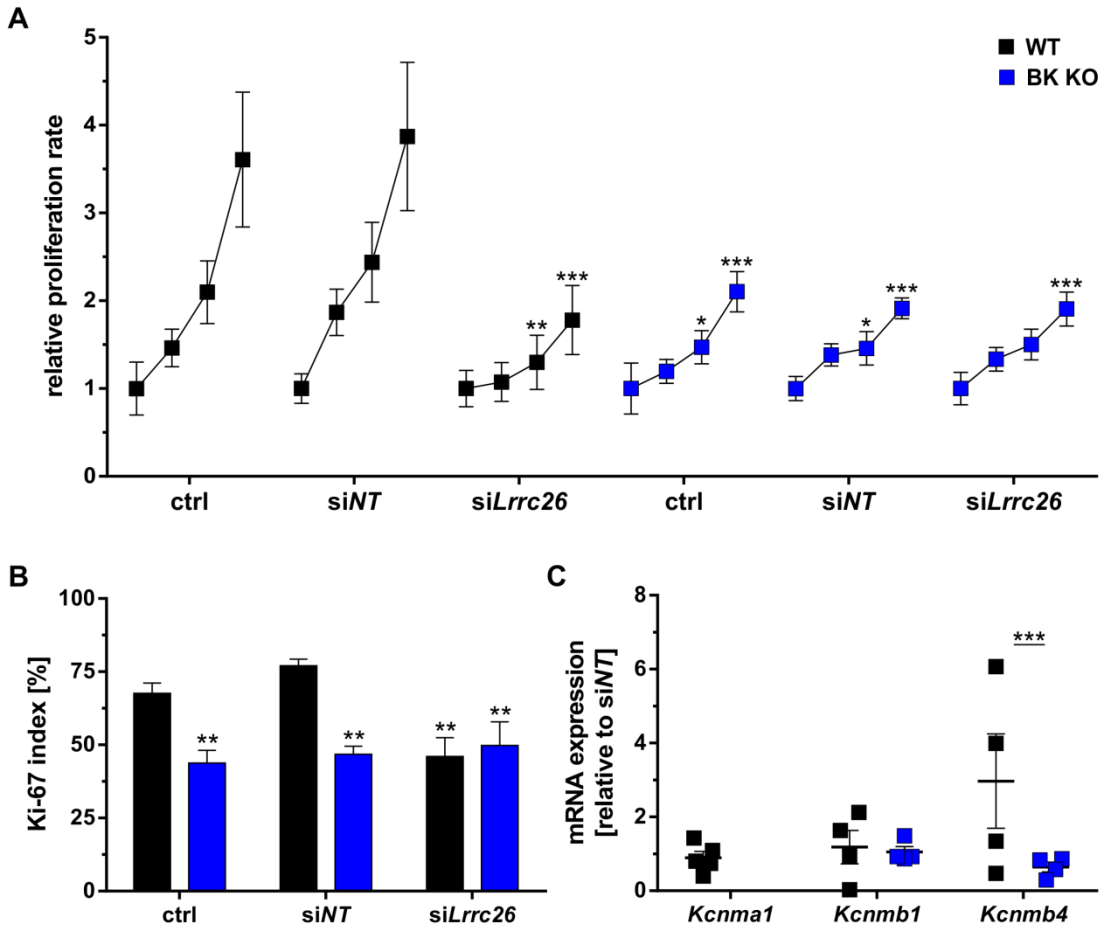

Figure 5.11: Proliferation of MMTV-PyMT$^{tg/+}$ WT and BK KO cells treated with *Lrrc26* siRNA
The BK-γ1 subunit transcript was knocked down with siRNA specifically targeting *Lrrc26* (si*Lrrc26*) in MMTV-PyMT$^{tg/+}$ WT and BK KO cells. Cultured tumour cells were transfected with siRNA during 72 h of serum starvation and the procedure was repeated for the 72 h period of restimulation with serum-supplemented medium. Proliferation of MMTV-PyMT$^{tg/+}$ WT and BK KO cells treated with si*NT* was used as reference. **(A)** The proliferation rate was studied in 8-well grid chamber slides 24, 48 and 72 h post restimulation and related to 0 h with each of the four time points in the diagram interconnected with lines. Proliferation of si*NT*-treated cells of both genotypes did not differ to their corresponding ctrl. However, the proliferation rate of MMTV-PyMT$^{tg/+}$ WT, but not that of BK KO cells was decreased by si*Lrrc26 (*two-way ANOVA with Sidak´s test). **(B)** The Ki-67 index after siRNA treatment was analysed 72 h after restimulation of cells grown in 8-well chamber slides in the presence or absence of siRNA. si*NT* treatment did not alter Ki-67 index when compared to ctrl treatment in both genotypes. si*Lrrc26* reduced the fraction of Ki-67-positive MMTV-PyMT$^{tg/+}$ WT cells to BK KO levels (by two-way repeated measures ANOVA and Tukey´s test). **(C)** Potential effects of si*Lrrc26* on the expression of representative BK subunit mRNAs were investigated in MMTV-PyMT$^{tg/+}$ WT and BK KO cells. Per genotype, 50,000 cells were seeded in each well of a 24-well plate in duplicate and treated as described above. Subsequent RNA analyses were performed 72 h after restimulation. *Kcnmb4* mRNA was upregulated in si*Lrrc26*-treated MMTV-PyMT$^{tg/+}$ WT cells, whereas *Kcnmb1* mRNA expression was not altered (Wilcoxon signed-rank tests). **(A - C)** Presented are means ± SEM. *p < 0.05, **p < 0.01 and ***p < 0.001 refer to 0 h MMTV-PyMT$^{tg/+}$ WT cells treated with si*NT* or were drawn between groups as indicated in n = 5 experiments.

In order to confirm these results and to examine the translational potential, the human MDA-MB-453 cell line was studied, which expresses high levels of BK-α and BK-γ1 mRNAs.

To test if BK-α and BK-γ1 mRNAs, namely *KCNMA1* and *LRRC26*, are crucial for the proliferative behaviour of MDA-MB-453 cells, the subunits were knocked down with siRNA (si*KCNMA1* and si*LRRC26*). The experiment was conducted as described in section 4.2.4 including ctrl, si*NT* and *GAPDH* siRNA (si*GAPDH*). Knockdown efficacies are shown in supplemental figure 9.7.

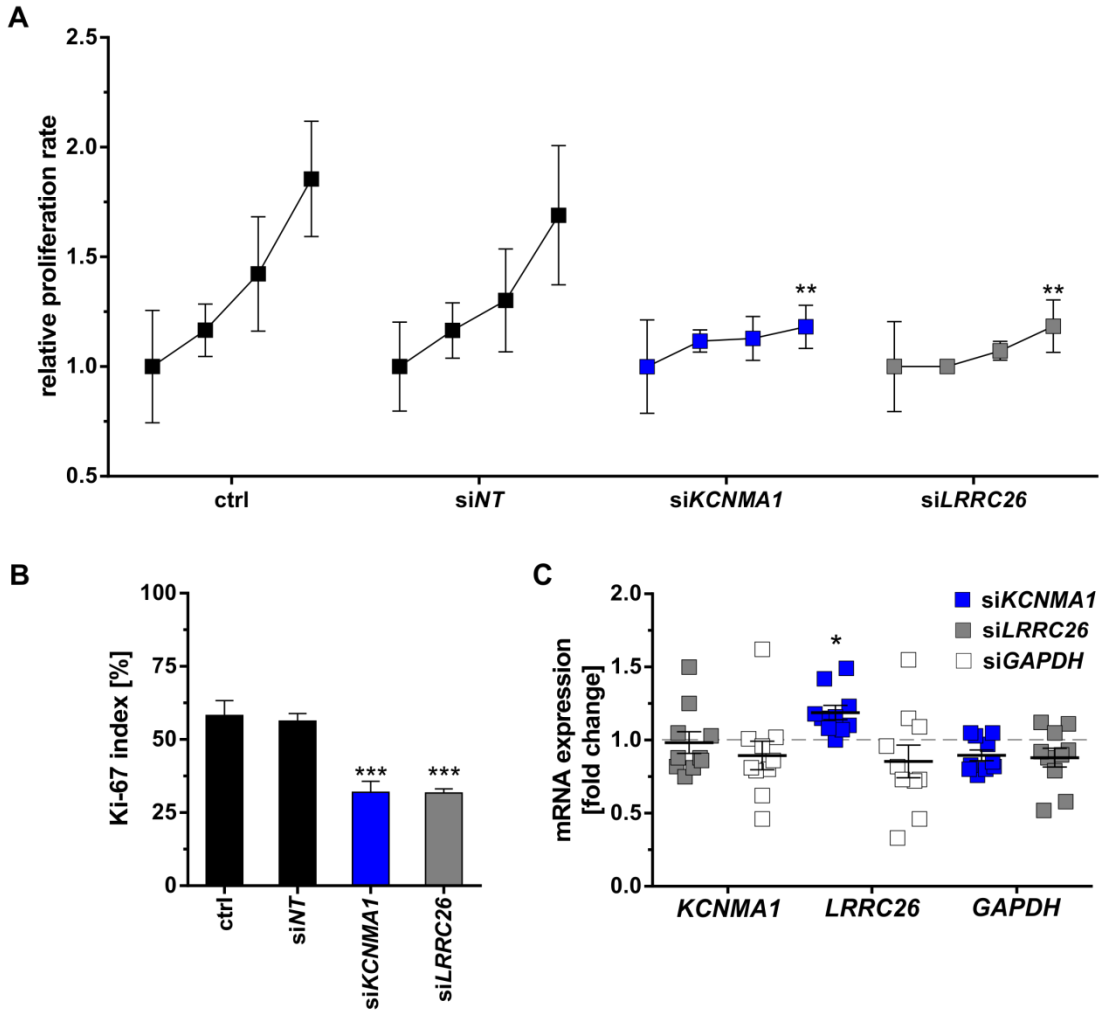

Figure 5.12: Proliferation response of MDA-MB-453 cells to siRNA-mediated depletion of *KCNMA1* or *LRRC26*

KCNMA1 and *LRRC26* knockdown experiments confirmed that the highly expressed BK-α and BK-γ1 subunits are required for MDA-MB-453 cell proliferation. **(A + B)** si*KCNMA1* or si*LRRC26* significantly decreased proliferation rates (two-way repeated measures ANOVA and Tukey´s test) and Ki-67 index (one-way ANOVA with Holm-Sidak test) as compared to si*NT* after 72 h (n = 5). **(C)** mRNAs isolated from **(A + B)** were pooled to investigate potential compensatory effects due to silencing of *KCNMA1*, *LRRC26* or the positive reference *GAPDH*. *KCNMA1* was upregulated in *LRRC26*-depleted cells (two-way repeated measures ANOVA with Dunnett´s test). *p < 0.05, **p < 0.01 and ***p < 0.001 refer to si*NT* treatment **(A + B)** at 0 h or **(C)** at 72 h or were drawn between groups as indicated.

The grid-based proliferation experiments revealed no difference between ctrl and si*NT*, whereas si*KCNMA1* and si*LRRC26* treatments resulted in significantly reduced proliferation rates. 72 h post restimulation, the relative proliferation rate in si*KCNMA1*- and

si*LRRC26*-treated MDA-MB-453 cells was similar (1.18 ± 0.10 fold and 1.18 ± 0.12 fold) and significantly lower compared to si*NT* treatment (1.69 ± 0.32 fold). Identical proliferation rates of si*KCNMA1*- and si*LRRC26*-depleted cells imply that BK-α and BK-γ1 subunits are essential in order to ensure proper BK channel function in the MDA-MB-453 cell line (figure 5.12 A). The Ki-67 index was investigated to provide additional information about the si*KCNMA1*- and si*LRRC26*-mediated effects on cell division in MDA-MB-453 cells. Similar fractions of Ki-67 were observed in ctrl (58.2 ± 5.1%) and si*NT* (56.3 ± 2.6%) groups, whereas Ki-67-positive MDA-MB-453 cells were reduced by si*KCNMA1* (32.0 ± 3.8%) or si*LRRC26* (31.7 ± 1.5%) (figure 5.12 B). *KCNMA1*, *LRRC26* and *GAPDH* mRNA expression levels were examined at 72 h in grid slide and Ki-67 siRNA experiments. As expected, *KCNMA1*, *LRRC26* and *GAPDH* mRNA expression was significantly downregulated after application of the respective siRNAs. Moreover, *LRRC26* mRNA was significantly upregulated (1.19 ± 0.09 fold) in si*KCNMA1*-treated MDA-MB-453 cells compared to si*NT* (figure 5.12 C).

5.2 Anti-/oestrogens and BK channels in breast cancer

The tumour-promoting role of BK could be confirmed in the MMTV-PyMT$^{tg/+}$ mouse model (figure 5.1 and figure 5.4) and in primary cells derived thereof (figure 5.11) as well as in human MDA-MB-453 breast tumour cells (figure 5.12). However, the mechanism of BK channel contribution to breast tumour cell proliferation remained unclear so far. Previous work suggests that selected hormones and anti-oestrogens at different concentrations control BK and thereby modulate breast cancer proliferation[202,207,220]. The herein performed SNP analysis in the BCAC dataset pointed into the same direction suggesting *KCNMB4* gene association with breast cancer increasing overall risk (OR 1.06) and ER-positive tumour risk (OR 1.07) (figure 5.5). In the following series of experiments, the interplay between ER status, ER-modulating agents and hormones as well as the BK channel complex was investigated with regard to the proliferative behaviour of MMTV-PyMT$^{tg/+}$ WT and BK KO cells as well as in selected human breast cancer cell lines, namely MDA-MB-453, MCF-7 and MDA-MB-157 cells.

5.2.1 Serum content as determinant of breast tumour cell proliferation via the BK

In the MMTV-PyMT$^{tg/+}$ model, proliferation of WT and BK KO cells in grid dishes was monitored 0, 24, 48 and 72 h after serum starvation and restimulation with 5% CCS or 5% FCS supplemented to the cell culture medium as well as in the absence of serum to resemble a prolonged period of serum starvation. As expected, the relative proliferation rate

was highest in FCS-stimulated MMTV-PyMT$^{tg/+}$ WT cells (1.00 ± 0.09, 1.87 ± 0.19, 3.78 ± 0.55 and 6.41 ± 1.06 fold for 0, 24, 48 and 72 h). For comparison, a significantly lower relative proliferation rate during the time course was seen in CCS (1.00 ± 0.13, 1.62 ± 0.12, 2.17 ± 0.22 and 2.85 ± 0.51 fold for 0, 24, 48 and 72 h) and no serum-treated (1.00 ± 0.18, 0.84 ± 0.06, 0.76 ± 0.05 and 0.73 ± 0.07 fold for 0, 24, 48 and 72 h) MMTV-PyMT$^{tg/+}$ WT cells, but also in MMTV-PyMT$^{tg/+}$ BK KO cells treated with FCS (1.00 ± 0.09, 1.55 ± 0.10, 2.39 ± 0.23 and 3.41 ± 0.44 fold for 0, 24, 48 and 72 h), CCS (1.00 ± 0.08, 1.60 ± 0.09, 2.07 ± 0.19 and 2.32 ± 0.37 fold for 0, 24, 48 and 72 h) or no serum (1.00 ± 0.16, 0.92 ± 0.06, 0.80 ± 0.06 and 0.72 ± 0.06 fold for 0, 24, 48 and 72 h) (figure 5.13 A).

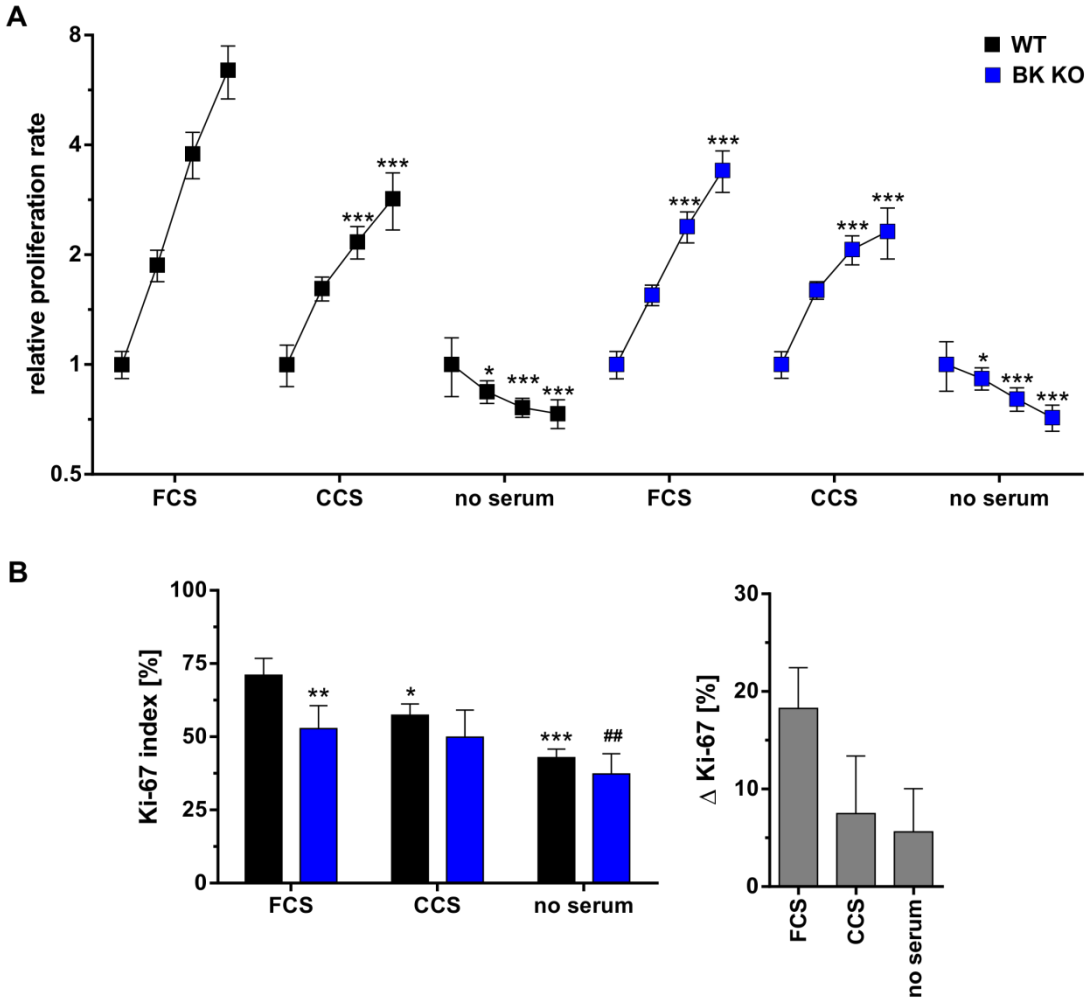

Figure 5.13: Serum-derived growth factors modify MMTV-PyMT$^{tg/+}$ WT and BK KO cell proliferation

MMTV-PyMT$^{tg/+}$ WT and BK KO cells were seeded in grid dishes or 8-well chamber slides. After 24 h of adhesion, cells were starved from serum for 72 h before restimulated with medium supplemented with either 5% FCS, 5% CCS or without serum. **(A)** During proliferation induced by restimulation, cell numbers were determined as described (figure 4.4) in grid dishes at 0, 24, 48 and 72 h as shown by squares and interconnected lines (n = 7, *p < 0.05, **p < 0.01 and ***p < 0.001 indicate significant difference compared to MMTV-PyMT$^{tg/+}$ WT FCS at the respective time points). **(B)** Ki-67 index was assessed 72 h after restimulation (n = 6, *p < 0.05, **/##p < 0.01 and ***p < 0.001 show significant difference compared to FCS treatment of MMTV-PyMT$^{tg/+}$ WT or BK KO cells, respectively).

(A + B) Both approaches revealed a higher proliferation status in MMTV-PyMT$^{tg/+}$ WT and lower levels in MMTV-PyMT$^{tg/+}$ BK KO cells treated with FCS. Cells growing in CCS-supplemented medium proliferated moderately and, importantly, genotype-dependent growth differences were abolished in the presence of CCS. In the absence of serum, progressive cell depletion was observed in the grid dishes in both genotypes, whereas a low fraction of cells was still Ki-67-positive probably representing cells arrested in G_1. Presented are means ± SEM and statistics were performed with two-way repeated measures ANOVA and Tukey´s test for the relative proliferation rate and Ki-67 index and with a one-way ANOVA with Tukey´s test for ∆ Ki-67.

The Ki-67 index was also highest MMTV-PyMT$^{tg/+}$ WT cells treated with FCS (71.1 ± 5.7%). A significantly lower Ki-67 index was found after 72 h of CCS treatment (57.3 ± 3.9%) or without serum (42.9 ± 2.9%) in the WT genotype, but also in MMTV-PyMT$^{tg/+}$ BK KO cells treated with FCS (52.8 ± 3.2%). In comparison with MMTV-PyMT$^{tg/+}$ BK KO cells treated with FCS, these treated with CCS (49.9 ± 3.8%) showed no significant different Ki-67 index, but did those treated without serum (37.3 ± 2.8%). Importantly, the calculated difference between MMTV-PyMT$^{tg/+}$ WT and BK KO cells with respect to the Ki-67 fraction (∆ Ki-67) was high in FCS (18.3 ± 4.2%) and much lower in CCS (7.5 ± 5.9%) and serum-free (5.6 ± 4.4%) conditions, but it was no significantly different between treatments (figure 5.13 B). This suggests the growth factor content in the serum as determinant of proliferation in a BK channel-dependent manner.

5.2.2 Influence of BK channel status on hormone-stimulated breast cancer cell proliferation

To clarify the interplay between breast cancer-associated hormones, BK status and proliferation, E2 and E2-BSA representing an E2 membrane-impermeable form bound to BSA, as well as progesterone and testosterone prepared at different concentrations were applied in CCS-containing media to serum-starved MMTV-PyMT$^{tg/+}$ WT and BK KO cells in grid dishes for 72 h comparing the different treatments to the CCS ctrl. As in previous experiments, FCS caused a significantly increased proliferation rate in MMTV-PyMT$^{tg/+}$ WT (2.20 ± 0.19 fold) as compared to BK KO cells (1.37 ± 0.16 fold). Accordingly, in the WT genotype, the physiological 0.1 nM concentration of E2 (1.39 ± 0.09 fold) and E2-BSA (1.44 ± 0.07 fold) as well as all testosterone concentrations tested (1.63 ± 0.11, 1.53 ± 0.14, 1.48 ± 0.10 and 1.50 ± 0.07 fold for 0.01, 0.1, 1 and 10 nM) significantly increased the relative proliferation rate. In contrast, none of these treatment conditions enhanced proliferation of BK-negative breast tumour cells (figure 5.14 A). These results were emphasised with regard to the Ki-67 status of MMTV-PyMT$^{tg/+}$ WT and BK KO cells. In detail, a significantly increased Ki-67 index was detected in MMTV-PyMT$^{tg/+}$ WT cells treated with FCS (1.29 ± 0.06 fold), 10 nM E2 (1.35 ± 0.06 fold) and 0.1 nM E2-BSA (1.30 ± 0.10 fold).

Compared to the BK KO genotype, MMTV-PyMT$^{tg/+}$ WT cells showed an increased Ki-67 index with 0.1 nM E2-BSA, 0.1 and 10 nM testosterone (figure 5.14 B).

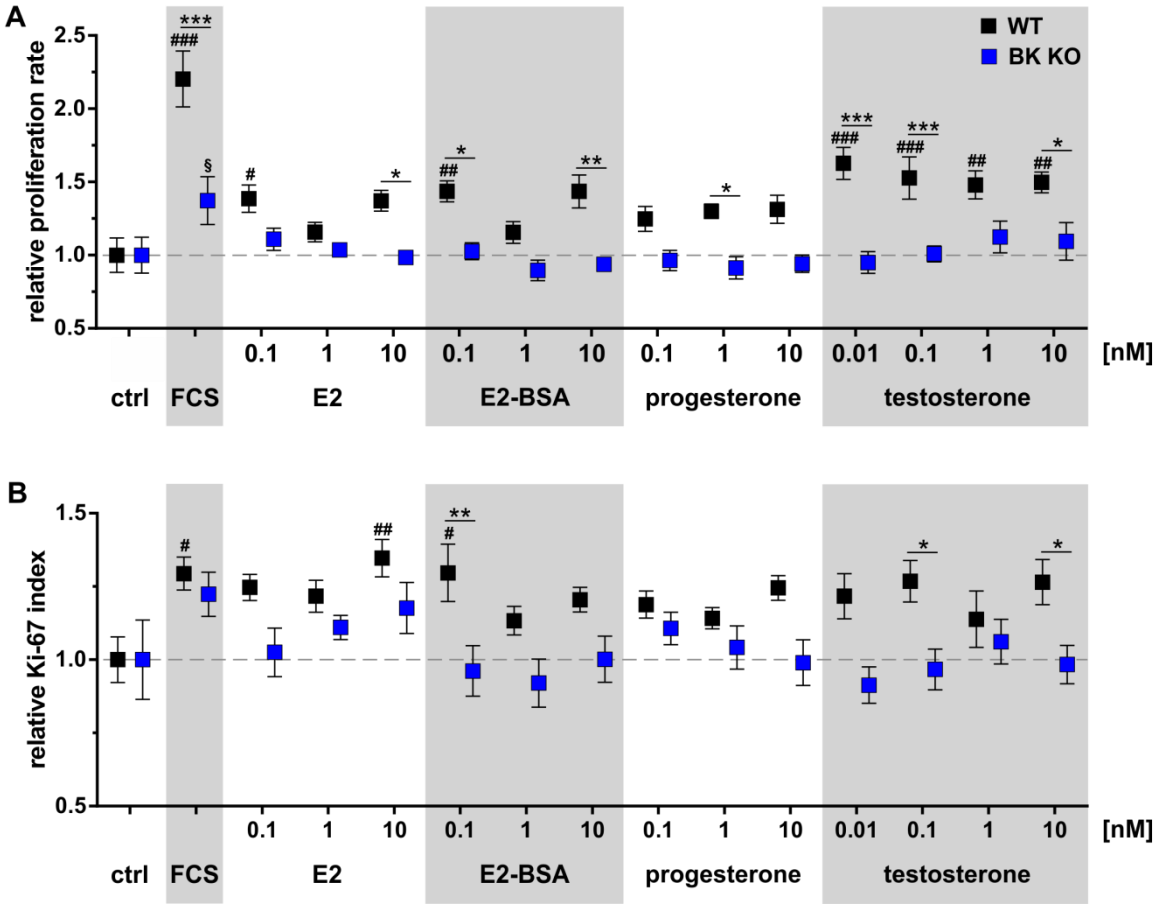

Figure 5.14: MMTV-PyMT$^{tg/+}$ WT and BK KO cell proliferation in response to growth factors
MMTV-PyMT$^{tg/+}$ WT and BK KO cells were seeded at a density of 80,000 in grid dishes as well as 50,000 in 8-well chamber slides. After 24 h, tumour cells were serum-starved for 72 h and then were restimulated for 72 h with different growth factor concentrations, as compared to ctrl treatment with CCS only. **(A)** The relative proliferation rate was assessed by the number of tumour cells after 72 h compared to initial cell numbers (n = 7). FCS treatment induced a significant increase of proliferation in both genotypes. The effect was significantly higher in MMTV-PyMT$^{tg/+}$ WT than in BK KO cells. Moreover, low concentrations of E2, its membrane-impermeable form E2-BSA, progesterone and testosterone stimulated proliferation of MMTV-PyMT$^{tg/+}$ WT cells, whereas BK-negative breast tumour cells did not respond to any of these treatments. **(B)** The results obtained in grid proliferation experiments were confirmed or at least showed similar tendencies with regard to Ki-67 index in MMTV-PyMT$^{tg/+}$ WT compared to BK KO cells (n = 6). **(A + B)** Means ± SEM are presented with */#/§p < 0.05, **/##p < 0.01, ***/###p < 0.001 show significant differences as indicated, according to MMTV-PyMT$^{tg/+}$ WT or MMTV-PyMT$^{tg/+}$ BK KO ctrl, respectively, in two-way ANOVA with Sidak´s test.

To corroborate these findings and to further test the relevance of BK's role for hormone-stimulated proliferation, several human breast cancer cell lines were analysed. In order to avoid or minimise hormone signalling via ERs, the ER-negative MDA-MB-453 apocrine breast cancer cell line, which expresses high BK-α and BK-γ1 levels, was studied for their response to a panel of sex hormones. As negative ctrl, the

ER-negative, BK-α-negative albeit BK-γ1-positive MDA-MB-157 triple-negative cell line was included in the analysis, whereas the ER-, BK-α- and BK-γ1-positive MCF-7 luminal cell line served as well-characterised positive reference for hormone-stimulated proliferation in breast cancer[202,368-370] (figure 5.15 A).

Stimulation with CCS-containing media for 72 h after serum withdrawal served as ctrl. In grid experiments, proliferation rates were lower in the absence of serum in all three cell lines (0.52 ± 0.08, 0.19 ± 0.01 and 0.60 ± 0.06 fold for MDA-MB-453, MCF-7 and MDA-MB-157 cells). On the contrary, FCS increased MDA-MB-453 (1.39 ± 0.05 fold) and MCF-7 (1.47 ± 0.05 fold) cell proliferation, whereas the proliferation rate of MDA-MB-157 cells was not affected (0.98 ± 0.05 fold). Albeit MDA-MB-453 cells were ER-negative, grid experiments revealed significantly increased proliferation rates when treated with the different E2 concentrations (1.51 ± 0.07, 1.35 ± 0.02 and 1.44 ± 0.12 fold for 0.1, 1 and 10 nM). This was similar to E2 treatment of ER-positive MCF-7 cells (1.26 ± 0.05, 1.30 ± 0.10 and 1.42 ± 0.01 fold for 0.1, 1 and 10 nM), whereas the ER- and BK-α-negative MDA-MB-157 cell line did not respond to any of the E2 concentrations tested. Regarding testosterone, the positive AR status with high expression levels in MDA-MB-453[371-373] and lower ones in MCF-7[368,374,375] but only one study with evidence for AR expression in MDA-MB-157[376] cells must be considered. MDA-MB-453 (1.57 ± 0.12, 1.39 ± 0.10, 1.42 ± 0.17 and 1.48 ± 0.06 fold for 0.1, 1 and 10 nM) and MCF-7 (1.25 ± 0.09, 1.18 ± 0.06, 1.23 ± 0.05 and 1.32 ± 0.02 fold for 0.1, 1 and 10 nM) cell proliferation was significantly increased at different testosterone concentrations tested without effect in MDA-MB-157 cells (figure 5.15 B). The Ki-67 index in ctrl conditions was different for the three cell lines with 62.0 ± 1.6, 93.6 ± 1.6 and 83.8 ± 1.5% for MDA-MB-453, MCF-7 and MDA-MB-157 cells, respectively. Therefore, absolute percentages of Ki-67-positive cells were plotted. In MDA-MB-453 cells, FCS (81.5 ± 3.8%) as well as 0.01 and 1 nM testosterone (77.2 ± 3.2 and 78.4 ± 2.9%) significantly increased the Ki-67 index. As MCF-7 cells showed already a very high basal Ki-67 index, the different treatments had no additive effect. Again, none of the treatments altered the Ki-67 status of the ER- and BK-α-negative MDA-MB-157 cell line (figure 5.15 C).

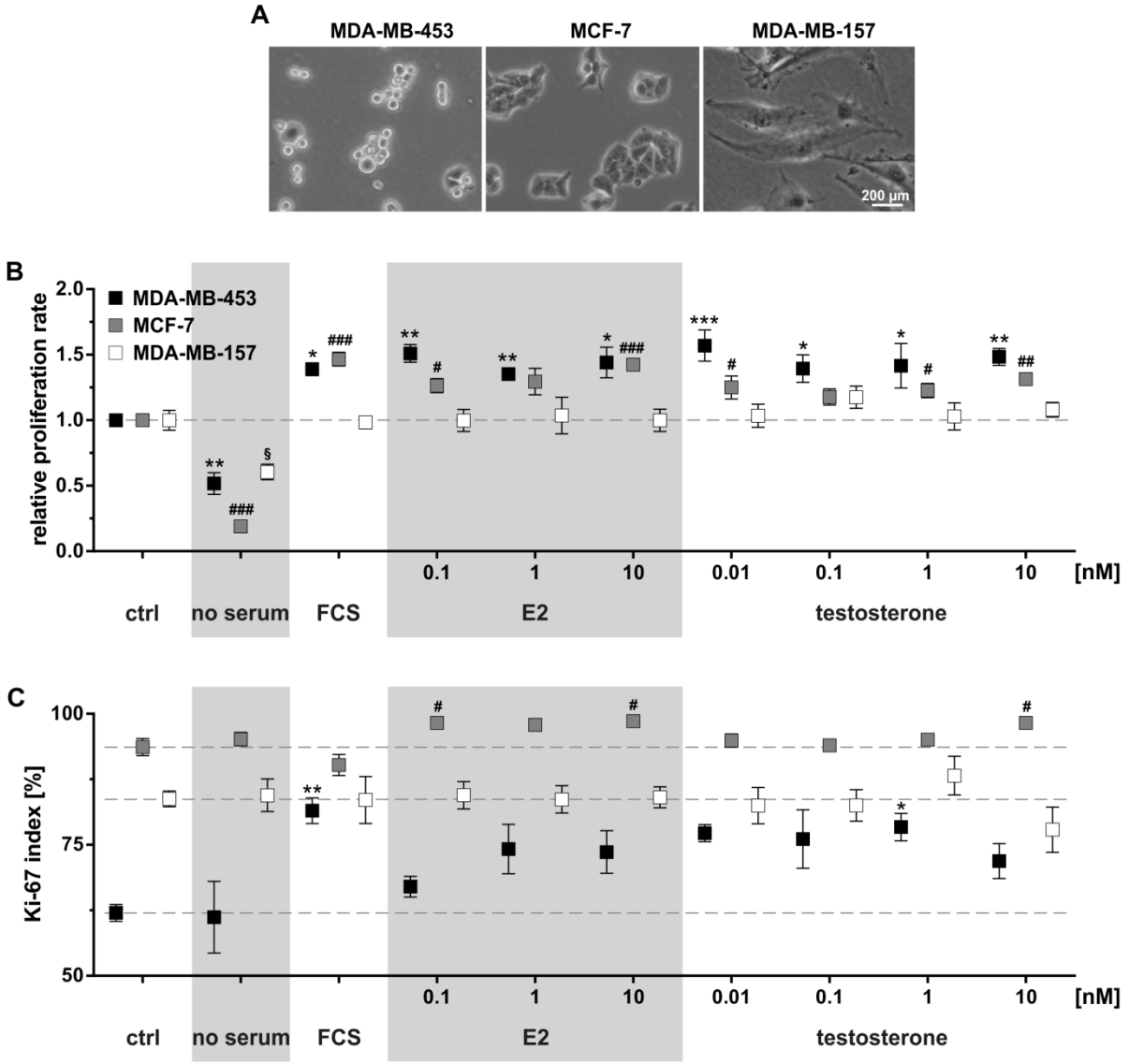

Figure 5.15: Growth factor-stimulated proliferation of human breast cancer cells
80,000 MDA-MB-453, 30,000 MCF-7 and 20,000 MDA-MB-157 cells per grid dish as well as 30,000 MDA-MB-453, 10,000 MCF-7 and 10,000 MDA-MB-157 cells in 8-well chamber slides were treated as described in previous figure 5.14. **(A)** Morphology of the three cell lines was different, as observed 24 h after seeding. **(B + C)** Grid proliferation rate (two-way ANOVA with Sidak´s test) and Ki-67 index (one-way repeated measures ANOVA with Dunnett´s tests for each cell line) were assessed in these cell lines. Serum deprivation for 72 h decreased cell numbers in all three selected human breast cancer cell lines compared to ctrl. In contrast, FCS but also various E2 and testosterone treatments for 72 h enhanced proliferation of the ER-negative and BK-α and -γ1-positive MDA-MB-453 as well as the ER-, BK-α and -γ1-positive MCF-7 cells, however not in ER- and BK-α-negative but BK-γ1-positive MDA-MB-157 cells. Shown are means ± SEM for n = 5 experiments. */#/§$p < 0.05$, **/##$p < 0.01$ or ***/###$p < 0.001$ show significant differences to MDA-MB-453, MCF-7 or MDA-MB-157, respectively.

5.2.3 Effects of anti-hormones and BK status on breast cancer cell proliferation

The available evidence suggests that besides growth factors including selected hormones, also anti-hormones and in particular anti-oestrogens can stimulate BK channel activity[207,220]. Hence, the effects of different concentrations of the pro-drug TAM and its active metabolites

(Z)-4-OH-TAM and (Z)-endoxifen as well as the pure anti-oestrogen fulvestrant were studied with regard to proliferation of MMTV-PyMT$^{tg/+}$ WT and BK KO cells and human MDA-MB-453, MCF-7 and MDA-MB-157 cells.

Experimental setups and readouts were similar to previous approaches (figure 5.14 and figure 5.15), hence MMTV-PyMT$^{tg/+}$ WT and BK KO cells were stimulated with anti-oestrogens in grid dishes for 72 h. Concentrations of 1, 10, 100 and up to 1,000 nM of TAM (0.72 ± 0.06, 0.75 ± 0.05, 0.72 ± 0.06 and 0.72 ± 0.05 fold), (Z)-4-OH-TAM (0.79 ± 0.05, 0.72 ± 0.03, 0.75 ± 0.06 and 0.76 ± 0.07 fold), (Z)-endoxifen (0.80 ± 0.05, 0.84 ± 0.03, 0.80 ± 0.04 and 0.73 ± 0.05 fold) and fulvestrant (0.85 ± 0.04, 0.72 ± 0.05, 0.75 ± 0.06 and 0.67 ± 0.04 fold) all showed either tendencies or significances towards decreased proliferation in MMTV-PyMT$^{tg/+}$ BK KO cells. This could be confirmed with 1,000 nM TAM (0.79 ± 0.04 fold), (Z)-4-OH-TAM (0.79 ± 0.04 fold) and (Z)-endoxifen (0.77 ± 0.04 fold) as well as 1, 10, 100 and 1,000 nM fulvestrant (0.89 ± 0.06, 0.79 ± 0.04, 0.81 ± 0.04 and 0.74 ± 0.02 fold) in MMTV-PyMT$^{tg/+}$ WT cells. However, the relative proliferation rate was strongly dependent on the test dose in the WT genotype. The 10 nM concentration of TAM (1.26 ± 0.07 fold) or (Z)-endoxifen (1.23 ± 0.05 fold) significantly stimulated rather than inhibited proliferation and 10 nM (Z)-4-OH-TAM (1.13 ± 0.03 fold) also showed a clear tendency towards increased proliferation in MMTV-PyMT$^{tg/+}$ WT cells, suggesting anti-hormone-induced and BK-mediated proliferation. In addition, the anti-proliferative effect of 1 and 100 nM TAM (1.07 ± 0.08 and 1.03 ± 0.07 fold), (Z)-4-OH-TAM (0.98 ± 0.04 and 0.90 ± 0.06 fold) and (Z)-endoxifen (1.00 ± 0.09 and 0.98 ± 0.03 fold) was diminished or absent in MMTV-PyMT$^{tg/+}$ WT cells. Moreover, proliferation responses reached statistical significance between WT and BK KO gentoypes for 1, 10 and 100 nM TAM, 10 nM (Z)-4-OH-TAM and 10 nM (Z)-endoxifen (figure 5.16 A).

Regarding the Ki-67 status of anti-oestrogen-treated MMTV-PyMT$^{tg/+}$ WT and BK KO cells, effects were comparable to the results in the grid experiments. Albeit not reaching significance in most test conditions, 1, 10, 100 and 1,000 nM of TAM (0.87 ± 0.05, 0.84 ± 0.05, 0.86 ± 0.04 and 0.80 ± 0.05 fold), (Z)-4-OH-TAM (0.95 ± 0.06, 0.79 ± 0.07, 0.83 ± 0.06 and 0.82 ± 0.07 fold), (Z)-endoxifen (0.82 ± 0.05, 0.72 ± 0.09, 0.80 ± 0.06 and 0.80 ± 0.05 fold) or fulvestrant (0.89 ± 0.05, 0.74 ± 0.09, 0.77 ± 0.04 and 0.78 ± 0.05 fold) treatments in the BK KO genotype showed decreased relative Ki-67 levels. In the WT genotype, 1, 10, 100 and 1,000 nM TAM (1.06 ± 0.07, 1.18 ± 0.01, 1.03 ± 0.03 and 0.86 ± 0.07 fold), (Z)-4-OH-TAM (0.98 ± 0.06, 1.34 ± 0.13, 1.02 ± 0.07 and 0.85 ± 0.07 fold), (Z)-endoxifen (1.07 ± 0.05, 1.35 ± 0.13, 0.87 ± 0.07 and 0.90 ± 0.13 fold) and fulvestrant (0.83 ± 0.04, 0.83 ± 0.10, 0.88 ± 0.04 and 0.62 ± 0.10 fold) confirmed the effects measured in

grid dishes. Also Ki-67 status did significantly differ between genotypes at 10 nM TAM, (Z)-4-OH-TAM or (Z)-endoxifen (figure 5.16 B).

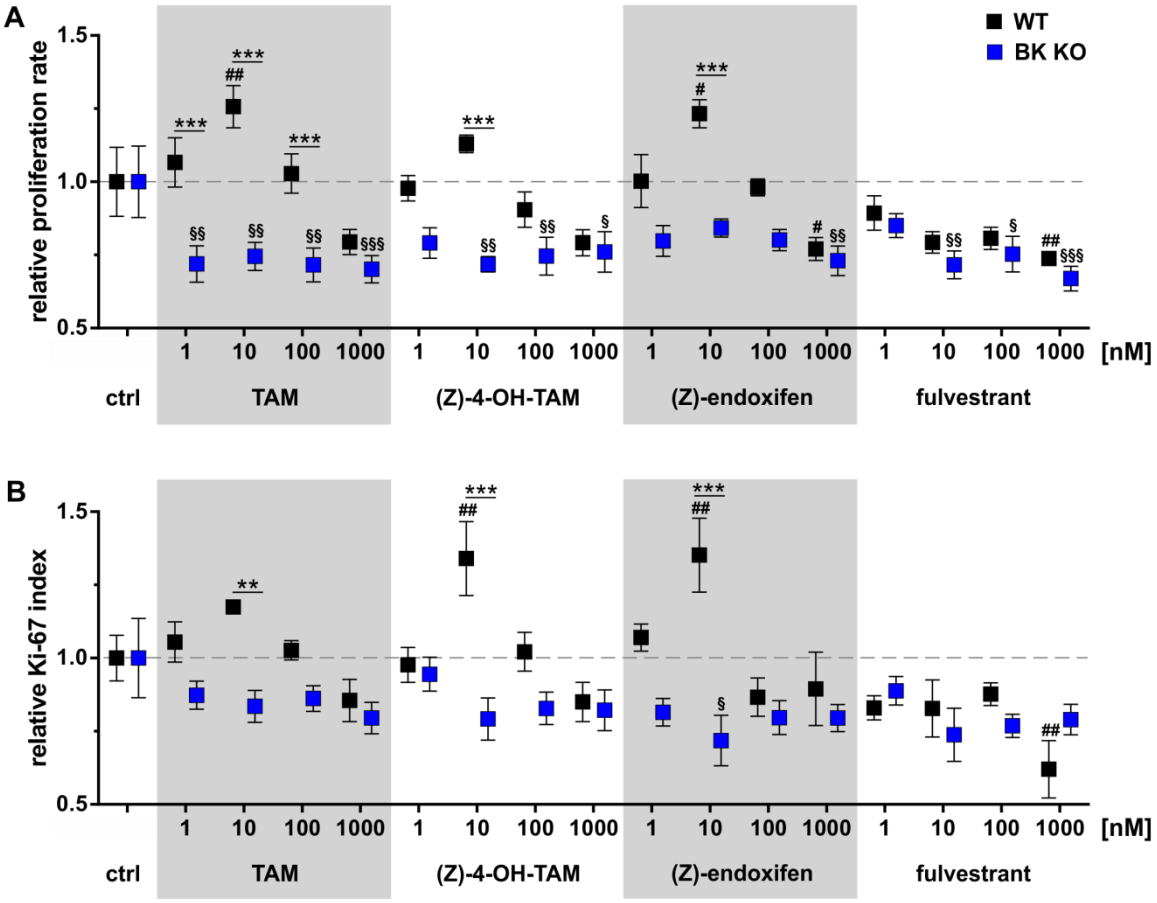

Figure 5.16: MMTV-PyMT$^{tg/+}$ WT and BK KO cell proliferation in response to anti-oestrogens
MMTV-PyMT$^{tg/+}$ WT and BK KO cells were treated with selected anti-oestrogens for **(A)** grid proliferation experiments and **(B)** Ki-67 index. The pro-drug TAM together with its active metabolites (Z)-4-OH-TAM and (Z)-endoxifen as well as fulvestrant decreased MMTV-PyMT$^{tg/+}$ BK KO cell proliferation in at least partly dose-dependent manner. MMTV-PyMT$^{tg/+}$ WT cells, on the contrary, differentially responded to the anti-oestrogen treatments with high concentrations also eliciting a negative impact on proliferation. Low concentrations of TAM and its metabolites increased rather than decreased proliferation of MMTV-PyMT$^{tg/+}$ cells in the presence of BK, though. Two-way ANOVA with Sidak´s test was performed for grid experiments (n = 7) and Ki-67 index (n = 6). Shown are means ± SEM with #/§p < 0.05, **/##/§§p < 0.01, ***/§§§p < 0.001 highlighting significant differences as indicated, according to MMTV-PyMT$^{tg/+}$ WT ctrl or according to MMTV-PyMT$^{tg/+}$ BK KO ctrl, respectively.

Anti-oestrogen treatments were also applied to human MDA-MB-453, MCF-7 and MDA-MB-157 cells growing in grid dishes. The ER-negative MDA-MB-453 cell line that showed high BK-α and BK-γ1 mRNA expression responded to all treatment conditions with a tendency or significance increased relative proliferation rate: 1, 10, 100 or 1,000 nM of TAM (1.28 ± 0.05, 1.40 ± 0.10, 1.40 ± 0.06 and 1.37 ± 0.09 fold), (Z)-4-OH-TAM (1.34 ± 0.07, 1.39 ± 0.05, 1.33 ± 0.03 and 1.23 ± 0.04 fold), (Z)-endoxifen (1.37 ± 0.07, 1.30 ± 0.11, 1.29 ± 0.07 and 1.28 ± 0.06 fold) or fulvestrant (1.24 ± 0.07, 1.29 ± 0.07, 1.30 ± 0.08 and 1.24

± 0.07 fold). In contrast, the ER-negative MDA-MB-157 cell line lacking BK-α did not respond to any treatment albeit BK-γ1 mRNA was expressed at low levels (figure 5.8): 1, 10, 100 or 1,000 nM of TAM (0.97 ± 0.11, 0.97 ± 0.10, 1.02 ± 0.10 and 0.93 ± 0.07 fold), (Z)-4-OH-TAM (0.97 ± 0.06, 0.95 ± 0.03, 0.94 ± 0.05 and 1.04 ± 0.04 fold), (Z)-endoxifen (1.01 ± 0.05, 0.98 ± 0.06, 1.01 ± 0.05 and 0.99 ± 0.05 fold) or fulvestrant (0.97 ± 0.06, 0.92 ± 0.05, 1.06 ± 0.09 and 0.98 ± 0.08 fold). The ER-positive, BK-α and BK-γ1-positive MCF-7 cell line differentially proliferated in dependence on anti-oestrogen concentrations: 1 and 10 nM TAM (1.17 ± 0.02 and 1.20 ± 0.03 fold), (Z)-4-OH-TAM (1.21 ± 0.04 and 1.34 ± 0.04 fold), (Z)-endoxifen (1.25 ± 0.03 and 1.33 ± 0.04 fold) and even the pure anti-oestrogen fulvestrant (1.20 ± 0.05 and 1.24 ± 0.04 fold) increased proliferation and thus lacked their desired anti-proliferative effect. Only high concentrations such as 100 and 1,000 nM of (Z)-4-OH-TAM (0.74 ± 0.08 and 0.61 ± 0.05 fold), (Z)-endoxifen (0.75 ± 0.06 and 0.64 ± 0.06 fold) and fulvestrant (0.73 ± 0.08 and 0.53 ± 0.05 fold) were sufficient to inhibit proliferation in comparison to ctrl. In contrast, TAM (0.98 ± 0.08 and 0.98 ± 0.10 fold) had no effect at these concentrations (figure 5.17 A).

Again, the grid-based proliferation assay was supplemented by investigating the Ki-67 index after 72 h of anti-oestrogen treatment for each of the three human cell lines. In MDA-MB-453 cells, the Ki-67 index was higher in all treatment conditions compared to ctrl (62.0 ± 1.6%): 1, 10, 100 or 1,000 nM TAM (78.0 ± 3.9, 78.8 ± 3.3, 73.6 ± 4.0 and 70.8 ± 2.1%), (Z)-4-OH-TAM (75.9 ± 2.4, 76.9 ± 2.2, 75.5 ± 3.7 and 71.8 ± 2.5%), (Z)-endoxifen (70.3 ± 2.5, 78.8 ± 4.5, 72.7 ± 2.4 and 75.2 ± 4.4%) and fulvestrant (77.9 ± 3.4, 70.7 ± 2.2, 77.8 ± 4.1 and 77.1 ± 3.0%). In MCF-7 cells and compared to ctrl conditions (93.6 ± 1.6), the different treatments showed no effect on Ki-67 index after 1, 10, 100 or 1,000 nM TAM application (96.6 ± 1.5, 97.0 ± 0.8, 96.0 ± 0.8 and 97.2 ± 0.8%) and only tendencies towards decreased Ki-67 levels for (Z)-4-OH-TAM (93.9 ± 2.3, 94.1 ± 1.3, 91.2 ± 2.1 and 92. 6 ± 3.1%), (Z)-endoxifen (90.5 ± 3.9, 95.7 ± 1.7, 89.5 ± 2.3 and 86.9 ± 2.5%) and fulvestrant (89.9 ± 2.3, 87.6 ± 3.1, 85.7 ± 2.6 and 83. 6 ± 1.4%) treatment. Apparently, in MCF-7 cells, only high anti-oestrogen concentrations had an impact on the pace of proliferation, which was assessed by the grid-based assay. In contrast, the Ki-67 marker, which serves as indicator of cells in the active phases of the cell cycle[97], seems less affected by the anti-oestrogen treatments in MCF-7 cells. In the MDA-MB-157 cell line, 1, 10, 100 and 1,000 nM TAM (83.8 ± 2.7, 80.9 ± 1.9, 82.8 ± 4.3 and 81.9 ± 2.1%), (Z)-4-OH-TAM (81.5 ± 1.3, 78.9 ± 1.6, 81.0 ± 3.7 and 80.3 ± 2.5%), (Z)-endoxifen (84.1 ± 2.2, 83.9 ± 1.4, 87.6 ± 4.3 and 80.0 ± 2.2%) or fulvestrant (80.0 ± 1.1, 80.8 ± 3.4, 82.4 ± 4.8 and 83.9 ± 2.1%) again did not differ from ctrl (83.8 ± 1.5%) (figure 5.17 B).

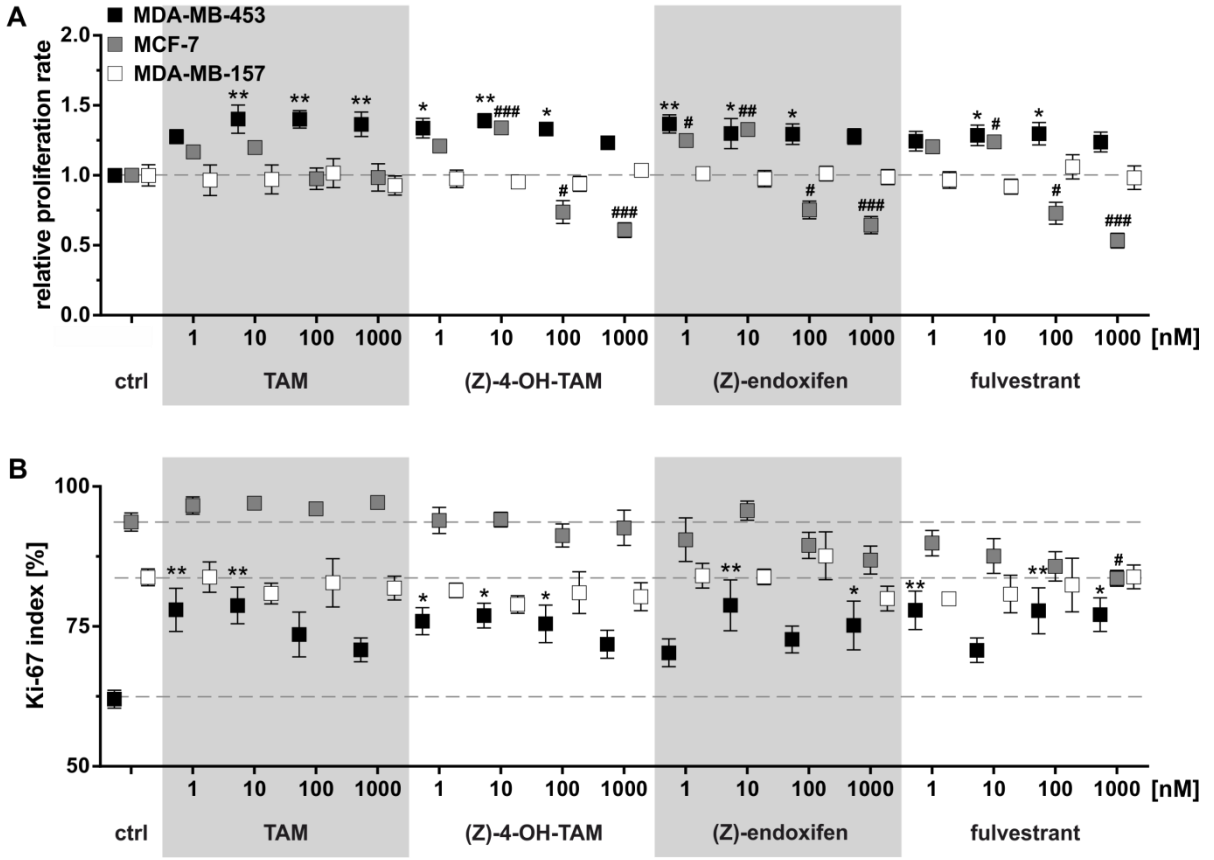

Figure 5.17: Effect of anti-oestrogens on proliferation of human breast cancer cells
The selected human breast cancer cell lines were seeded as described in figure 5.15 and treated with anti-oestrogens for **(A)** grid proliferation experiments rate (two-way ANOVA with Sidak´s test) and **(B)** Ki-67 index (one-way repeated measures ANOVA with Dunnett´s tests for each cell line). The ER-negative and BK-α- and γ1-positive MDA-MB-453 cell line responded to anti-oestrogen treatments in a pro-proliferative manner, whereas no effect to any of the selected substances and concentrations was observed for the ER- and BK-α-negative but BK-γ1-positive MDA-MB-157 cell line. For the ER-, BK-α- and -γ1-positive MCF-7 cells, either increased proliferation tendencies or significant effects were detected in response to low concentrations of the different anti-oestrogens. At higher concentrations, (Z)-4-OH-TAM, (Z)-endoxifen and fulvestrant diminished MCF-7 cell proliferation, as reported by others[377-379]. Plots show means ± SEM for n = 5 experiments. */#p < 0.05, **/##p < 0.01 and ###p < 0.001 show significant differences to MDA-MB-453 or MCF-7, whereas no statistically significant effects of the treatments were observed in MDA-MB-157 cells.

5.2.4 *In vivo* TAM therapy of MMTV-PyMT$^{tg/+}$ WT and BK KO tumours

TAM therapy has been successful in many breast cancer patients, although its use is limited by side effects, therapy failure and the development of therapy resistance[1,21,380]. Whether the BK channel status of breast tumours affects tumour growth *in vivo* has remained elusive so far. Therefore, a first translational approach aimed at dose-finding and at exploring the murine TAM metabolism followed by tumour growth monitoring in MMTV-PyMT$^{tg/+}$ WT and BK KO after implantation of TAM and placebo pellets in mice. TAM metabolism (see figure 1.4) in mice was studied by the use of 0.5 or 5 mg TAM or placebo pellets with a release time

of 60 d. At an age of 12 weeks, mice were ovariectomised. After one week of recovery, pellets were implanted subcutaneously at the lateral side of the neck. The continuous release of TAM or placebo, as guaranteed by the implanted pellet, avoided the necessity of repeated drug administration and the induction of peak concentrations after application. 7, 14 and 21 d post pellet implantation, retrobulbary plasma was collected (figure 5.18 A).

HPLC analyses of TAM and its main metabolites were conducted by Dr. Thomas Mürdter (AG Prof. Dr. Brauch, IKP Stuttgart) after setting the lower level of quantification according to an in-house human patient reference. 0.5 mg/60 d placebo pellets revealed no TAM or any of the metabolites in the plasma samples except for some background concentrations of (E)-DM-TAM-4-O-Gluc at 7 and 21 d (figure 5.18 B). In 0.5 mg/60 d TAM pellet-implanted mice, moderate TAM concentrations (3.89 ± 1.23, 2.25 ± 0.22 and 1.89 ± 0.14 nM for 7, 14 and 21 d) were measured as well as low concentrations of many of the tested metabolites including (Z)-4-OH-TAM (0.41 ± 0.15, 0.21 ± 0.02 and 0.16 ± 0.02 nM for 7, 14 and 21 d) and (Z)-endoxifen (0.14 ± 0.14 for 7 d) (figure 5.18 C). The 5 mg/60 d placebo pellet revealed only background levels for (Z)-DM-TAM-4-O-Gluc and (E)-DM-TAM-4-O-Gluc at 14 d post pellet implantation (figure 5.18 D), whereas TAM (6.92 ± 0.38, 6.93 ± 0.69 and 7.34 ± 0.97 nM) and many metabolites were detected in the plasma samples in 5 mg/60 d TAM pellets at 7, 14 and 21 d post implantation. Amongst these were the two major active TAM metabolites[90,381], (Z)-4-OH-TAM (0.73 ± 0.05, 0.69 ± 0.13 and 0.61 ± 0.08 nM) and (Z)-endoxifen (0.23 ± 0.02, 0.21 ± 0.03 and 0.20 ± 0.01 nM) (figure 5.18 E).

As in humans, none of the mouse plasma samples showed high α-OH-TAM concentrations when compared to TAM metabolism in rats, which is known to render rats prone to the development of liver cancer[86,87]. During the time course of 21 d, TAM metabolite concentrations in plasma from the TAM pellet-implanted mice were stable with steady-state concentrations reached already after 7 d. In the 0.5 mg/60 d TAM group, the TAM concentration was significantly higher at 7 d compared to 14 d and 21 d. Besides, a significant difference existed in (Z)-TAM-4-O-Gluc concentrations between 7 d and 21 d in the 5 mg/60 d TAM group.

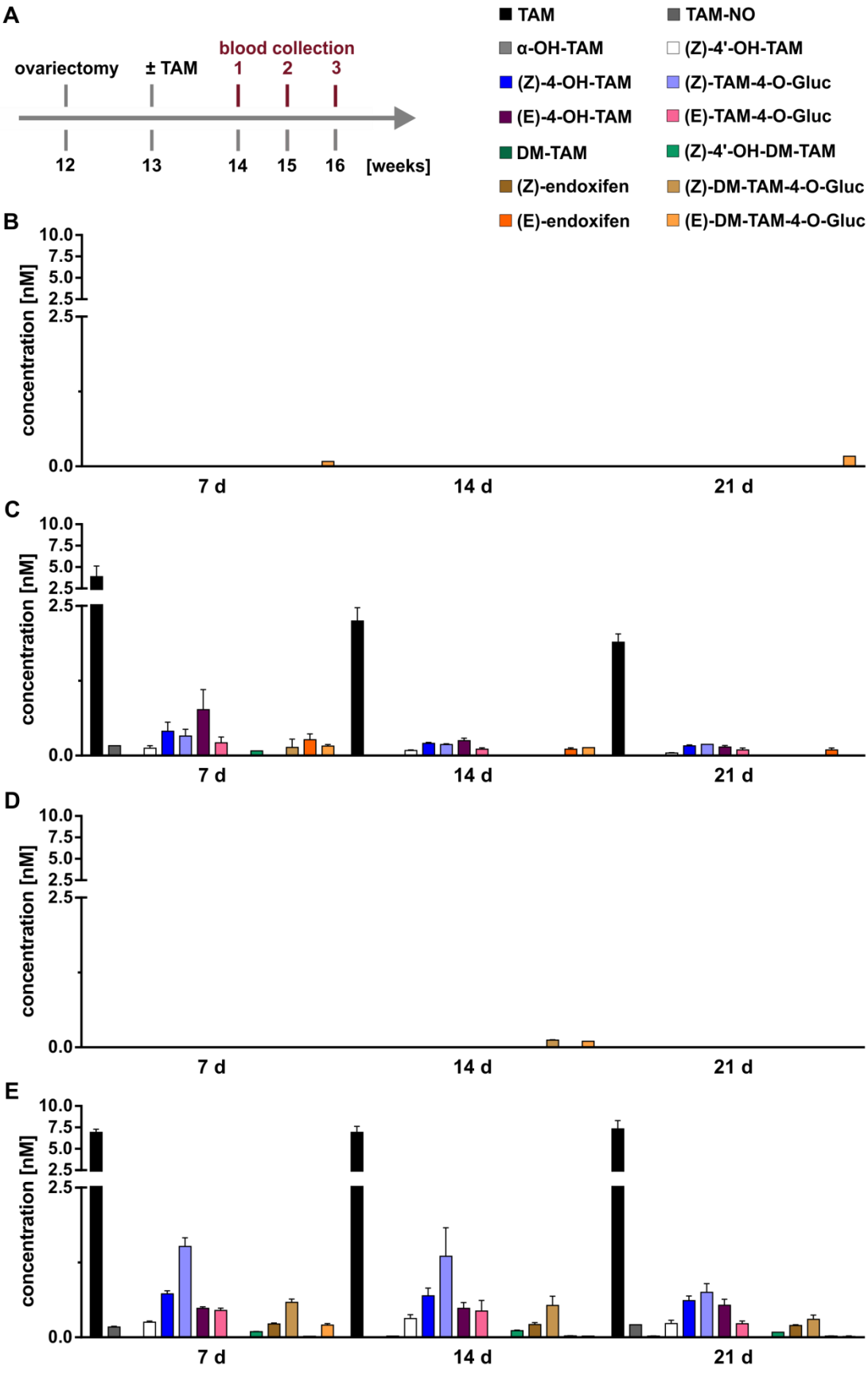
A
ovariectomy
± TAM
blood collection
1
2
3
12
13
14
15
16
[weeks]
TAM
TAM-NO
α-OH-TAM
(Z)-4'-OH-TAM
(Z)-4-OH-TAM
(Z)-TAM-4-O-Gluc
(E)-4-OH-TAM
(E)-TAM-4-O-Gluc
DM-TAM
(Z)-4'-OH-DM-TAM
(Z)-endoxifen
(Z)-DM-TAM-4-O-Gluc
(E)-endoxifen
(E)-DM-TAM-4-O-Gluc
B
C
D
E
concentration [nM]
10.0
7.5
5.0
2.5
2.5
0.0
7 d
14 d
21 d

Figure 5.18: TAM metabolism after pellet implantation in mice
(A) Mice were ovariectomised 7 d before implantation of placebo or TAM pellets with continuous release of 0.5 or 5 mg within 60 d. HPLC measurements of TAM and its metabolites was obtained from retrobulbary blood taken 7, 14 or 21 d after pellet implantation. **(B)** The lower level of quantification was set according to an in-house human patient reference. TAM and its metabolites were not detected in 0.5 mg/60 d placebo pellets. **(C)** TAM pellets with 0.5 mg/60 d release resulted in TAM accumulation and many known TAM metabolites in the plasma samples. Similar effects were seen with **(D)** placebo and **(E)** TAM pellets with 5 mg/60 d release, respectively, albeit overall metabolite levels were higher as compared to 0.5 mg/60 d TAM pellets. **(B - E)** Bar graphs show means ± SEM for mice implanted with low-dose or high-dose pellets of TAM (each n = 4) or placebo (each n = 2) and statistically tested with two-way repeated measures ANOVA and Tukey´s test.

For further experiments, the 5 mg/60 d TAM and placebo pellets were chosen because TAM release dose of these pellets was comparable to 20-40 mg TAM per day in the human system when BW (25 g for mouse and 70 kg for woman) and the roughly sevenfold-increased metabolic rate of a mouse are considered appropriately[382,383].

To investigate the role of BK for tumour growth in 5 mg/60 d TAM-treated mice, MMTV-PyMT$^{tg/+}$ WT and BK KO cells were orthotopically transplanted into FVB/N mice at an age of 12 weeks (section 4.1.5). Ovariectomy ensured equal conditions and avoidance of tumour growth disturbances by endogenous E2 and was conducted at a tumour volume of approximately 62.5 mm³ (section 4.1.6). The experiment was terminated at an eightfold-increased tumour volume compared to the day of pellet implantation (figure 5.19 A). At the end of the experiment, monitoring of uterus weight compared to total BW showed a significant increase in the TAM group (0.172 ± 0.109 and 0.207 ± 0.016%) compared to placebo (0.103 ± 0.017 and 0.082 ± 0.005%) for both WT and BK KO genotypes (figure 5.19 B). Tumour growth and thus survival time between genotypes reached a significant different response in WT and BK KO genotypes according to TAM therapy. MMTV-PyMT$^{tg/+}$ WT tumour growth under TAM treatment needed 90.5 ± 10.1% of the time to reach the experimental endpoint compared to placebo. In contrast, MMTV-PyMT$^{tg/+}$ BK KO tumour growth was delayed under TAM treatment, as the eightfold-increased tumour volume was reached 1.78 ± 0.42 fold later than in the respective placebo treatment group (figure 5.19 C). qRT-PCR analysis of mRNA levels in tumour tissues at the end of the experiment revealed no statistically significant differences between genotypes and treatment groups for *Esr1* or *Esr2* as well as the accessory subunits expressed in the cells, i.e. *Kcnmb1*, *Kcnmb4* and *Lrrc26* (supplemental figure 9.8). Macroscopically visible lung metastasis was absent in MMTV-PyMT$^{tg/+}$ BK KO tumour-bearing mice treated with placebo. In TAM-treated mice and in the MMTV-PyMT$^{tg/+}$ WT tumour-bearing and placebo-treated mice, one lung metastasis was detected in 2-3 of the 9 mice investigated, but this differences between groups did not reach statistical significance (data not shown). Along the same line, TAM treatment had no

effect on the migratory capacity of MMTV-PyMT$^{tg/+}$ WT and BK KO cells *in vitro*, which was investigated with the xCELLigence system (supplemental figure 9.9).

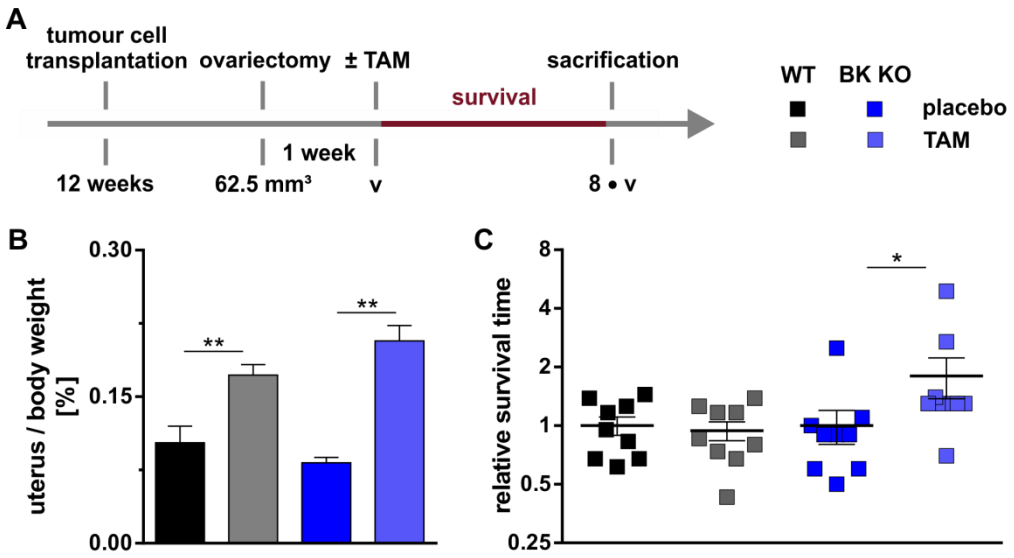

Figure 5.19: Growth progression of MMTV-PyMT$^{tg/+}$ WT and BK KO breast tumours ± TAM
(A) Female FVB/N mice received MMTV-PyMT$^{tg/+}$ WT or BK KO cells and were ovariectomised at a tumour volume (v) of approximately 62.5 mm³. 1 week after ovariectomy, mice were implanted TAM or placebo pellets with 5 mg/60 d release. Tumour growth was monitored three times per week with a digital calliper. Survival was defined as the time frame necessary to reach an eightfold-increased tumour volume compared to the initial tumour size at the day of pellet implantation. **(B)** Uterus weight was increased in TAM-implanted tumour-bearing mice of both genotypes, when related to whole BW (one-way ANOVA and Tukey´s test). **(C)** Relative survival was compared between genotypes with placebo set to a relative survival time = 1. The growth of MMTV-PyMT$^{tg/+}$ WT tumours was not significantly affected by TAM even showing a tendency towards decreased survival under TAM therapy, whereas a significantly prolonged relative survival time was detected in MMTV-PyMT$^{tg/+}$ BK KO tumour-bearing mice (Mann-Whitney test). **(B + C)** n = 9 experiments were performed and plotted are means ± SEM with *p < 0.05 and **p < 0.01.

5.2.5 Combined TAM and radiation therapy

Breast cancer therapy often involves multiple approaches to reach maximum success. Hence, surgery, radiotherapy, chemotherapy and targeted therapies are used either in combination or sequentially. Therefore, the BK-dependent pro- and anti-proliferative effects of TAM were assessed during radiation therapy. TAM (10 or 1,000 nM) was applied to MMTV-PyMT$^{tg/+}$ WT and BK KO cells 1 h prior to irradiation with 0 or 2 Gy. The BK KO genotype generally did not exhibit a radiosensitising effect when compared to WT cells (supplemental figure 9.10).

Accordingly, clonogenic assays 24 h after TAM and IR revealed no significant differences in ctrl conditions between genotypes (0.73 ± 0.05 for WT and 0.64 ± 0.05 for BK KO). In the BK KO genotype, both low and high TAM concentrations increased clonogenic survival (0.78 ± 0.07 and 0.87 ± 0.09 for 10 and 1,000 nM TAM), presumably via an ER-mediated

stimulation of cell cycle arrest, as radiation-induced cell cycle arrest is important to allow for DNA repair[38]. The WT genotype revealed differential responses to IR with an increase of the cell survival fraction exposed to 1,000 nM TAM (0.57 ± 0.08) and a decrease in survival with 10 nM TAM (0.90 ± 0.03) (figure 5.20 A).

IR by inducing DNA damage results in mitotic catastrophe and cell death especially of cells with low DNA repair capacity such as tumour cells[38,39,384] (section 1.1.3). Residual DNA damage 24 h post IR was detected by staining and counting γH2AX foci. In the absence of BK, TAM did not alter γH2AX numbers per cell and hence the DNA repair processes (1.49 ± 0.08, 1.28 ± 0.12 and 1.24 ± 0.14 for ctrl, 10 and 1,000 nM TAM). However, γH2AX foci numbers were increased in 10 nM TAM-treated MMTV-PyMT$^{tg/+}$ WT cells (2.15 ± 0.18 for 10 nM TAM and 1.74 ± 0.14 for ctrl) (figure 5.20 B). Besides DNA repair, potential genotype-dependent differences in DNA damage induction by TAM was investigated by γH2AX analysis 30 min and thus shortly after irradiation. The number of γH2AX foci did not differ in the presence of TAM within each genotype, although the number of γH2AX foci in MMTV-PyMT$^{tg/+}$ WT cells was significantly higher after 1,000 nM TAM application than in the BK KO genotype (36.3 ± 5.1 versus 26.5 ± 4.7 DSBs per cell) (figure 5.20 C).

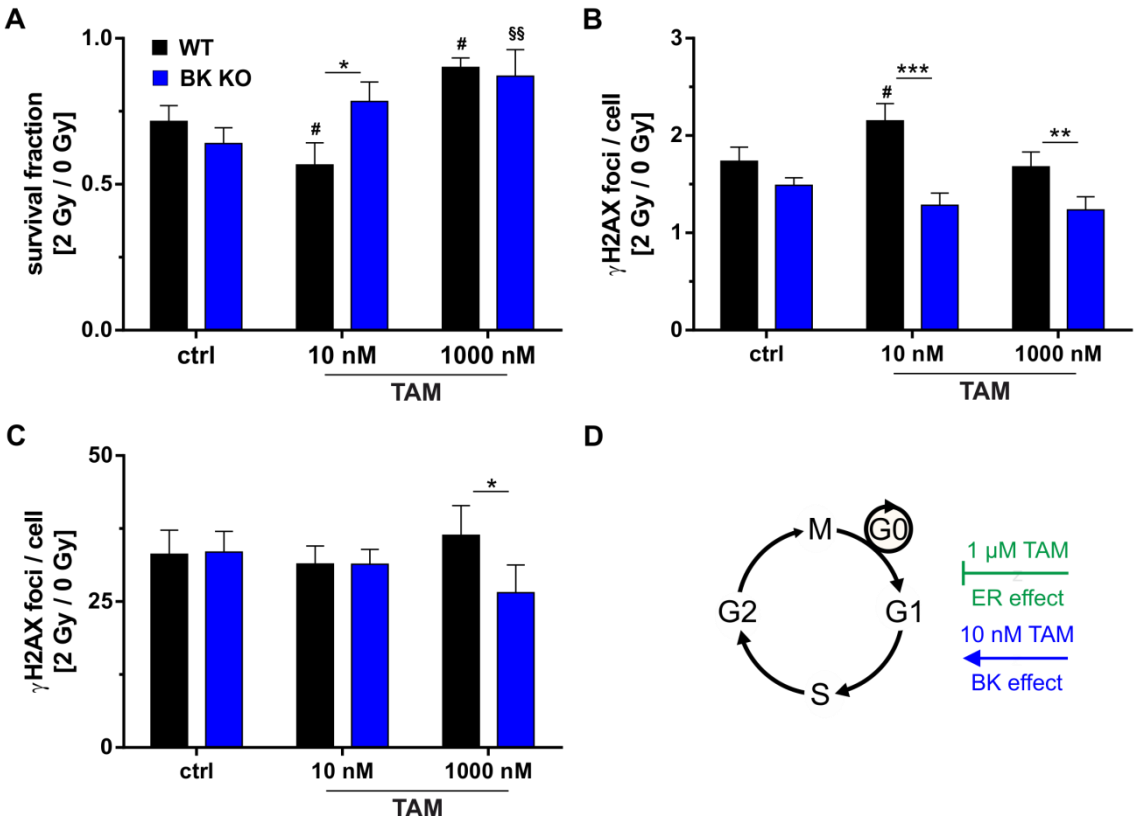

Figure 5.20: Combined TAM and radiation therapy in MMTV-PyMT$^{tg/+}$ WT and BK KO cells
MMTV-PyMT$^{tg/+}$ WT and BK KO cells were seeded with 600,000 cells per 25 cm² cell flask for clonogenic survival assays or with 50,000 cells in 12-well chamber slides for γH2AX DNA damage assessment. After 72 h growth in 5% CCS-containing medium, stimulation with TAM at low

(10 nM) or high (1,000 nM) concentration occurred 1 h before irradiation with 0 or 2 Gy. Therefore, the putative pro- or anti-proliferative effects of different TAM concentrations were investigated in the BK-mediated response to IR. **(A)** Relative survival after 2 Gy was not different between genotypes in ctrl conditions (see also supplemental figure 9.10). TAM increased survival of MMTV-PyMT$^{tg/+}$ BK KO cells at both concentrations and of 1,000 nM TAM-treated MMTV-PyMT$^{tg/+}$ WT cells, which may be attributable to the anti-proliferative effect of TAM. Administration of 10 nM TAM to MMTV-PyMT$^{tg/+}$ WT cells resulted in the opposite effect by reducing clonogenic survival thereby contributing to a genotype-dependent effect at this concentration. **(B)** 24 h after IR, residual DNA damage was elevated in 10 nM TAM-treated MMTV-PyMT$^{tg/+}$ WT cells, which was not observed after treatment with 1,000 nM TAM. In the BK KO genotype, residual γH2AX foci numbers did not differ between treatments, but generally were lower compared to the WT genotype. **(C)** TAM treatment or genotype had no influence on DNA damage 30 min after IR, except for a significant genotype-dependent difference with 1,000 nM TAM. **(D)** Radiation-induced cell cycle arrest is necessary for DNA damage repair and survival (figure 1.2). The anti-proliferative effect of TAM and thus decreased residual DNA damage and increased survival was verified in MMTV-PyMT$^{tg/+}$ BK KO cells at low and high TAM concentrations and in 1,000 nM TAM-treated MMTV-PyMT$^{tg/+}$ WT cells. The opposite effect was observed in 10 nM TAM-treated MMTV-PyMT$^{tg/+}$ WT cells, which may be attributable to a BK-dependent pro-proliferative effect of low-dose TAM. **(A - C)** Bar graphs present as means ± SEM of n = 5 experiments. Shown are relative effects of 2 Gy IR corrected for baseline (0 Gy) effects in the various treatments and genotypes. */#$p < 0.05$, **/§§$p < 0.01$ or ***$p < 0.001$ represent statistical outcome after two-way repeated measures ANOVA with Sidak´s test for the different experiments.

To conclude, the anti-proliferative effect of TAM may lead to decreased residual DNA damage and increased clonogenic survival in the BK KO genotype and in 1,000 nM TAM-treated MMTV-PyMT$^{tg/+}$ WT cells. In contrast, a BK-mediated pro-proliferative effect of 10 nM low-dose TAM may be responsible for elevated residual DNA damage and lower clonogenic survival in BK-proficient tumour cells. The impact of these *in vitro* findings for combinational TAM and IR therapy with regard to BK status of breast cancer patients remains elusive (figure 5.20 D).

5.3 The IK channel in breast cancer development and survival

5.3.1 Spontaneous breast cancer in MMTV-PyMT$^{tg/+}$ WT and IK KO mice

The IK channel is well described for its tumour-promoting properties (section 1.4.3) including cell cycle progression and proliferation in the ER-positive MCF-7 cell line[260,261,263] as well as in basal-like MDA-MB-231 cells where IK also modulates apoptosis, migration and epithelial-mesenchymal transition[264]. IK contribution to Ca^{2+} signalling and proliferation has been confirmed in detail in a primary cell system derived from the MMTV-PyMT$^{tg/+}$ mouse model[385]. Besides, IK channel expression is increased in human breast tumours and it correlates with tumour grade and metastasis[265,386].

In the spontaneous breast tumour-developing MMTV-PyMT$^{tg/+}$ model, survival parameters were studied in the absence and the presence of IK. Statistics revealed no influence of IK channel status on TFS with a HR of 0.60 (CI 0.12 - 1.27) (figure 5.21 A). Also OS was not affected by IK status in the MMTV-PyMT$^{tg/+}$ model with a HR of 1.77 (CI 0.78 - 8.18) (figure 5.21 B). BW during tumour progression was neither different between genotypes (data not shown). These results were in line with previous investigations on spontaneous tumour development and progression in MMTV-PyMT$^{tg/+}$ WT and IK KO mice[385].

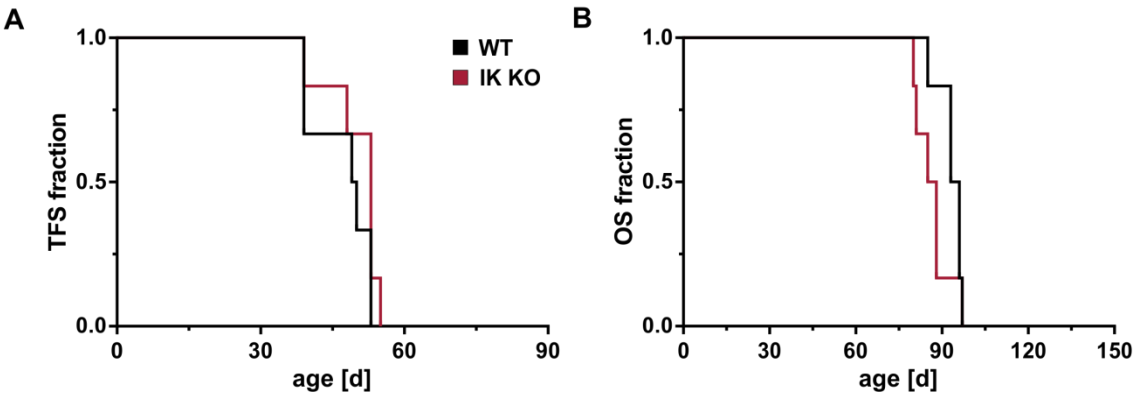

Figure 5.21: Spontaneous tumourigenesis and progression of tumour growth in MMTV-PyMT$^{tg/+}$ WT and IK KO mice
(A) Tumour-free survival (TFS) and **(B)** overall survival (OS) of MMTV-PyMT$^{tg/+}$ mice lacking IK and their WT littermates were investigated. No statistically significant differences were detected between the two genotypes for TFS or OS with log-rank tests of each n = 6 experiments.

In order to verify that IK did not alter tumour classification, the ER and HER2 status were determined in MMTV-PyMT$^{tg/+}$ WT and IK KO tissue and primary cell cultures. *Esr1*, *Esr2* and *Erbb2* mRNAs coding for ER-α, ER-β and HER2 were present in tissues (figure 5.22 A) and cells (figure 5.22 B) from both MMTV-PyMT$^{tg/+}$ WT and IK KO tumours. ER-α expression was further confirmed on the protein level in tissues (figure 5.22 C) and cells (figure 5.22 D) of both genotypes.

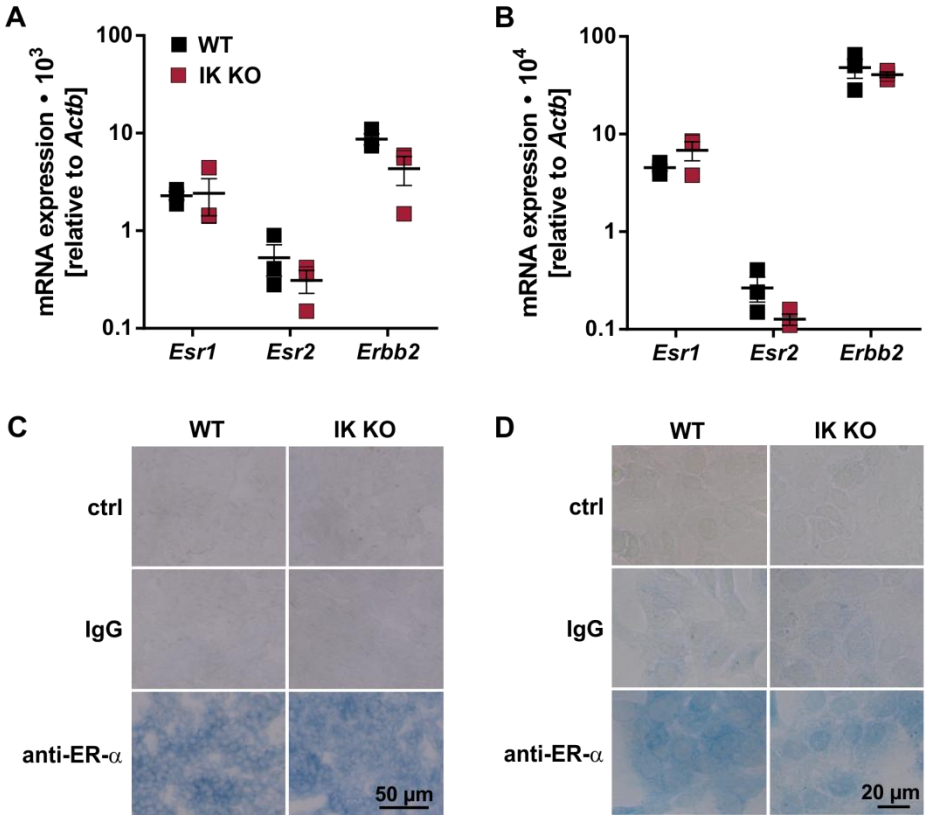

Figure 5.22: Characterisation of MMTV-PyMT$^{tg/+}$ WT and IK KO tissues and cells
MMTV-PyMT$^{tg/+}$ WT and IK KO **(A)** tumours and **(B)** cells were employed for qRT-PCR analysis of *Esr1*, *Esr2* and *Erbb2* mRNA expression coding for ER-α and ER-β as well as the HER2 protein. Differences between genotypes were not observed in n = 3 experiments, presented as means ± SEM, of a two-way repeated measures ANOVA and Sidak´s test. **(C)** Tissue sections and **(D)** cells of MMTV-PyMT$^{tg/+}$ WT and IK KO genotype were also positive for ER-α protein.

Moreover, K_{Ca} mRNA expression status and levels were measured with qRT-PCR in MMTV-PyMT$^{tg/+}$ WT and IK KO tumour tissues and cells. Tissue samples of both genotypes expressed *Kcnma1*, *Kcnmb1*, *Kcnmb2*, *Kcnmb4*, *Lrrc26*, *Kcnn1*, *Kcnn2* and *Kcnn3* mRNA coding for BK-α, BK-β1, BK-β2, BK-β4, BK-γ1 and SK1 - SK3 with similar abundances. As expected, *Kcnn4* mRNA encoding the IK channel was detected in MMTV-PyMT$^{tg/+}$ WT but not in IK KO tissue. *Kcnmb3*, *Lrrc38*, *Lrrc52* and *Lrrc55* mRNA expression coding for BK-β3, BK-γ4, BK-γ2 and BK-γ3 was absent (figure 5.23 A). Tumour cells of both genotypes revealed a K_{Ca} mRNA expression pattern similar to tissue except for the expression status of *Kcnmb2* and *Kcnn3*, which could not be confirmed in cells (figure 5.23 B).

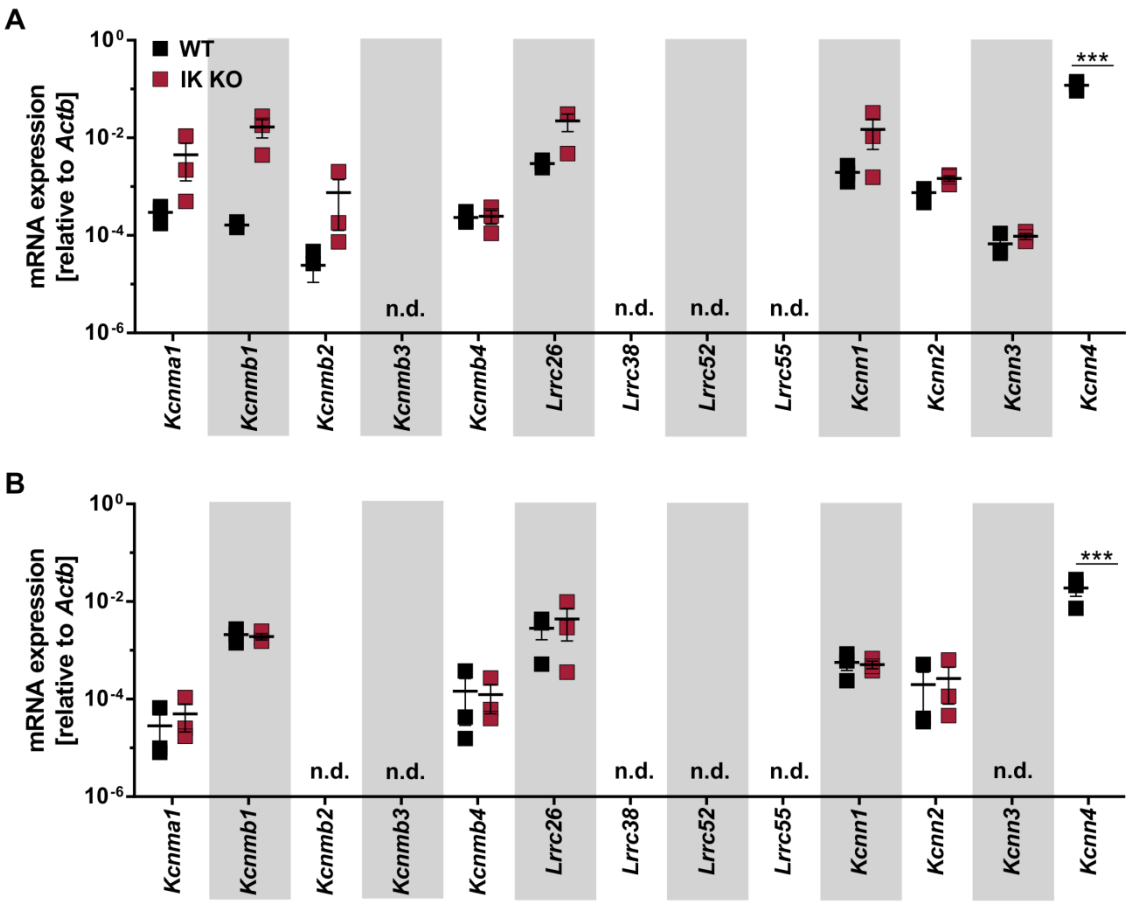

Figure 5.23: K_{Ca} channel mRNA expression pattern of MMTV-PyMT$^{tg/+}$ WT and IK KO tumours
mRNA expression levels of the different K_{Ca} channels and subunits were measured with qRT-PCR in samples derived from the MMTV-PyMT$^{tg/+}$ mouse model. **(A)** Tissues of both genotypes were positive for *Kcnma1*, *Kcnmb1*, *Kcnmb2*, *Kcnmb4* and *Lrrc26* as well as *Kcnn1 - 3* mRNA. *Kcnn4* mRNA was expressed in the WT, but was not detected (n.d.) in the IK KO genotype. **(B)** In primary cells of MMTV-PyMT$^{tg/+}$ WT and IK KO genotypes, the mRNA pattern observed in tissue could be confirmed except for *Kcnmb2* and *Kcnn3* mRNA expression. Means ± SEM are shown for n = 3 experiments. ***p < 0.001 was calculated with separate two-way repeated measures ANOVA and Sidak´s test for tissues and cells, respectively.

5.3.2 Role of the IK channel in human breast cancer

The possible contribution of IK channels to tumourigenesis was further considered with regard to the individual genomic risk of *KCNN4* SNPs (n = 77) used from the BCAC (section 4.5.3). The iCOGS array together with the imputation of SNPs delivered breast cancer-associated variants with the eleven most interesting candidates modulating overall and ER-positive, but not ER-negative tumour development. Of these SNPs, rs12609846, rs1685191 and rs12463319 significantly decreased breast cancer risk (OR 0.94), whereas the remaining *KCNN4* SNPs led to a significantly increased breast cancer risk (OR 1.05 or 1.06). Population frequencies of the SNPs varied with MAFs of 21 to 41% (figure 5.24 A)[347]. Interestingly, all SNPs were found in intron 1-2 of the *KCNN4* gene containing in total nine

exons. Their intronic localisation may be a hint for up-stream regulatory functions[336,361] (figure 5.24 B). No ERE was detected in the *KCNN4* gene (data not shown). Linkage disequilibrium was 62 - 100% between rs73048670, rs62116961, rs12609846, rs1685191, rs56681946, rs12463319, rs11879798 and rs11083720, except for lacking linkage between rs11879798 and rs11083720. rs56344893, rs200380818 and rs34144623 were inherited independently from all other SNPs (figure 5.24 C).

A

	SNP number	MAF	All		ER$^+$ BC		ER$^-$ BC	
			OR	p	OR	p	OR	p
1	rs73048670	T = 0.21	1.05	1.1×10^{-6}	1.05	4.2×10^{-5}	1.04	0.05
2	rs62116961	C = 0.25	1.06	1.7×10^{-7}	1.07	6.4×10^{-7}	1.04	0.04
3	rs12609846	C = 0.41	0.94	1.2×10^{-8}	0.93	6.0×10^{-9}	0.96	0.07
4	rs1685191	C = 0.36	0.94	1.2×10^{-8}	0.93	5.7×10^{-9}	0.96	0.07
5	rs56681946	C = 0.23	1.06	3.0×10^{-7}	1.07	7.8×10^{-7}	1.04	0.04
6	rs12463319	T = 0.36	0.94	1.0×10^{-8}	0.93	4.4×10^{-9}	0.96	0.07
7	rs56344893	A = 0.23	1.06	3.5×10^{-7}	1.06	1.2×10^{-6}	1.04	0.05
8	rs11879798	A = 0.23	1.06	2.1×10^{-7}	1.06	1.1×10^{-6}	1.05	0.03
9	rs200380818	TC = 0.23	1.06	2.2×10^{-7}	1.06	1.1×10^{-6}	1.05	0.03
10	rs11083720	T = 0.23	1.06	5.8×10^{-7}	1.06	9.1×10^{-6}	1.05	0.04
11	rs34144623	C = 0.24	1.06	2.3×10^{-6}	1.06	1.4×10^{-5}	1.04	0.11

B

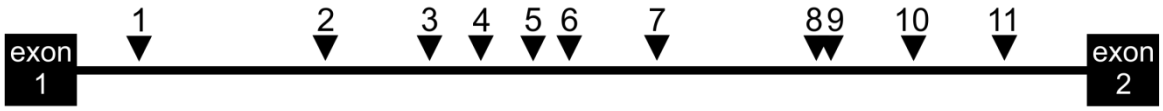

C

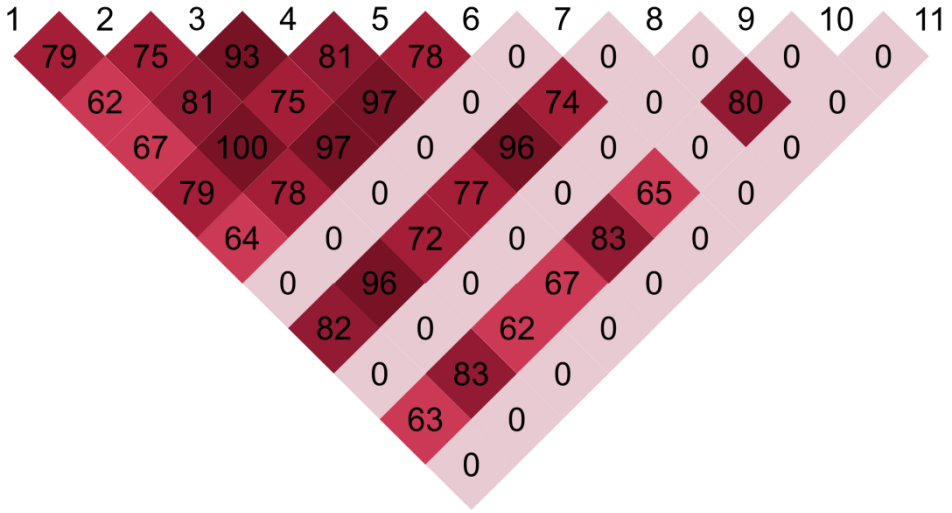

Figure 5.24: Breast cancer risk assessment of *KCNN4* variants
KCNN4 SNPs identified by the iCOGS array were analysed together with *KCNN4* SNPs that were imputed due to their genetic linkage with other genes tested on the array. In addition to overall risk assessment in all tested specimen, breast cancer risk could be further stratified according to the development of an ER-positive or -negative tumour. Besides, *KCNN4* risk SNPs were allocated for

their chromosomal position and tested for genetic linkage. **(A)** *KCNN4* SNPs directly retrieved from the array were not found to significantly modify breast cancer risk (data not shown). Imputation of SNPs tested on the iCOGS array allowed the detection of eleven *KCNN4* SNPs that altered overall and particularly ER-positive breast cancer risk. Frequencies of these SNPs in the population varied between 21 and 41%[347]. **(B)** These significant SNPs all were located in intron 1-2 of the *KCNN4* gene. **(C)** Linkage amongst the SNPs was verified among eight of the eleven SNPs with variabilities between 62 and 100%. In contrast, inheritance of rs56344893, rs200380818 and rs34144623 was independent from the other SNPs. *Abbreviations:* Minor allele frequency, MAF; Odds ratio, OR; Single nucleotide polymorphism, SNP.

Among the experimental proteins binding to the distinct SNP regions, the most frequent candidate was Early B-cell factor 1 (EBF1). However, there was no significant Spearman correlation in *EBF1* and *KCNN4* mRNA expression levels according to breast cancer data from TCGA (data not shown). Nevertheless, EBF1 was related to several SNPs, i.e. rs73048670, rs12609846, rs56681946 and rs12463319. This association may reflect the participation of IK, which is well studied for its roles in immune cells, in B cell development and activity[275,387], as EBF1 is important for proper maturation and function of B cells[388,389]. Interestingly, EBF1 is further shown to interact with ER-β. The EBF1 binding motif is enriched at sites of ER-β genomic binding and EBF1 together with E2 enhance ER-β recruitment[390]. Moreover, the Ebf1 protein in mice is described to act as tumour suppressor with reduced Ebf1 levels leading to enhanced DNA damage. Ebf1 further contributes to the regulation of DNA repair due to its influence on DNA repair gene expression. In addition, the induction of DNA damage by IR was shown to decrease *EBF1* mRNA expression of human cells. As a result, loss-of-function mutations in *Ebf1* are associated with the development of leukaemia[391-393]. After stratification of *EBF1* to its mRNA expression levels in breast cancer, the KM plotter revealed no influence on OS or distant metastasis-free survival. However, RFS differed according to *EBF1* with high mRNA expression resulting in an increased RFS in general with $p = 2.4 \bullet 10^{-8}$ (HR 0.72 (0.64 - 0.81)) as well as ER-positive breast cancer with $p = 8.3 \bullet 10^{-7}$ (HR 0.71 (0.62 - 0.81)). Nonetheless, TAM treatment had no *EBF1*-dependent impact on RFS in ER-positive breast cancer (data not shown).

In TCGA-derived data generated from established human breast tumours, *KCNN1*, *KCNN2*, *KCNN3* and *KCNN4* mRNA expression levels were further investigated in comparison to healthy breast tissues (section 4.5.1). mRNA expression for all four channels was present with no significant difference between healthy and tumour tissues (figure 5.25).

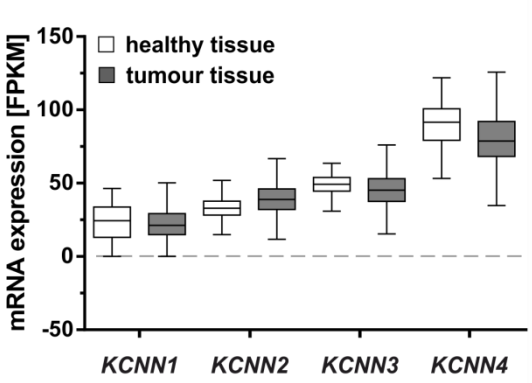

Figure 5.25: *KCNN1 - 4* mRNA expression in healthy and tumour tissues derived from TCGA
mRNA expression levels for the different SK1 - 3 (*KCNN1*, *KCNN2*, *KCNN3*) and IK (*KCNN4*) channel-encoding genes were extracted from TCGA database. No significant differences were found in fragments per kilobase of transcript per million mapped reads (FPKM) values, obtained by quantitative sequencing, in tumour tissues (n = 1,095) compared to healthy parts (n = 113) of the breast. Box plots show means ± SEM.

Moreover, the influence of *KCNN4* mRNA expression levels on OS outcome was studied in data obtained from TCGA (section 4.5.1) and the KM plotter (section 4.5.2). In TCGA, OS stratified by *KCNN4* mRNA expression levels did not lead to a significant difference over the time course of less than 10 years (figure 5.26 A). In contrast, the KM plotter allowed a follow-up time of 25 years revealing that high *KCNN4* mRNA levels significantly shortened OS with a HR of 1.37. Over this time range, patient numbers dropped more extremely in patients whose tumours had high (372, 254, 105, 23, 4, 1 and 0 patients for 0, 50, 100, 150, 200, 250 and 300 months, respectively) compared to low (1,030, 829, 372, 106, 17, 2 and 0 patients for 0, 50, 100, 150, 200, 250 and 300 months) *KCNN4* mRNA expression levels (figure 5.26 B).

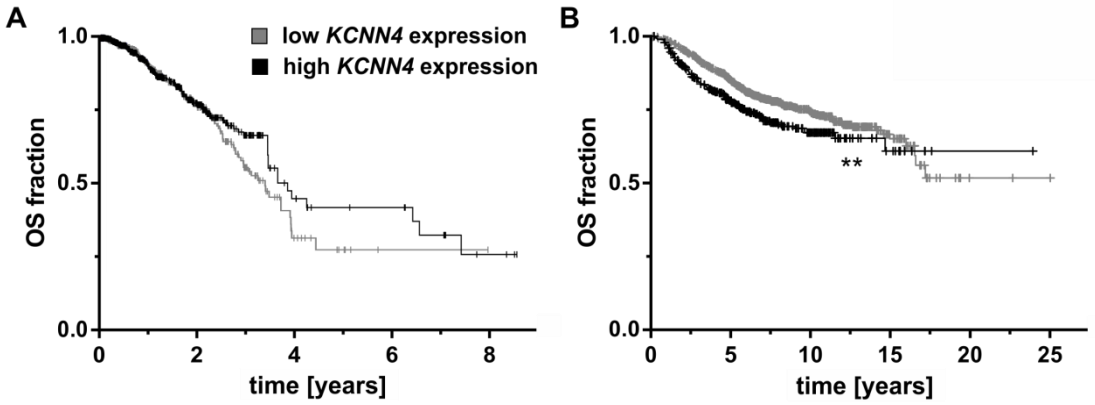

Figure 5.26: Kaplan-Meier survival analysis of breast cancer patients stratified for tumour *KCNN4* mRNA expression
Data on overall survival (OS) was retrieved from open access databases, which compared survival of patients with low or high *KCNN4* mRNA expression levels. **(A)** The available follow-up time in the TCGA dataset was less than 10 years and OS was similar between groups expressing either high or

low levels of *KCNN4*. **(B)** The KM plotter dataset allowed a follow-up time of 25 years during which a significantly decreased OS was associated with high *KCNN4* mRNA expression levels. **p < 0.01 in log-rank test for n = 599 for high and n = 601 for low *KCNN4* mRNA expression in TCGA and n = 372 for high and n = 1,030 for low *KCNN4* mRNA expression in the KM plotter.

5.3.3 IK channel contribution to proliferation in the MMTV-PyMT$^{tg/+}$ model

The Ki-67 status was determined in tissue sections and primary cells derived from MMTV-PyMT$^{tg/+}$ WT and IK KO tumours. *Mki67* mRNA expression between genotypes did not differ in tissues (figure 5.27 A) but did in primary cell cultures (1.00 ± 0.03 in IK KO and 2.41 ± 0.31 in WT) (figure 5.27 B). Tissue protein distribution was neither different between genotypes (figure 5.27 C). However, Ki-67 status in primary MMTV-PyMT$^{tg/+}$ WT and IK KO cells revealed a significantly reduced fraction of proliferating cells in the IK KO genotype after restimulation with serum-containing medium with 62.5 ± 5.5, 66.5 ± 8.6 and 74.0 ± 5.6% WT and 39.8 ± 3.6, 35.3 ± 3.6 and 37.8 ± 2.1% IK KO proliferating cells at 24, 48 and 72 h (figure 5.27 D). These results formed part of a recent publication[385].

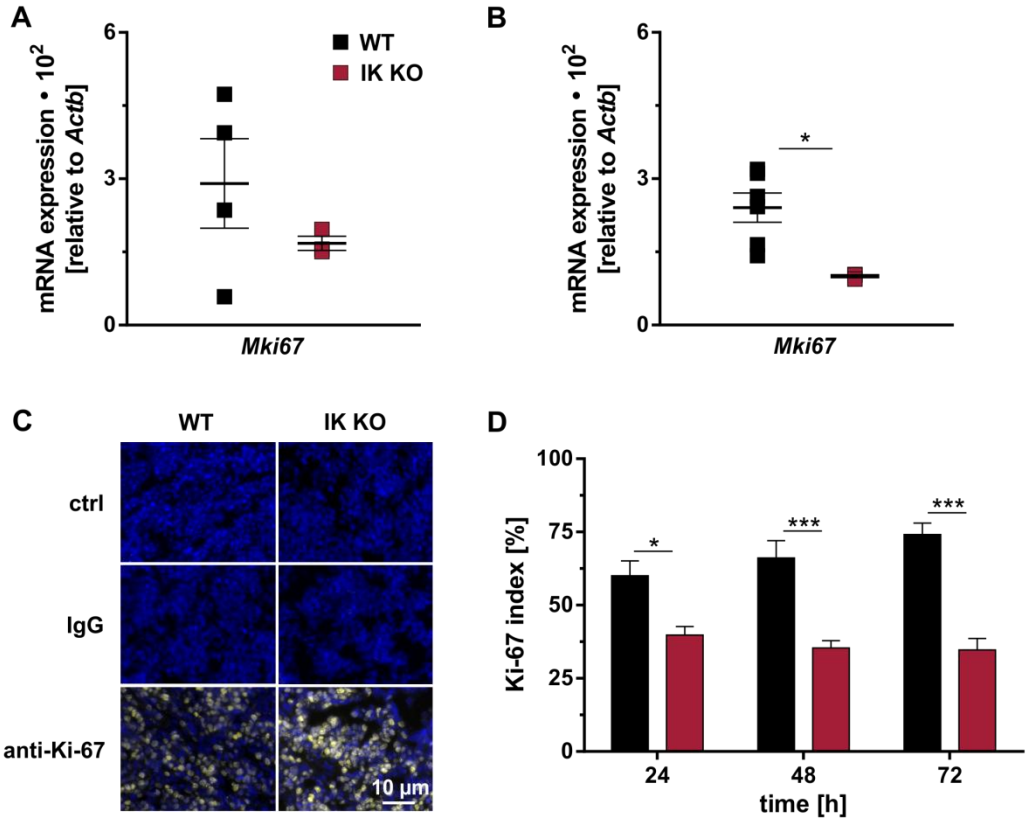

Figure 5.27: Ki-67 proliferation status of MMTV-PyMT$^{tg/+}$ WT and IK KO tissues and cells
Abundance of Ki-67-encoding mRNA was assessed in **(A)** tumour biopsies and **(B)** cells from spontaneously developed MMTV-PyMT$^{tg/+}$ WT and IK KO tumours. No difference was detected in tumour biopsies, whereas *Mki67* expression was significantly lower in IK KO cells. Ki-67 protein was investigated in MMTV-PyMT$^{tg/+}$ WT and IK KO **(C)** tissue sections (n = 4) and **(D)** cells (n = 6) with again no difference in tumour tissue, but a lower Ki-67 index in primary cell cultures with IK KO as compared to WT genotype. **(A, B, D)** Presented are means ± SEM with *p < 0.05, **p < 0.01 and

***p < 0.001. *Mki67* expression in tumour biopsies (n = 4 for WT and n = 3 for IK KO) and cells (n = 6 for WT and n = 3 for IK KO) was assessed with unpaired t-tests and Ki-67 index of cells was analysed by one-way ANOVA and Bonferroni correction.

To further elucidate the contribution of the IK channel to proliferation of tumour cells in the MMTV-PyMT$^{tg/+}$ model, the IK inhibitor TRAM-34 was studied in grid dishes for a time course of 0, 24, 48 and 72 after serum restimulation of cells with WT (figure 5.28 A) or IK KO (figure 5.28 B) genotype.

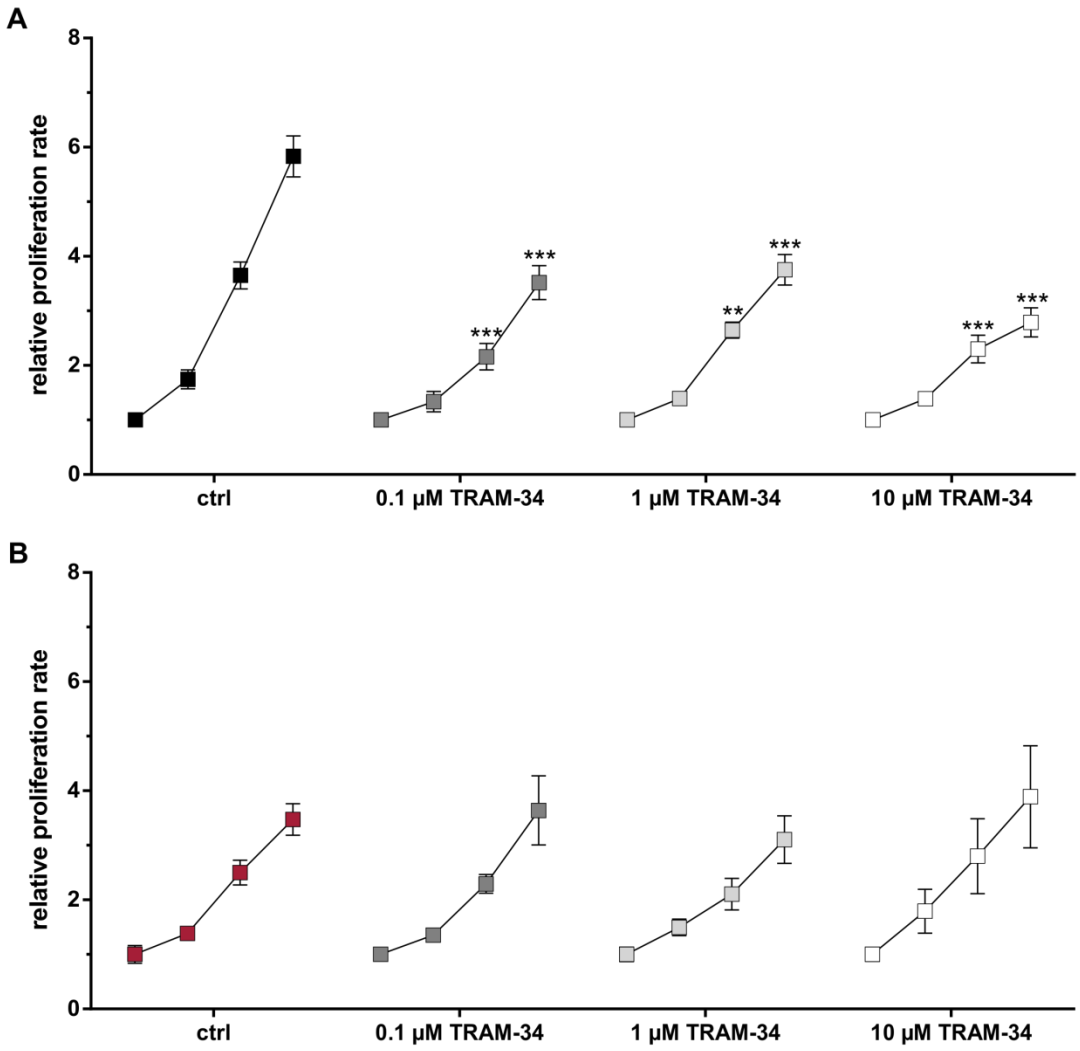

Figure 5.28: Proliferation of MMTV-PyMT$^{tg/+}$ WT and IK KO cells treated with TRAM-34
MMTV-PyMT$^{tg/+}$ WT and IK KO cells were seeded in grid dishes and allowed to adhere for 24 h before serum withdrawal for 72 h. Restimulation with 0.1, 1, and 10 µM TRAM-34 or ethanol as solvent ctrl was carried out with serum-containing medium for 3 d. **(A)** The proliferation of MMTV-PyMT$^{tg/+}$ WT cells was significantly decreased after 48 and 72 h of treatment with the different TRAM-34 concentrations. **(B)** In contrast, TRAM-34 did not modulate proliferation of IK KO cells over the entire time course. Of note, relative proliferation rates in the absence of IK were in the range of **(A)** TRAM-34-treated MMTV-PyMT$^{tg/+}$ WT cells. Means ± SEM of n = 5 experiments are plotted. **p < 0.01 and ***p < 0.001 of a two-way repeated measures ANOVA with Tukey´s test show significant difference according to the respective time point of ctrl treatment.

MMTV-PyMT$^{tg/+}$ WT cells showed the highest relative proliferation rate in ctrl (1.75 ± 0.17, 3.65 ± 0.25 and 5.83 ± 0.38 fold at 24, 48 and 72), whereas 0.1 µM (2.16 ± 0.24 and 3.52 ± 0.31 fold), 1 µM (2.65 ± 0.15 and 3.76 ± 0.28 fold) or 10 µM (2.30 ± 0.25 and 2.79 ± 0.27 fold) TRAM-34 significantly decreased proliferation in an IK-dependent manner at 48 and 72 h (figure 5.26 A). Proliferation of MMTV-PyMT$^{tg/+}$ IK KO cells showed no differences in ctrl (1.38 ± 0.09, 2.50 ± 0.23 and 3.47 ± 0.29 fold), 0.1 µM (1.35 ± 0.09, 2.29 ± 0.17 and 3.64 ± 0.63 fold), 1 µM (1.50 ± 0.15, 2.10 ± 0.29 and 3.11 ± 0.44 fold) and 10 µM (2.80 ± 0.40, 3.65 ± 0.69 and 3.89 ± 0.94 fold) TRAM-34 at 24, 48 and 72 h (figure 5.26 B). These in parts published experiments confirmed that TRAM-34-sensitive IK channels play an important role for the proliferation of MMTV-PyMT$^{tg/+}$ cells *in vitro*[385].

5.4 IK channels and the tumour microenvironment

5.4.1 Tumour immune cell status in the spontaneous MMTV-PyMT$^{tg/+}$ model

The IK channel is expressed in different cell types that constitute the tumour microenvironment and is especially described for its functions in both the innate and adaptive immune system (see section 1.4.4). Hence, IK channels were assessed for their contribution to an altered immune cell status of MMTV-PyMT$^{tg/+}$-derived tumours. Immune cells were distinguished from other cell types by their positive CD45 status (section 4.4.4). Immune cell infiltration in tumour tissue was recognised for the WT (11.9 ± 2.3 CD45-positive cells per 150 mm²), but was rare for the IK KO genotype (1.2 ± 0.5 CD45-positive cells per 150 mm²). Difference between MMTV-PyMT$^{tg/+}$ WT and IK KO tumour infiltration by CD45-positive cells reached statistical significance (figure 5.29 A). Moreover, CD45-positive cells in the tumour stroma were highly abundant in MMTV-PyMT$^{tg/+}$ WT (26.5 ± 2.7 CD45-positive cells per 150 mm²) and uncommon in IK KO (3.4 ± 1.1 CD45-positive cells per 150 mm²) samples (figure 5.29 B) allowing the conclusion that IK in tumour cells and in immune cells is important for the phenotype of the MMTV-PyMT$^{tg/+}$ model. Importantly, the interplay of IK in the different cell types could be one of the reasons for the apparent disparity between the *in vivo* and *in vitro* results.

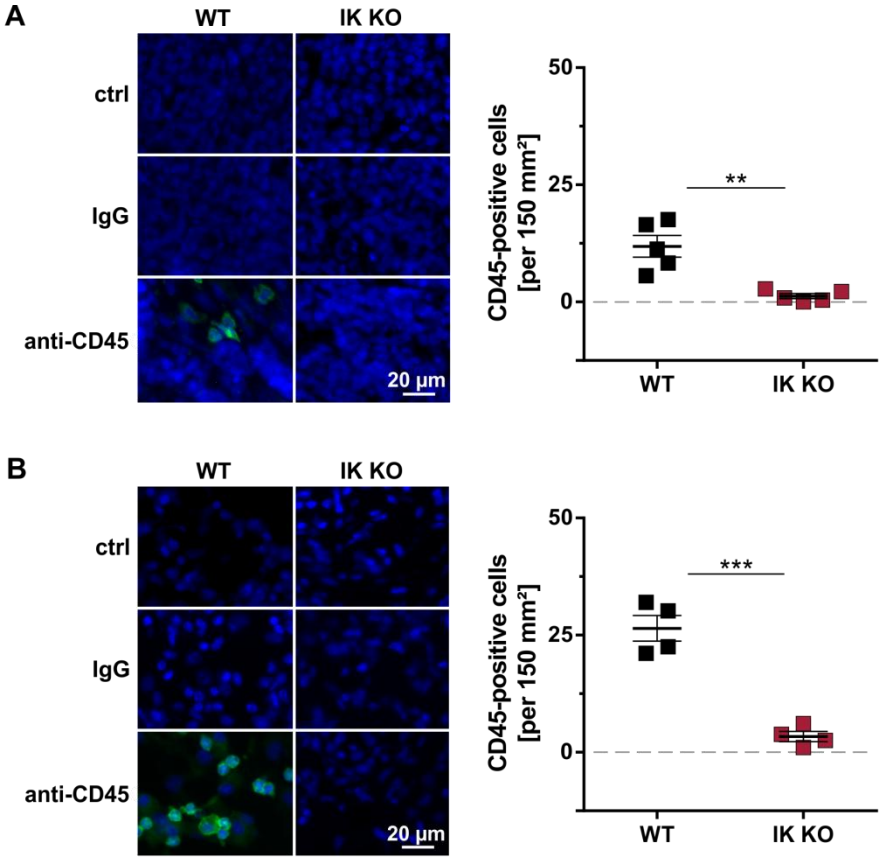

Figure 5.29: Presence of CD45-positive cells in MMTV-PyMT$^{tg/+}$ WT and IK KO tumours
Immune cell infiltration in tumour tissue and the surrounding stroma was detected by immunofluorescence staining against the CD45 pan immune cell marker. The presence of CD45-positive cells was significantly lower in tissue sections of **(A)** tumours and **(B)** surrounding stroma from MMTV-PyMT$^{tg/+}$ IK KO compared to WT samples. Shown are means ± SEM. Unpaired t-tests of n = 5 experiments revealed **p < 0.01 and ***p < 0.001 between genotypes.

5.4.2 Role of the IK channel in the MMTV-PyMT$^{tg/+}$ orthotopic transplant model

To study the contribution of the IK channel to tumour growth in dependence on its stromal expression *in vivo*, orthotopic MMTV-PyMT$^{tg/+}$ WT and IK KO cell transplantations were performed in the fourth right mammary gland of FVB/N mice (section 4.1.5). WT mice received MMTV-PyMT$^{tg/+}$ WT or IK KO cells. In a reverse approach, MMTV-PyMT$^{tg/+}$ WT cells were transplanted in IK KO mice. Log-rank tests revealed no differences regarding TFS of MMTV-PyMT$^{tg/+}$ IK KO cells in WT mice (HR 1.16 (CI 0.43 - 3.52)) and MMTV-PyMT$^{tg/+}$ WT cells in IK KO mice (HR 1.42 (CI 0.58 - 4.90)) in comparison with MMTV-PyMT$^{tg/+}$ WT cells in WT mice (figure 5.30 A). In contrast, OS was significantly prolonged in MMTV-PyMT$^{tg/+}$ IK KO cells implanted into WT mice (HR 0.35 (CI 0.06 - 0.63)) and MMTV-PyMT$^{tg/+}$ WT cells implanted into IK KO mice (HR 0.33 (CI 0.05 - 0.59)) compared to MMTV-PyMT$^{tg/+}$ WT cells implanted into WT mice with 74.0 ± 9.1, 67.4 ± 3.6 and 52.4 ± 5.6 d, respectively. The hereby presented findings suggest that a positive IK status in tumour cells especially, but also in

stromal cells, drive tumour progression (figure 5.30 B). Nevertheless, differences in tumour volume increase in the first 28 d after initial tumour palpation did not reach statistical significance between the groups (figure 5.30 C). In line with the results obtained in the spontaneous MMTV-PyMT$^{tg/+}$ model, *Esr1* and *Esr2* mRNA expression was not significantly different in tumours obtained from the various groups (supplemental figure 9.11). Macroscopic lung metastases neither showed significant differences between groups (0.33 ± 0.21, 1.00 ± 0.32 and 0.33 ± 0.21 metastases/lung for MMTV-PyMT$^{tg/+}$ WT cells in WT mice, MMTV-PyMT$^{tg/+}$ IK KO cells in WT mice and MMTV-PyMT$^{tg/+}$ WT cells in IK KO mice) (figure 5.30 D).

Moreover, immune cell infiltration and the presence of immune cells in the stroma were assessed in WT and IK KO recipients with either MMTV-PyMT$^{tg/+}$ WT or IK KO cells. CD45-positive cell numbers were analysed in MMTV-PyMT$^{tg/+}$ WT tumours with anti-CD45 staining performed by Alice Dragoi for her Master´s thesis project. Tumour immune cell infiltration was counted and revealed significantly lower numbers of CD45-positive cells in IK KO than in WT mice transplanted with MMTV-PyMT$^{tg/+}$ WT cells (0.68 ± 0.31 versus 2.62 ± 0.64 CD45-positive cells per 150 mm²) (figure 5.30 E). However, immune cell numbers in the stroma did not differ significantly (8.34 ± 4.13 or 7.93 ± 4.28 CD45-positive cells per 150 mm²) after transplantation of MMTV-PyMT$^{tg/+}$ WT cells into WT or IK KO mice (figure 5.30 F). Of note, only the CD45 status of MMTV-PyMT$^{tg/+}$ WT cells transplanted into WT and IK KO mice was considered. MMTV-PyMT$^{tg/+}$ IK KO primary cell cultures were derived from different mice and may present with an altered immunogenic potential when transplanted into immunocompetent FVB/N recipients.

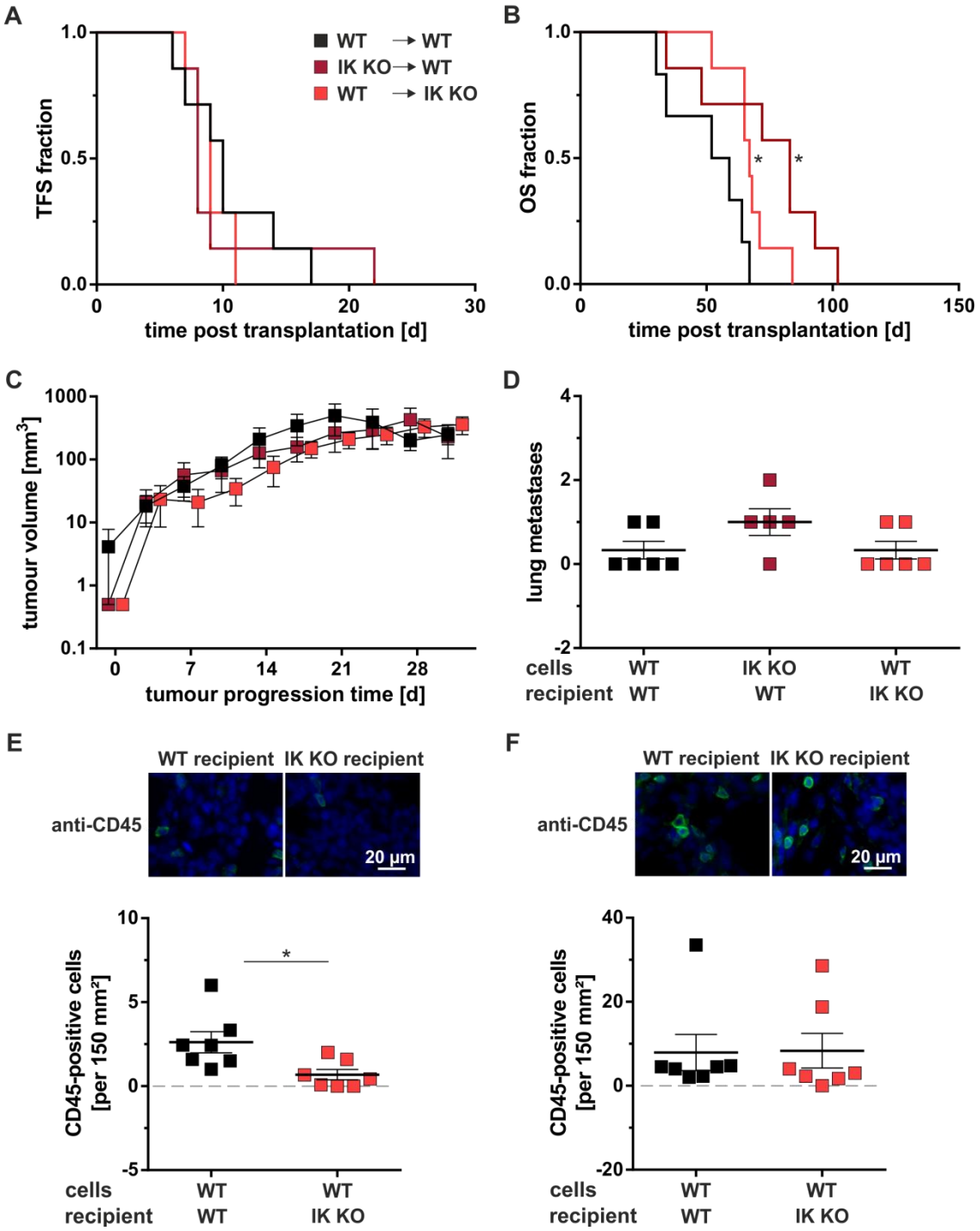

Figure 5.30: Tumour formation of MMTV-PyMT$^{tg/+}$ WT and IK KO cells after allotransplantation
Cells for transplantation derived from passages 6 to 12 of *in vitro*-propagated MMTV-PyMT$^{tg/+}$ tumour cells. Orthotopic transplantation was performed into the fat pad of the fourth mammary gland of FVB/N mice. Transplantation of MMTV-PyMT$^{tg/+}$ WT and IK KO cells in WT recipients allowed conclusions on the impact of the tumour cell IK channel for tumour induction and progression. Besides, the transplantation of MMTV-PyMT$^{tg/+}$ WT cells in WT or IK KO recipients was employed to investigate the role of the environmental IK channel to modulate these processes. **(A)** Tumour-free survival (TFS) did not differ between the transplant groups (log-rank test). **(B)** Overall survival (OS) was prolonged by IK ablation either in the tumour cell itself or in the microenvironment (log-rank test). **(C)** Tumour volume increase (two-way ANOVA with Tukey´s test) and **(D)** lung metastasis (Kruskal-Wallis test and Dunn´s post hoc analysis) showed no significant differences between groups. **(E)** Immune cell infiltration in the tumour was assessed by the detection of CD45-positive cells and revealed lower levels when

MMTV-PyMT$^{tg/+}$ WT cells were transplanted in IK KO recipients compared to WT recipients (unpaired t-test). **(F)** In contrast, no significant difference was observed with regard to CD45-positive cell numbers in the stroma of MMTV-PyMT$^{tg/+}$ WT tumours formed in WT or IK KO recipients (Mann-Whitney test). Plots present means ± SEM of n = 7 experiments with *p < 0.05.

5.5 Radiotherapy of IK-proficient and -deficient MMTV-PyMT$^{tg/+}$ cells and orthotopic tumour transplants

5.5.1 DNA repair and breast cancer cell survival after irradiation

Radiotherapy was first performed in MMTV-PyMT$^{tg/+}$ WT cells in the presence and absence of the IK inhibitor TRAM-34 as well as in IK KO cells. Clonogenic assays were carried out by seeding cells 24 h after 0, 2, 4 or 6 Gy IR in 6-well plates. Colony formation was studied after 14 d by coomassie blue staining and colonies of at least 50 cells of size, representing original tumour cells that survived irradiation, were counted (see figure 4.5). Moreover, IR induces direct and indirect DNA damage with malignant cells possessing a lower DNA repair capacity and thus decreased survival due to apoptosis by mitotic catastrophe when compared to healthy cells[38,39,384]. To examine if IK channel function modulates DNA repair, γH2AX foci as a measure of DNA damage were analysed. Previous work identified interplay between IK and IR-induced γH2AX levels in glioblastoma[296].

IK channel inhibition was carried out by application of the IK channel inhibitor TRAM-34 in comparison to ctrl treatment of MMTV-PyMT$^{tg/+}$ WT cells prior to IR. As shown in figure 5.31, colony formation assays were performed with clonogenic survival diminishing with increasing doses of IR. Survival fractions after 2, 4 and 6 Gy differed significantly or showed a tendency between ctrl (0.79 ± 0.03, 0.47 ± 0.06 and 0.20 ± 0.04) and TRAM-34 treatment (0.49 ± 0.05, 0.28 ± 0.06 and 0.13 ± 0.03).

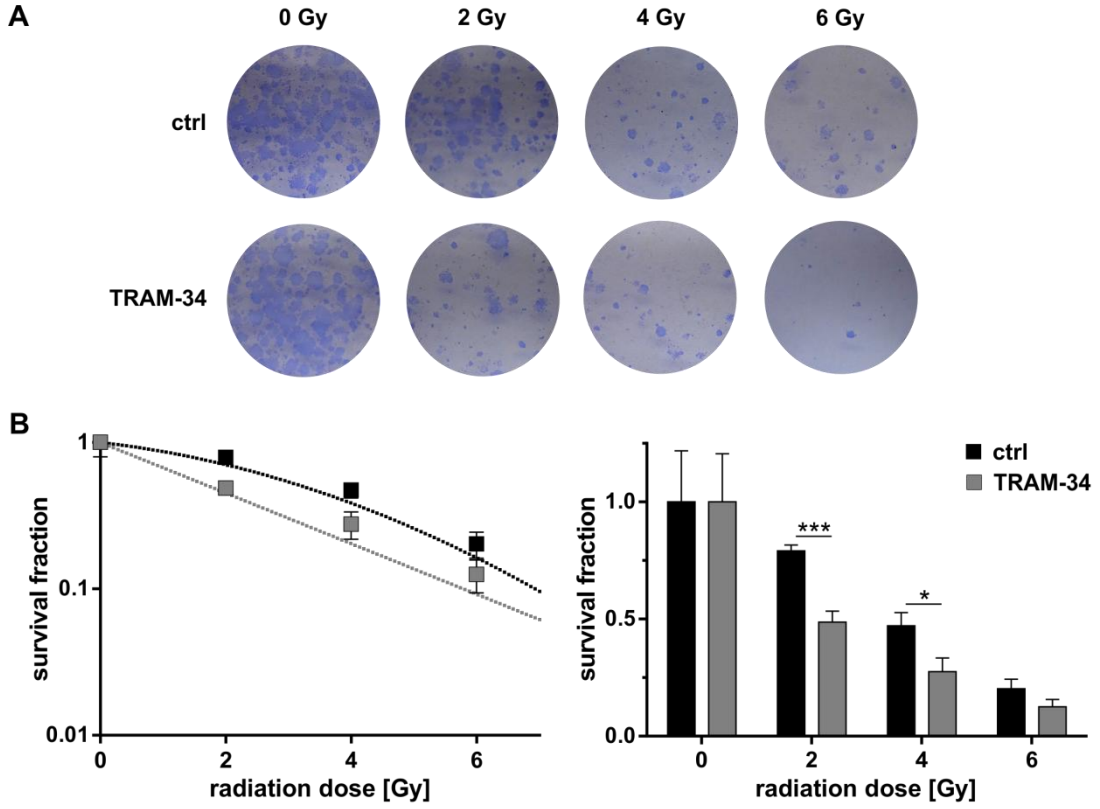

Figure 5.31: Influence of TRAM-34 treatment on survival of MMTV-PyMT$^{tg/+}$ WT cells after IR
After seeding, MMTV-PyMT$^{tg/+}$ WT cells were allowed to adhere and grow for 72 h prior to stimulation of the cells with 10 µM TRAM-34 or ethanol (ctrl), which occurred 1 h before IR. 24 h after irradiation with 0, 2, 4 or 6 Gy, cells were allowed to adhere and form colonies in 6-well plates for 14 d. **(A)** Colony formation ability of TRAM-34-treated or ctrl cells after irradiation is shown in the representative images. **(B)** The survival curve after increasing doses of IR (left) and the corresponding bar graphs (right) showed diminished colony formation after TRAM-34 treatment as compared to ctrl. Results are shown as means ± SEM of n = 5 experiments with *$p < 0.05$ and ***$p < 0.001$ in a one-way ANOVA with Sidak´s test.

In order to assess whether the decreased clonogenic survival after TRAM-34 treatment of the MMTV-PyMT$^{tg/+}$ WT cells resulted from an impaired DNA repair capacity, γH2AX foci (sections 1.1.3 and 4.4.4) were measured 30 min after IR for DNA damage induction and 24 h after IR for DNA repair (figure 5.32 A). IR with 2 Gy highly upregulated γH2AX foci numbers at 30 min with no differences in ctrl and TRAM-34 treatments (1.14 ± 0.08 versus 30.30 ± 0.44 and 1.12 ± 0.04 versus 29.78 ± 0.21 γH2AX foci/cell for 0 versus 2 Gy regarding ctrl and TRAM-34) (figure 5.32 B). However, residual γH2AX foci 24 h after IR with 2, 4 and 6 Gy and thus incomplete DNA repair, were significantly higher in TRAM-34-treated (1.59 ± 0.05, 2.74 ± 0.22 and 3.68 ± 0.31 γH2AX foci/cell) than in ctrl-treated MMTV-PyMT$^{tg/+}$ WT (1.31 ± 0.06, 2.15 ± 0.11 and 3.14 ± 0.36 γH2AX foci/cell) cells (figure 5.32 C).

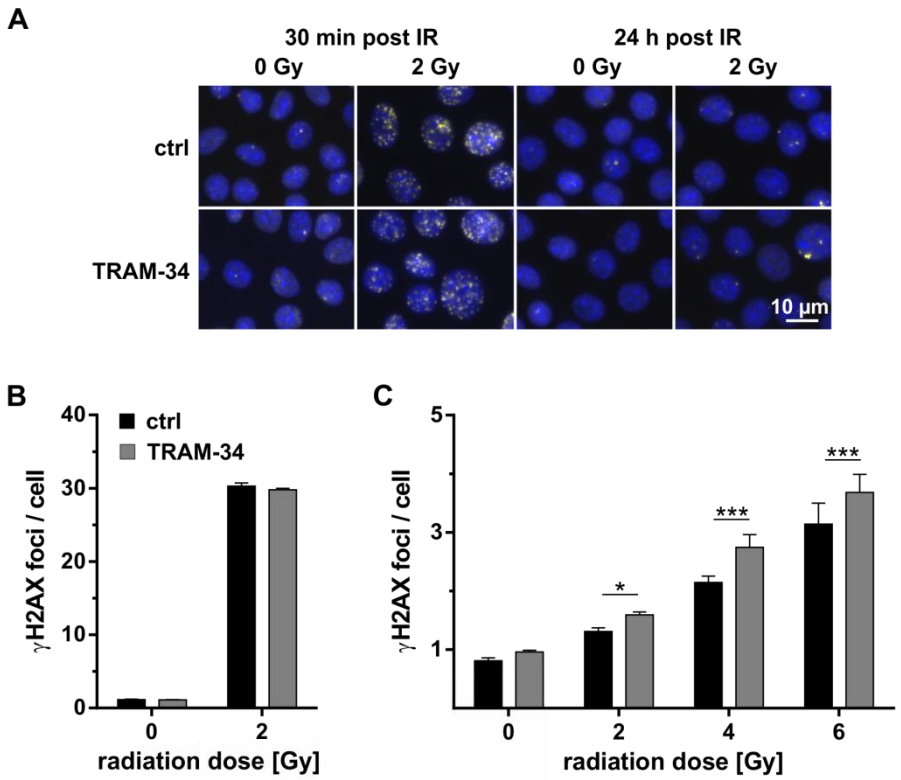

Figure 5.32: Effect of TRAM-34 treatment on MMTV-PyMT$^{tg/+}$ WT cell DNA damage induction and repair by IR

(A) MMTV-PyMT$^{tg/+}$ WT cells were seeded in 12-well chamber slides for γH2AX assay. After 72 h, cells were treated with 10 µM TRAM-34 or the solvent (ctrl) 1 h prior to irradiation with 0, 2, 4 or 6 Gy. 30 min and 24 h after IR, respectively, cells were fixed to investigate DNA damage induction and repair. **(B)** γH2AX foci induction 30 min after IR did not differ between ctrl and TRAM-34 treatments. **(C)** Residual γH2AX foci 24 h after IR were significantly higher in TRAM-34-treated compared to ctrl-treated MMTV-PyMT$^{tg/+}$ WT cells. n = 5 experiments were carried out as presented with means ± SEM. *p < 0.05 and ***p < 0.001 show significant differences according to a two-way repeated measures ANOVA with Sidak´s multiple comparison test.

To confirm these results, clonogenic survival together with analysis of residual γH2AX foci after irradiation were assessed in MMTV-PyMT$^{tg/+}$ WT and IK KO cells. Again, survival of MMTV-PyMT$^{tg/+}$ WT cells decreased in a dose-dependent manner with 0.73 ± 0.04, 0.35 ± 0.02 and 0.13 ± 0.01 for 2, 4 and 6 Gy, respectively. A much higher vulnerability to IR was observed in IK-deficient cells, which also responded with a dose-dependent but much steeper decline in survival (0.36 ± 0.03, 0.15 ± 0.02 and 0.06 ± 0.01 for 2, 4 and 6 Gy, respectively). Differences between genotypes were significant for 2 and 4 Gy. The low number of colonies formed with 6 Gy in both genotypes, compared to 0, 2 and 4 Gy, might explain why results for this IR dose lack significance (figure 5.33).

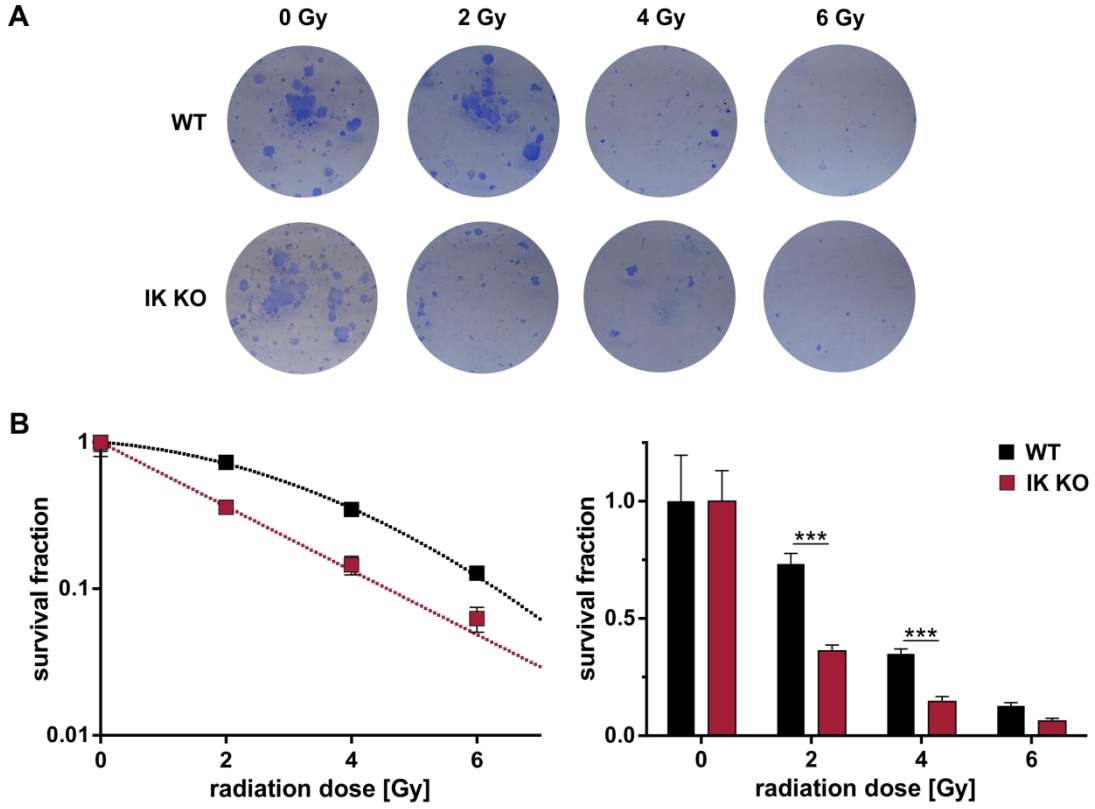

Figure 5.33: Clonogenic survival of MMTV-PyMT$^{tg/+}$ WT and IK KO cells after IR
To test for clonogenic survival after IR, MMTV-PyMT$^{tg/+}$ WT and IK KO cells were plated in 6-well plates (n=6 technical replicates per experiment) 24 h after irradiation. Colony formation was studied after 14 d in fixed and coomassie blue-stained cultures. Survival of MMTV-PyMT$^{tg/+}$ WT and IK KO cells after IR was measured as colonies with ≥ 50 cells. **(A)** Representative images show tumour cells from both genotypes irradiated with the different radiation doses. The density of colonies was lower in MMTV-PyMT$^{tg/+}$ IK KO than in WT samples. **(B)** Colony formation ability, presented in the survival curve (left) and corresponding bar graphs (right), was significantly diminished in MMTV-PyMT$^{tg/+}$ IK KO compared to WT cells after 2 and 4 Gy of IR. Means ± SEM of n = 9 experiments revealed **p < 0.01 and ***p< 0.001 in a one-way ANOVA with Sidak´s post hoc test.

In addition, γH2AX foci were counted 30 min and 24 h after irradiation in order to analyse genotype-specific differences in irradiation-evoked DSB formation and remaining DNA damage after DNA repair (figure 5.34 A). Formation of γH2AX foci was detected by immunofluorescence and firstly measured 30 min post IR. γH2AX foci were strongly induced by 2 Gy with no differences between genotypes (1.20 ± 0.21 versus 30.27 ± 2.06 and 1.05 ± 0.16 versus 32.01 ± 1.82 γH2AX foci/cell for 0 versus 2 Gy in WT and IK KO (figure 5.34 B). Residual γH2AX foci were counted 24 h after IR as a measure of remaining DSBs after DNA repair. With 0.76 ± 0.14 and 1.00 ± 0.19 γH2AX foci/cell in MMTV-PyMT$^{tg/+}$ WT and IK KO cells at 24 h, 0 Gy-irradiated cells did not differ in the number of γH2AX foci, which were in the same range as at the 30 min time point. After 24 h and contrary to 30 min, however, 0 Gy IR induced a significant increase in γH2AX foci numbers in the IK KO genotype, which surprisingly imply diminished DNA repair in this genotype at basal

conditions already. 24 h after IR, administration of 2, 4 and 6 Gy resulted in significantly increased residual γH2AX foci numbers in MMTV-PyMT$^{tg/+}$ IK KO (1.95 ± 0.26, 2.84 ± 0.32 and 3.78 ± 0.27 γH2AX foci/cell) compared to WT cells (1.41 ± 0.21, 2.08 ± 0.26 and 2.60 ± 0.25 γH2AX foci/cell) (figure 5.34 C). Together, the impaired DNA repair capacity of MMTV-PyMT$^{tg/+}$ IK KO cells might explain the decreased clonogenic survival of IK-deficient cells after irradiation.

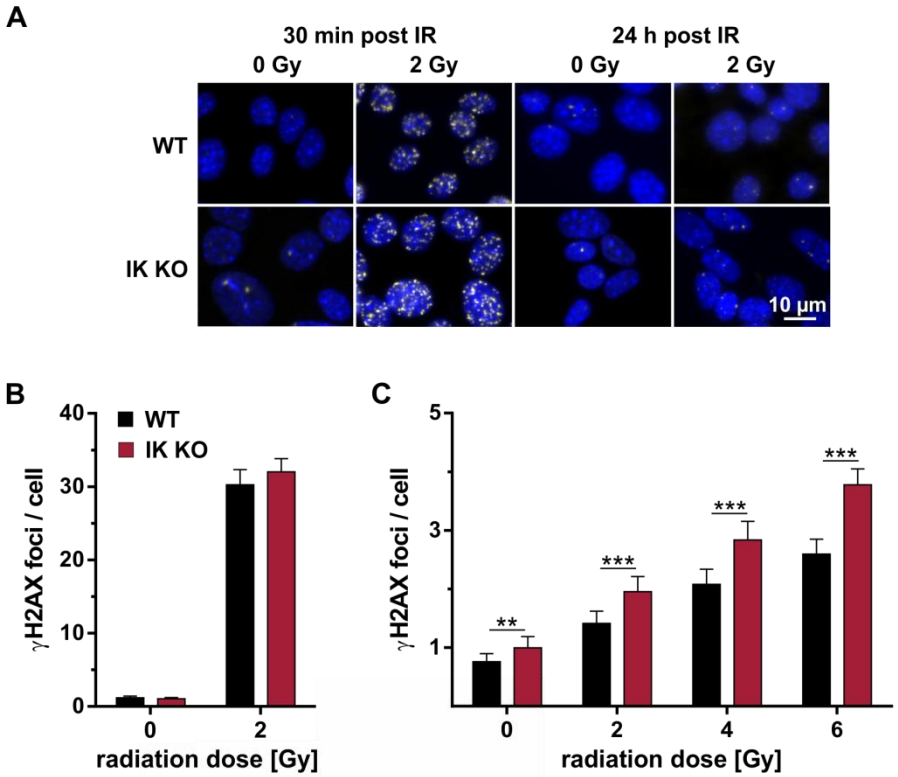

Figure 5.34: DNA damage induction and repair in MMTV-PyMT$^{tg/+}$ WT and IK KO cells after IR
(A) Representative images show the formation of γH2AX foci 30 min upon irradiation with 2 Gy. The number of γH2AX foci 24 h after irradiation was lower in MMTV-PyMT$^{tg/+}$ WT compared to IK KO cells indicating that DNA repair processes are impaired. Nuclei were counter-stained with DAPI (blue) and γH2AX foci present in the cell nuclei are visualised in yellow colour. Counting the number of nuclei and the total number of γH2AX foci allowed determination of γH2AX foci per cell. **(B)** γH2AX foci numbers did not differ between genotypes 30 min after IR. **(C)** 24 h post IR, residual γH2AX foci numbers, a measure of incomplete DNA repair, were elevated with increasing doses of IR and particularly in the IK KO compared to the WT genotype. n = 7 experiments are presented as means ± SEM. **p < 0.01 and ***p < 0.001 show significant differences between genotypes as calculated by two-way repeated measures ANOVA and Sidak´s test.

5.5.2 Survival and growth of MMTV-PyMT$^{tg/+}$ WT and IK KO tumours in mice after radiotherapy

To test for the relevance of IK channels in the response to radiotherapy, IR was delivered to MMTV-PyMT$^{tg/+}$ WT and IK KO tumours growing in FVB/N mice after orthotopic transplantation for five consecutive days (sections 4.1.5 and 4.1.7). An appropriate IR dose, which would lead to moderate tumour regression and allowing for regrowth, i.e. an

eightfold-increased tumour volume compared to the beginning of irradiation, was tested in MMTV-PyMT$^{tg/+}$ WT tumours in advance. 2.5, 5 and 7 Gy per day significantly increased survival times as reflected by increased HRs of 0.24 (CI 0.02 - 0.29), 0.21 (CI 0.01 - 0.02) and 0.21 (CI 0.01 - 0.02) with p-values ≤ 0.0009, 0.0001 and 0.0001 compared to 0 Gy. Within the 7 Gy group, one animal had full tumour regression and showed no regrowth over the time course of 120 d after the start of irradiation (figure 5.35 A).

The 2.5 Gy dose was used for irradiation of MMTV-PyMT$^{tg/+}$ IK KO tumours, as the *in vitro* data implied a higher radiosensitivity after IK channel inhibition or ablation (figures 5.31 and 5.33). 2.5 Gy in MMTV-PyMT$^{tg/+}$ IK KO tumours induced improved survival with a HR of 0.31 (CI 0.07 - 0.44) compared to 0 Gy (figure 5.35 B). Monitoring of tumour volumes after IR in both genotypes showed a more profound regression with increasing radiation doses (figure 5.35 C). Accordingly, survival times were dose-dependent with 20.43 ± 2.30, 35.29 ± 2.43, 48.29 ± 3.87 and 80.14 ± 10.77 d for 0, 2.5, 5 and 7 Gy in MMTV-PyMT$^{tg/+}$ WT as well as 34.86 ± 4.00 and 63.00 ± 9.62 d for 0 and 2.5 Gy in MMTV-PyMT$^{tg/+}$ IK KO tumour-bearing mice. As a result, there was a significant increase in survival time of mice with 2.5 Gy-irradiated MMTV-PyMT$^{tg/+}$ IK KO tumours as well as 5 and 7 Gy-irradiated MMTV-PyMT$^{tg/+}$ WT tumours compared to 0 Gy-irradiated MMTV-PyMT$^{tg/+}$ WT tumours. Besides, MMTV-PyMT$^{tg/+}$ IK KO tumour and therefore survival after 2.5 Gy was higher than after 0 Gy in IK KO tumours or MMTV-PyMT$^{tg/+}$ WT tumours irradiated in 2.5 Gy doses (figure 5.35 D).

Analysis of tumour mRNA levels at the end of the experiment showed no significant difference for H2AX between genotypes and radiation doses. Also, *Kcnn4* mRNA expression was not significantly in irradiated MMTV-PyMT$^{tg/+}$ WT tumours, albeit it was absent in the IK KO as expected (supplemental figure 9.12). In addition, no significant difference in macroscopic lung metastasis was detected between mice with MMTV-PyMT$^{tg/+}$ WT and IK KO tumours (data not shown). These results suggest a radiosensitising effect after interference with the IK channel to improve local tumour control.

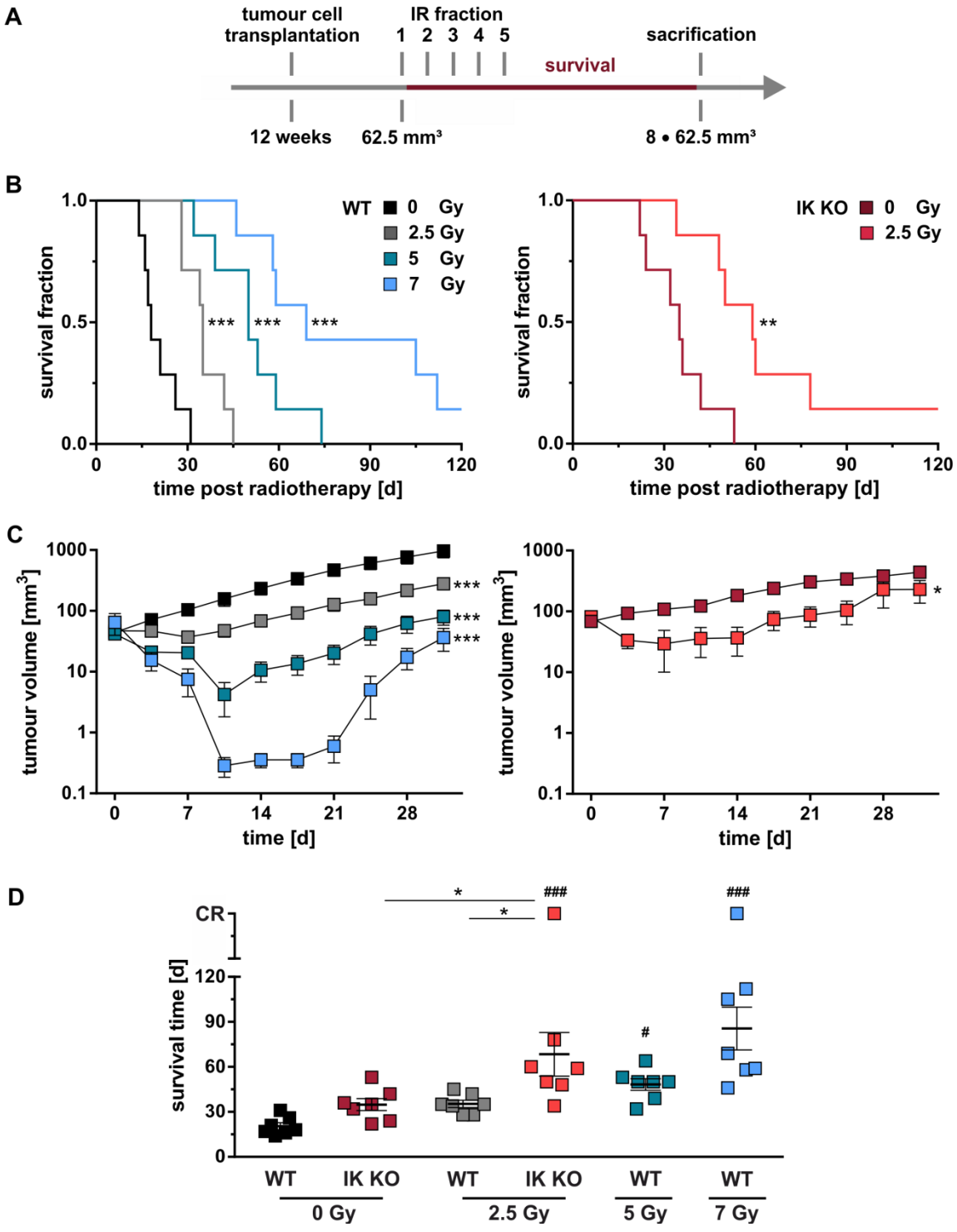

Figure 5.35: Radiotherapy of MMTV-PyMT$^{tg/+}$ WT and IK KO tumours in mice
(A) FVB/N mice transplanted with MMTV-PyMT$^{tg/+}$ WT or IK cells received localised radiotherapy at a tumour volume of about 62.5 mm³. Irradiation of the tumours occurred for five consecutive days at doses of 0, 2.5, 5 or 7 Gy, respectively. Tumour regression and regrowth were assessed until tumours reached an eightfold-increased tumour volume compared to the first day of irradiation (n = 7). **(B)** In comparison with 0 Gy, escalating doses of IR led to significantly improved overall survival of mice transplanted with MMTV-PyMT$^{tg/+}$ WT or IK KO tumour cells in log-rank tests. **(C)** Tumour volumes decreased by IR in a dose-dependent manner (means ± SEM, two-way repeated measures ANOVA and Tukey´s test). **(B + C)** *p < 0.05, **p < 0.01 and ***p < 0.001 show significant differences to the respective 0 Gy genotype control. **(D)** Survival time was increased in 2.5 Gy-irradiated IK KO

compared to 0 Gy and 2.5 Gy WT and 0 Gy IK KO tumour-bearing mice. Each one mouse in IK KO 2.5 Gy and WT 7 Gy showed complete response (CR). One-way ANOVA with Sidak´s post hoc test calculated *$p < 0.05$ as indicated in the figure or #$p < 0.05$ and ###$p < 0.001$ compared to 0 Gy-irradiated MMTV-PyMT$^{tg/+}$ WT tumour-bearing mice.

6. Discussion

6.1 The BK channel contributes to breast tumourigenesis and cancer progression

Ion channels are aberrantly expressed in cancer and they contribute to the characteristics of tumours from different entities including breast cancer[131,135]. In hormone-related cancers, the BK channel is known to promote the proliferation of breast, cervix, ovarian and prostate cancer cells[179,180,187]. By the use of different breast cancer cell lines and human patient data, BK contribution to cell cycle progression, high tumour stage and poor prognosis were confirmed[187,191].

6.1.1 BK KO modifies survival in spontaneous and engrafted MMTV-PyMT$^{tg/+}$ murine breast cancer models

In an earlier work, increased TFS without effect on OS was observed in the breast cancer-prone MMTV-PyMT$^{tg/+}$ BK KO compared to WT mouse. Animal numbers in this study were low due to mating problems and generation of the KO genotype with n = 5 for TFS and n = 4 for OS[315]. Thus, a first aim of the present work was to repeat the respective experiments albeit with an increased number of mice. As a result, both TFS (n = 16 for BK KO genotype) and OS (n = 8 for BK KO genotype) were prolonged in the MMTV-PyMT$^{tg/+}$ BK KO compared to the WT genotype (figure 5.1). Moreover, the transplantation of primary MMTV-PyMT$^{tg/+}$ BK KO cells into WT recipients increased TFS (figure 5.4 B), but had no effect on OS (figure 5.4 C) when compared to MMTV-PyMT$^{tg/+}$ WT tumours propagated in WT hosts. With regard to its physiological role, the BK channel is ubiquitously expressed in different tissues including smooth muscle, neurons and cochlear hair cells, contributing to many physiological functions such as vascular tonus, neuronal excitability and hearing[394,395]. Tumour formation and growth of primary MMTV-PyMT$^{tg/+}$ cells generally depend on the tumour microenvironment. A modulatory effect of BK on TFS and OS seems also to stem from microenvironmental cells, as MMTV-PyMT$^{tg/+}$ WT cells propagated in BK KO mice had shorter TFS but no difference with respect to OS when compared to their transplantation into WT mice (figure 5.4 B + C). Presently, it is unclear why BK-deficient tumour engraftments do not affect OS, whereas MMTV-PyMT$^{tg/+}$ BK KO mice that spontaneously develop breast cancer show a prolonged OS time. Presumably, the generally faster tumour formation and progression in the transplant model, as reflected by a decreased observation period of the tumours until termination criteria are reached, may explain the difference compared to the spontaneous model. This higher aggressiveness of the transplant model may derive from selection pressure of tumour clones during primary tumour growth in the spontaneous model,

during the establishment of primary cell cultures together with their cultivation, and underlies the successful implantation in the recipient. Thus, in the transplant model, BK deficiency may be compensated in certain tumour clones with regard to tumour growth.

Furthermore, BK in glioblastoma is described to promote metastasis. Glioblastoma cells express high levels of a glioma-specific BK splice variant, which seems to stimulate the migratory properties of this type of malignant tumour cells[186,396]. Therefore, metastasis to the lungs was also investigated with regard to BK channel status in the spontaneous MMTV-PyMT$^{tg/+}$ breast cancer model. As counted from the right lung, there were no differences in macroscopically visible numbers of metastases (figure 5.1 C). However, micrometastases counted after haematoxylin/eosin staining in the left lung showed an increase in spontaneous MMTV-PyMT$^{tg/+}$ BK KO compared to WT tumour-bearing mice (figure 5.1 D). This surprising result might be explained by the elevated overall observation time of the tumour-prone BK KO genotype. In the transplant model, macroscopic lung metastasis numbers did neither differ (figure 5.4 E) and micrometastasis detection by haematoxylin/eosin staining was absent (data not shown). For explanation and in contrast to subcutaneous MMTV-PyMT$^{tg/+}$ cell injection as site of tumour cell transplantation, MMTV-PyMT$^{tg/+}$ cells injected in the mammary pad and thus their site of origin express a differential gene pattern and can lose their metastatic potential[397].

6.1.2 Tumour *KCNMA1* mRNA expression levels modulate human breast cancer outcome

Molecular breast cancer subtypes can be distinguished according to the PAM50 classification and they determine clinical characteristics and survival outcome according to gene expression patterns[8,26,398]. In order to test a potential influence of BK channel mRNA expression on OS, human patient samples stratified for BK channel mRNA expression levels were investigated. The data was collected as part of TCGA and the KM plotter. Strikingly, the two web tools delivered contrary results with high BK channel mRNA expression acting as modifier that decreased OS in TCGA but increased OS in the KM plotter (figure 5.6). To test for the contradictory OS outcomes derived from Kaplan Meier estimations in TCGA and the KM plotter, data collection and conductance of the survival analyses must be compared for differential technical approaches. For mRNA expression analyses, n = 1,200 samples for both *KCNMA1* and *KCNN4* were provided in TCGA, whereas only n = 626 samples for *KCNMA1* but n = 1,402 samples for *KCNN4* were available in the KM plotter. In TCGA, a sequencing library was created from total RNA and sequencing was carried out on an IlluminaHiSeq2000 microarray platform. In contrast, data in the KM plotter derived from publications that provided raw data and included clinical survival data, at least 30 patients in

the cohort and Affymetrix HG-U133A and HG-U133 Plus 2.0 microarrays. Follow-up time in the survival analyses was less than 9 years for TCGA and 25 years for the KM plotter[342,399,400]. In conclusion, TCGA may provide more reliable information with regard to survival outcome, but its use in the breast cancer data set is limited due to a relatively short follow-up time at the moment.

6.1.3 The Ki-67 proliferation marker is decreased in MMTV-PyMT$^{tg/+}$ BK KO tumours

The Ki-67 protein is an established marker for proliferation. It is detectable through all active phases of the cell cycle while absent in quiescent cells[97]. Ki-67 expression in tissues and cells derived from MMTV-PyMT$^{tg/+}$ WT and BK KO tumours served to further assess BK channel contribution to proliferation and thus tumour progression. The Ki-67 status of MMTV-PyMT$^{tg/+}$ BK KO tissues and cells was lower than in the WT genotype (figure 5.10). These *in vitro* results confirmed the increased OS survival of the BK KO genotype *in vivo* and were in line with previous results on the role of the BK channel in breast cancer proliferation[187,190].

6.1.4 ER and HER2 expression in murine breast cancer as well as immune cell infiltration are not affected by BK status

The most prominent biomarkers to define breast cancer subtypes are ER, PR and HER2[7]. The ER forms a homodimer or heterodimer composed of α and β subunits and it is expressed in the majority of breast tumours. ER activation by oestrogens leads to receptor dimerisation and translocation in the nucleus where it binds EREs. Thereby, gene expression is regulated in favour of proliferation and anti-apoptosis with the ER-α subunit dominating the oncogenic characteristics of the ER. Less is known about ER-β, albeit it seems to possess counter-regulatory properties to ER-α[401,402]. A positive ER status is often accompanied by PR expression because the latter is induced by ER signalling. PR signalling contributes to proliferation and thus represents a risk factor for breast cancer development. However, the presence of the PR is associated with an ameliorated prognosis in established breast cancer due to its context-dependent action, for example the interference with E2-induced and ER-α-mediated tumour cell growth[403-406]. HER2 overexpression is found in 20 - 30% of all breast tumours. It is associated with aggressive tumour characteristics and poor outcome, but anti-HER2 therapy in particular in combination with chemotherapy is quite successful[96,407-409].

As breast cancer subtype is a predictor of recurrence and survival outcome[13,410], classification of MMTV-PyMT$^{tg/+}$ WT and BK KO tumours and differences between genotypes were studied. Tumour tissues and cells from both genotypes were positive for ER and HER2 expression (figure 5.2). As further confirmation, expression patterns of BK channel subunits were detected in human breast cancer cell lines of different intrinsic subtypes and thus different hormone receptor and HER2 status (figure 5.8). In addition, the presence of immune cells in tumours and stroma was detected in both spontaneous and transplant MMTV-PyMT$^{tg/+}$ WT and BK KO tumours with the pan leukocyte marker CD45. Immune cell infiltration in stroma and tumour tissue was not dependent on the BK status, hence identical in MMTV-PyMT$^{tg/+}$ WT and BK KO samples (figures 5.3 and 5.4). Thus, BK genotype-specific effects on the interplay of these factors with tumourigenesis and tumour growth were excluded.

6.2 BK channel accessory subunits are important determinants of breast cancer risk and progression

The BK-α pore-forming subunit is ubiquitously expressed and its activity is determined by both membrane potential and $[Ca^{2+}]_i$. The tissue-specific association of BK-α with accessory BK-β and BK-γ subunits allows BK channel activity at decreased voltages and lower $[Ca^{2+}]_i$ concentrations[153,411]. Therefore, it was speculated that BK channel activity and function in normal breast and breast cancer relies on the tissue- and cell type-specific expression of its subunits.

6.2.1 SNPs in the *KCNMB4* gene can increase breast cancer risk

Gene expression is regulated by complex hierarchical signalling networks. Moreover, steady-state mRNA levels differ between individuals due to the impact of genetic variation, as can be found by the analysis of eQTLs[412-414]. In order to test for genetic variation in the genes associated with the BK channel complex and their impact on breast cancer risk, SNP data from the iCOGS array was used from the BCAC[347]. SNPs in the *KCNMB4* gene were found that increased overall breast cancer risk and further were associated with the development of ER-positive tumours. Moreover, all SNPs were located in the first two introns of the *KCNMB4* gene and thus may have upstream regulatory properties. In the context of *KCNMB4* protein expression, BK-β4 was reported to stimulate or inhibit BK channel activity in a Ca^{2+} concentration-dependent manner[163,415]. Further, BK-β4 was shown to decrease sensitivity to BK-interacting agents such as the pharmacological inhibitors charybdotoxin and iberiotoxin[164]. Nevertheless, the functional significance of the *KCNMB4* variants must be

further clarified. 8 of the 9 SNPs were in high linkage disequilibrium (figure 5.5). Thus, it would also be possible that these variants are inherited in linkage disequilibrium with various SNPs from other genes that functionally contribute to breast cancer development. In addition to breast cancer development, variants in BK channel genes potentially modulate therapy success and survival outcome in breast cancer[416].

6.2.2 BK channel subunits are differentially expressed in breast cancer subtypes

BK subunit mRNA expression was further regarded in human healthy and breast tumour tissue data retrieved from TCGA. No differences were seen between the two groups with the presence of all subunits spread across the samples except for *LRRC38* encoding BK-γ4, for which no data was available, and the testis-specific *LRRC52* encoding the BK-γ2 subunit (figure 5.7). As the expression of different BK subunits may be very patient-specific including patients without any BK expression and as diverse subunits may potentially compensate for each other, individual differences might be masked by this approach.

The K_{Ca} mRNA expression profile was analysed in a set of 15 human normal breast and breast cancer cell lines of different molecular subtypes and revealed a high frequency of *KCNMA1*, but also *KCNMB3*, *KCNMB4* and *LRRC26*. Apart from *LRRC26*, mRNA expression of the other BK-γ-encoding subunits, namely *LRRC38*, *LRRC52* and *LRRC55* was rarely seen (figure 5.8). K_{Ca} mRNA expression analysis in MMTV-PyMT$^{tg/+}$ WT and BK KO tumour tissues and cells confirmed the positive BK-α status in the WT genotype on mRNA level while it was absent in the BK KO genotype. Besides, the qRT-PCR analysis revealed abundances of *Lrrc26* as well as *Kcnn4* mRNA in both genotypes with significantly increased amounts in BK KO cells (figure 5.9). Due to their tissue-specific expression, specific BK-β and BK-γ subunits are present in breast cancer and enable oncogenic BK functions. In the case of breast cancer, especially BK-β4 and BK-γ1 may represent novel modifiers and molecular targets for tumour formation and growth and in particular BK-γ1 was identified because of its abundance in breast and prostate cancer[153,165].

6.2.3 BK channel subunits stimulate proliferation of breast tumour cells

Due to its high expression in breast tumour cells and in breast cancer in general[165], the functional contribution of BK-α and BK-γ1 to the proliferation of MMTV-PyMT$^{tg/+}$ WT and BK KO mouse as well as of MDA-MB-453 human breast tumour cells was further tested by the use of siRNA. In line with decreased Ki-67 expression after BK-α ablation (figure 5.10), si*Lrrc26* markedly attenuated the proliferation of MMTV-PyMT$^{tg/+}$ WT cells to levels of

MMTV-PyMT$^{tg/+}$ BK KO cells, in which the *Lrrc26* depletion showed no additional and thus BK-α-independent effect. Furthermore, si*Lrrc26* led to increased *Kcnmb4* mRNA levels in MMTV-PyMT$^{tg/+}$ WT cells with no effect in the BK KO genotype (figure 5.11). In MDA-MB-453 cells having very high mRNA expression levels for *KCNMA1* and *LRRC26*, si*KCNMA1* and si*LRRC26* each diminished relative proliferation rates as compared to si*NT*-treated cells. In addition, the si*KCNMA1*-mediated depletion of BK-α induced *LRRC26* mRNA upregulation, which may point to a counter-regulatory effect due to a lack of BK activity (figure 5.12). In sum, BK-γ1 served as fundamental factor for proper BK function in terms of proliferation in the tested murine and human breast tumour cells. The downregulation of BK-γ1 decreased proliferation in dependence on the presence of BK-α. In order to compensate for lacking or absent BK function, upregulation of other BK subunits that constitute the BK channel complex occurred. Hence, the different accessory subunits may, at least in part, have influence on each other's expression. Questions rise to which extent the oncogenic potential of the BK channel relies on distinct BK-β and BK-γ subunits and in how far their modulation is reversed by compensatory expression of other subunits.

As BK-β and BK-γ subunits are expressed in a tissue-specific manner, their targeting may represent a promising tool to modulate BK function in a more specific way with fewer side effects. As BK-α is ubiquitously expressed and linked to important physiologic functions, pharmacological targeting *in vivo* gives rise to multiple problems. In this context, BK deficiency induces different conditions, e.g. cerebellar ataxia[316], an increased blood pressure due to hyperaldosteronism[417], progressive hearing loss[418] or osteopenia[419]. With regard to cell types that constitute the tumour microenvironment, BK channel expression status affects maturation and insulin signalling in adipocytes[357,420] and it responds to nitric oxide application in fibroblasts[421]. Furthermore, the BK channel modulates endothelial-dependent vasodilation as well as smooth muscle cells and thus the vascular tone[422,423], but has no impact on endothelial cell proliferation and therefore angiogenesis[424]. In clinical trials, BK channel modulation was tested without satisfactory success so far. The number of candidates to enter clinical trials has been low, which can derive from lacking selectivity or potency and from toxicities. One small molecule BK activator reached phase III clinical trials investigating stroke, but failed because it showed no difference compared to placebo treatment[425-427].

6.3 Interaction of BK with different growth factors and anti-/oestrogens promotes tumour cell proliferation and tumour growth

6.3.1 Growth factors present in serum and selected hormones induce BK-dependent breast tumour cell proliferation *in vitro*

The assembly of the BK channel complex acts as determinant of BK function and action. Nevertheless, the BK channel assembly does not represent a sufficient explanation for its mechanistic contribution to breast cancer. However, it is known that BK channel activity is not only dependent on the membrane potential, $[Ca^{2+}]_i$ and accessory subunits. Rather, the BK channel responds to activation by ligands such as a diversity of growth factors and it may serve as transducer for extracellular stimuli[220]. Therefore, a first approach investigated the proliferation response of MMTV-PyMT$^{tg/+}$ WT and BK KO cells to standard FCS-containing media in comparison to media supplemented with CCS or without serum. As expected, proliferation rates were higher in MMTV-PyMT$^{tg/+}$ WT cells treated with FCS compared to the BK KO genotype and compared to CCS or serum-free treatments in both genotypes (figure 5.13). BK channel activation by growth factors is rapid, as measured by electrophysiological approaches, thus suggesting direct effects on the BK channel with physiological but also pathophysiological consequences such as an increased proliferation of MCF-7 cells after stimulation also with a membrane-impermeable form of E2[202].

A complementary approach utilised MMTV-PyMT$^{tg/+}$ WT and BK KO mouse as well as MDA-MB-453, MCF-7 and MDA-MB-157 human breast tumour cells, which were stimulated by different growth factors, i.e. E2, E2-BSA, progesterone or testosterone, in a range of physiological concentrations and up to 10 nM, the concentration with the putatively largest effect on BK channel activation[202], in a logarithmic scale. Proliferation outcomes were primarily dependent on BK channel status and less on the hormone concentrations applied to the tumour cells (figures 5.14 and 5.15). Interestingly, however, E2 was previously shown to stimulate the mRNA expression of BK-α and its accessory subunits via ER genomic signalling and it is known to promote the expression of distinct BK-α isoforms through the regulation of alternative splicing[217,428,429]. To conclude, BK channel-positive tumours seem to benefit from extracellular circulating growth factors, which may stimulate proliferation of the corresponding tumour cells. Canonical BK channels are usually present at the plasma membrane. Besides, intracellular BK channels are found in different cell types, especially on the inner mitochondrial membrane and the outer membrane of the nucleus[430,431]. For signalling, especially the nucleus is an interesting target. Nuclear BK channels in hippocampal neurons are described to regulate nuclear Ca^{2+} concentration and signalling as well as to regulate transcription mediated by the cyclic adenosine monophosphate response element-binding protein[432]. As the non-membrane-permeable E2-BSA conjugate showed a

pro-proliferative effect in MMTV-PyMT$^{tg/+}$ WT cells (figure 5.14), it was excluded that intracellular BK channels or ERs were involved. In addition, patch-clamp experiments revealed changes in BK K^+ currents upon hormone applications[201,202].

Despite these promising results, also some opposing effects were described when comparing the work of different research groups using various cell types. BK channel activation and signalling by oestrogens may be cell type- and context-dependent. Besides, oestrogens may also stimulate other ion channels potentially superimposing the beneficial effects linked to the depletion of BK activity[220]. Therefore, a comparative study investigating different cell types, growth factors in different concentrations and a variety of functional assays, i.e. electrophysiology and proliferation, would allow for a better understanding of the integration of hormone-stimulated BK channel activation in breast cancer.

6.3.2 Anti-hormones modulate proliferation of BK channel-positive breast tumour cells in a concentration-dependent manner

The BK channel has also been described for its activation by different anti-hormones and may thus intervene with endocrine breast cancer therapy. Indeed, stimulation of the BK by TAM is a concentration-dependent process with maximum activation at 10 nM TAM inducing MCF-7 breast tumour cell proliferation[207]. In a comprehensive approach, MMTV-PyMT$^{tg/+}$ WT and BK KO cells as well as MDA-MB-453, MCF-7 and MDA-MB-157 cells were exposed to 1, 10, 100 or 1,000 nM TAM, (Z)-4-OH-TAM, (Z)-endoxifen or fulvestrant. At high concentrations (1,000 nM) the various drugs produced the clinically desired effect of lower proliferation in the ER-positive MMTV-PyMT$^{tg/+}$ WT and BK KO as well as MCF-7 cells. In the BK-α-positive MMTV-PyMT$^{tg/+}$ WT and MCF-7 cells, proliferation-stimulating rather than inhibitory effects were observed at lower doses of TAM (1 to 10 nM) in different experimental settings. In MMTV-PyMT$^{tg/+}$ BK KO cells, all drugs tested showed an anti-proliferative tendency or no effect emphasising BK to be responsible for the pro-proliferative effect of anti-oestrogens. In line, the ER- and BK-α-negative as well as BK-γ1-positive MDA-MB-157 cell line did not respond to any of these treatments, suggesting that BK-γ1 is not sufficient to promote either pro- or anti-proliferative effects of the anti-hormones. However, proliferation rates in ER-negative MDA-MB-453 cells, which express high levels of BK-α and BK-γ1, were significantly enhanced by TAM and its metabolites (figures 5.16 and 5.17), hence, it was concluded that this occurred independently from genomic signalling controlled by the ER.

Regarding hormone signalling via the ER, the classic ER-α and ER-β homodimer or heterodimer resides mainly in the nucleus and less in the cytoplasm even in absence of ligand binding, which leads to rearrangement of the ER pattern within the nucleus[433].

Besides, the nuclear pore complex regulates shuttling of the ER between cytoplasm and nucleus. ER activation is involved in gene transcription with its role as transcription factor but also as coregulator by the interaction with other transcription factors[434,435]. Moreover, two ER-α isoforms, namely ER36 and ER46 with molecular weights of 36 and 46 kDa were found to be associated with the membrane via palmitoylation. Adaptor and scaffolding proteins facilitate ER-α membrane localisation and enable multi-protein signalling complexes. Both isoforms are E2-responsive and the presence of ER36 in breast cancer cells is independent from their nuclear ER status[435-437]. Therefore, ER-α membrane localisation may also explain, at least partly, the pro-proliferative effects after E2 application in MMTV-PyMT$^{tg/+}$ WT murine as well as MDA-MB-453 and MCF-7 human tumour cells. However, it is not a valid explanation for the pro-proliferative effect after anti-oestrogen application, as agonistic effects of the anti-oestrogens tested on mammary ER isoforms have not been described so far (figures 5.14 and 5.15).

Besides ER36 and ER46, the GPER residing in the plasma membrane was identified in various cell types. In breast cancer cell lines, GPER expression is independent from ER status albeit interactions are described. In this context, GPER stimulation by E2 leads to breast cancer cell proliferation. E2-evoked and ER-independent non-genomic effects via GPERs occur in a rapid manner by interaction with signalling pathways. Not only E2, but also TAM and its metabolite (Z)-4-OH-TAM as well as fulvestrant show agonistic effects on the GPER. In addition, the GPER is associated with oestrogen-related diseases such as cancers of the reproductive system, obesity or osteoporosis[438-442]. This raises the question whether the pro-proliferative effect after application of hormones or anti-oestrogens in MMTV-PyMT$^{tg/+}$ WT and BK KO mouse as well as the differential outcome in MDA-MB-453, MCF-7 and MDA-MB-157 human breast tumour cells (figures 5.14 - 5.17) may derive from interaction of the BK channel with the GPER. However, there exist conflicting results on the putative localisation and function of the GPER in the endoplasmic reticulum, the cytoplasm and nucleus, which needs to be clarified[443]. In the context of breast cancer, high cytoplasmic GPER expression is claimed to result in better survival outcome also in patients receiving endocrine therapy, and associates with low stage and luminal A or luminal B subtypes. On the contrary, nuclear GPER expression is an indicator for less differentiated and triple-negative breast cancer[444,445]. Another study compared membrane to total GPER expression. Opposite to total GPER, membrane GPER expression is an indicator for high histological grade and poor prognosis[446]. In line, GPER expression is associated with TAM resistance, which can be explained by the agonistic effect of TAM on the GPER as well as the consequent induction of aromatase expression[445,447]. Further, GPER expression in breast cancer-associated fibroblasts may modulate the migration and epithelial-mesenchymal transition in breast tumour cells[448]. Moreover, it was recently shown that activity of the

TREK-1 two-pore domain K^+ channel is increased by GPER signalling after E2 stimulation, whereas E2 has no direct effect on TREK-1 activity[449]. GPER is also expressed in the MMTV-PyMT$^{tg/+}$ model, in which it has no obvious impact on tumourigenesis, but contributes to tumour progression[450]. Therefore, future studies should investigate the potential interaction of BK channels and GPER at the membrane that may stimulate anti-/hormone-induced BK currents and downstream signalling[202,207].

Generally, interaction of membrane proteins and induction of signalling processes are enabled in lipid rafts, which are sphingolipid and cholesterol-enriched domains of the membrane. Caveolae are such tube-like invaginations, which are further characterised by the expression of caveolins-1 - 3 serving as scaffold proteins. In particular, caveolin-1 is described for its ambiguous function in cancer[451,452]. In breast cancer, caveolin-1 has a dual role as tumour suppressor and oncoprotein. Absence of caveolin-1 is associated with cellular transformation and proliferation. MMTV-PyMT$^{tg/+}$ caveolin-1 KO mice show decreased TFS leading to a higher tumour burden[453]. Besides, the absence of caveolin-1 in tumour stroma correlates with tumour stage, recurrence and a decreased progression-free survival. In TAM-treated patients, it further predicts poor prognosis[454]. In advanced breast cancer, however, caveolin-1 overexpression is found and functions to promote proliferation in established tumour cells. Moreover, TAM application increases caveolin-1 expression, whereas this is repressed after acquisition of TAM resistance[453,455]. As scaffolding protein, caveolin-1 possesses versatile functions during tumourigenesis, tumour progression and TAM resistance. Deciphering its controversial effects and the direct interaction partners of caveolin-1 for the accomplishment of its different pro-oncogenic and tumour-suppressive functions would be beneficial for better comprehension and the development of intervention strategies[456]. Interestingly, TAM and its metabolites, E2 as well as cholesterol to a minor extent, decrease membrane fluidity in breast cancer cells. This effect is dose-dependent and observed at high doses in particular[457-459]. The BK channel is found in cholesterol-rich microdomains of the membrane from vascular endothelial cells, especially in caveolae where its activity is diminished by the interaction with caveolin-1[460]. In myometrial cells, the BK has been associated with caveolin-1, but also caveolin-2, however not with caveolin-3. Lipid raft disruption in these cells also increases BK channel activity[461].

In addition to its rationale for the therapy of especially ER-positive breast tumours, TAM shows anti-fungal and anti-viral actions and modulates natural killer cell cytotoxicity[458,462-464]. Strikingly, TAM application to ER-negative tumour cells is described to promote anti-proliferative and anti-migrative properties, apoptotic events as well as the reversion of epithelial-mesenchymal transition. Further, the oncolytic effect of TAM is not completely reversible by high-dose E2 administration. Regarding ER-independent actions of TAM, these

are accompanied by an increase in $[Ca^{2+}]_i$, which is associated with elevated levels of ROS and c-Jun N-terminal kinase activation. Interestingly, this may represent the underlying mechanism for an observed increase in proteasomal degradation and EGFR level reduction by TAM. Besides, TAM-evoked protein kinase C reduction may result from direct EGFR down-stream signalling via the phospholipase C-γ1/phosphatidylinositol 4,5-bisphosphate/diacylglycerol pathway[465-467]. Whether BK channel activation by TAM is involved in these processes is unclear at present.

To summarise this part, BK channel status served as determinant of anti-oestrogen-induced proliferation. This effect was not dependent on genomic ER signalling usually attenuating the proliferation response of breast tumour cells. It can thus be proposed that patients with BK channel-positive tumours may especially benefit from anti-oestrogen therapy when applied at sufficiently high concentrations reaching steady-state conditions early after the start of therapy in order to circumvent a potentially undesired pro-proliferative effect mediated by BK. On the other side, BK-positive tumour clones with declining ER status may benefit from continuous endocrine therapy through BK channel-mediated stimulation of proliferation. Therefore, BK channel-positive tumours may be more prone to develop anti-oestrogen resistance, as clones with low ER expression that form during disease progression would respond less to the beneficial effects of the endocrine therapy leading to their clonal expansion. As an example provided in the murine p53 null transplant model, ER-positive premalignant lesions develop to ER-positive or ER-negative tumours. Here, TAM administration reduces tumour incidence, delays tumour onset and leads to the formation of ER-negative tumours in particular. Whether the ER-negative tumours arising in this model form from previously ER-positive tumour cells or whether there is a direct selection towards ER-negative tumour cells remains elusive[468].

6.3.3 Efficacy of TAM therapy *in vivo* is decreased in breast tumours with positive BK channel status

TAM is the pioneering drug used for endocrine intervention as part of breast cancer therapy. Before the approval of TAM, synthetic oestrogens at very high doses were applied to treat tumours of the breast. Due to the grand success of TAM, which was initially developed as contraceptive, it has been prescribed to many patients[77,78,469]. Nevertheless, TAM itself is a pro-drug with a diversity of metabolites including (Z)-4-OH-TAM and (Z)-endoxifen possessing much elevated affinities for binding the ER[470]. (Z)-endoxifen is accepted the main contributor to the anti-cancer effects of TAM therapy, because it reaches higher systemic levels compared to (Z)-4-OH-TAM albeit high inter-patient variability is observed that is influenced by CYP2D6 activity[90,471-473]. Due to the pro-proliferative effect of TAM and its

metabolites seen in BK channel-positive breast tumour cells (figures 5.16 and 5.17), the potential relevance of this interplay was further assessed in the MMTV-PyMT$^{tg/+}$ model *in vivo*.

First, TAM metabolism was determined in mice in order to compare to the well-studied metabolism in humans. In murine plasma, concentrations of TAM and its metabolites were dependent on the dose and thus lower in 0.5 mg/60 d than in 5 mg/60 d release pellets. Steady-state conditions were already reached at the first measurement time point at 7 d post pellet implantation. When comparing the main metabolites, TAM reached highest concentrations compared to (Z)-4-OH-TAM, which was higher than (Z)-endoxifen, while N-DM-TAM was below the lower limit of quantification in most samples (figure 5.18). These results are in line with previously published data in the mouse[472]. However, TAM is excessively metabolised to N-DM-TAM in the human system. Therefore, human plasma concentrations are even higher for N-DM-TAM than TAM and (Z)-endoxifen levels are higher than levels of (Z)-4-OH-TAM[474,475]. In addition, serum steady-state conditions of TAM in humans are only reached within a time frame of four weeks[89]. Besides, TAM and its metabolites accumulate especially in tumour tissue compared to plasma levels, but tissue concentrations diminish with circulating levels of E2[476,477]. Comparing murine CYP2D and human CYP2D6 activity, a similar expression pattern is confirmed in liver and kidney, but not in intestine and brain[478]. Although metabolite accumulation differs between the human and the murine system, experimental TAM therapy in the MMTV-PyMT$^{tg/+}$ model is established. Dose and application frequency vary according to the application routes such as i.p.[479,480] or s.c.[481] injections, per oral gavage[472,482] or subcutaneous pellet implants[483-486].

For investigating growth differences during TAM therapy according to BK channel status, the 5 mg/60 d release pellet was chosen as clinically relevant dose. The use of drug pellets ensures continuous release without necessity of daily application and thus repeated handling and stress for the MMTV-PyMT$^{tg/+}$ WT or BK KO tumour-bearing and ovariectomised mice. TAM successfully decreased tumour growth in MMTV-PyMT$^{tg/+}$ BK KO mice. However, there was no significantly prolonged tumour growth detected with TAM in the WT genotype. Apparently, TAM therapy was less effective in the presence of BK in the MMTV-PyMT$^{tg/+}$ mouse model (figure 5.19). Hints for growth-stimulatory effects at the beginning of TAM therapy are described in patients as well as in mice transplanted with MCF-7 cells[487]. Further, TAM induces an accelerated tumour onset in a mouse model of *Brca1* mutation-related breast cancer[488]. With respect to MMTV-PyMT$^{tg/+}$ mice, this model develops HER2- and ER-positive breast tumours with the latter declining in late stage carcinomas[312]. In MMTV-PyMT$^{tg/+}$ explants grown in ovariectomised mice, the maintenance of low ER expression and experimentally dose-dependent E2-stimulated growth of tumours *in vivo* are

confirmed. However, it is known that high-dose application of E2 downregulates ER expression and thus can result in a loss of ER status and thereby leading to differential results. It is also important to note that the MMTV promoter possesses no ERE, thus it should not respond to E2 and ER-mediated signalling directly. However, MMTV promoter activity is controlled by other steroids such as progesterone and glucocorticoids[489]. Further, the interplay between ER and HER2 was investigated in human breast cancer cell lines with E2 but also TAM repressing HER2 transcription via their action on the ER[490]. In male FVB/N MMTV-PyMT$^{tg/+}$ mice, TAM treatment reduces the number of mammary pads developing a tumour, but it has no impact on growth once a tumour is established. TAM also increases ER-α expression in mammary gland tumours in male mice while ER-β and HER2 are decreased[479]. In female FVB/N MMTV-PyMT$^{tg/+}$ mice, TAM shows prolonged tumourigenesis also resulting in delayed progression as measured by tumour growth[480]. To some extent, other studies report the absence of ER in late-stage MMTV-PyMT$^{tg/+}$ tumours with induction of high AR expression. However, the course of hormone receptor and HER2 expression during MMTV-PyMT$^{tg/+}$ tumour progression is substrain-specific[312,491]. This can partly be explained by substrain-specific SNPs, which are already shown to determine the metastatic potential of the MMTV-PyMT$^{tg/+}$ model[492]. In that context, a positive ER status in MMTV-PyMT$^{tg/+}$ tumour tissues and cells utilised in this approach was confirmed and further emphasised by the use of littermate animals for the experimental purposes (section 4.1.4 and figure 5.2).

6.3.4 TAM modifies survival outcome of breast cancer cells after IR

According to the German S3 guideline for breast cancer, endocrine therapy and radiotherapy can safely be delivered in a sequential or in a concurrent manner[80,493,494]. In one study, the combination of the AI anastrozole and radiotherapy shows a reduction in the 5-year ipsilateral breast tumour recurrence-free survival rate as compared to anastrozole alone. This effect could not be replicated when replacing anastrozole with TAM[495]. However, other studies describe an improved local control when radiotherapy is added to TAM treatment[496-498]. In general, continuous TAM application to reach therapeutically-relevant high concentrations in the tumour tissue induces G_1 cell cycle arrest of breast tumour cells, which may support their DNA repair capacity and thus survival[499-501]. Assuming that proliferation determines survival outcome after IR, the opposing pro-proliferative and anti-proliferative effects of either 10 or 1,000 nM TAM (see figure 5.16) need further consideration especially in BK channel-positive breast tumours. The experimental setup used was based on MMTV-PyMT$^{tg/+}$ WT and BK KO cells stimulated with TAM prior to irradiation. Survival and residual γH2AX foci numbers were dependent on treatment conditions with 1,000 nM TAM

resulting in a better outcome in both genotypes compared to ctrl. In contrast, 10 nM TAM decreased survival of MMTV-PyMT$^{tg/+}$ WT cells, whereas the opposite was observed in MMTV-PyMT$^{tg/+}$ BK KO cells (figure 5.20). Importantly, lack of BK did not alter radiosensitivity per se (supplemental figure 9.10). A possible explanation for these differential cell behaviours between genotypes and with regard to TAM concentration is the interplay between BK channel-stimulated and ER-prohibited proliferation, as cell cycle arrest is important to allow for DNA repair and to overcome mitotic catastrophe[502].

In one study from 1989, an increased radioresistance of MCF-7 cells treated with 1,000 nM TAM was observed, which was confirmed in further *in vitro* studies[503,504]. On the contrary, other studies suggest an increased radiosensitivity of combined TAM and radiotherapy. In these studies, TAM was applied after IR only and actually did not test for concurrent TAM and radiotherapy[505,506]. Moreover, a beneficial radiosensitising effect of combined TAM and radiotherapy is also claimed in two rat models[504]. However, one of these two rat model tested for the tumourigenic potency of radiotherapy and thus TAM was applied only 14 or 15 d after IR[507]. The second rat model used the carcinogen 1-methyl-1-nitrosurea for induction of multiple ER-positive breast tumours, where 25 fractions of IR in combination with daily s.c. administration of 500 mg/kg BW TAM resulted in decreased tumour volumes, as also observed with IR or TAM alone. The suitability of this model is questionable, as the application of IR in this model is known to induce further carcinogenesis leading to the formation of additional tumours[508]. Compared to the daily standard application of 20 mg TAM for the therapy of breast cancer patients assuming an average BW of less than 70 kg, the TAM dose chosen in these rats was approximately 150 times higher and may therefore lack clinical relevance[509,510]. Besides, the liver carcinogenic effects of the TAM metabolite α-OH-TAM, which extensively accumulates in rats but not in mice or humans, also limits the use of *in vivo* rat cancer models for the analysis of TAM-mediated effects[86,87]. Regarding clinical trials, only data from retrospective analyses of the combined effect of TAM and radiotherapy are available. So far, these reports do not find evidence for altered radioresistance when TAM application overlaps for at least two weeks with radiotherapy. With regard to toxicity, an increase in radiotherapy-induced lung and mammary fibrosis is observed with simultaneous TAM treatment, which is attributable to the release of pro-inflammatory cytokines by both therapies[504].

In view of BK as prognostic factor and predictor of therapy outcome, the frequency of BK expression in human breast tumours and thus the clinical importance of BK channels as breast cancer biomarker must be established. In this attempt, BK channel mRNA expression was screened and showed a positive status in most of the 15 human normal breast and breast cancer cell lines from different molecular subtypes (figure 5.8). However, the majority

of commercially available breast cancer cell lines were initially isolated from sites of metastasis instead of the primary tumour. Hence, the frequency of BK channel expression in the primary disease remains largely unclear and conclusions being drawn are further restricted by the fact that migration and thus metastasis of the tumour cells may be attributed to the tumour-promoting functions of the BK channel. With regard to highly invasive malignancies, BK contributes to radiation-induced migration in glioblastoma[186,222]. Also in breast cancer, BK channel inhibition by different penitrems decreases migratory and invasive properties of MDA-MB-231 cells[511].

6.4 The IK channel is implicated in breast cancer development and survival outcome

6.4.1 *KCNN4* SNPs modify human breast cancer risk and *KCNN4* gene expression may determine survival outcome

The clinical relevance of the IK channel was investigated with human breast cancer genetic data. BCAC analysis revealed eleven SNPs in the first intron of the *KCNN4* gene, which were associated with an altered overall risk for breast cancer development and the risk to develop ER-positive tumours. Of special interest were three SNPs with high MAFs of 0.36 or 0.41, namely rs12609846, rs1685191 and rs12463319, which decreased overall and ER-positive breast cancer risk to 0.94 or 0.93 with very low p-values (figure 5.24)[347]. Based on the TCGA dataset, mRNA expression for *KCNN1 - 4* did not differ between established breast tumours and healthy breast tissue (figure 5.25). Stratification of breast cancer patients by *KCNN4* mRNA expression levels revealed differential survival outcomes with high expression leading to decreased OS in the KM plotter. OS analysis in TCGA showed no influence of *KCNN4* mRNA expression levels (figure 5.26). This might be explained by the shorter follow-up time in TCGA or differences in other experimental aspects such as sample numbers and microarray platforms, as already stated in section 6.1.2.

6.4.2 Lack of IK does not alter TFS and OS in the spontaneous MMTV-PyMT$^{tg/+}$ model, but contributes to proliferation *in vitro*

In the spontaneous MMTV-cNeu$^{tg/+}$ murine breast cancer model, IK KO results in prolonged TFS and OS[385]. The characteristic of this model is the overexpression of cNeu, the rat homologue of human HER2. Due to the unactivated form of cNeu in the MMTV-cNeu$^{tg/+}$ model meaning intrinsic tyrosine kinase activity, but no activating mutations as are observed in human HER2-enriched breast cancer, tumours form with a long latency and resemble the

luminal B type[29,512,513]. In contrast to MMTV-cNeu$^{tg/+}$, no effects on TFS and OS are observed in the spontaneous MMTV-PyMT$^{tg/+}$ mouse model[385]. In another attempt to investigate the role of IK channels for breast cancer induction and progression *in vivo*, no effects on TFS and OS were confirmed in the IK-deficient MMTV-PyMT$^{tg/+}$ model (figure 5.21). The oncoprotein in the MMTV-PyMT$^{tg/+}$ model is the polyoma middle T antigen and this mouse breast cancer model is characterised by the formation of multiple tumour foci[312]. Comparing the two models investigated, they differ in their aggressiveness and show strain-specific latencies. MMTV-cNeu$^{tg/+}$ mice on FVB/N background develop tumours at an average age of 7 - 12 months, whereas the F1 generation of mixed FVB/N x C57Bl/6 MMTV-cNeu$^{tg/+}$ mice shows a TFS of > 18 months[514,515]. MMTV-PyMT$^{tg/+}$ mice have an average TFS of 53 d on FVB/N background and 92 d on C57Bl/6 background[302,313]. Therefore, tumour induction is much faster in MMTV-PyMT$^{tg/+}$ compared to MMTV-cNeu$^{tg/+}$ mice. However, all breast cancer-developing mice utilised in the presented analyses were on FVB/N background. Moreover, both MMTV-cNeu$^{tg/+}$ and MMTV-PyMT$^{tg/+}$ mice develop luminal tumours with pulmonary metastasis. Besides, MMTV-cNeu$^{tg/+}$ and MMTV-PyMT$^{tg/+}$ tumours cluster tightly in gene expression with luminal epithelial profiling. With regard to the ten subgroups of breast cancer, both mouse models cluster in group VI and thus luminal cell phenotype[29,516-518]. Therefore, it may be the fundamental aggressiveness of the MMTV-PyMT$^{tg/+}$ model to mask moderate effects on survival outcome such as induced by IK channel ablation.

Further, analysis of Ki-67 mRNA and protein expression revealed no difference between genotypes in tissue sections derived from such tumours. However, significant differences were obtained for isolated primary MMTV-PyMT$^{tg/+}$ cells with decreased Ki-67 levels in the IK KO genotype (figure 5.27). Besides, proliferation assays were performed in grid dishes where MMTV-PyMT$^{tg/+}$ IK KO cells had a significantly lower relative proliferation rate compared to WT. IK channel contribution to proliferation was additionally confirmed by the application of the IK inhibitor TRAM-34, which significantly decreased cell proliferation at any of the concentration tested in the presence of IK (figure 5.28). The lacking effect of the IK channel on tumour growth *in vivo* and Ki-67 status *in situ* compared to the decreased proliferation status after IK channel ablation or inhibition *in vitro* point to an altered proliferation response due to tumour cell cultivation or to microenvironmental cells and factors, which are absent in the established primary cell cultures.

6.4.3 ER, HER2 and K_{Ca} molecular patterns are not dependent on IK channels

For classification of MMTV-PyMT$^{tg/+}$ WT and IK KO tumours, mRNA expression analyses of the genes coding for K_{Ca} channels, ERs and HER2 together with ER-α protein staining were performed in MMTV-PyMT$^{tg/+}$ tissues and cells from both genotypes. Genotype-dependent

alterations except for the expected absence of *Kcnn4* mRNA in the IK KO genotype were not observed (figures 5.22 and 5.23). Apparently, alterations in breast cancer subtype or K_{Ca} mRNA expression are not responsible for the discrepant results in MMTV-PyMT$^{tg/+}$ tissues and cells.

6.4.4 Tumour infiltration of immune cells is determined by IK channel expression

Despite advances in the exploration of its contribution to cancer, one prominent role of the IK is its expression and function in a diversity of cells constituting the immune system. These comprise T cells[519,520] and B cells[275,521], dendritic cells[278,522], macrophages[277,523], natural killer cells[276], but also granulocytes[279] and mast cells[280,524]. The IK channel is important for the activation of these immune cell subsets to fulfil their particular functions. The importance of the immune system to recognise malignant cells but also manipulation of immune cell functions by established tumours to promote their own growth are well described. This altered response of the immune system comprises decreased anti-tumour functions of immune cells, enhanced infiltration of suppressive immune cells and the modulation of immune cells to support tumour characteristics[282,525]. Immune cell presence in the stroma and the infiltration in tumours of spontaneously breast cancer-prone MMTV-PyMT$^{tg/+}$ WT and IK KO mice were assessed by immunofluorescence stainings against the pan leukocyte marker CD45. Both stromal and tumour CD45-positive cell numbers were lower and thus immune cell homing to the tumour was significantly decreased in the IK KO genotype (figure 5.29). The available evidence imply that IK KO mice have no modified immune cell counts per se and that the distribution of immune cell subsets neither is changed in the absence of IK. Nevertheless, not only the number of immune cells, but also their maturation and activation status determine the success of an immune response[279,526]. Due to the importance of the IK channel for proper function of the different immune cell subsets, immune cells with IK KO genotype may be more insufficiently targeted to the tumour site to interfere with both carcinogenesis and tumour progression. Cell surveillance by the immune system might be impaired in IK KO immune cells meaning a lower detection and elimination of aberrant cells. This would promote tumourigenesis and decrease TFS time in MMTV-PyMT$^{tg/+}$ IK KO mice. Besides, IK KO immune cells may increase OS in the MMTV-PyMT$^{tg/+}$ model by releasing different or altered portions of cytokines that are usually employed by the tumour to stimulate its progression.

To test for IK-mediated functions in the tumour microenvironment of the MMTV-PyMT$^{tg/+}$ breast cancer model, MMTV-PyMT$^{tg/+}$ WT and IK KO cells were transplanted into WT recipient mice and MMTV-PyMT$^{tg/+}$ WT cells were further transplanted into IK KO recipients. As a result, TFS did not significantly differ between groups (figure 5.30 A). As both

MMTV-PyMT$^{tg/+}$ WT and IK KO cells were transplanted into WT recipients, IK channel status of tumour cells seemed to have no influence on initial tumour formation. Besides, MMTV-PyMT$^{tg/+}$ WT cells did not reveal differential tumour formation in WT and IK KO mice suggesting microenvironmental IK channels are not important for early tumour formation. In this context, it is well accepted that mouse strain determines the aggressiveness of MMTV-PyMT$^{tg/+}$ tumourigenesis, which can be attributed to immunosurveillance and immunoediting processes. Therefore, an intact immune system, as provided in the C57Bl/6 strain, increases tumour latency. On the opposite, interference with the immune response in the FVB/N strain has no impact on MMTV-PyMT$^{tg/+}$ tumour development[527,528]. Therefore, a potential immuno-oncological influence of the IK channel with regard to TFS may be masked on FVB/N strain background. In an earlier preliminary attempt, TFS was found significantly increased in MMTV-PyMT$^{tg/+}$ IK KO than WT cell-engrafted WT mice. However, these observations were carried out with lower animal numbers and lack results on tumour progression and OS, as experiments were terminated already 60 d after tumour inoculation[315,385]. In the current approach, at least three different cell lines per genotype were employed for representative results also with regard to cell line-specific spontaneous tumour regression[529-531].

Contrary to TFS, OS was significantly prolonged in MMTV-PyMT$^{tg/+}$ IK KO compared to WT tumours propagated in WT recipients (figure 5.30 B). MMTV-PyMT$^{tg/+}$ IK KO cell proliferation was probably impaired by direct interference with cell cycle progression[260,261]. Regarding MMTV-PyMT$^{tg/+}$ WT tumour growth in IK KO compared to WT recipients, the prolonged OS in IK KO recipients may be attributable to effects provoked by microenvironmental cells. As measured at the end of the experiment, CD45-positive cell numbers were significantly decreased in tumour tissue, but not in the stroma of MMTV-PyMT$^{tg/+}$ IK KO compared to WT tumours (figure 5.30 E + F). In conclusion, low IK KO immune cell infiltration to the tumours may contribute, at least partly, to an increased OS outcome explained by lower tumour-promoting inflammation in such tumours[282,525]. Interestingly, IK channel functions in immune cells were already related to cancer-modulating effects. In chronic lymphocytic leukaemia cells, IK channel mRNA and protein expression associate with tumour cell proliferation, which can be prohibited by TRAM-34 application[245]. In addition, TRAM-34 treatment in chronic myelogenous leukaemia leads to a better tumour growth control by inhibition of IK channels expressed on adherent natural killer cells[276]. Furthermore, T cell infiltration in tumour tissue of head and neck squamous cell carcinoma was described to be dependent on IK channels and to be modulated by adenosine accumulation in the tumour tissue[532]. Moreover, invasiveness of LoVo colon cancer cells correlates with IK channel expression in tumour-associated macrophages[284]. A similar effect is observed in glioma cells, which induce an anti-inflammatory phenotype in microglia, the brain-resident macrophages.

This diminishes glioma cell detection by the immune system and increases glioma malignancy. Besides, the anti-inflammatory state of the microglia is accompanied by abundant IK channel expression, whose targeting with TRAM-34 switches microglia back into their pro-inflammatory cytokine-releasing anti-tumour phenotype[285,533,534].

Albeit the modulation of immune cell functions represents its pioneering involvement, the IK channel is also present in other cells constituting the microenvironment. IK channel expression is confirmed in adipose precursor cells, although conflicting roles for down-stream signalling and proliferation in these cells are described so far[269,535,536]. With regard to breast cancer, adipose tissue is not only a site of energy storage, but also represents a major endocrine organ[267,268]. Moreover, many factors for the construction of the extracellular matrix, but also which promote different tumour characteristics such as growth, angiogenesis and metastasis, are produced by fibroblasts[271]. Basic fibroblast growth factor, but also transforming growth-factor-β upregulate the IK channel in fibroblasts, which promotes fibroblast proliferation and myogenesis[270,273]. With further regard to angiogenesis and vessel-constituting cell types, vascular smooth muscle cell proliferation mediated by platelet-derived growth factor is sensitive to TRAM-34 treatment[537]. Furthermore, a common feature of the tumour vasculature is excessive proliferation of endothelial cells[5,282]. Proliferation, but also migration of endothelial cells involves IK channel expression induced by different stimuli such as basic fibroblast growth factor, vascular endothelial growth factor or epidermal growth factor. This effect is confirmed by diminished angiogenesis *in vivo* after application of TRAM-34[424,538]. Therefore, it cannot be concluded that the putative microenvironmental effects on OS in the transplant model (figure 5.30 B) are solely dependent on IK channel-mediated modulation of the immune system. Rather, tumour progression apart from tumour cell characteristics may be the consequence of the interplay between different stromal cell types.

6.5 IK contributes to breast tumour cell survival after radiotherapy

6.5.1 The IK channel enhances DNA repair and breast tumour cell survival after IR

The standard procedure in the therapy of non-advanced invasive breast cancer is the conduction of breast-conserving surgery followed by radiotherapy[80]. Altered $[Ca^{2+}]_i$ mobilisation, signal transduction and DNA repair are detected in lymphocytes following IR[539,540]. Moreover, Ca^{2+} entry and down-stream activation of CaMK II in K562 leukaemia cells occurs via non-selective cation channels following IR. Inhibition of CaMK II is accompanied by a decrease in clonogenic survival after IR but not in ctrl[541]. Interestingly, IK activation by $[Ca^{2+}]_i$ involves channel interaction with calmodulin leading to downstream

signalling via CaMK II[230,234]. In order to study the contribution of IK channels to clonogenic survival after IR in breast cancer, the putative radiosensitising role of the IK channel was tested in the MMTV-PyMT$^{tg/+}$ model. Compared to MMTV-PyMT$^{tg/+}$ WT cells, irradiation of MMTV-PyMT$^{tg/+}$ IK KO cells or MMTV-PyMT$^{tg/+}$ WT TRAM-34-treated cells led to decreased clonogenic cell survival and increased residual γH2AX foci, a measure of DNA damage and thus a marker for decreased DNA repair (figures 5.31 - 5.34). These results confirm previous findings in glioblastoma, where the IK channel was inhibited by TRAM-34 or knocked down with short hairpin RNA prior to IR. In this study, radiation-induced IK activity was related to modified Ca^{2+} signalling, lower G_2/M arrest, and increased residual γH2AX foci resulting in diminished clonogenic survival. Further, TRAM-34 increased the radiosensitivity of an ectopic glioblastoma *in vivo* model[296].

IK channel participation in the radiation response may involve several mechanisms according to the 5Rs of radiotherapy, which comprise radiosensitivity, reassortment, repair, reoxygenation and repopulation[542-544]. Hereby, cell cycle arrest upon DNA damage induction by IR is essential for DNA repair in order to avoid mitotic catastrophe[545]. Cellular DNA repair capacity and therefore radiosensitivity depends on the cell cycle phase with high sensitivity in late G_1 phase and mitosis, and lower sensitivity in S phase due to the overexpression of DNA repair enzymes[39,542]. Thus, IK channel ablation or inhibition may render cells more prone to die from irradiation due to an increased G_1 arrest and a decreased G_2/M arrest[260,291]. Additionally, it may be interesting to investigate whether the IK channel is involved in cell cycle reassortment of tumour cells after repeated irradiation[542]. Moreover, DNA repair is highly energy-consuming, thus energy crisis after IR is a common phenomenon and intracellular ATP concentrations drop following IR[546]. Tumour cells mainly use glucose for energy fuelling. They exert anaerobic glycolysis and lactic acid fermentation for energy supply rather than mitochondrial respiration, a phenomenon known as the Warburg effect. Glucose provides carbohydrates for acetyl-CoA synthesis, which is used for histone acetylation and DNA decondensation. High glucose uptake and availability in the cell, even against the chemical glucose gradient, is enabled by aberrant expression of Na^+-coupled glucose cotransporters in many tumour cells. Hereby, Na^+ influx can be facilitated by radiogenic K^+ channel activation to hyperpolarise the plasma membrane[291]. Regarding hyperpolarisation, IK channels are involved in the secretion of Cl^- ions in a Ca^{2+}-dependent manner[547-551]. On the contrary, the inhibition of Cl^- channels also affects IK channel activity[552]. With regard to tumour hypoxia and reoxygenation, H_2O_2 formation consequently to IR application leads to an increase in $[Ca^{2+}]_i$ and thus IK channel activation[291]. In glioblastoma, IK channel upregulation is also observed in cancer stem cells[545]. Whether and in how far IK may contribute to repopulation, meaning a compensatory and accelerated tumour cell proliferation stimulated by releasing factors from dying cells, is not determined so far[553].

6.5.2 The IK channel increases tumour progression after radiotherapy *in vivo*

Irradiation of MMTV-PyMT$^{tg/+}$ tumours formed after tumour cell transplantation into WT recipient mice increased survival time in a dose-dependent manner. The effect of IR was more prominent in MMTV-PyMT$^{tg/+}$ IK KO tumours, which additionally showed a prolonged tumour growth per se (figure 5.35). To conclude, the IK channel is a potential target for dose reduction during radiotherapy. Its inhibition results in decreased numbers of surviving tumour cells and a delay of tumour regrowth and progression.

A possible candidate to be investigated in this respect is senicapoc. This drug was first investigated *in vitro* to test for its inhibitory potential on IK and its efficacy in the prevention of red blood cell dehydration in sickle cell anaemia. These effects were confirmed *in vivo* after oral senicapoc administration in mice[241]. In addition to its efficacy, the safety of senicapoc in humans was tested up to phase III clinical trials. Senicapoc had a positive impact on haematocrit, haemoglobin and the number of sickled red blood cells, even so the trial was terminated early because the frequency of sickle cell painful crisis could not be reduced[240,242]. As an older IK channel inhibitor, clotrimazole is also safe for use in patients with mild adverse effects including dysuria and increased transaminase levels[554]. However, the use of clotrimazole to support radiotherapy is limited due to its low IK selectivity[226,236].

7. Summary

Breast cancer is the most frequent malignancy in women in the Western world. Despite advances in the pathophysiological understanding and different therapeutic approaches, breast cancer remains the second leading cause of cancer death in women[1]. In this context, tumour subtypes are principally distinguished according to the expression of ER, PR and HER2 as well as gene expression signatures such as PAM50. On this basis, response to therapy as well as prognosis are determined[7,26]. At the same time, new biomarkers for further tumour sub-classification are needed allowing for earlier and more efficient treatment strategies, as they are better tailored to the individual needs of each patient. As such, ion channels are often aberrantly expressed or active in different tumour entities and amongst them, K^+ channels are the largest and most diverse group. BK and IK are associated with breast cancer and as such “oncochannels”, they contribute to the proliferation and migration of breast tumour cells[131,135,137]. Therefore, this work aimed at the identification of BK and IK channels as new classifiers in murine and human breast cancer. To further investigate the mechanisms underlying their pro-oncogenic effects, the assembly of the BK channel complex and the role of the microenvironmental IK channel were assessed among other features such as BK´s and IK´s role for tumour cell behaviours in the presence of established breast cancer therapies i.e. endocrine and radiation therapy (figure 7.1).

Both channels were expressed in the MMTV-PyMT$^{tg/+}$ murine breast cancer model and they contributed to tumour cell proliferation *in vitro*. *In vivo*, BK channel ablation was an overall determinant for an increased TFS and it also increased OS in the spontaneous MMTV-PyMT$^{tg/+}$ model. In contrast, IK channel ablation had no influence on TFS, but caused an increase in OS after orthotopic allotransplantation of MMTV-PyMT$^{tg/+}$ primary cell cultures. Interestingly, the BK channel exists as a complex of its pore-forming α subunit, which is complemented by the tissue-specific expression of four β and four γ subunits. Amongst these, nine SNPs in the *KCNMB4* gene encoding the BK-β4 subunit were found from the BCAC consortium to increase overall and in particular ER-positive breast cancer risk[347]. Moreover, the BK-γ1 subunit was most abundantly expressed in the MMTV-PyMT$^{tg/+}$ model, but also in MDA-MB-453 human breast cancer cells and, in both models, its mRNA knockdown depleted tumour cell proliferation rates to the same extent as a lack of the pore-forming BK-α subunit. Importantly, the pro-proliferative effect of BK was attributed to growth factor stimulation and an ER-independent hormonal control of breast cancer. With regard to the IK channel gene, eleven SNPs were identified to modify overall and ER-positive breast cancer risk[347]. IK channel ablation impaired breast tumour cell proliferation and it seemed to affect the tumour microenvironment *i.e.* CD45-positive immune cell infiltration.

Accordingly, immune cell infiltration in MMTV-PyMT$^{tg/+}$ tumour tissue was decreased in the absence of IK.

Besides controlling breast cancer initiation and disease progression, BK and IK channels interfered with certain therapy regimens of breast cancer such as TAM therapy and radiotherapy. Although their initial purpose is the inhibition of the ER and thus to evoke a decrease in proliferation, anti-oestrogens in addition to serum growth factors stimulated proliferation in a BK channel-dependent manner *in vitro*. Intriguingly, MMTV-PyMT$^{tg/+}$ WT tumours *in vivo* did not respond to TAM, whereas tumour progression in the BK KO genotype was significantly delayed suggesting that TAM-mediated BK activation contributed to tumour growth. Finally, low and high TAM concentrations interfered with DNA repair and survival outcome after IR in dependence on WT and BK KO genotypes with no differential outcome observed between genotypes with radiotherapy alone. In contrast, improved DNA repair and clonogenic survival after irradiation were observed in the presence of IK in MMTV-PyMT$^{tg/+}$ tumour-derived cells *in vitro* supporting the higher susceptibility of IK-deficient tumours towards radiotherapy in the allotransplant model.

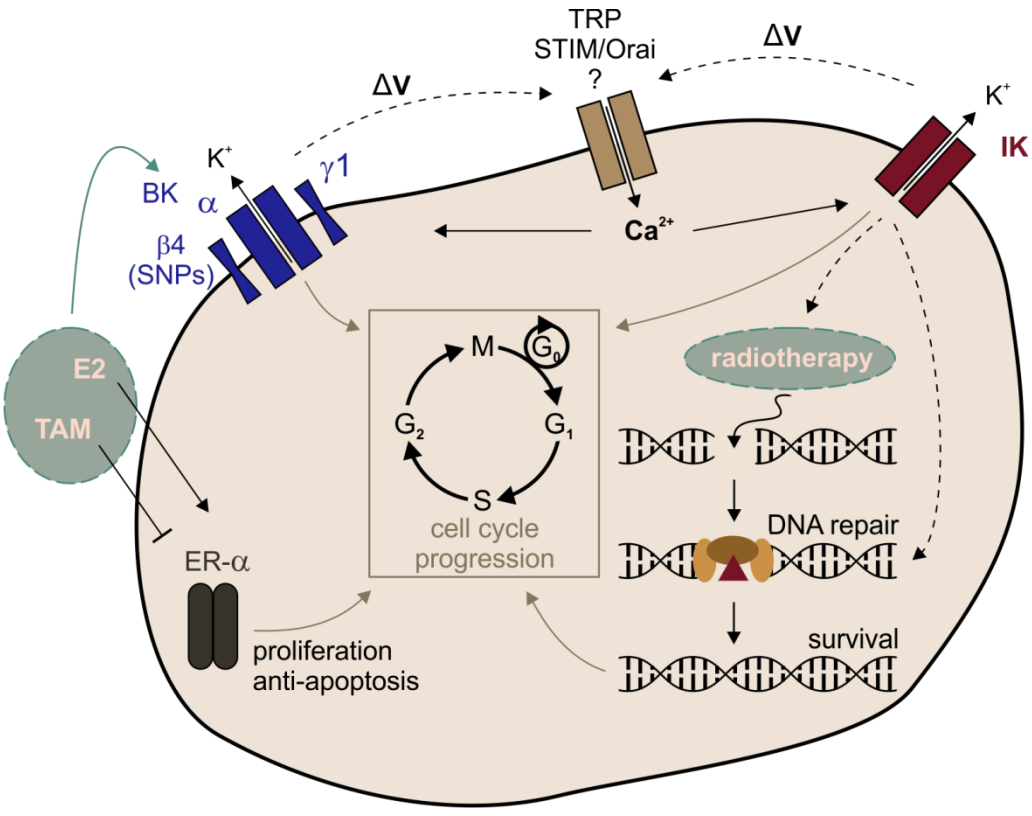

Figure 7.1: Summary
BK and IK channels contribute to breast tumour cell proliferation. The BK consists as a complex of its pore-forming α subunit and accessory β1 - 4 and γ1 - 4 subunits that modulate channel activity in a tissue-specific manner. BK-β4 SNPs can alter breast cancer risk[347] and BK-γ1 is necessary for BK-mediated proliferation *in vitro*. Growth factors such as E2, but also anti-oestrogens such as the selective ER modulator TAM stimulate BK-mediated proliferation. Breast tumour and stromal cell IK channels promote proliferation and tumour growth. IK also seems to contribute to DNA repair and

survival processes after radiotherapy. Influence of other molecules or signalling pathways on these processes to modulate BK and IK activity, e.g. TRP or STIM/Orai and Ca^{2+} signalling, need further elucidation. *Abbreviations:* Big conductance for potassium, BK; Intermediate conductance for potassium, IK; Potassium ion, K^{+}; Calcium ion, Ca^{2+}; Single nucleotide polymorphism, SNP; Difference in membrane potential, ΔV; Transient receptor potential, TRP; Stromal interaction molecule, STIM; 17β-oestradiol, E2; Tamoxifen, TAM; Oestrogen receptor, ER; Cell cycle phases Gap, G / Synthesis, S / Mitosis, M; Deoxyribonucleic acid, DNA.

8. Zusammenfassung

Das Mammakarzinom hat die häufigste Inzidenz und die zweithöchste Mortalität unter den Krebsneuerkrankungen der Frau[1]. Trotz zunehmendem Verständnis pathophysiologischer Mechanismen und der Verfügbarkeit zielgerichteter Therapien limitieren unerwünschte Wirkungen, Therapieversagen sowie Resistenzentwicklungen die Lebensqualität sowie das Gesamtüberleben der betroffenen Patientinnen. Neben der Einteilung von Brusttumoren in molekulare Subgruppen, die unter anderem anhand des Status für ER, PR und HER2 sowie der Expression bestimmter Genexpressionsmuster erfolgt, bedarf es zusätzlicher funktionaler Biomarker zur Verbesserung von Diagnostik und Therapie[7,26]. Solche Zielstrukturen könnten Ionenkanäle und darunter insbesondere K^+-Kanäle darstellen, deren veränderte Expression und Aktivität bereits in unterschiedlichen Tumorentitäten nachgewiesen wurde. Mitunter durch ihre Beiträge zu charakteristischen Merkmalen maligner Tumorzellen sind besonders die in dieser Arbeit untersuchten BK- und IK-Kanäle für die Entstehung und Metastasierung des Mammakarzinoms interessant[131,135,137].

Die vorliegenden Befunde implizieren, dass beide Kanäle im MMTV-PyMT$^{tg/+}$-Mausmodell zur Proliferation der Brusttumorzellen beitragen. Der BK-KO-Genotyp verlängerte generell das tumorfreie Überleben, aber auch das Gesamtüberleben bei spontaner Tumorinduktion. Ein IK-KO-Genotyp in Tumorzellen oder Empfängertieren hingegen verlängerte insbesondere das Gesamtüberleben nach orthotoper Allotransplantation. Der BK-Kanal besteht als Komplex aus seiner porenbildenden α-Untereinheit sowie je vier beschriebenen gewebsspezifisch exprimierten β- und γ-Untereinheiten. Neun SNPs des für BK-β4-kodierenden *KCNMB4*-Gens erhöhten das Brustkrebsrisiko[347] und die BK-γ1-Untereinheit war notwendig für die BK-Kanal-vermittelte proliferative Wirkung *in vitro*. Insbesondere Serum-enthaltene Wachstumsfaktoren und E2, jedoch auch Antiöstrogene stimulierten den BK-Kanal und förderten so die Tumorprogression *in vitro* sowie Therapieversagen unter TAM-Behandlung *in vivo*. Die IK-Kanal-vermittelte Wirkung beim Mammakarzinom obliegt nicht nur den Tumorzellen, sondern insbesondere auch seiner Bedeutung im angeborenen und erworbenen Immunsystem. Entsprechend war die Präsenz sowie die Infiltration von Immunzellen in MMTV-PyMT$^{tg/+}$-Tumoren im IK-KO-Genotyp verringert. Mechanistisch bedürfen die Details der hier identifizierten IK-Expression in den CD45-positiven Zellen sowie deren Abundanz im IK-negativen Mammakarzinom weiterer Aufklärung. Die Bedeutung des IK-Kanalstatus wurde außerdem beim Erfolg der Strahlentherapie ersichtlich. Hier scheint die Aktivität des IK-Kanals für eine geordnete Reduktion des DNA-Schadens durch DNA-Reparaturprozesse sowie für das zelluläre Überleben essenziell zu sein. Der Übertrag dieser *in vitro*-Befunde auf das tumortragende Tiermodell bestätigte die radiosensitivierende

Wirkung der IK-Kanalablation durch ein verlängertes relatives Überleben. Zusammengenommen implizieren die vorliegenden Befunde, dass BK- und IK-Kanäle *in vivo* vielversprechende Kandidaten für die weitere prä-/klinische Überprüfung sind. Zielführend in Bezug auf eine Risikoreduktion für die Entstehung des Mammakarzinoms sowie dessen Therapie scheinen dabei sowohl pharmakologische Ansätze zur Modulation der Kanalaktivität von BK und IK als auch der mögliche Einfluss krankheitsassoziierter Genvarianten im Kontext bereits etablierter Behandlungsmethoden zu sein.

9. Supplement

9.1 Primer sequences

Genotyping

Primers	Nomenclature	Sequence 5' - 3'	Manufacturer
BK	F1	TGGTCTTCTTCATCCTCGGG	Eurofins
	F2	AAGGGCCATTTTGAAGACGTC	
	R1	CCAGCCACAGTGTTTGTTGG	
IK	F1	TAAGTGCTTGCTGAGTCTGGA	Eurofins
	F2	CAGGAAGCACAGGCACTGC	
	R1	AGGAGAGTGACTGTAGGTGAG	
MMTV-PyMT	F1	GGAAGCAAGTACTTCACAAGGG	Eurofins
	R1	GGAAAGTCACTAGGAGCAGGG	
	Fctrl	CAAATGTTGCTTGTCTGGTG	
	Rctrl	GTCAGTCGAGTGCACAGTTT	

siRNA

siRNA	Reference number	Sequence 5' - 3'	Manufacturer
GAPDH	D-001830-10-05	GUCAACGGAUUUGGUCGUA	Dharmacon
		CAACGGAUUUGGUCGUAUU	
		GACCUCAACUACAUGGUUU	
		UGGUUUACAUGUUCCAAUA	
Gapdh	D-001830-20-05	GUGUGAACCACGAGAAAUA	Dharmacon
		GGAGAAACCUGCCAAGUAU	
		UCAAGAAGGUGGUGAAGCA	
		UGGUGAAGCAGGCAUCUGA	
KCNMA1	L-006267-00-0005	GACCUGAUCUUCUGCUUAA	Dharmacon
		GAUCCAAGAAGGUACUUUA	
		GAAUUUACCGGCUGAGAGA	
		UCGAAUAUCAUGAGAGUAA	
LRRC26	L-029447-01-0005	CGUCAACAAGCGACACAGA	Dharmacon
		GGGACCUGGCCGUGGUUUA	
		CACUCAGCCUGCAGGACAA	
		GCUGGAAGCACUGGCACCA	
Lrrc26	L-053374-01-0005	CGGCAAUCGAGGCGGGUUU	Dharmacon
		AGUCACUAGCAGCGCGAGA	
		CAAUAGACAAAACCCGAAA	
		CUGCAGGACAAUUCACUAC	
Non-targeting	D-001810-10-05	UGGUUUACAUGUCGACUAA	Dharmacon
		UGGUUUACAUGUUGUGUGA	
		UGGUUUACAUGUUUUCUGA	

	UGGUUUACAUGUUUUCCUA

qRT-PCR

Primers		Sequence 5’ - 3’	Manufacturer
ACTB	F	CCGTCTTCCCCTCCATCGT	Eurofins
	R	GATGCCTCTCTTGCTCTGGG	
Actb	F	GACGGCCAGGTCATCACTAT	Eurofins
	R	CCACAGGATTCCATACCCAAG	
Erbb2	F	CCAATCTGCACCATCGACGT	Eurofins
	R	TACCAACTCCCGGAATCTCG	
Esr1	F	CCATGACCCTTCACACCAAAG	Eurofins
	R	CCAGCTCGTTCCCTTGGAT	
Esr2	F	TCCTTGGTGTGAAGCAAGATCA	Eurofins
	R	CCGCCAAGCTTCCTCTTCAG	
GAPDH	F	CATGGCCTCCAAGGAGTAAG	Eurofins
	R	GGTTGAGCACAGGGTACTTTA	
Gapdh	F	GGTGCTGAGTATGTCGTGGAG	Eurofins
	R	CGGAGATGATGACCCTTTTG	
KCNMA1	F	TGCCTTCGTGGTCTGTCCTTCC	Eurofins
	R	CGCTTTCGGCTTCGGCTCTCT	
Kcnma1	F	GACGCCTCTTCATGGTCTTC	Eurofins
	R	TAGGAGCCCCCGTATTTCTT	
Kcnmb1	F	GTACAACTGTGCTGCCCCTC	Eurofins
	R	TCTTGCCCTCCAGCTCTTCC	
Kcnmb2	F	GCCGGACCTCTTCATCTTACA	Eurofins
	R	GTCCTCCCCAGCCTTCAGAG	
Kcnmb3	F	GGACCACTGTGTTGAAGCCC	Eurofins
	R	AAAGTCCAGCCCGTCATCCA	
Kcnmb4	F	CGTGAACAACTCCGAGTCCA	Eurofins
	R	GGGCGGGATATAGGAGCACT	
Kcnn1	F	TGTACCACGCCCGAGAGATC	Eurofins
	R	TCCAGCGAGATCAGGGACAC	
Kcnn2	F	TCTCTCCACGATCATCCTGCT	Eurofins
	R	CTGCTCCATTGTCCACCATGA	
Kcnn3	F	CGCCTATCACACAAGGGAAGT	Eurofins
	R	ACGCTCGTAGGTCATGGCTA	
Kcnn4	F	ATGTGGGGCAAGATTGTCTG	Eurofins
	R	GTGTTTCTCCGCCTTGTTGA	
LRRC26	F	CCCTGACTGCCTTTTCCGAC	Eurofins
	R	TGACGAGGAAGGAGGCCG	
Lrrc26	F	GCCTACTGACAGCTTTTCCG	Eurofins
	R	GGGGTCTAGCTGTCTCCTTAG	

Lrrc38	F	CGCTCACCTCTTCTCCTGGA	Eurofins
	R	CCTCCATGGGCAGTGAACAC	
Lrrc52	F	GTGGTGCTCCAGACTCTGTACCTA	Eurofins
	R	CCGTACACGTGGCGTTCTGGGCAT	
Lrrc55	F	AGCCCTTGCTGAAGTGGCTGCGGA	Eurofins
	R	TTGAAGCTCTCTTCAGTGAGTGAA	
Mki67	F	TGCCCGACCCTACAA	Eurofins
	R	TGCTGCTTCTCCTTC	

9.2 Backcrossing of the BK L2 allele to FVB/N background

For the generation of tumour-bearing mice with breast tissue-specific BK ablation, BK L2 allele-carrying mice on a hybrid 129/Sv x C57Bl/6 background [316] were used to establish a pre-mutant BK L2 strain on FVB/N background[313]. This was accomplished by crossing heterozygous BK L2-carrying mice with FVB/N WT mice for nine generations (figure 9.1).

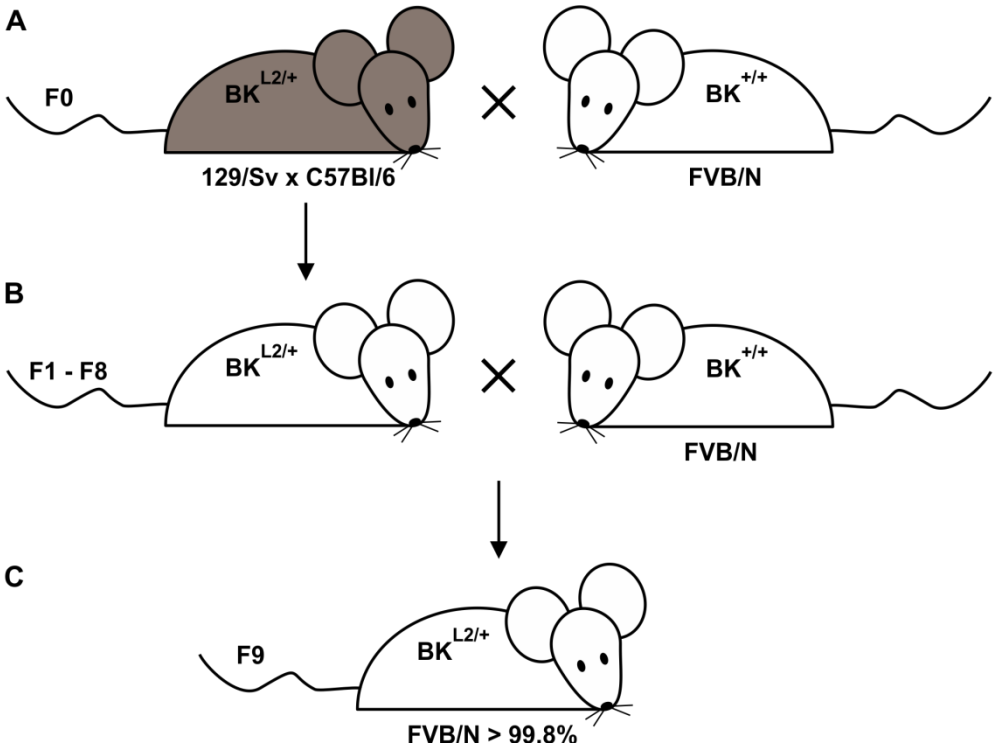

Figure 9.1: Establishment of the BK L2 mouse strain on FVB/N background
For future studies on the breast tissue-specific role of the BK *in vivo*, the BK L2 allele was established on FVB/N background. **(A)** 129/Sv x C57Bl/6 mice carrying the BK L2 allele were mated with FVB/N mice. **(B)** The F1 offspring was further mated with FVB/N mice to reach F9. **(C)** The F9 offspring generation reached an estimated > 99.8% pure genetic FVB/N background, which allows investigation of cell type-specific functions of BK in murine breast cancer models upon targeting the pre-mutant BK L2/L2 alleles with Cre recombinase.

9.3 BW of spontaneous MMTV-PyMT$^{tg/+}$ WT and BK KO mice

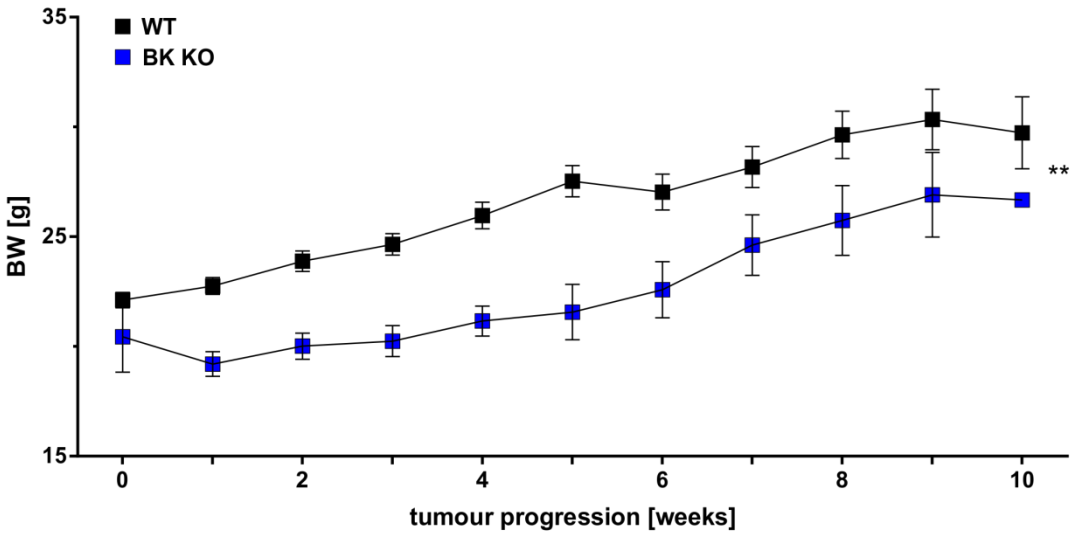

Figure 9.2: BW of MMTV-PyMT$^{tg/+}$ WT and BK KO mice during tumour progression
Body weight (BW) was monitored in spontaneous MMTV-PyMT$^{tg/+}$ WT and BK KO mice from the day of first positive tumour palpation and until overall survival was reached (figure 5.1). Plotted are means ± SEM with overall **p < 0.01 in an unpaired t-test.

9.4 ER and BK mRNA expression in allotransplanted MMTV-PyMT$^{tg/+}$ WT and BK KO tumours

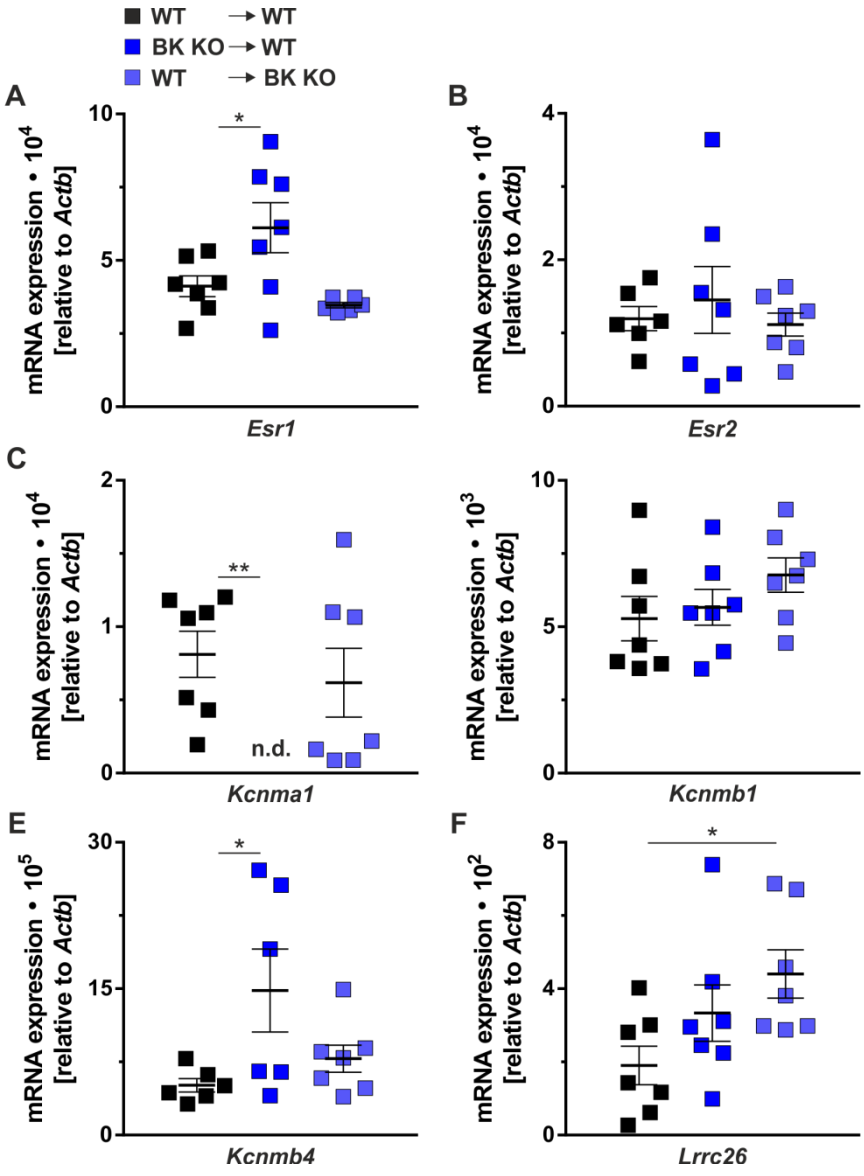

Figure 9.3: ER and BK mRNA expression profiles in transplanted MMTV-PyMT$^{tg/+}$ WT and BK KO tumours

MMTV-PyMT$^{tg/+}$ WT and BK KO cells were engrafted to the fourth right mammary gland of WT and BK KO mice. At the end of the experiment, the tumour formed in each mouse was removed and RNA was isolated from a tumour piece. Subsequent analyses were performed by Alice Dragoi as part of her Master´s thesis project. **(A + B)** *Esr1* and *Esr2* mRNA, encoding the ER subunits α and β, did not differ between groups, except for an increased *Esr1* mRNA expression in MMTV-PyMT$^{tg/+}$ BK KO compared to WT tumours propagated in WT recipients. **(C - F)** BK channel complex-encoding mRNAs that had been detected in the primary cell cultures (figure 5.9), i.e. *Kcnma1*, *Kcnmb1*, *Kcnmb4* and *Lrrc26*, were further assessed. **(C)** BK-α-encoding *Kcnma1* mRNA expression was confirmed in MMTV-PyMT$^{tg/+}$ WT, but not detected (n.d.) in BK KO tumours. **(D)** *Kcnmb1* representing BK-β1 was detected in all groups at similar levels. **(E)** Interestingly, *Kcnmb4* mRNA coding for BK-β4 was upregulated in MMTV-PyMT$^{tg/+}$ BK KO as compared to WT tumours engrafted in WT recipients. **(F)** Also BK-γ1-encoding *Lrrc26* mRNA showed a tendency to be increased in MMTV-PyMT$^{tg/+}$ BK KO tumours propagated in WT recipients, and was significantly increased in MMTV-PyMT$^{tg/+}$ WT formed in BK KO recipients, as compared to MMTV-PyMT$^{tg/+}$ WT tumours grown in WT recipients. Presented are

means ± SEM of n = 7 experiments with *p < 0.05 and **p < 0.01 as indicated by separate one-way ANOVAs with Dunnett´s test.

9.5 Ki-67 expression in MMTV-PyMT$^{tg/+}$ WT and BK KO tumours

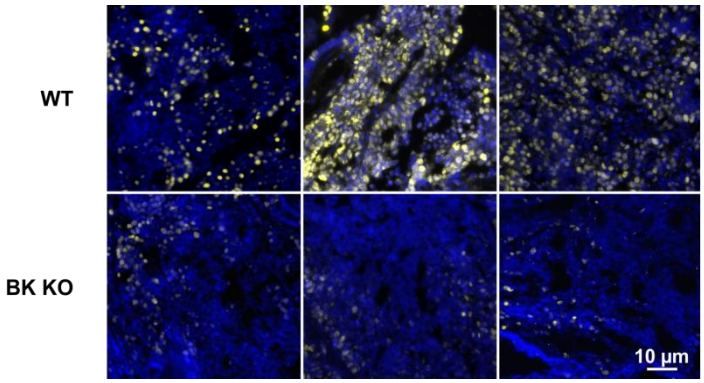

Figure 9.4: Ki-67 expression in spontaneous MMTV-PyMT$^{tg/+}$ WT and BK KO tumours
Tissue sections from MMTV-PyMT$^{tg/+}$ tumours showed a high portion of Ki-67-positive cells in the WT genotype, whereas Ki-67 status was much lower in the BK KO genotype. Representative results from n = 3 independent tumours per genotype are shown.

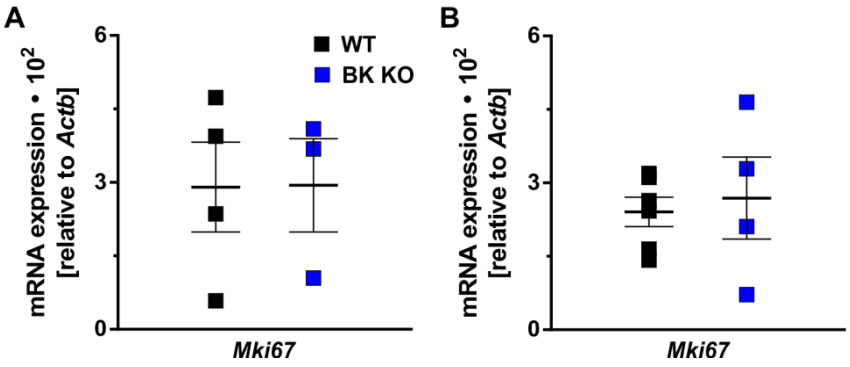

Figure 9.5: *Mki67* mRNA expression in spontaneous MMTV-PyMT$^{tg/+}$ WT and BK KO tumours
Mki67, the transcript coding for Ki-67 was measured with qRT-PCR in MMTV-PyMT$^{tg/+}$ WT and BK KO tumour tissues and cells. No significant differences were observed in **(A)** tumours and **(B)** cells derived from MMTV-PyMT$^{tg/+}$ WT and BK KO mice for n = 3 experiments in unpaired t-tests.

9.6 Knockdown efficacies in siRNA experiments

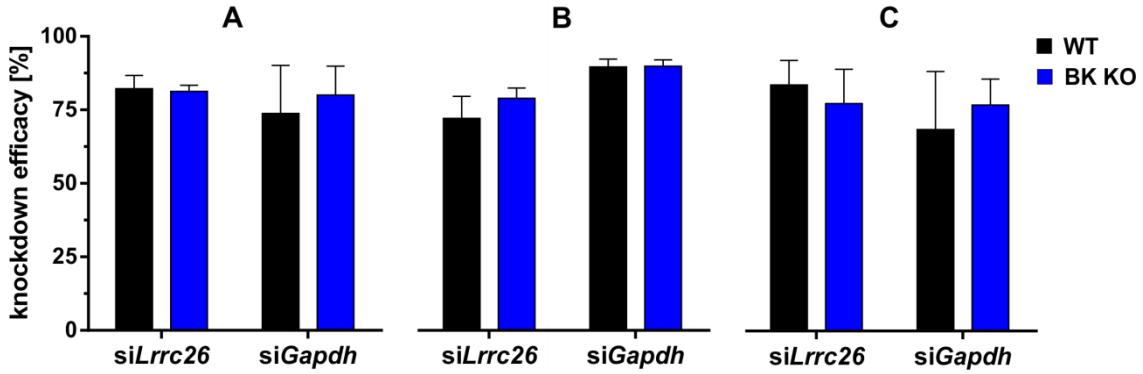

Figure 9.6: Knockdown efficacies in murine siRNA experiments
siRNA-mediated knockdown of *Lrrc26* or *Gapdh* mRNA was analysed with qRT-PCR in MMTV-PyMT$^{tg/+}$ WT and BK KO cell experiments of n = 5. Presented are means ± SEM with knockdown efficacies of **(A)** 82.2 ± 4.5% and 73.8 ± 16.4% as well as 81.3 ± 2.1% and 80.1 ± 9.8% for grid-based proliferation (figure 5.11 A), **(B)** 72.1 ± 7.5% and 89.6 ± 2.7% as well as 79.0 ± 3.5% and 89.9 ± 2.1% for Ki-67 index (figure 5.11 B), **(C)** 83.7 ± 8.3% and 68.6 ± 19.7% as well as 79.0 ± 3.5% and 89.9 ± 2.1% for mRNA compensation attempts (figure 5.11 C) for si*Lrrc26* and si*Gapdh* in WT as well as BK KO genotypes, respectively.

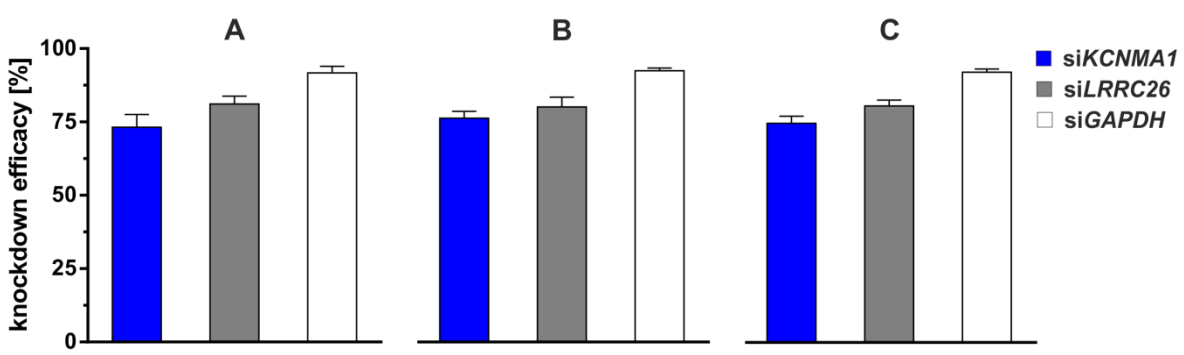

Figure 9.7: Knockdown efficacies in human siRNA experiments
The MDA-MB-453 breast tumour cell line was employed for targeting *KCNMA1* and *LRRC26* as well as the positive reference *GAPDH* with a siRNA. Knockdown efficacies for *KCNMA1*, *LRRC26* and *GAPDH* were **(A)** 73.2 ± 4.3%, 81.1 ± 2.7% and 91.7 ± 2.2% for grid-based proliferation (figure 5.12 A), **(B)** 76.3 ± 2.4%, 80.1 ± 3.3% and 92.4 ± 1.0% for Ki-67 index (figure 5.12 B) and **(C)** 74.8 ± 2.4%, 80.6 ± 2.0% and 92.1 ± 1.2% for mRNA compensation (figure 5.12 C), respectively. Bar graphs shown means ± SEM of n = 5 experiments **(A + B)**, whose mRNA samples were pooled for analysis of **(C)**.

9.7 Effect of TAM on ER and BK mRNA expression and migration in the MMTV-PyMT$^{tg/+}$ WT and BK KO model

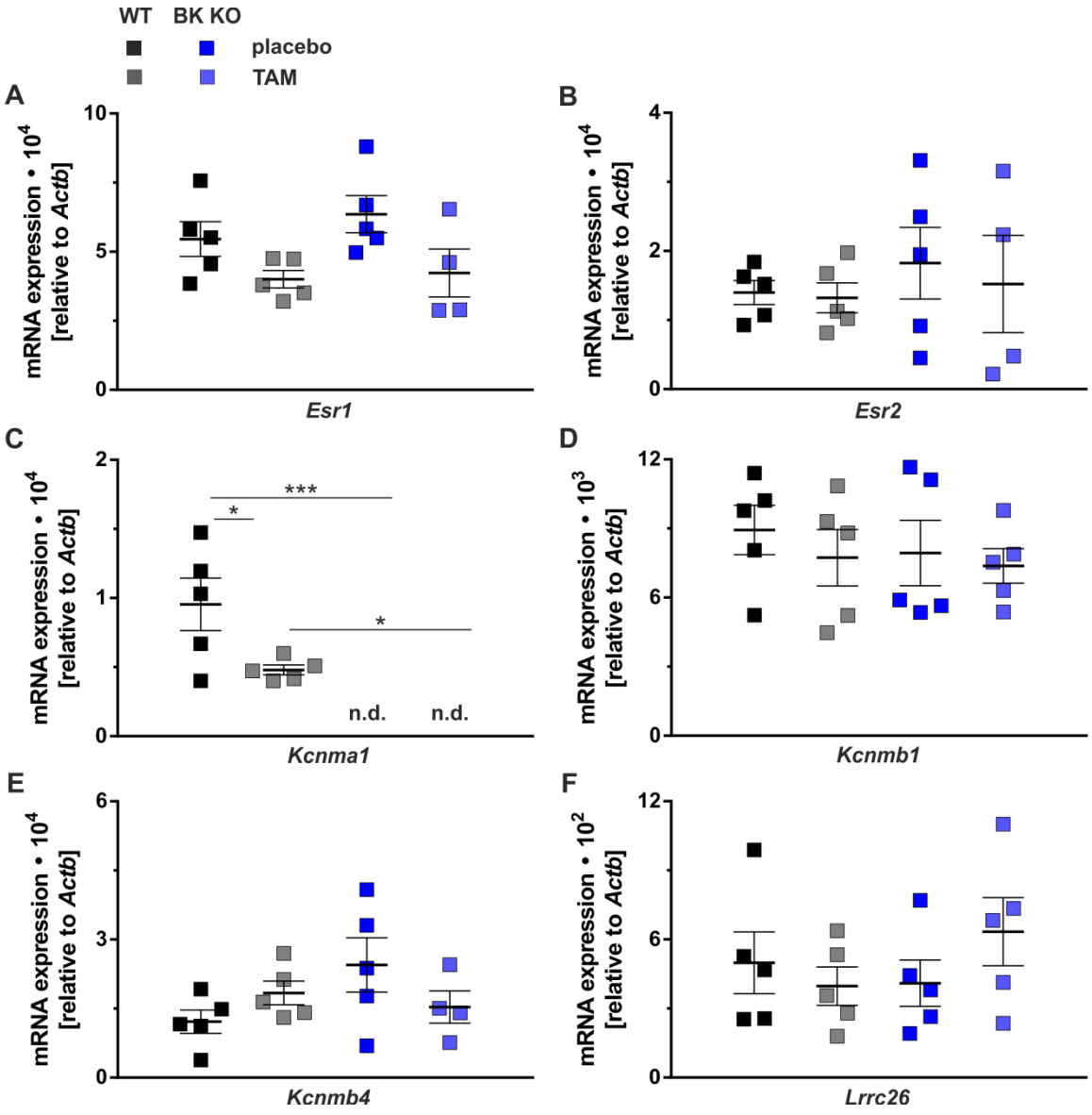

Figure 9.8: ER and BK mRNA expression in MMTV-PyMT$^{tg/+}$ WT and BK KO tumour engraftments after TAM therapy
MMTV-PyMT$^{tg/+}$ WT and BK tumours were inoculated into the mammary fat pad of the fourth right gland of WT mice treated with a 5 mg/60 d-releasing TAM or placebo pellet. RNA isolation and subsequent expression analyses were performed by Alice Dragoi from a piece of the tumour at the end of the experiment. **(A + B)** *Esr1* and *Esr2* mRNA expression was not significantly different between genotypes and treatments. However, *Esr1* mRNA levels showed a tendency towards decreased levels under TAM therapy. **(C)** *Kcnma1* mRNA was not detected (n.d.) in MMTV-PyMT$^{tg/+}$ BK KO tumours. Besides, *Kcnma1* mRNA was significantly downregulated in MMTV-PyMT$^{tg/+}$ WT tumours treated with TAM. **(D - F)** None of the tested BK channel accessory subunits, namely *Kcnmb1*, *Kcnmb4* and *Lrrc26* showed differential mRNA expression levels between genotypes or treatments. n = 4-5 experiments were performed with *p < 0.05 and ***p < 0.001 calculated by one-way ANOVA and Sidak´s test.

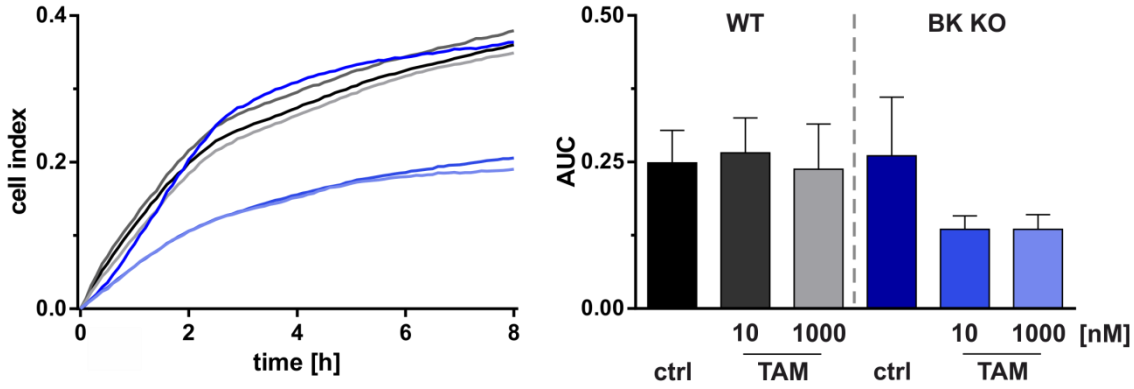

Figure 9.9: Effect of TAM on migration of MMTV-PyMT$^{tg/+}$ WT and BK KO tumour cells
MMTV-PyMT$^{tg/+}$ WT and BK KO cells were seeded at a density of 1.5 million in 25 cm² cell flasks and allowed to adhere for 24 h before serum removal for 72 h. After pre-incubation with 10 or 1,000 nM TAM or DMSO used as vehicle, the cells were trypsinised and seeded in TAM or DMSO-containing 16-well impedance plates to monitor cell migration in the xCELLigence system for 8 h (left). The area under the curve (AUC) of cell index was plotted for the entire time frame of 8 h (right). The experiment did not reach statistical significance, but showed a trend towards decreased migration in MMTV-PyMT$^{tg/+}$ BK KO cells treated with TAM, whereas this was not observed in ctrl or in any treatment condition of the WT genotype. Means ± SEM are shown in the bar graphs of n = 8 experiments analysed with two-way repeated measures ANOVA and Sidak´s multiple comparison test.

9.8 Influence of IR on MMTV-PyMT$^{tg/+}$ WT and BK KO cell survival

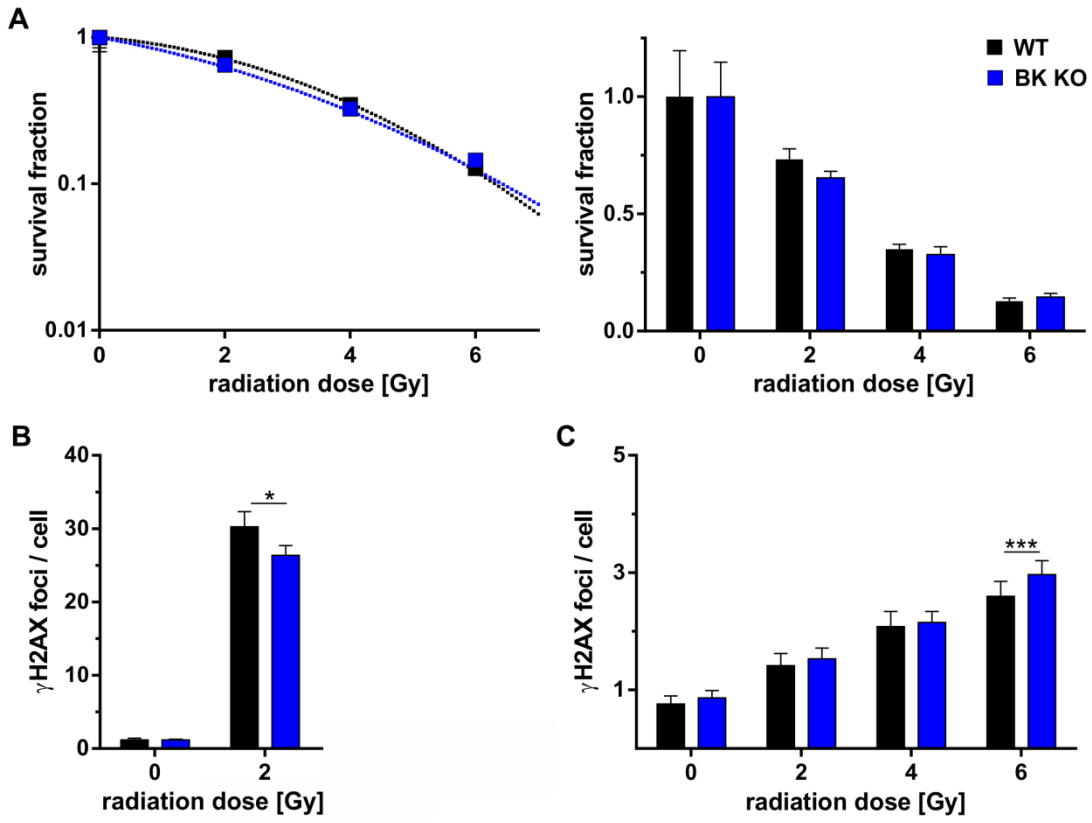

Figure 9.10: DNA repair and survival of MMTV-PyMT$^{tg/+}$ WT and BK KO cells after irradiation
MMTV-PyMT$^{tg/+}$ WT and BK KO cells were seeded at a density of 600,000 cells per 25 cm² cell flask or 50,000 cells per well of a 12-well chamber slide. After 72 h, irradiation with 0, 2, 4 or 6 Gy was performed. **(A)** After 24 h of recovery from irradiation, MMTV-PyMT$^{tg/+}$ WT and BK KO cells were trypsinised and seeded in 6-well plates at 3,500 cells/well with six technical replicates. 14 d later, cells were fixed and stained with coomassie blue and colonies with ≥ 50 cells were counted. No significant differences were observed between WT and BK KO genotypes (n = 9 in one-way ANOVA with Sidak´s test). **(B)** 30 min or **(C)** 24 h after irradiation, the numbers of γH2AX foci as indicator of DNA damage were determined. Significant differences between genotypes were found with 2 Gy and 6 Gy after 30 min and 24 h, respectively (n = 7 in two-way repeated measures ANOVA with Sidak´s test). Bar graphs show means ± SEM for with *p < 0.05 and ***p < 0.001.

9.9 ER, IK and H2AX mRNA expression in MMTV-PyMT$^{tg/+}$ WT and IK KO tumours engraftments

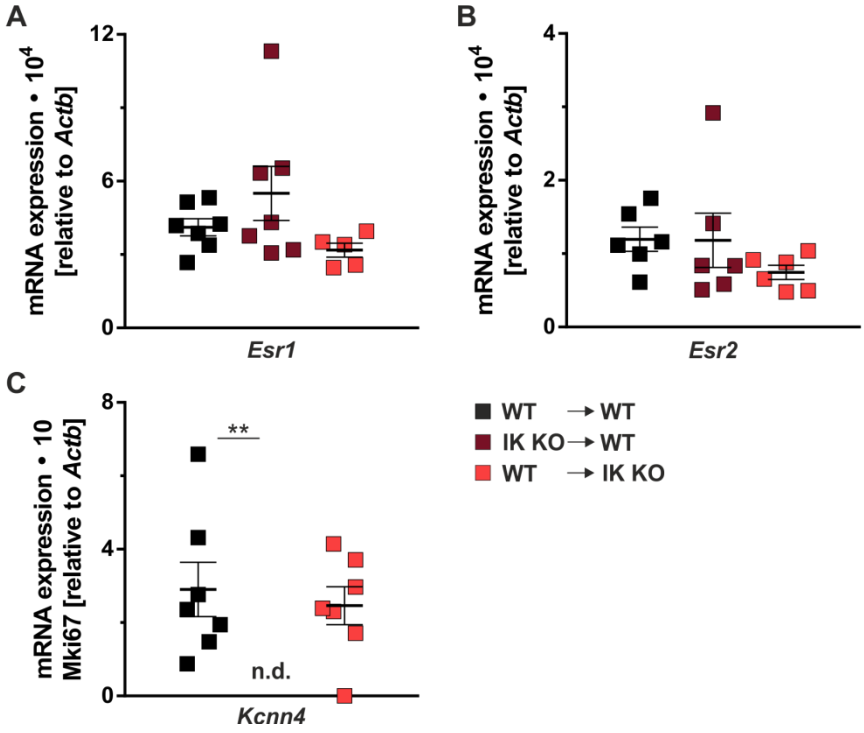

Figure 9.11: ER and IK mRNA expression in MMTV-PyMT$^{tg/+}$ WT and IK KO tumour engraftments
MMTV-PyMT$^{tg/+}$ WT and IK KO cells were transplanted in WT and IK KO recipients. Tumour formation and progression were monitored and RNA was isolated from a tumour piece of each mouse after scarification as part of Alice Dragoi´s Master´s thesis project. **(A + B)** *Esr1* and *Esr2* mRNA expression did not significantly differ between groups. **(C)** *Kcnn4* mRNA, encoding the IK channel, was not detected (n.d.) in MMTV-PyMT$^{tg/+}$ IK KO tumours grown in WT mice, whereas it was detectable in MMTV-PyMT$^{tg/+}$ WT tumours propagated in either WT or IK KO mice with no effect of the recipient´s genotype on the *Kcnn4* level. n = 7 experiments were performed with $^{**}p < 0.01$ indicating for a significant difference according to one-way ANOVA with Sidak´s test.

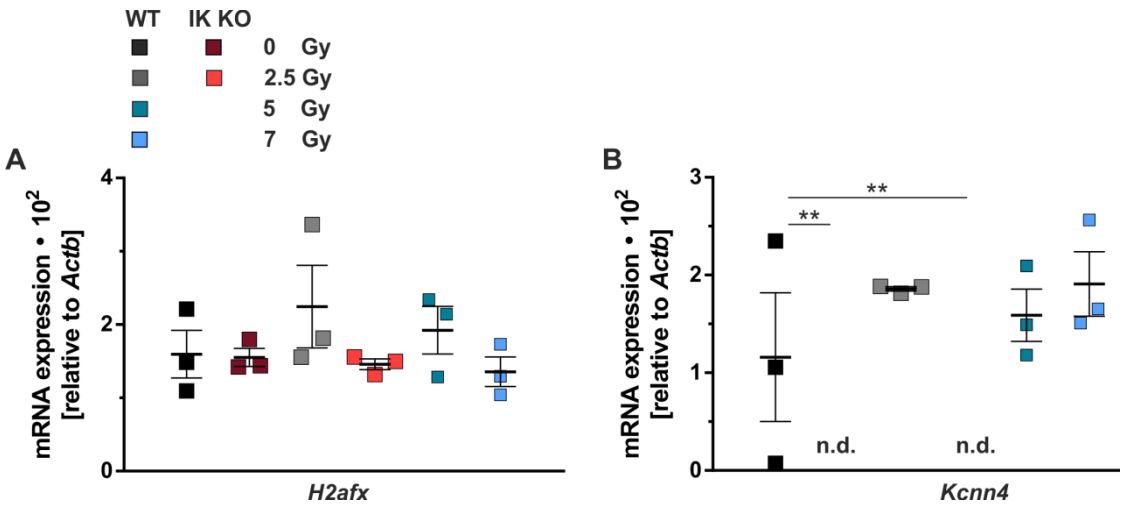

Figure 9.12: H2AX and IK mRNA expression in transplanted MMTV-PyMT$^{tg/+}$ WT and IK KO tumours after radiotherapy

MMTV-PyMT$^{tg/+}$ WT and IK KO tumours propagated in WT recipients were irradiated for five consecutive days. Tumour regression and regrowth were assessed and RNA was isolated (performed by Alice Dragoi) from a tumour piece after termination of the experiment. **(A)** *H2afx* mRNA levels coding for the H2AX DNA damage marker were not significantly different between genotypes and radiation doses. **(B)** *Kcnn4* mRNA expression was not detected (n.d.) in MMTV-PyMT$^{tg/+}$ IK KO tumours, but did not differ between the different irradiation groups in the presence of IK. **p < 0.01 in one-way ANOVA and Sidak´s test indicates for a significant in n = 3 experiments.

10. Bibliography

1 Siegel, R. L., Miller, K. D. & Jemal, A. Cancer statistics, 2018. *CA Cancer J Clin* **68**, 7-30, doi:10.3322/caac.21442 (2018).

2 Tubbs, A. & Nussenzweig, A. Endogenous DNA Damage as a Source of Genomic Instability in Cancer. *Cell* **168**, 644-656, doi:10.1016/j.cell.2017.01.002 (2017).

3 Knudson, A. G., Jr. Mutation and cancer: statistical study of retinoblastoma. *Proc Natl Acad Sci U S A* **68**, 820-823 (1971).

4 Walsh, T. *et al.* Spectrum of mutations in BRCA1, BRCA2, CHEK2, and TP53 in families at high risk of breast cancer. *JAMA* **295**, 1379-1388, doi:10.1001/jama.295.12.1379 (2006).

5 Hanahan, D. & Weinberg, R. A. The hallmarks of cancer. *Cell* **100**, 57-70 (2000).

6 Sims, A. H., Howell, A., Howell, S. J. & Clarke, R. B. Origins of breast cancer subtypes and therapeutic implications. *Nat Clin Pract Oncol* **4**, 516-525, doi:10.1038/ncponc0908 (2007).

7 Sorlie, T. *et al.* Gene expression patterns of breast carcinomas distinguish tumor subclasses with clinical implications. *Proc Natl Acad Sci U S A* **98**, 10869-10874, doi:10.1073/pnas.191367098 (2001).

8 Sorlie, T. *et al.* Repeated observation of breast tumor subtypes in independent gene expression data sets. *Proc Natl Acad Sci U S A* **100**, 8418-8423, doi:10.1073/pnas.0932692100 (2003).

9 Cejalvo, J. M. *et al.* Intrinsic Subtypes and Gene Expression Profiles in Primary and Metastatic Breast Cancer. *Cancer Res* **77**, 2213-2221, doi:10.1158/0008-5472.CAN-16-2717 (2017).

10 Bloom, H. J. & Richardson, W. W. Histological grading and prognosis in breast cancer; a study of 1409 cases of which 359 have been followed for 15 years. *Br J Cancer* **11**, 359-377 (1957).

11 Elston, C. W. & Ellis, I. O. Pathological prognostic factors in breast cancer. I. The value of histological grade in breast cancer: experience from a large study with long-term follow-up. *Histopathology* **19**, 403-410 (1991).

12 Cheang, M. C. *et al.* Ki67 index, HER2 status, and prognosis of patients with luminal B breast cancer. *J Natl Cancer Inst* **101**, 736-750, doi:10.1093/jnci/djp082 (2009).

13 Uscanga-Perales, G. I., Santuario-Facio, S. K. & Ortiz-Lopez, R. Triple negative breast cancer: Deciphering the biology and heterogeneity. *Medicina Universitaria* (2016).

14 Sonnenblick, A., Fumagalli, D., Sotiriou, C. & Piccart, M. Is the differentiation into molecular subtypes of breast cancer important for staging, local and systemic therapy, and follow up? *Cancer Treat Rev* **40**, 1089-1095, doi:10.1016/j.ctrv.2014.07.005 (2014).

15 Farmer, P. *et al.* Identification of molecular apocrine breast tumours by microarray analysis. *Oncogene* **24**, 4660-4671, doi:10.1038/sj.onc.1208561 (2005).

16 Vranic, S., Feldman, R. & Gatalica, Z. Apocrine carcinoma of the breast: A brief update on the molecular features and targetable biomarkers. *Bosn J Basic Med Sci* **17**, 9-11, doi:10.17305/bjbms.2016.1811 (2017).

17 Naderi, A., Meyer, M. & Dowhan, D. H. Cross-regulation between FOXA1 and ErbB2 signaling in estrogen receptor-negative breast cancer. *Neoplasia* **14**, 283-296 (2012).

18 Ni, M. *et al.* Targeting androgen receptor in estrogen receptor-negative breast cancer. *Cancer Cell* **20**, 119-131, doi:10.1016/j.ccr.2011.05.026 (2011).

19 Basile, D. *et al.* Androgen receptor in estrogen receptor positive breast cancer: Beyond expression. *Cancer Treat Rev* **61**, 15-22, doi:10.1016/j.ctrv.2017.09.006 (2017).

20 Christenson, J. L. *et al.* Harnessing a Different Dependency: How to Identify and Target Androgen Receptor-Positive Versus Quadruple-Negative Breast Cancer. *Horm Cancer* **9**, 82-94, doi:10.1007/s12672-017-0314-5 (2018).

21 Leitlinie. Interdisziplinäre S3-Leitlinie für die Früherkennung, Diagnostik, Therapie und Nachsorge des Mammakarzinoms. *Leitlinienprogramm Onkologie* (2017).

22 Wong, E. Breast cancer pathogenesis and histologic vs. molecular subtypes. *McMaster Pathophysiology Review* (2012).

23 Li, Z. *et al.* The differences in ultrasound and clinicopathological features between basal-like and normal-like subtypes of triple negative breast cancer. *PLoS One* **10**, e0114820, doi:10.1371/journal.pone.0114820 (2015).

24 Zeng, Z. *et al.* Mammography and ultrasound effective features in differentiating basal-like and normal-like subtypes of triple negative breast cancer. *Oncotarget* **8**, 79670-79679, doi:10.18632/oncotarget.19053 (2017).

25 Milioli, H. H., Tishchenko, I., Riveros, C., Berretta, R. & Moscato, P. Basal-like breast cancer: molecular profiles, clinical features and survival outcomes. *BMC Med Genomics* **10**, 19, doi:10.1186/s12920-017-0250-9 (2017).

26 Parker, J. S. *et al.* Supervised risk predictor of breast cancer based on intrinsic subtypes. *J Clin Oncol* **27**, 1160-1167, doi:10.1200/JCO.2008.18.1370 (2009).

27 Curtis, C. *et al.* The genomic and transcriptomic architecture of 2,000 breast tumours reveals novel subgroups. *Nature* **486**, 346-352, doi:10.1038/nature10983 (2012).

28 Russnes, H. G., Lingjaerde, O. C., Borresen-Dale, A. L. & Caldas, C. Breast Cancer Molecular Stratification: From Intrinsic Subtypes to Integrative Clusters. *Am J Pathol* **187**, 2152-2162, doi:10.1016/j.ajpath.2017.04.022 (2017).

29 Herschkowitz, J. I. *et al.* Identification of conserved gene expression features between murine mammary carcinoma models and human breast tumors. *Genome Biol* **8**, R76, doi:10.1186/gb-2007-8-5-r76 (2007).

30 Pinnaro, P. *et al.* Impact of Sequencing Radiation Therapy and Chemotherapy on Long-Term Local Toxicity for Early Breast Cancer: Results of a Randomized Study at 15-Year Follow-Up. *Int J Radiat Oncol Biol Phys* **95**, 1201-1209, doi:10.1016/j.ijrobp.2016.03.016 (2016).

31 Kreienberg, R. *et al.* Interdisziplinäre S3-Leitlinie für die Früherkennung, Diagnostik, Therapie und Nachsorge des Mammakarzinoms. *Leitlinienprogramm Onkologie* **Langversion 3.0** (2012).

32 Anampa, J., Makower, D. & Sparano, J. A. Progress in adjuvant chemotherapy for breast cancer: an overview. *BMC Med* **13**, 195, doi:10.1186/s12916-015-0439-8 (2015).

33 Early Breast Cancer Trialists' Collaborative, G. *et al.* Comparisons between different polychemotherapy regimens for early breast cancer: meta-analyses of long-term outcome among 100,000 women in 123 randomised trials. *Lancet* **379**, 432-444, doi:10.1016/S0140-6736(11)61625-5 (2012).

34 da Ros, M. *et al.* The Use of Anthracyclines for Therapy of CNS Tumors. *Anticancer Agents Med Chem* **15**, 721-727 (2015).

35 Early Breast Cancer Trialists' Collaborative, G. *et al.* Effect of radiotherapy after breast-conserving surgery on 10-year recurrence and 15-year breast cancer death: meta-analysis of individual patient data for 10,801 women in 17 randomised trials. *Lancet* **378**, 1707-1716, doi:10.1016/S0140-6736(11)61629-2 (2011).

36 Ebctcg *et al.* Effect of radiotherapy after mastectomy and axillary surgery on 10-year recurrence and 20-year breast cancer mortality: meta-analysis of individual patient data for 8135 women in 22 randomised trials. *Lancet* **383**, 2127-2135, doi:10.1016/S0140-6736(14)60488-8 (2014).

37 Puck, T. T., Morkovin, D., Marcus, P. I. & Cieciura, S. J. Action of x-rays on mammalian cells. II. Survival curves of cells from normal human tissues. *J Exp Med* **106**, 485-500 (1957).

38 Eriksson, D. & Stigbrand, T. Radiation-induced cell death mechanisms. *Tumour Biol* **31**, 363-372, doi:10.1007/s13277-010-0042-8 (2010).

39 Hubenak, J. R., Zhang, Q., Branch, C. D. & Kronowitz, S. J. Mechanisms of injury to normal tissue after radiotherapy: a review. *Plast Reconstr Surg* **133**, 49e-56e, doi:10.1097/01.prs.0000440818.23647.0b (2014).

40 Kuerbitz, S. J., Plunkett, B. S., Walsh, W. V. & Kastan, M. B. Wild-type p53 is a cell cycle checkpoint determinant following irradiation. *Proc Natl Acad Sci U S A* **89**, 7491-7495 (1992).

41 Yamada, M. & Puck, T. T. Action of radiation on mammalian cells. IV. Reversible mitotic lag in the S3 HeLa cell produced by low doses of x-rays. *Proc Natl Acad Sci U S A* **47**, 1181-1191 (1961).

42 Little, J. B. Delayed initiation of DNA synthesis in irradiated human diploid cells. *Nature* **218**, 1064-1065 (1968).

43 Willers, H. *et al.* DNA Damage Response Assessments in Human Tumor Samples Provide Functional Biomarkers of Radiosensitivity. *Semin Radiat Oncol* **25**, 237-250, doi:10.1016/j.semradonc.2015.05.007 (2015).

44 Goldstein, M. & Kastan, M. B. The DNA damage response: implications for tumor responses to radiation and chemotherapy. *Annu Rev Med* **66**, 129-143, doi:10.1146/annurev-med-081313-121208 (2015).

45 Celeste, A. *et al.* Genomic instability in mice lacking histone H2AX. *Science* **296**, 922-927, doi:10.1126/science.1069398 (2002).

46 Bassing, C. H. *et al.* Increased ionizing radiation sensitivity and genomic instability in the absence of histone H2AX. *Proc Natl Acad Sci U S A* **99**, 8173-8178, doi:10.1073/pnas.122228699 (2002).

47 Budach, W., Bolke, E. & Matuschek, C. Hypofractionated Radiotherapy as Adjuvant Treatment in Early Breast Cancer. A Review and Meta-Analysis of Randomized Controlled Trials. *Breast Care (Basel)* **10**, 240-245, doi:10.1159/000439007 (2015).

48 Whelan, T. J. *et al.* Long-term results of hypofractionated radiation therapy for breast cancer. *N Engl J Med* **362**, 513-520, doi:10.1056/NEJMoa0906260 (2010).

49 Haviland, J. S. *et al.* The UK Standardisation of Breast Radiotherapy (START) trials of radiotherapy hypofractionation for treatment of early breast cancer: 10-year follow-up results of two randomised controlled trials. *Lancet Oncol* **14**, 1086-1094, doi:10.1016/S1470-2045(13)70386-3 (2013).

50 group, F. T. *et al.* First results of the randomised UK FAST Trial of radiotherapy hypofractionation for treatment of early breast cancer (CRUKE/04/015). *Radiother Oncol* **100**, 93-100, doi:10.1016/j.radonc.2011.06.026 (2011).

51 Veronesi, U. *et al.* Intraoperative radiotherapy versus external radiotherapy for early breast cancer (ELIOT): a randomised controlled equivalence trial. *Lancet Oncol* **14**, 1269-1277, doi:10.1016/S1470-2045(13)70497-2 (2013).

52 Vaidya, J. S. *et al.* Risk-adapted targeted intraoperative radiotherapy versus whole-breast radiotherapy for breast cancer: 5-year results for local control and overall

survival from the TARGIT-A randomised trial. *Lancet* **383**, 603-613, doi:10.1016/S0140-6736(13)61950-9 (2014).

53 Strnad, V. *et al.* 5-year results of accelerated partial breast irradiation using sole interstitial multicatheter brachytherapy versus whole-breast irradiation with boost after breast-conserving surgery for low-risk invasive and in-situ carcinoma of the female breast: a randomised, phase 3, non-inferiority trial. *Lancet* **387**, 229-238, doi:10.1016/S0140-6736(15)00471-7 (2016).

54 Romestaing, P. *et al.* Role of a 10-Gy boost in the conservative treatment of early breast cancer: results of a randomized clinical trial in Lyon, France. *J Clin Oncol* **15**, 963-968, doi:10.1200/JCO.1997.15.3.963 (1997).

55 Bartelink, H. *et al.* Whole-breast irradiation with or without a boost for patients treated with breast-conserving surgery for early breast cancer: 20-year follow-up of a randomised phase 3 trial. *Lancet Oncol* **16**, 47-56, doi:10.1016/S1470-2045(14)71156-8 (2015).

56 Maranzano, E. *et al.* A prospective observational trial on emesis in radiotherapy: analysis of 1020 patients recruited in 45 Italian radiation oncology centres. *Radiother Oncol* **94**, 36-41, doi:10.1016/j.radonc.2009.11.001 (2010).

57 Shaitelman, S. F. *et al.* Acute and Short-term Toxic Effects of Conventionally Fractionated vs Hypofractionated Whole-Breast Irradiation: A Randomized Clinical Trial. *JAMA Oncol* **1**, 931-941, doi:10.1001/jamaoncol.2015.2666 (2015).

58 Polgar, C. *et al.* Late side-effects and cosmetic results of accelerated partial breast irradiation with interstitial brachytherapy versus whole-breast irradiation after breast-conserving surgery for low-risk invasive and in-situ carcinoma of the female breast: 5-year results of a randomised, controlled, phase 3 trial. *Lancet Oncol* **18**, 259-268, doi:10.1016/S1470-2045(17)30011-6 (2017).

59 Darby, S. C. *et al.* Risk of ischemic heart disease in women after radiotherapy for breast cancer. *N Engl J Med* **368**, 987-998, doi:10.1056/NEJMoa1209825 (2013).

60 Berrington de Gonzalez, A. *et al.* Proportion of second cancers attributable to radiotherapy treatment in adults: a cohort study in the US SEER cancer registries. *Lancet Oncol* **12**, 353-360, doi:10.1016/S1470-2045(11)70061-4 (2011).

61 Blakemore, J. & Naftolin, F. Aromatase: Contributions to Physiology and Disease in Women and Men. *Physiology (Bethesda)* **31**, 258-269, doi:10.1152/physiol.00054.2015 (2016).

62 Choe, H. K. *et al.* Synchronous activation of gonadotropin-releasing hormone gene transcription and secretion by pulsatile kisspeptin stimulation. *Proc Natl Acad Sci U S A* **110**, 5677-5682, doi:10.1073/pnas.1213594110 (2013).

63 Matzuk, M. M. & Lamb, D. J. The biology of infertility: research advances and clinical challenges. *Nat Med* **14**, 1197-1213, doi:10.1038/nm.f.1895 (2008).

64 Lobo, R. A., March, C. M., Goebelsmann, U. & Mishell, D. R., Jr. The modulating role of obesity and 17 beta-estradiol (E2) on bound and unbound E2 and adrenal androgens in oophorectomized women. *J Clin Endocrinol Metab* **54**, 320-324, doi:10.1210/jcem-54-2-320 (1982).

65 Lee, A. J., Cai, M. X., Thomas, P. E., Conney, A. H. & Zhu, B. T. Characterization of the oxidative metabolites of 17beta-estradiol and estrone formed by 15 selectively expressed human cytochrome p450 isoforms. *Endocrinology* **144**, 3382-3398, doi:10.1210/en.2003-0192 (2003).

66 Dewailly, D. *et al.* Interactions between androgens, FSH, anti-Mullerian hormone and estradiol during folliculogenesis in the human normal and polycystic ovary. *Hum Reprod Update* **22**, 709-724, doi:10.1093/humupd/dmw027 (2016).

67 Maybin, J. A. & Critchley, H. O. Steroid regulation of menstrual bleeding and endometrial repair. *Rev Endocr Metab Disord* **13**, 253-263, doi:10.1007/s11154-012-9228-2 (2012).

68 Doshi, S. B. & Agarwal, A. The role of oxidative stress in menopause. *J Midlife Health* **4**, 140-146, doi:10.4103/0976-7800.118990 (2013).

69 Patel, S., Zhou, C., Rattan, S. & Flaws, J. A. Effects of Endocrine-Disrupting Chemicals on the Ovary. *Biol Reprod* **93**, 20, doi:10.1095/biolreprod.115.130336 (2015).

70 Kuiper, G. G. *et al.* Comparison of the ligand binding specificity and transcript tissue distribution of estrogen receptors alpha and beta. *Endocrinology* **138**, 863-870, doi:10.1210/endo.138.3.4979 (1997).

71 Jameera Begam, A., Jubie, S. & Nanjan, M. J. Estrogen receptor agonists/antagonists in breast cancer therapy: A critical review. *Bioorg Chem* **71**, 257-274, doi:10.1016/j.bioorg.2017.02.011 (2017).

72 Williams, C. & Lin, C. Y. Oestrogen receptors in breast cancer: basic mechanisms and clinical implications. *Ecancermedicalscience* **7**, 370, doi:10.3332/ecancer.2013.370 (2013).

73 Bondesson, M., Hao, R., Lin, C. Y., Williams, C. & Gustafsson, J. A. Estrogen receptor signaling during vertebrate development. *Biochim Biophys Acta* **1849**, 142-151, doi:10.1016/j.bbagrm.2014.06.005 (2015).

74 Louie, M. C. & Sevigny, M. B. Steroid hormone receptors as prognostic markers in breast cancer. *Am J Cancer Res* **7**, 1617-1636 (2017).

75 Yager, J. D. & Davidson, N. E. Estrogen carcinogenesis in breast cancer. *N Engl J Med* **354**, 270-282, doi:10.1056/NEJMra050776 (2006).

76 Beatson, G. T. On the treatment of inoperable cases of carcinoma of the mamma: Suggestions for a new method of treatment with illustrative cases. *The Lancet* (1896).

77 Haddow, A., Watkinson, J. M., Paterson, E. & Koller, P. C. Influence of Synthetic Oestrogens on Advanced Malignant Disease. *Br Med J* **2**, 393-398 (1944).

78 Jordan, V. C. Tamoxifen: a most unlikely pioneering medicine. *Nat Rev Drug Discov* **2**, 205-213, doi:10.1038/nrd1031 (2003).

79 Tremont, A., Lu, J. & Cole, J. T. Endocrine Therapy for Early Breast Cancer: Updated Review. *Ochsner J* **17**, 405-411 (2017).

80 Albert, U.-S. *et al.* Interdisziplinäre S3-Leitlinie für die Früherkennung, Diagnostik, Therapie und Nachsorge des Mammakarzinoms. *Leitlinienprogramm Onkologie* **Langversion 4.0** (2017).

81 Eroglu, A. Tamoxifen-associated thromboembolism in breast cancer. *Thromb Res* **131**, 566, doi:10.1016/j.thromres.2012.08.308 (2013).

82 Chen, J. Y. *et al.* Endometrial cancer incidence in breast cancer patients correlating with age and duration of tamoxifen use: a population based study. *J Cancer* **5**, 151-155, doi:10.7150/jca.8412 (2014).

83 Harper, M. J. & Walpole, A. L. A new derivative of triphenylethylene: effect on implantation and mode of action in rats. *J Reprod Fertil* **13**, 101-119 (1967).

84 Robertson, D. W., Katzenellenbogen, J. A., Long, D. J., Rorke, E. A. & Katzenellenbogen, B. S. Tamoxifen antiestrogens. A comparison of the activity, pharmacokinetics, and metabolic activation of the cis and trans isomers of tamoxifen. *J Steroid Biochem* **16**, 1-13 (1982).

85 Brauch, H., Murdter, T. E., Eichelbaum, M. & Schwab, M. Pharmacogenomics of tamoxifen therapy. *Clin Chem* **55**, 1770-1782, doi:10.1373/clinchem.2008.121756 (2009).

86 Brown, K. Breast cancer chemoprevention: risk-benefit effects of the antioestrogen tamoxifen. *Expert Opin Drug Saf* **1**, 253-267 (2002).

87 Brown, K. Is tamoxifen a genotoxic carcinogen in women? *Mutagenesis* **24**, 391-404, doi:10.1093/mutage/gep022 (2009).

88 Coezy, E., Borgna, J. L. & Rochefort, H. Tamoxifen and metabolites in MCF7 cells: correlation between binding to estrogen receptor and inhibition of cell growth. *Cancer Res* **42**, 317-323 (1982).

89 Jordan, V. C. Metabolites of tamoxifen in animals and man: identification, pharmacology, and significance. *Breast Cancer Res Treat* **2**, 123-138 (1982).

90 Murdter, T. E. *et al.* Activity levels of tamoxifen metabolites at the estrogen receptor and the impact of genetic polymorphisms of phase I and II enzymes on their concentration levels in plasma. *Clin Pharmacol Ther* **89**, 708-717, doi:10.1038/clpt.2011.27 (2011).

91 Khosrow-Khavar, F. *et al.* Cardiotoxicity of aromatase inhibitors and tamoxifen in postmenopausal women with breast cancer: a systematic review and meta-analysis of randomized controlled trials. *Ann Oncol* **28**, 487-496, doi:10.1093/annonc/mdw673 (2017).

92 Ryden, L., Heibert Arnlind, M., Vitols, S., Hoistad, M. & Ahlgren, J. Aromatase inhibitors alone or sequentially combined with tamoxifen in postmenopausal early breast cancer compared with tamoxifen or placebo - Meta-analyses on efficacy and adverse events based on randomized clinical trials. *Breast* **26**, 106-114, doi:10.1016/j.breast.2016.01.006 (2016).

93 Limonta, P. *et al.* GnRH receptors in cancer: from cell biology to novel targeted therapeutic strategies. *Endocr Rev* **33**, 784-811, doi:10.1210/er.2012-1014 (2012).

94 Boer, K. Fulvestrant in advanced breast cancer: evidence to date and place in therapy. *Ther Adv Med Oncol* **9**, 465-479, doi:10.1177/1758834017711097 (2017).

95 Rahim, B. & O'Regan, R. AR Signaling in Breast Cancer. *Cancers (Basel)* **9**, doi:10.3390/cancers9030021 (2017).

96 Slamon, D. J. *et al.* Human breast cancer: correlation of relapse and survival with amplification of the HER-2/neu oncogene. *Science* **235**, 177-182 (1987).

97 Scholzen, T. & Gerdes, J. The Ki-67 protein: from the known and the unknown. *J Cell Physiol* **182**, 311-322, doi:10.1002/(SICI)1097-4652(200003)182:3<311::AID-JCP1>3.0.CO;2-9 (2000).

98 Gerdes, J., Schwab, U., Lemke, H. & Stein, H. Production of a mouse monoclonal antibody reactive with a human nuclear antigen associated with cell proliferation. *Int J Cancer* **31**, 13-20 (1983).

99 Sobecki, M. *et al.* The cell proliferation antigen Ki-67 organises heterochromatin. *Elife* **5**, e13722, doi:10.7554/eLife.13722 (2016).

100 Cidado, J. *et al.* Ki-67 is required for maintenance of cancer stem cells but not cell proliferation. *Oncotarget* **7**, 6281-6293, doi:10.18632/oncotarget.7057 (2016).

101 Sun, X. *et al.* Ki-67 Contributes to Normal Cell Cycle Progression and Inactive X Heterochromatin in p21 Checkpoint-Proficient Human Cells. *Mol Cell Biol* **37**, doi:10.1128/MCB.00569-16 (2017).

102 Cuylen, S. *et al.* Ki-67 acts as a biological surfactant to disperse mitotic chromosomes. *Nature* **535**, 308-312, doi:10.1038/nature18610 (2016).

103 Takagi, M., Nishiyama, Y., Taguchi, A. & Imamoto, N. Ki67 antigen contributes to the timely accumulation of protein phosphatase 1gamma on anaphase chromosomes. *J Biol Chem* **289**, 22877-22887, doi:10.1074/jbc.M114.556647 (2014).

104 Matheson, T. D. & Kaufman, P. D. The p150N domain of chromatin assembly factor-1 regulates Ki-67 accumulation on the mitotic perichromosomal layer. *Mol Biol Cell* **28**, 21-29, doi:10.1091/mbc.E16-09-0659 (2017).

105 Goldhirsch, A. *et al.* Personalizing the treatment of women with early breast cancer: highlights of the St Gallen International Expert Consensus on the Primary Therapy of Early Breast Cancer 2013. *Ann Oncol* **24**, 2206-2223, doi:10.1093/annonc/mdt303 (2013).

106 Inwald, E. C. *et al.* Ki-67 is a prognostic parameter in breast cancer patients: results of a large population-based cohort of a cancer registry. *Breast Cancer Res Treat* **139**, 539-552, doi:10.1007/s10549-013-2560-8 (2013).

107 Inari, H. *et al.* Clinicopathological and prognostic significance of Ki-67 immunohistochemical expression of distant metastatic lesions in patients with metastatic breast cancer. *Breast Cancer* **24**, 748-755, doi:10.1007/s12282-017-0774-z (2017).

108 Sonnenblick, A. *et al.* Final 10-year results of the Breast International Group 2-98 phase III trial and the role of Ki67 in predicting benefit of adjuvant docetaxel in patients with oestrogen receptor positive breast cancer. *Eur J Cancer* **51**, 1481-1489, doi:10.1016/j.ejca.2015.03.018 (2015).

109 Acs, B. *et al.* Ki-67 as a controversial predictive and prognostic marker in breast cancer patients treated with neoadjuvant chemotherapy. *Diagn Pathol* **12**, 20, doi:10.1186/s13000-017-0608-5 (2017).

110 Mengel, M. *et al.* Inter-laboratory and inter-observer reproducibility of immunohistochemical assessment of the Ki-67 labelling index in a large multi-centre trial. *J Pathol* **198**, 292-299, doi:10.1002/path.1218 (2002).

111 Leung, S. C. Y. *et al.* Analytical validation of a standardized scoring protocol for Ki67: phase 3 of an international multicenter collaboration. *NPJ Breast Cancer* **2**, 16014, doi:10.1038/npjbcancer.2016.14 (2016).

112 Dowsett, M. *et al.* Assessment of Ki67 in breast cancer: recommendations from the International Ki67 in Breast Cancer working group. *J Natl Cancer Inst* **103**, 1656-1664, doi:10.1093/jnci/djr393 (2011).

113 Varga, Z. *et al.* An international reproducibility study validating quantitative determination of ERBB2, ESR1, PGR, and MKI67 mRNA in breast cancer using MammaTyper(R). *Breast Cancer Res* **19**, 55, doi:10.1186/s13058-017-0848-z (2017).

114 Sinn, H. P. *et al.* Comparison of immunohistochemistry with PCR for assessment of ER, PR, and Ki-67 and prediction of pathological complete response in breast cancer. *BMC Cancer* **17**, 124, doi:10.1186/s12885-017-3111-1 (2017).

115 Wallden, B. *et al.* Development and verification of the PAM50-based Prosigna breast cancer gene signature assay. *BMC Med Genomics* **8**, 54, doi:10.1186/s12920-015-0129-6 (2015).

116 van 't Veer, L. J. *et al.* Gene expression profiling predicts clinical outcome of breast cancer. *Nature* **415**, 530-536, doi:10.1038/415530a (2002).

117 Glas, A. M. *et al.* Converting a breast cancer microarray signature into a high-throughput diagnostic test. *BMC Genomics* **7**, 278, doi:10.1186/1471-2164-7-278 (2006).

118 Cardoso, F. *et al.* 70-Gene Signature as an Aid to Treatment Decisions in Early-Stage Breast Cancer. *N Engl J Med* **375**, 717-729, doi:10.1056/NEJMoa1602253 (2016).

119 Paik, S. *et al.* A multigene assay to predict recurrence of tamoxifen-treated, node-negative breast cancer. *N Engl J Med* **351**, 2817-2826, doi:10.1056/NEJMoa041588 (2004).

120 Petkov, V. I. *et al.* Breast-cancer-specific mortality in patients treated based on the 21-gene assay: a SEER population-based study. *NPJ Breast Cancer* **2**, 16017, doi:10.1038/npjbcancer.2016.17 (2016).

121 Albain, K. S. *et al.* Prognostic and predictive value of the 21-gene recurrence score assay in postmenopausal women with node-positive, oestrogen-receptor-positive breast cancer on chemotherapy: a retrospective analysis of a randomised trial. *Lancet Oncol* **11**, 55-65, doi:10.1016/S1470-2045(09)70314-6 (2010).

122 Sparano, J. A. *et al.* Prospective Validation of a 21-Gene Expression Assay in Breast Cancer. *N Engl J Med* **373**, 2005-2014, doi:10.1056/NEJMoa1510764 (2015).

123 Filipits, M. *et al.* A new molecular predictor of distant recurrence in ER-positive, HER2-negative breast cancer adds independent information to conventional clinical risk factors. *Clin Cancer Res* **17**, 6012-6020, doi:10.1158/1078-0432.CCR-11-0926 (2011).

124 Martin, M. *et al.* Clinical validation of the EndoPredict test in node-positive, chemotherapy-treated ER+/HER2- breast cancer patients: results from the GEICAM 9906 trial. *Breast Cancer Res* **16**, R38, doi:10.1186/bcr3642 (2014).

125 Pelaez-Garcia, A. *et al.* Comparison of risk classification between EndoPredict and MammaPrint in ER-positive/HER2-negative primary invasive breast cancer. *PLoS One* **12**, e0183452, doi:10.1371/journal.pone.0183452 (2017).

126 Bosl, A. *et al.* MammaPrint versus EndoPredict: Poor correlation in disease recurrence risk classification of hormone receptor positive breast cancer. *PLoS One* **12**, e0183458, doi:10.1371/journal.pone.0183458 (2017).

127 Bartlett, J. M. *et al.* Comparing Breast Cancer Multiparameter Tests in the OPTIMA Prelim Trial: No Test Is More Equal Than the Others. *J Natl Cancer Inst* **108**, doi:10.1093/jnci/djw050 (2016).

128 Ge, L. *et al.* Big Potassium (BK) ion channels in biology, disease and possible targets for cancer immunotherapy. *Int Immunopharmacol* **22**, 427-443, doi:10.1016/j.intimp.2014.06.040 (2014).

129 Benarroch, E. E. Potassium channels: brief overview and implications in epilepsy. *Neurology* **72**, 664-669, doi:10.1212/01.wnl.0000343739.72081.4e (2009).

130 Shieh, C. C., Coghlan, M., Sullivan, J. P. & Gopalakrishnan, M. Potassium channels: molecular defects, diseases, and therapeutic opportunities. *Pharmacol Rev* **52**, 557-594 (2000).

131 Pardo, L. A. & Stuhmer, W. The roles of K(+) channels in cancer. *Nat Rev Cancer* **14**, 39-48, doi:10.1038/nrc3635 (2014).

132 Otto, T. & Sicinski, P. Cell cycle proteins as promising targets in cancer therapy. *Nat Rev Cancer* **17**, 93-115, doi:10.1038/nrc.2016.138 (2017).

133 Urrego, D., Tomczak, A. P., Zahed, F., Stuhmer, W. & Pardo, L. A. Potassium channels in cell cycle and cell proliferation. *Philos Trans R Soc Lond B Biol Sci* **369**, 20130094, doi:10.1098/rstb.2013.0094 (2014).

134 Wonderlin, W. F., Woodfork, K. A. & Strobl, J. S. Changes in membrane potential during the progression of MCF-7 human mammary tumor cells through the cell cycle. *J Cell Physiol* **165**, 177-185, doi:10.1002/jcp.1041650121 (1995).

135 Huang, X. & Jan, L. Y. Targeting potassium channels in cancer. *J Cell Biol* **206**, 151-162, doi:10.1083/jcb.201404136 (2014).

136 Kunzelmann, K. Ion channels and cancer. *J Membr Biol* **205**, 159-173, doi:10.1007/s00232-005-0781-4 (2005).
137 Gueguinou, M. *et al.* KCa and Ca(2+) channels: the complex thought. *Biochim Biophys Acta* **1843**, 2322-2333, doi:10.1016/j.bbamcr.2014.02.019 (2014).
138 Roderick, H. L. & Cook, S. J. Ca2+ signalling checkpoints in cancer: remodelling Ca2+ for cancer cell proliferation and survival. *Nat Rev Cancer* **8**, 361-375, doi:10.1038/nrc2374 (2008).
139 Latorre, R., Oberhauser, A., Labarca, P. & Alvarez, O. Varieties of calcium-activated potassium channels. *Annu Rev Physiol* **51**, 385-399, doi:10.1146/annurev.ph.51.030189.002125 (1989).
140 Vergara, C., Latorre, R., Marrion, N. V. & Adelman, J. P. Calcium-activated potassium channels. *Curr Opin Neurobiol* **8**, 321-329 (1998).
141 Kohler, M. *et al.* Small-conductance, calcium-activated potassium channels from mammalian brain. *Science* **273**, 1709-1714 (1996).
142 Elkins, T., Ganetzky, B. & Wu, C. F. A Drosophila mutation that eliminates a calcium-dependent potassium current. *Proc Natl Acad Sci U S A* **83**, 8415-8419 (1986).
143 Butler, A., Tsunoda, S., McCobb, D. P., Wei, A. & Salkoff, L. mSlo, a complex mouse gene encoding "maxi" calcium-activated potassium channels. *Science* **261**, 221-224 (1993).
144 Pallanck, L. & Ganetzky, B. Cloning and characterization of human and mouse homologs of the Drosophila calcium-activated potassium channel gene, slowpoke. *Hum Mol Genet* **3**, 1239-1243 (1994).
145 Tseng-Crank, J. *et al.* Cloning, expression, and distribution of functionally distinct Ca(2+)-activated K+ channel isoforms from human brain. *Neuron* **13**, 1315-1330 (1994).
146 Liu, X., Chang, Y., Reinhart, P. H., Sontheimer, H. & Chang, Y. Cloning and characterization of glioma BK, a novel BK channel isoform highly expressed in human glioma cells. *J Neurosci* **22**, 1840-1849 (2002).
147 Singh, H. *et al.* MitoBK(Ca) is encoded by the Kcnma1 gene, and a splicing sequence defines its mitochondrial location. *Proc Natl Acad Sci U S A* **110**, 10836-10841, doi:10.1073/pnas.1302028110 (2013).
148 Xie, J. & McCobb, D. P. Control of alternative splicing of potassium channels by stress hormones. *Science* **280**, 443-446 (1998).
149 Chen, L. *et al.* Functionally diverse complement of large conductance calcium- and voltage-activated potassium channel (BK) alpha-subunits generated from a single site of splicing. *J Biol Chem* **280**, 33599-33609, doi:10.1074/jbc.M505383200 (2005).
150 Fodor, A. A. & Aldrich, R. W. Convergent evolution of alternative splices at domain boundaries of the BK channel. *Annu Rev Physiol* **71**, 19-36, doi:10.1146/annurev.physiol.010908.163124 (2009).
151 Shen, K. Z. *et al.* Tetraethylammonium block of Slowpoke calcium-activated potassium channels expressed in Xenopus oocytes: evidence for tetrameric channel formation. *Pflugers Arch* **426**, 440-445 (1994).
152 Wang, L. & Sigworth, F. J. Structure of the BK potassium channel in a lipid membrane from electron cryomicroscopy. *Nature* **461**, 292-295, doi:10.1038/nature08291 (2009).
153 Latorre, R. *et al.* Molecular Determinants of BK Channel Functional Diversity and Functioning. *Physiol Rev* **97**, 39-87, doi:10.1152/physrev.00001.2016 (2017).

154 Yuan, P., Leonetti, M. D., Hsiung, Y. & MacKinnon, R. Open structure of the Ca2+ gating ring in the high-conductance Ca2+-activated K+ channel. *Nature* **481**, 94-97, doi:10.1038/nature10670 (2011).

155 Bian, S., Favre, I. & Moczydlowski, E. Ca2+-binding activity of a COOH-terminal fragment of the Drosophila BK channel involved in Ca2+-dependent activation. *Proc Natl Acad Sci U S A* **98**, 4776-4781, doi:10.1073/pnas.081072398 (2001).

156 Cui, J., Cox, D. H. & Aldrich, R. W. Intrinsic voltage dependence and Ca2+ regulation of mslo large conductance Ca-activated K+ channels. *J Gen Physiol* **109**, 647-673 (1997).

157 Horrigan, F. T. & Aldrich, R. W. Coupling between voltage sensor activation, Ca2+ binding and channel opening in large conductance (BK) potassium channels. *J Gen Physiol* **120**, 267-305 (2002).

158 Stefani, E. *et al.* Voltage-controlled gating in a large conductance Ca2+-sensitive K+channel (hslo). *Proc Natl Acad Sci U S A* **94**, 5427-5431 (1997).

159 Yan, J. & Aldrich, R. W. LRRC26 auxiliary protein allows BK channel activation at resting voltage without calcium. *Nature* **466**, 513-516, doi:10.1038/nature09162 (2010).

160 Knaus, H. G. *et al.* Primary sequence and immunological characterization of beta-subunit of high conductance Ca(2+)-activated K+ channel from smooth muscle. *J Biol Chem* **269**, 17274-17278 (1994).

161 Brenner, R. *et al.* Vasoregulation by the beta1 subunit of the calcium-activated potassium channel. *Nature* **407**, 870-876, doi:10.1038/35038011 (2000).

162 Uebele, V. N. *et al.* Cloning and functional expression of two families of beta-subunits of the large conductance calcium-activated K+ channel. *J Biol Chem* **275**, 23211-23218, doi:10.1074/jbc.M910187199 (2000).

163 Brenner, R., Jegla, T. J., Wickenden, A., Liu, Y. & Aldrich, R. W. Cloning and functional characterization of novel large conductance calcium-activated potassium channel beta subunits, hKCNMB3 and hKCNMB4. *J Biol Chem* **275**, 6453-6461 (2000).

164 Meera, P., Wallner, M. & Toro, L. A neuronal beta subunit (KCNMB4) makes the large conductance, voltage- and Ca2+-activated K+ channel resistant to charybdotoxin and iberiotoxin. *Proc Natl Acad Sci U S A* **97**, 5562-5567, doi:10.1073/pnas.100118597 (2000).

165 Egland, K. A. *et al.* High expression of a cytokeratin-associated protein in many cancers. *Proc Natl Acad Sci U S A* **103**, 5929-5934, doi:10.1073/pnas.0601296103 (2006).

166 Gessner, G. *et al.* BKCa channels activating at resting potential without calcium in LNCaP prostate cancer cells. *J Membr Biol* **208**, 229-240, doi:10.1007/s00232-005-0830-z (2005).

167 Almassy, J. & Begenisich, T. The LRRC26 protein selectively alters the efficacy of BK channel activators. *Mol Pharmacol* **81**, 21-30, doi:10.1124/mol.111.075234 (2012).

168 Olesen, S. P., Munch, E., Moldt, P. & Drejer, J. Selective activation of Ca(2+)-dependent K+ channels by novel benzimidazolone. *Eur J Pharmacol* **251**, 53-59 (1994).

169 Gonzalez-Perez, V., Xia, X. M. & Lingle, C. J. Functional regulation of BK potassium channels by gamma1 auxiliary subunits. *Proc Natl Acad Sci U S A* **111**, 4868-4873, doi:10.1073/pnas.1322123111 (2014).

170 Yan, J. & Aldrich, R. W. BK potassium channel modulation by leucine-rich repeat-containing proteins. *Proc Natl Acad Sci U S A* **109**, 7917-7922, doi:10.1073/pnas.1205435109 (2012).

171 Yang, C. *et al.* Knockout of the LRRC26 subunit reveals a primary role of LRRC26-containing BK channels in secretory epithelial cells. *Proc Natl Acad Sci U S A* **114**, E3739-E3747, doi:10.1073/pnas.1703081114 (2017).

172 Brelidze, T. I. & Magleby, K. L. Protons block BK channels by competitive inhibition with K+ and contribute to the limits of unitary currents at high voltages. *J Gen Physiol* **123**, 305-319, doi:10.1085/jgp.200308951 (2004).

173 Yellen, G. Ionic permeation and blockade in Ca2+-activated K+ channels of bovine chromaffin cells. *J Gen Physiol* **84**, 157-186 (1984).

174 Nardi, A., Calderone, V., Chericoni, S. & Morelli, I. Natural modulators of large-conductance calcium-activated potassium channels. *Planta Med* **69**, 885-892, doi:10.1055/s-2003-45095 (2003).

175 Knaus, H. G. *et al.* Tremorgenic indole alkaloids potently inhibit smooth muscle high-conductance calcium-activated potassium channels. *Biochemistry* **33**, 5819-5828 (1994).

176 Zhou, Y. & Lingle, C. J. Paxilline inhibits BK channels by an almost exclusively closed-channel block mechanism. *J Gen Physiol* **144**, 415-440, doi:10.1085/jgp.201411259 (2014).

177 Sanchez, M. & McManus, O. B. Paxilline inhibition of the alpha-subunit of the high-conductance calcium-activated potassium channel. *Neuropharmacology* **35**, 963-968 (1996).

178 Imlach, W. L. *et al.* The molecular mechanism of "ryegrass staggers," a neurological disorder of K+ channels. *J Pharmacol Exp Ther* **327**, 657-664, doi:10.1124/jpet.108.143933 (2008).

179 Bloch, M. *et al.* KCNMA1 gene amplification promotes tumor cell proliferation in human prostate cancer. *Oncogene* **26**, 2525-2534, doi:10.1038/sj.onc.1210036 (2007).

180 Han, X. *et al.* Heat shock proteins and p53 play a critical role in K+ channel-mediated tumor cell proliferation and apoptosis. *Apoptosis* **12**, 1837-1846, doi:10.1007/s10495-007-0101-9 (2007).

181 Samuel, P. *et al.* Over-expression of miR-31 or loss of KCNMA1 leads to increased cisplatin resistance in ovarian cancer cells. *Tumour Biol* **37**, 2565-2573, doi:10.1007/s13277-015-4081-z (2016).

182 Vereb, G., Jr. *et al.* Depletion of intracellular calcium stores facilitates the influx of extracellular calcium in platelet derived growth factor stimulated A172 glioblastoma cells. *Cytometry* **24**, 64-73, doi:10.1002/(SICI)1097-0320(19960501)24:1<64::AID-CYTO8>3.0.CO;2-I (1996).

183 Ransom, C. B. & Sontheimer, H. BK channels in human glioma cells. *J Neurophysiol* **85**, 790-803, doi:10.1152/jn.2001.85.2.790 (2001).

184 Weaver, A. K., Liu, X. & Sontheimer, H. Role for calcium-activated potassium channels (BK) in growth control of human malignant glioma cells. *J Neurosci Res* **78**, 224-234, doi:10.1002/jnr.20240 (2004).

185 Rosa, P. *et al.* Overexpression of Large-Conductance Calcium-Activated Potassium Channels in Human Glioblastoma Stem-Like Cells and Their Role in Cell Migration. *J Cell Physiol* **232**, 2478-2488, doi:10.1002/jcp.25592 (2017).

186 Edalat, L. *et al.* BK K+ channel blockade inhibits radiation-induced migration/brain infiltration of glioblastoma cells. *Oncotarget* **7**, 14259-14278, doi:10.18632/oncotarget.7423 (2016).
187 Oeggerli, M. *et al.* Role of KCNMA1 in breast cancer. *PLoS One* **7**, e41664, doi:10.1371/journal.pone.0041664 (2012).
188 Khaitan, D. *et al.* Role of KCNMA1 gene in breast cancer invasion and metastasis to brain. *BMC Cancer* **9**, 258, doi:10.1186/1471-2407-9-258 (2009).
189 Gambade, A. *et al.* Activation of TRPV2 and BKCa channels by the LL-37 enantiomers stimulates calcium entry and migration of cancer cells. *Oncotarget* **7**, 23785-23800, doi:10.18632/oncotarget.8122 (2016).
190 Ouadid-Ahidouch, H., Roudbaraki, M., Ahidouch, A., Delcourt, P. & Prevarskaya, N. Cell-cycle-dependent expression of the large Ca2+-activated K+ channels in breast cancer cells. *Biochem Biophys Res Commun* **316**, 244-251, doi:10.1016/j.bbrc.2004.02.041 (2004).
191 Mound, A., Rodat-Despoix, L., Bougarn, S., Ouadid-Ahidouch, H. & Matifat, F. Molecular interaction and functional coupling between type 3 inositol 1,4,5-trisphosphate receptor and BKCa channel stimulate breast cancer cell proliferation. *Eur J Cancer* **49**, 3738-3751, doi:10.1016/j.ejca.2013.07.013 (2013).
192 Tajima, N., Itokazu, Y., Korpi, E. R., Somerharju, P. & Kakela, R. Activity of BK(Ca) channel is modulated by membrane cholesterol content and association with Na+/K+-ATPase in human melanoma IGR39 cells. *J Biol Chem* **286**, 5624-5638, doi:10.1074/jbc.M110.149898 (2011).
193 Olsen, M. L., Weaver, A. K., Ritch, P. S. & Sontheimer, H. Modulation of glioma BK channels via erbB2. *J Neurosci Res* **81**, 179-189, doi:10.1002/jnr.20543 (2005).
194 Schickling, B. M. *et al.* BKCa channel inhibitor modulates the tumorigenic ability of hormone-independent breast cancer cells via the Wnt pathway. *Oncol Rep* **33**, 533-538, doi:10.3892/or.2014.3617 (2015).
195 Duerson, K., White, R. E., Jiang, F., Schonbrunn, A. & Armstrong, D. L. Somatostatin stimulates BKCa channels in rat pituitary tumor cells through lipoxygenase metabolites of arachidonic acid. *Neuropharmacology* **35**, 949-961 (1996).
196 Rezzonico, R. *et al.* Prostaglandin E2 induces interaction between hSlo potassium channel and Syk tyrosine kinase in osteosarcoma cells. *J Bone Miner Res* **17**, 869-878, doi:10.1359/jbmr.2002.17.5.869 (2002).
197 Florio, T. *et al.* Chemokine stromal cell-derived factor 1alpha induces proliferation and growth hormone release in GH4C1 rat pituitary adenoma cell line through multiple intracellular signals. *Mol Pharmacol* **69**, 539-546, doi:10.1124/mol.105.015255 (2006).
198 Denson, D. D., Wang, X., Worrell, R. T. & Eaton, D. C. Effects of fatty acids on BK channels in GH(3) cells. *Am J Physiol Cell Physiol* **279**, C1211-1219, doi:10.1152/ajpcell.2000.279.4.C1211 (2000).
199 Gilligan, D. M., Badar, D. M., Panza, J. A., Quyyumi, A. A. & Cannon, R. O., 3rd. Acute vascular effects of estrogen in postmenopausal women. *Circulation* **90**, 786-791 (1994).
200 White, R. E. *et al.* Endothelium-independent effect of estrogen on Ca(2+)-activated K(+) channels in human coronary artery smooth muscle cells. *Cardiovasc Res* **53**, 650-661 (2002).
201 Valverde, M. A. *et al.* Acute activation of Maxi-K channels (hSlo) by estradiol binding to the beta subunit. *Science* **285**, 1929-1931 (1999).

202 Coiret, G., Matifat, F., Hague, F. & Ouadid-Ahidouch, H. 17-beta-estradiol activates maxi-K channels through a non-genomic pathway in human breast cancer cells. *FEBS Lett* **579**, 2995-3000, doi:10.1016/j.febslet.2005.02.085 (2005).

203 De Wet, H. *et al.* Modulation of the BK channel by estrogens: examination at single channel level. *Mol Membr Biol* **23**, 420-429, doi:10.1080/09687860600802803 (2006).

204 Dick, G. M., Rossow, C. F., Smirnov, S., Horowitz, B. & Sanders, K. M. Tamoxifen activates smooth muscle BK channels through the regulatory beta 1 subunit. *J Biol Chem* **276**, 34594-34599, doi:10.1074/jbc.M104689200 (2001).

205 Dick, G. M., Hunter, A. C. & Sanders, K. M. Ethylbromide tamoxifen, a membrane-impermeant antiestrogen, activates smooth muscle calcium-activated large-conductance potassium channels from the extracellular side. *Mol Pharmacol* **61**, 1105-1113 (2002).

206 Duncan, R. K. Tamoxifen alters gating of the BK alpha subunit and mediates enhanced interactions with the avian beta subunit. *Biochem Pharmacol* **70**, 47-58, doi:10.1016/j.bcp.2005.03.026 (2005).

207 Coiret, G., Borowiec, A. S., Mariot, P., Ouadid-Ahidouch, H. & Matifat, F. The antiestrogen tamoxifen activates BK channels and stimulates proliferation of MCF-7 breast cancer cells. *Mol Pharmacol* **71**, 843-851, doi:10.1124/mol.106.028290 (2007).

208 Dick, G. M. The pure anti-oestrogen ICI 182,780 (Faslodex) activates large conductance Ca(2+)-activated K(+) channels in smooth muscle. *Br J Pharmacol* **136**, 961-964, doi:10.1038/sj.bjp.0704807 (2002).

209 Liu, Y. C., Lo, Y. C., Huang, C. W. & Wu, S. N. Inhibitory action of ICI-182,780, an estrogen receptor antagonist, on BK(Ca) channel activity in cultured endothelial cells of human coronary artery. *Biochem Pharmacol* **66**, 2053-2063 (2003).

210 Wallner, M., Meera, P. & Toro, L. Determinant for beta-subunit regulation in high-conductance voltage-activated and Ca(2+)-sensitive K+ channels: an additional transmembrane region at the N terminus. *Proc Natl Acad Sci U S A* **93**, 14922-14927 (1996).

211 Morrow, J. P. *et al.* Defining the BK channel domains required for beta1-subunit modulation. *Proc Natl Acad Sci U S A* **103**, 5096-5101, doi:10.1073/pnas.0600907103 (2006).

212 Liu, G. *et al.* Locations of the beta1 transmembrane helices in the BK potassium channel. *Proc Natl Acad Sci U S A* **105**, 10727-10732, doi:10.1073/pnas.0805212105 (2008).

213 Wu, R. S. *et al.* Location of the beta 4 transmembrane helices in the BK potassium channel. *J Neurosci* **29**, 8321-8328, doi:10.1523/JNEUROSCI.6191-08.2009 (2009).

214 King, J. T. *et al.* Beta2 and beta4 subunits of BK channels confer differential sensitivity to acute modulation by steroid hormones. *J Neurophysiol* **95**, 2878-2888, doi:10.1152/jn.01352.2005 (2006).

215 Han, G. *et al.* Estrogen receptor alpha mediates acute potassium channel stimulation in human coronary artery smooth muscle cells. *J Pharmacol Exp Ther* **316**, 1025-1030, doi:10.1124/jpet.105.093542 (2006).

216 Nishimura, I. *et al.* 17beta-estradiol at physiological concentrations augments Ca(2+) -activated K+ currents via estrogen receptor beta in the gonadotropin-releasing hormone neuronal cell line GT1-7. *Endocrinology* **149**, 774-782, doi:10.1210/en.2007-0759 (2008).

217 Li, X. T. & Qiu, X. Y. 17beta-Estradiol Upregulated Expression of alpha and beta Subunits of Larger-Conductance Calcium-Activated K(+) Channels (BK) via Estrogen Receptor beta. *J Mol Neurosci* **56**, 799-807, doi:10.1007/s12031-015-0502-0 (2015).

218 Kim, D. Y. & Yang, E. K. 17Beta-Estradiol Inhibits Calcium-Activated Potassium Channel Expressions in Rat Whole Bladder. *Int Neurourol J* **20**, 18-25, doi:10.5213/inj.1630492.246 (2016).

219 Korovkina, V. P., Brainard, A. M., Ismail, P., Schmidt, T. J. & England, S. K. Estradiol binding to maxi-K channels induces their down-regulation via proteasomal degradation. *J Biol Chem* **279**, 1217-1223, doi:10.1074/jbc.M309158200 (2004).

220 Kow, L. M. & Pfaff, D. W. Rapid estrogen actions on ion channels: A survey in search for mechanisms. *Steroids* **111**, 46-53, doi:10.1016/j.steroids.2016.02.018 (2016).

221 Zhang, L. *et al.* Direct binding of estradiol enhances Slack (sequence like a calcium-activated potassium channel) channels' activity. *Neuroscience* **131**, 275-282, doi:10.1016/j.neuroscience.2004.10.042 (2005).

222 Steinle, M. *et al.* Ionizing radiation induces migration of glioblastoma cells by activating BK K(+) channels. *Radiother Oncol* **101**, 122-126, doi:10.1016/j.radonc.2011.05.069 (2011).

223 Kizub, I. V., Pavlova, O. O., Ivanova, I. V. & Soloviev, A. I. Protein kinase C-dependent inhibition of BK(Ca) current in rat aorta smooth muscle cells following gamma-irradiation. *Int J Radiat Biol* **86**, 291-299, doi:10.3109/09553000903564042 (2010).

224 Soloviev, A. *et al.* Functional and molecular consequences of ionizing irradiation on large conductance Ca2+-activated K+ channels in rat aortic smooth muscle cells. *Life Sci* **84**, 164-171, doi:10.1016/j.lfs.2008.11.015 (2009).

225 Gardos, G. The function of calcium in the potassium permeability of human erythrocytes. *Biochim Biophys Acta* **30**, 653-654 (1958).

226 Ishii, T. M. *et al.* A human intermediate conductance calcium-activated potassium channel. *Proc Natl Acad Sci U S A* **94**, 11651-11656 (1997).

227 Joiner, W. J., Wang, L. Y., Tang, M. D. & Kaczmarek, L. K. hSK4, a member of a novel subfamily of calcium-activated potassium channels. *Proc Natl Acad Sci U S A* **94**, 11013-11018 (1997).

228 Hoffman, J. F. *et al.* The hSK4 (KCNN4) isoform is the Ca2+-activated K+ channel (Gardos channel) in human red blood cells. *Proc Natl Acad Sci U S A* **100**, 7366-7371, doi:10.1073/pnas.1232342100 (2003).

229 Kaczmarek, L. K. *et al.* International Union of Basic and Clinical Pharmacology. C. Nomenclature and Properties of Calcium-Activated and Sodium-Activated Potassium Channels. *Pharmacol Rev* **69**, 1-11, doi:10.1124/pr.116.012864 (2017).

230 Fanger, C. M. *et al.* Calmodulin mediates calcium-dependent activation of the intermediate conductance KCa channel, IKCa1. *J Biol Chem* **274**, 5746-5754 (1999).

231 Marcelo, K. L., Means, A. R. & York, B. The Ca(2+)/Calmodulin/CaMKK2 Axis: Nature's Metabolic CaMshaft. *Trends Endocrinol Metab* **27**, 706-718, doi:10.1016/j.tem.2016.06.001 (2016).

232 Adelman, J. P. SK channels and calmodulin. *Channels (Austin)* **10**, 1-6, doi:10.1080/19336950.2015.1029688 (2016).

233 Sharma, R. K. & Parameswaran, S. Calmodulin-binding proteins: A journey of 40 years. *Cell Calcium* **75**, 89-100, doi:10.1016/j.ceca.2018.09.002 (2018).

234 Takai, J. *et al.* Laminar shear stress upregulates endothelial Ca(2)(+)-activated K(+) channels KCa2.3 and KCa3.1 via a Ca(2)(+)/calmodulin-dependent protein kinase kinase/Akt/p300 cascade. *Am J Physiol Heart Circ Physiol* **305**, H484-493, doi:10.1152/ajpheart.00642.2012 (2013).

235 Benzaquen, L. R., Brugnara, C., Byers, H. R., Gatton-Celli, S. & Halperin, J. A. Clotrimazole inhibits cell proliferation in vitro and in vivo. *Nat Med* **1**, 534-540 (1995).

236 Wulff, H. *et al.* Design of a potent and selective inhibitor of the intermediate-conductance Ca2+-activated K+ channel, IKCa1: a potential immunosuppressant. *Proc Natl Acad Sci U S A* **97**, 8151-8156 (2000).

237 Agarwal, J. J., Zhu, Y., Zhang, Q. Y., Mongin, A. A. & Hough, L. B. TRAM-34, a putatively selective blocker of intermediate-conductance, calcium-activated potassium channels, inhibits cytochrome P450 activity. *PLoS One* **8**, e63028, doi:10.1371/journal.pone.0063028 (2013).

238 Crankshaw, D. J., Shen, P., Makaji, E. & Holloway, A. C. Tram-34 inhibits rat CYP450 2B1, 2C6 and 3A2. *Proceedings of the British Pharmacological Society 7* (2009).

239 Toyama, K. *et al.* The intermediate-conductance calcium-activated potassium channel KCa3.1 contributes to atherogenesis in mice and humans. *J Clin Invest* **118**, 3025-3037, doi:10.1172/JCI30836 (2008).

240 Ataga, K. I. *et al.* Efficacy and safety of the Gardos channel blocker, senicapoc (ICA-17043), in patients with sickle cell anemia. *Blood* **111**, 3991-3997, doi:10.1182/blood-2007-08-110098 (2008).

241 Stocker, J. W. *et al.* ICA-17043, a novel Gardos channel blocker, prevents sickled red blood cell dehydration in vitro and in vivo in SAD mice. *Blood* **101**, 2412-2418, doi:10.1182/blood-2002-05-1433 (2003).

242 Ataga, K. I. *et al.* Improvements in haemolysis and indicators of erythrocyte survival do not correlate with acute vaso-occlusive crises in patients with sickle cell disease: a phase III randomized, placebo-controlled, double-blind study of the Gardos channel blocker senicapoc (ICA-17043). *Br J Haematol* **153**, 92-104, doi:10.1111/j.1365-2141.2010.08520.x (2011).

243 Devor, D. C., Singh, A. K., Frizzell, R. A. & Bridges, R. J. Modulation of Cl- secretion by benzimidazolones. I. Direct activation of a Ca(2+)-dependent K+ channel. *Am J Physiol* **271**, L775-784, doi:10.1152/ajplung.1996.271.5.L775 (1996).

244 Kovalenko, I. *et al.* Identification of KCa3.1 Channel as a Novel Regulator of Oxidative Phosphorylation in a Subset of Pancreatic Carcinoma Cell Lines. *PLoS One* **11**, e0160658, doi:10.1371/journal.pone.0160658 (2016).

245 Grossinger, E. M. *et al.* Targeting proliferation of chronic lymphocytic leukemia (CLL) cells through KCa3.1 blockade. *Leukemia* **28**, 954-958, doi:10.1038/leu.2014.37 (2014).

246 Lai, W. *et al.* PRL-3 promotes the proliferation of LoVo cells via the upregulation of KCNN4 channels. *Oncol Rep* **26**, 909-917, doi:10.3892/or.2011.1366 (2011).

247 Lai, W. *et al.* KCNN4 channels participate in the EMT induced by PRL-3 in colorectal cancer. *Med Oncol* **30**, 566, doi:10.1007/s12032-013-0566-z (2013).

248 Freise, C., Ruehl, M., Seehofer, D., Hoyer, J. & Somasundaram, R. The inhibitor of Ca(2+)-dependent K+ channels TRAM-34 blocks growth of hepatocellular carcinoma cells via downregulation of estrogen receptor alpha mRNA and nuclear factor-kappaB. *Invest New Drugs* **31**, 452-457, doi:10.1007/s10637-012-9879-6 (2013).

249 Yin, M. Z. *et al.* Activation of K(+) channel by 1-EBIO rescues the head and neck squamous cell carcinoma cells from Ca(2+) ionophore-induced cell death. *Korean J Physiol Pharmacol* **20**, 25-33, doi:10.4196/kjpp.2016.20.1.25 (2016).

250 Chen, Y. *et al.* miR-497-5p inhibits cell proliferation and invasion by targeting KCa3.1 in angiosarcoma. *Oncotarget* **7**, 58148-58161, doi:10.18632/oncotarget.11252 (2016).

251 Bulk, E. *et al.* Epigenetic dysregulation of KCa 3.1 channels induces poor prognosis in lung cancer. *Int J Cancer* **137**, 1306-1317, doi:10.1002/ijc.29490 (2015).

252 Rabjerg, M. *et al.* High expression of KCa3.1 in patients with clear cell renal carcinoma predicts high metastatic risk and poor survival. *PLoS One* **10**, e0122992, doi:10.1371/journal.pone.0122992 (2015).

253 Schmidt, J., Friebel, K., Schonherr, R., Coppolino, M. G. & Bosserhoff, A. K. Migration-associated secretion of melanoma inhibitory activity at the cell rear is supported by KCa3.1 potassium channels. *Cell Res* **20**, 1224-1238, doi:10.1038/cr.2010.121 (2010).

254 Ruggieri, P. *et al.* The inhibition of KCa3.1 channels activity reduces cell motility in glioblastoma derived cancer stem cells. *PLoS One* **7**, e47825, doi:10.1371/journal.pone.0047825 (2012).

255 Klumpp, L., Sezgin, E. C., Skardelly, M., Eckert, F. & Huber, S. M. KCa3.1 channels and glioblastoma: in vitro studies. *Curr Neuropharmacol*, doi:10.2174/1570159X15666170808115821 (2017).

256 Wang, Z. H. *et al.* Blockage of intermediate-conductance-Ca(2+) -activated K(+) channels inhibits progression of human endometrial cancer. *Oncogene* **26**, 5107-5114, doi:10.1038/sj.onc.1210308 (2007).

257 Zhang, Y., Feng, Y., Chen, L. & Zhu, J. Effects of Intermediate-Conductance Ca(2+)-Activated K(+) Channels on Human Endometrial Carcinoma Cells. *Cell Biochem Biophys* **72**, 515-525, doi:10.1007/s12013-014-0497-0 (2015).

258 Liu, L. *et al.* Intermediate-Conductance-Ca2-Activated K Channel IKCa1 Is Upregulated and Promotes Cell Proliferation in Cervical Cancer. *Med Sci Monit Basic Res* **23**, 45-57 (2017).

259 Zhao, H. *et al.* KCNN4 and S100A14 act as predictors of recurrence in optimally debulked patients with serous ovarian cancer. *Oncotarget* **7**, 43924-43938, doi:10.18632/oncotarget.9721 (2016).

260 Ouadid-Ahidouch, H. *et al.* Functional and molecular identification of intermediate-conductance Ca(2+)-activated K(+) channels in breast cancer cells: association with cell cycle progression. *Am J Physiol Cell Physiol* **287**, C125-134, doi:10.1152/ajpcell.00488.2003 (2004).

261 Faouzi, M. *et al.* Functional cooperation between KCa3.1 and TRPC1 channels in human breast cancer: Role in cell proliferation and patient prognosis. *Oncotarget* **7**, 36419-36435, doi:10.18632/oncotarget.9261 (2016).

262 Liu, H., Li, Y. & Raisch, K. P. Clotrimazole induces a late G1 cell cycle arrest and sensitizes glioblastoma cells to radiation in vitro. *Anticancer Drugs* **21**, 841-849, doi:10.1097/CAD.0b013e32833e8022 (2010).

263 Faouzi, M., Chopin, V., Ahidouch, A. & Ouadid-Ahidouch, H. Intermediate Ca2+-sensitive K+ channels are necessary for prolactin-induced proliferation in breast cancer cells. *J Membr Biol* **234**, 47-56, doi:10.1007/s00232-010-9238-5 (2010).

264 Zhang, P. *et al.* Inhibition of SK4 Potassium Channels Suppresses Cell Proliferation, Migration and the Epithelial-Mesenchymal Transition in Triple-Negative Breast Cancer Cells. *PLoS One* **11**, e0154471, doi:10.1371/journal.pone.0154471 (2016).

265 Haren, N. *et al.* Intermediate conductance Ca2+ activated K+ channels are expressed and functional in breast adenocarcinomas: correlation with tumour grade and metastasis status. *Histol Histopathol* **25**, 1247-1255, doi:10.14670/HH-25.1247 (2010).

266 Panaccione, A., Guo, Y., Yarbrough, W. G. & Ivanov, S. V. Expression Profiling of Clinical Specimens Supports the Existence of Neural Progenitor-Like Stem Cells in Basal Breast Cancers. *Clin Breast Cancer* **17**, 298-306 e297, doi:10.1016/j.clbc.2017.01.007 (2017).

267 Baglietto, L. *et al.* Circulating steroid hormone concentrations in postmenopausal women in relation to body size and composition. *Breast Cancer Res Treat* **115**, 171-179, doi:10.1007/s10549-008-0069-3 (2009).

268 Bulun, S. E., Chen, D., Moy, I., Brooks, D. C. & Zhao, H. Aromatase, breast cancer and obesity: a complex interaction. *Trends Endocrinol Metab* **23**, 83-89, doi:10.1016/j.tem.2011.10.003 (2012).

269 Zhang, X. H., Zhang, Y. Y., Sun, H. Y., Jin, M. W. & Li, G. R. Functional ion channels and cell proliferation in 3T3-L1 preadipocytes. *J Cell Physiol* **227**, 1972-1979, doi:10.1002/jcp.22925 (2012).

270 Pena, T. L., Chen, S. H., Konieczny, S. F. & Rane, S. G. Ras/MEK/ERK Up-regulation of the fibroblast KCa channel FIK is a common mechanism for basic fibroblast growth factor and transforming growth factor-beta suppression of myogenesis. *J Biol Chem* **275**, 13677-13682 (2000).

271 Qiao, A., Gu, F., Guo, X., Zhang, X. & Fu, L. Breast cancer-associated fibroblasts: their roles in tumor initiation, progression and clinical applications. *Front Med* **10**, 33-40, doi:10.1007/s11684-016-0431-5 (2016).

272 Friebel, K., Schonherr, R., Kinne, R. W. & Kunisch, E. Functional role of the KCa3.1 potassium channel in synovial fibroblasts from rheumatoid arthritis patients. *J Cell Physiol* **230**, 1677-1688, doi:10.1002/jcp.24924 (2015).

273 Grgic, I. *et al.* Renal fibrosis is attenuated by targeted disruption of KCa3.1 potassium channels. *Proc Natl Acad Sci U S A* **106**, 14518-14523, doi:10.1073/pnas.0903458106 (2009).

274 Khanna, R., Chang, M. C., Joiner, W. J., Kaczmarek, L. K. & Schlichter, L. C. hSK4/hIK1, a calmodulin-binding KCa channel in human T lymphocytes. Roles in proliferation and volume regulation. *J Biol Chem* **274**, 14838-14849 (1999).

275 Kim, U. *et al.* Identification of transcription coactivator OCA-B-dependent genes involved in antigen-dependent B cell differentiation by cDNA array analyses. *Proc Natl Acad Sci U S A* **100**, 8868-8873, doi:10.1073/pnas.1033108100 (2003).

276 Koshy, S. *et al.* Blocking KCa3.1 channels increases tumor cell killing by a subpopulation of human natural killer lymphocytes. *PLoS One* **8**, e76740, doi:10.1371/journal.pone.0076740 (2013).

277 Hanley, P. J. *et al.* Extracellular ATP induces oscillations of intracellular Ca2+ and membrane potential and promotes transcription of IL-6 in macrophages. *Proc Natl Acad Sci U S A* **101**, 9479-9484, doi:10.1073/pnas.0400733101 (2004).

278 Crottes, D. *et al.* Immature human dendritic cells enhance their migration through KCa3.1 channel activation. *Cell Calcium* **59**, 198-207, doi:10.1016/j.ceca.2016.02.008 (2016).

279 Henriquez, C. *et al.* The calcium-activated potassium channel KCa3.1 plays a central role in the chemotactic response of mammalian neutrophils. *Acta Physiol (Oxf)* **216**, 132-145, doi:10.1111/apha.12548 (2016).

280 Shumilina, E. *et al.* Blunted IgE-mediated activation of mast cells in mice lacking the Ca2+-activated K+ channel KCa3.1. *J Immunol* **180**, 8040-8047 (2008).

281 Dunn, G. P., Old, L. J. & Schreiber, R. D. The three Es of cancer immunoediting. *Annu Rev Immunol* **22**, 329-360, doi:10.1146/annurev.immunol.22.012703.104803 (2004).

282 Hanahan, D. & Weinberg, R. A. Hallmarks of cancer: the next generation. *Cell* **144**, 646-674, doi:10.1016/j.cell.2011.02.013 (2011).

283 Wang, M. *et al.* Mechanism of immune evasion in breast cancer. *Onco Targets Ther* **10**, 1561-1573, doi:10.2147/OTT.S126424 (2017).

284 Xu, H. *et al.* Tumor-associated macrophage-derived IL-6 and IL-8 enhance invasive activity of LoVo cells induced by PRL-3 in a KCNN4 channel-dependent manner. *BMC Cancer* **14**, 330, doi:10.1186/1471-2407-14-330 (2014).

285 Grimaldi, A. *et al.* KCa3.1 inhibition switches the phenotype of glioma-infiltrating microglia/macrophages. *Cell Death Dis* **7**, e2174, doi:10.1038/cddis.2016.73 (2016).

286 Lee, E. L., Hasegawa, Y., Shimizu, T. & Okada, Y. IK1 channel activity contributes to cisplatin sensitivity of human epidermoid cancer cells. *Am J Physiol Cell Physiol* **294**, C1398-1406, doi:10.1152/ajpcell.00428.2007 (2008).

287 Pillozzi, S. *et al.* The combined activation of KCa3.1 and inhibition of Kv11.1/hERG1 currents contribute to overcome Cisplatin resistance in colorectal cancer cells. *Br J Cancer* **118**, 200-212, doi:10.1038/bjc.2017.392 (2018).

288 D'Alessandro, G. *et al.* KCa3.1 channel inhibition sensitizes malignant gliomas to temozolomide treatment. *Oncotarget* **7**, 30781-30796, doi:10.18632/oncotarget.8761 (2016).

289 Yeh, P. S. *et al.* Evidence for the Inhibition by Temozolomide, an Imidazotetrazine Family Alkylator, of Intermediate-Conductance Ca2+-Activated K+ Channels in Glioma Cells. *Cell Physiol Biochem* **38**, 1727-1742, doi:10.1159/000443112 (2016).

290 Joiner, M. & van der Kogel, A. Basic Clinical Radiobiology. (2009).

291 Stegen, B. *et al.* K(+) channel signaling in irradiated tumor cells. *Eur Biophys J* **45**, 585-598, doi:10.1007/s00249-016-1136-z (2016).

292 Roth, B. *et al.* Low-dose photon irradiation alters cell differentiation via activation of hIK channels. *Pflugers Arch* **467**, 1835-1849, doi:10.1007/s00424-014-1601-4 (2015).

293 Gibhardt, C. S. *et al.* X-ray irradiation activates K+ channels via H2O2 signaling. *Sci Rep* **5**, 13861, doi:10.1038/srep13861 (2015).

294 Rosenzweig, A., Blenis, J. & Gomes, A. P. Beyond the Warburg Effect: How Do Cancer Cells Regulate One-Carbon Metabolism? *Front Cell Dev Biol* **6**, 90, doi:10.3389/fcell.2018.00090 (2018).

295 Hofmann, P. Cancer and Exercise: Warburg Hypothesis, Tumour Metabolism and High-Intensity Anaerobic Exercise. *Sports (Basel)* **6**, doi:10.3390/sports6010010 (2018).

296 Stegen, B. *et al.* Ca2+-Activated IK K+ Channel Blockade Radiosensitizes Glioblastoma Cells. *Mol Cancer Res* **13**, 1283-1295, doi:10.1158/1541-7786.MCR-15-0075 (2015).

297 Brown, B. M., Pressley, B. & Wulff, H. KCa3.1 Channel Modulators as Potential Therapeutic Compounds for Glioblastoma. *Curr Neuropharmacol* **16**, 618-626, doi:10.2174/1570159X15666170630164226 (2018).

298 Taketo, M. *et al.* FVB/N: an inbred mouse strain preferable for transgenic analyses. *Proc Natl Acad Sci U S A* **88**, 2065-2069 (1991).

299 Mahler, J. F., Stokes, W., Mann, P. C., Takaoka, M. & Maronpot, R. R. Spontaneous lesions in aging FVB/N mice. *Toxicol Pathol* **24**, 710-716, doi:10.1177/019262339602400606 (1996).

300 Wong, K. *et al.* Sequencing and characterization of the FVB/NJ mouse genome. *Genome Biol* **13**, R72, doi:10.1186/gb-2012-13-8-r72 (2012).

301 Pugh, P. L., Ahmed, S. F., Smith, M. I., Upton, N. & Hunter, A. J. A behavioural characterisation of the FVB/N mouse strain. *Behav Brain Res* **155**, 283-289, doi:10.1016/j.bbr.2004.04.021 (2004).

302 Guy, C. T., Cardiff, R. D. & Muller, W. J. Induction of mammary tumors by expression of polyomavirus middle T oncogene: a transgenic mouse model for metastatic disease. *Mol Cell Biol* **12**, 954-961 (1992).

303 Taneja, P. *et al.* MMTV mouse models and the diagnostic values of MMTV-like sequences in human breast cancer. *Expert Rev Mol Diagn* **9**, 423-440, doi:10.1586/erm.09.31 (2009).
304 Ross, S. R. Mouse mammary tumor virus molecular biology and oncogenesis. *Viruses* **2**, 2000-2012, doi:10.3390/v2092000 (2010).
305 Callahan, R. & Smith, G. H. Common integration sites for MMTV in viral induced mouse mammary tumors. *J Mammary Gland Biol Neoplasia* **13**, 309-321, doi:10.1007/s10911-008-9092-6 (2008).
306 Truss, M., Bartsch, J., Mows, C., Chavez, S. & Beato, M. Chromatin structure of the MMTV promoter and its changes during hormonal induction. *Cell Mol Neurobiol* **16**, 85-101 (1996).
307 Truss, M., Chalepakis, G. & Beato, M. Interplay of steroid hormone receptors and transcription factors on the mouse mammary tumor virus promoter. *J Steroid Biochem Mol Biol* **43**, 365-378 (1992).
308 Archer, T. K. *et al.* Steroid hormone receptor status defines the MMTV promoter chromatin structure in vivo. *J Steroid Biochem Mol Biol* **53**, 421-429 (1995).
309 Salmons, B. & Gunzburg, W. H. Revisiting a role for a mammary tumor retrovirus in human breast cancer. *Int J Cancer* **133**, 1530-1535, doi:10.1002/ijc.28210 (2013).
310 Dilworth, S. M. Polyoma virus middle T antigen and its role in identifying cancer-related molecules. *Nat Rev Cancer* **2**, 951-956, doi:10.1038/nrc946 (2002).
311 Fluck, M. M. & Schaffhausen, B. S. Lessons in signaling and tumorigenesis from polyomavirus middle T antigen. *Microbiol Mol Biol Rev* **73**, 542-563, Table of Contents, doi:10.1128/MMBR.00009-09 (2009).
312 Lin, E. Y. *et al.* Progression to malignancy in the polyoma middle T oncoprotein mouse breast cancer model provides a reliable model for human diseases. *Am J Pathol* **163**, 2113-2126, doi:10.1016/S0002-9440(10)63568-7 (2003).
313 Davie, S. A. *et al.* Effects of FVB/NJ and C57Bl/6J strain backgrounds on mammary tumor phenotype in inducible nitric oxide synthase deficient mice. *Transgenic Res* **16**, 193-201, doi:10.1007/s11248-006-9056-9 (2007).
314 Lifsted, T. *et al.* Identification of inbred mouse strains harboring genetic modifiers of mammary tumor age of onset and metastatic progression. *Int J Cancer* **77**, 640-644 (1998).
315 Steudel, F. A. Die Bedeutung der Ca^{2+}-aktivierten Kaliumkanäle vom IK- und BK-Typ für die Entstehung und Therapie von Brustkrebs. (2016).
316 Sausbier, M. *et al.* Cerebellar ataxia and Purkinje cell dysfunction caused by Ca2+-activated K+ channel deficiency. *Proc Natl Acad Sci U S A* **101**, 9474-9478, doi:10.1073/pnas.0401702101 (2004).
317 Sausbier, M. *et al.* Distal colonic K(+) secretion occurs via BK channels. *J Am Soc Nephrol* **17**, 1275-1282, doi:10.1681/ASN.2005101111 (2006).
318 Strom, J. O., Theodorsson, A., Ingberg, E., Isaksson, I. M. & Theodorsson, E. Ovariectomy and 17beta-estradiol replacement in rats and mice: a visual demonstration. *J Vis Exp*, e4013, doi:10.3791/4013 (2012).
319 St Aubin, J., Steciw, S., Kirkby, C. & Fallone, B. G. An integrated 6 MV linear accelerator model from electron gun to dose in a water tank. *Med Phys* **37**, 2279-2288, doi:10.1118/1.3397455 (2010).
320 Baumann, M. *et al.* Radiation oncology in the era of precision medicine. *Nat Rev Cancer* **16**, 234-249, doi:10.1038/nrc.2016.18 (2016).
321 Richards, J., Imagawa, W., Balakrishnan, A., Edery, M. & Nandi, S. The lack of effect of phenol red or estradiol on the growth response of human, rat, and mouse

mammary cells in primary culture. *Endocrinology* **123**, 1335-1340, doi:10.1210/endo-123-3-1335 (1988).

322 Welshons, W. V., Wolf, M. F., Murphy, C. S. & Jordan, V. C. Estrogenic activity of phenol red. *Mol Cell Endocrinol* **57**, 169-178 (1988).

323 Cooper, S. & Gonzalez-Hernandez, M. Experimental reconsideration of the utility of serum starvation as a method for synchronizing mammalian cells. *Cell Biol Int* **33**, 71-77, doi:10.1016/j.cellbi.2008.09.009 (2009).

324 Takeuchi, R., Matsumoto, H., Akimoto, Y. & Fujii, A. Inhibition of G(1) cell cycle arrest in human gingival fibroblasts exposed to phenytoin. *Fundam Clin Pharmacol* **28**, 114-119, doi:10.1111/j.1472-8206.2012.01065.x (2014).

325 Gil-Gil, M. J. *et al.* Breast cancer brain metastases: a review of the literature and a current multidisciplinary management guideline. *Clin Transl Oncol* **16**, 436-446, doi:10.1007/s12094-013-1110-5 (2014).

326 Redig, A. J. & McAllister, S. S. Breast cancer as a systemic disease: a view of metastasis. *J Intern Med* **274**, 113-126, doi:10.1111/joim.12084 (2013).

327 Lorusso, G. & Ruegg, C. New insights into the mechanisms of organ-specific breast cancer metastasis. *Semin Cancer Biol* **22**, 226-233, doi:10.1016/j.semcancer.2012.03.007 (2012).

328 Li, W. *et al.* Tamoxifen promotes apoptosis and inhibits invasion in estrogenpositive breast cancer MCF7 cells. *Mol Med Rep* **16**, 478-484, doi:10.3892/mmr.2017.6603 (2017).

329 Hoelting, T., Siperstein, A. E., Duh, Q. Y. & Clark, O. H. Tamoxifen inhibits growth, migration, and invasion of human follicular and papillary thyroid cancer cells in vitro and in vivo. *J Clin Endocrinol Metab* **80**, 308-313, doi:10.1210/jcem.80.1.7829632 (1995).

330 Piccolella, M., Crippa, V., Messi, E., Tetel, M. J. & Poletti, A. Modulators of estrogen receptor inhibit proliferation and migration of prostate cancer cells. *Pharmacol Res* **79**, 13-20, doi:10.1016/j.phrs.2013.10.002 (2014).

331 Tsai, C. L. *et al.* Estradiol and tamoxifen induce cell migration through GPR30 and activation of focal adhesion kinase (FAK) in endometrial cancers with low or without nuclear estrogen receptor alpha (ERalpha). *PLoS One* **8**, e72999, doi:10.1371/journal.pone.0072999 (2013).

332 Li, Y. *et al.* 4-Hydroxytamoxifen-stimulated processing of cyclin E is mediated via G protein-coupled receptor 30 (GPR30) and accompanied by enhanced migration in MCF-7 breast cancer cells. *Toxicology* **309**, 61-65, doi:10.1016/j.tox.2013.04.012 (2013).

333 Yu, X. *et al.* Activation of G protein-coupled estrogen receptor induces endothelium-independent relaxation of coronary artery smooth muscle. *Am J Physiol Endocrinol Metab* **301**, E882-888, doi:10.1152/ajpendo.00037.2011 (2011).

334 Evanson, K. W., Goldsmith, J. A., Ghosh, P. & Delp, M. D. The G protein-coupled estrogen receptor agonist, G-1, attenuates BK channel activation in cerebral arterial smooth muscle cells. *Pharmacol Res Perspect* **6**, e00409, doi:10.1002/prp2.409 (2018).

335 Zhang, J. D. Introduction to the Data Analysis of the Roche xCELLigence. (2015).

336 Zerbino, D. R. *et al.* Ensembl 2018. *Nucleic Acids Res* **46**, D754-D761, doi:10.1093/nar/gkx1098 (2018).

337 Untergasser, A. *et al.* Primer3--new capabilities and interfaces. *Nucleic Acids Res* **40**, e115, doi:10.1093/nar/gks596 (2012).

338 Koressaar, T. & Remm, M. Enhancements and modifications of primer design program Primer3. *Bioinformatics* **23**, 1289-1291, doi:10.1093/bioinformatics/btm091 (2007).

339 Altschul, S. F., Gish, W., Miller, W., Myers, E. W. & Lipman, D. J. Basic local alignment search tool. *J Mol Biol* **215**, 403-410, doi:10.1016/S0022-2836(05)80360-2 (1990).

340 Malkawi, S. R., Abu-Hazeem, R. M. & Easa, M. O. Effect of water softening on the colour intensity of routine haematoxylin and eosin stain. *East Mediterr Health J* **9**, 1109-1113 (2003).

341 Ciriello, G. *et al.* Comprehensive Molecular Portraits of Invasive Lobular Breast Cancer. *Cell* **163**, 506-519, doi:10.1016/j.cell.2015.09.033 (2015).

342 Gyorffy, B. *et al.* An online survival analysis tool to rapidly assess the effect of 22,277 genes on breast cancer prognosis using microarray data of 1,809 patients. *Breast Cancer Res Treat* **123**, 725-731, doi:10.1007/s10549-009-0674-9 (2010).

343 Sakoda, L. C., Jorgenson, E. & Witte, J. S. Turning of COGS moves forward findings for hormonally mediated cancers. *Nat Genet* **45**, 345-348, doi:10.1038/ng.2587 (2013).

344 Bahcall, O. G. iCOGS collection provides a collaborative model. Foreword. *Nat Genet* **45**, 343, doi:10.1038/ng.2592 (2013).

345 Michailidou, K. *et al.* Large-scale genotyping identifies 41 new loci associated with breast cancer risk. *Nat Genet* **45**, 353-361, 361e351-352, doi:10.1038/ng.2563 (2013).

346 Amos, C. I. *et al.* The OncoArray Consortium: A Network for Understanding the Genetic Architecture of Common Cancers. *Cancer Epidemiol Biomarkers Prev* **26**, 126-135, doi:10.1158/1055-9965.EPI-16-0106 (2017).

347 Michailidou, K. *et al.* Association analysis identifies 65 new breast cancer risk loci. *Nature* **551**, 92-94, doi:10.1038/nature24284 (2017).

348 Church, D. M. *et al.* Modernizing reference genome assemblies. *PLoS Biol* **9**, e1001091, doi:10.1371/journal.pbio.1001091 (2011).

349 Lu, Z. PubMed and beyond: a survey of web tools for searching biomedical literature. *Database (Oxford)* **2011**, baq036, doi:10.1093/database/baq036 (2011).

350 Sherry, S. T. *et al.* dbSNP: the NCBI database of genetic variation. *Nucleic Acids Res* **29**, 308-311 (2001).

351 Johnson, A. D. *et al.* SNAP: a web-based tool for identification and annotation of proxy SNPs using HapMap. *Bioinformatics* **24**, 2938-2939, doi:10.1093/bioinformatics/btn564 (2008).

352 Yuan, Y., Tian, L., Lu, D. & Xu, S. Analysis of genome-wide RNA-sequencing data suggests age of the CEPH/Utah (CEU) lymphoblastoid cell lines systematically biases gene expression profiles. *Sci Rep* **5**, 7960, doi:10.1038/srep07960 (2015).

353 Ward, L. D. & Kellis, M. HaploReg: a resource for exploring chromatin states, conservation, and regulatory motif alterations within sets of genetically linked variants. *Nucleic Acids Res* **40**, D930-934, doi:10.1093/nar/gkr917 (2012).

354 Arnold, M., Raffler, J., Pfeufer, A., Suhre, K. & Kastenmuller, G. SNiPA: an interactive, genetic variant-centered annotation browser. *Bioinformatics* **31**, 1334-1336, doi:10.1093/bioinformatics/btu779 (2015).

355 Yang, T. P. *et al.* Genevar: a database and Java application for the analysis and visualization of SNP-gene associations in eQTL studies. *Bioinformatics* **26**, 2474-2476, doi:10.1093/bioinformatics/btq452 (2010).

356 Goda, A. A., Siddique, A. B., Mohyeldin, M., Ayoub, N. M. & El Sayed, K. A. The Maxi-K (BK) Channel Antagonist Penitrem A as a Novel Breast Cancer-Targeted Therapeutic. *Mar Drugs* **16**, doi:10.3390/md16050157 (2018).

357 Illison, J. *et al.* Obesogenic and Diabetogenic Effects of High-Calorie Nutrition Require Adipocyte BK Channels. *Diabetes* **65**, 3621-3635, doi:10.2337/db16-0245 (2016).

358 Rheinlander, A., Schraven, B. & Bommhardt, U. CD45 in human physiology and clinical medicine. *Immunol Lett* **196**, 22-32, doi:10.1016/j.imlet.2018.01.009 (2018).

359 Trowbridge, I. S. & Thomas, M. L. CD45: an emerging role as a protein tyrosine phosphatase required for lymphocyte activation and development. *Annu Rev Immunol* **12**, 85-116, doi:10.1146/annurev.iy.12.040194.000505 (1994).

360 Saunders, A. E. & Johnson, P. Modulation of immune cell signalling by the leukocyte common tyrosine phosphatase, CD45. *Cell Signal* **22**, 339-348, doi:10.1016/j.cellsig.2009.10.003 (2010).

361 Fagerberg, L. *et al.* Analysis of the human tissue-specific expression by genome-wide integration of transcriptomics and antibody-based proteomics. *Mol Cell Proteomics* **13**, 397-406, doi:10.1074/mcp.M113.035600 (2014).

362 Lee, H., Palm, J., Grimes, S. M. & Ji, H. P. The Cancer Genome Atlas Clinical Explorer: a web and mobile interface for identifying clinical-genomic driver associations. *Genome Med* **7**, 112, doi:10.1186/s13073-015-0226-3 (2015).

363 Lanczky, A. *et al.* miRpower: a web-tool to validate survival-associated miRNAs utilizing expression data from 2178 breast cancer patients. *Breast Cancer Res Treat* **160**, 439-446, doi:10.1007/s10549-016-4013-7 (2016).

364 Wesolowski, S., Birtwistle, M. R. & Rempala, G. A. A Comparison of Methods for RNA-Seq Differential Expression Analysis and a New Empirical Bayes Approach. *Biosensors (Basel)* **3**, 238-258, doi:10.3390/bios3030238 (2013).

365 Torres, Y. P., Granados, S. T. & Latorre, R. Pharmacological consequences of the coexpression of BK channel alpha and auxiliary beta subunits. *Front Physiol* **5**, 383, doi:10.3389/fphys.2014.00383 (2014).

366 Williams, J. A. Origin of transmembrane potentials in non-excitable cells. *J Theor Biol* **28**, 287-296 (1970).

367 Cervera, J., Alcaraz, A. & Mafe, S. Membrane potential bistability in nonexcitable cells as described by inward and outward voltage-gated ion channels. *J Phys Chem B* **118**, 12444-12450, doi:10.1021/jp508304h (2014).

368 Subik, K. *et al.* The Expression Patterns of ER, PR, HER2, CK5/6, EGFR, Ki-67 and AR by Immunohistochemical Analysis in Breast Cancer Cell Lines. *Breast Cancer (Auckl)* **4**, 35-41 (2010).

369 Oba, T. & Ito, K. I. Combination of two anti-tubulin agents, eribulin and paclitaxel, enhances anti-tumor effects on triple-negative breast cancer through mesenchymal-epithelial transition. *Oncotarget* **9**, 22986-23002, doi:10.18632/oncotarget.25184 (2018).

370 Liu, X. *et al.* Androgen receptor and heat shock protein 27 co-regulate the malignant potential of molecular apocrine breast cancer. *J Exp Clin Cancer Res* **37**, 90, doi:10.1186/s13046-018-0762-y (2018).

371 Hall, R. E., Birrell, S. N., Tilley, W. D. & Sutherland, R. L. MDA-MB-453, an androgen-responsive human breast carcinoma cell line with high level androgen receptor expression. *Eur J Cancer* **30A**, 484-490 (1994).

372 Dai, X., Cheng, H., Bai, Z. & Li, J. Breast Cancer Cell Line Classification and Its Relevance with Breast Tumor Subtyping. *J Cancer* **8**, 3131-3141, doi:10.7150/jca.18457 (2017).

373 Speers, C. *et al.* Androgen receptor as a mediator and biomarker of radioresistance in triple-negative breast cancer. *NPJ Breast Cancer* **3**, 29, doi:10.1038/s41523-017-0038-2 (2017).

374 Magklara, A., Brown, T. J. & Diamandis, E. P. Characterization of androgen receptor and nuclear receptor co-regulator expression in human breast cancer cell lines exhibiting differential regulation of kallikreins 2 and 3. *Int J Cancer* **100**, 507-514, doi:10.1002/ijc.10520 (2002).

375 Macedo, L. F. *et al.* Role of androgens on MCF-7 breast cancer cell growth and on the inhibitory effect of letrozole. *Cancer Res* **66**, 7775-7782, doi:10.1158/0008-5472.CAN-05-3984 (2006).

376 Zhang, W. *et al.* BRCA1 inhibits AR-mediated proliferation of breast cancer cells through the activation of SIRT1. *Sci Rep* **6**, 22034, doi:10.1038/srep22034 (2016).

377 Pratt, S. E. & Pollak, M. N. Estrogen and antiestrogen modulation of MCF7 human breast cancer cell proliferation is associated with specific alterations in accumulation of insulin-like growth factor-binding proteins in conditioned media. *Cancer Res* **53**, 5193-5198 (1993).

378 Coopman, P. *et al.* Anti-proliferative and anti-estrogenic effects of ICI 164,384 and ICI 182,780 in 4-OH-tamoxifen-resistant human breast-cancer cells. *Int J Cancer* **56**, 295-300 (1994).

379 de Vries Schultink, A. H. *et al.* An Antiestrogenic Activity Score for tamoxifen and its metabolites is associated with breast cancer outcome. *Breast Cancer Res Treat* **161**, 567-574, doi:10.1007/s10549-016-4083-6 (2017).

380 Martin, H. L., Smith, L. & Tomlinson, D. C. Multidrug-resistant breast cancer: current perspectives. *Breast Cancer (Dove Med Press)* **6**, 1-13, doi:10.2147/BCTT.S37638 (2014).

381 Helland, T. *et al.* The active tamoxifen metabolite endoxifen (4OHNDtam) strongly down-regulates cytokeratin 6 (CK6) in MCF-7 breast cancer cells. *PLoS One* **10**, e0122339, doi:10.1371/journal.pone.0122339 (2015).

382 Perlman, R. L. Mouse models of human disease: An evolutionary perspective. *Evol Med Public Health* **2016**, 170-176, doi:10.1093/emph/eow014 (2016).

383 Rangarajan, A. & Weinberg, R. A. Opinion: Comparative biology of mouse versus human cells: modelling human cancer in mice. *Nat Rev Cancer* **3**, 952-959, doi:10.1038/nrc1235 (2003).

384 Caruso, R. *et al.* Mitotic catastrophe in malignant epithelial tumors: the pathologist's viewpoint. *Ultrastruct Pathol* **35**, 66-71, doi:10.3109/01913123.2010.543753 (2011).

385 Steudel, F. A. *et al.* SK4 channels modulate Ca(2+) signalling and cell cycle progression in murine breast cancer. *Mol Oncol* **11**, 1172-1188, doi:10.1002/1878-0261.12087 (2017).

386 Biasiotta, A., D'Arcangelo, D., Passarelli, F., Nicodemi, E. M. & Facchiano, A. Ion channels expression and function are strongly modified in solid tumors and vascular malformations. *J Transl Med* **14**, 285, doi:10.1186/s12967-016-1038-y (2016).

387 Wulff, H., Knaus, H. G., Pennington, M. & Chandy, K. G. K+ channel expression during B cell differentiation: implications for immunomodulation and autoimmunity. *J Immunol* **173**, 776-786 (2004).

388 Liao, D. Emerging roles of the EBF family of transcription factors in tumor suppression. *Mol Cancer Res* **7**, 1893-1901, doi:10.1158/1541-7786.MCR-09-0229 (2009).
389 Vilagos, B. *et al.* Essential role of EBF1 in the generation and function of distinct mature B cell types. *J Exp Med* **209**, 775-792, doi:10.1084/jem.20112422 (2012).
390 Le, T. P., Sun, M., Luo, X., Kraus, W. L. & Greene, G. L. Mapping ERbeta genomic binding sites reveals unique genomic features and identifies EBF1 as an ERbeta interactor. *PLoS One* **8**, e71355, doi:10.1371/journal.pone.0071355 (2013).
391 Prasad, M. A. *et al.* Ebf1 heterozygosity results in increased DNA damage in pro-B cells and their synergistic transformation by Pax5 haploinsufficiency. *Blood* **125**, 4052-4059, doi:10.1182/blood-2014-12-617282 (2015).
392 Wang, C. *et al.* Non-Lethal Ionizing Radiation Promotes Aging-Like Phenotypic Changes of Human Hematopoietic Stem and Progenitor Cells in Humanized Mice. *PLoS One* **10**, e0132041, doi:10.1371/journal.pone.0132041 (2015).
393 Georgopoulos, K. Ebf1 in DNA repair and leukemogenesis. *Blood* **125**, 3969-3971, doi:10.1182/blood-2015-05-639427 (2015).
394 Contreras, G. F. *et al.* A BK (Slo1) channel journey from molecule to physiology. *Channels (Austin)* **7**, 442-458, doi:10.4161/chan.26242 (2013).
395 Kyle, B. D. & Braun, A. P. The regulation of BK channel activity by pre- and post-translational modifications. *Front Physiol* **5**, 316, doi:10.3389/fphys.2014.00316 (2014).
396 Rosa, P. *et al.* BK channels blockage inhibits hypoxia-induced migration and chemoresistance to cisplatin in human glioblastoma cells. *J Cell Physiol* **233**, 6866-6877, doi:10.1002/jcp.26448 (2018).
397 Werbeck, J. L. *et al.* Tumor microenvironment regulates metastasis and metastasis genes of mouse MMTV-PymT mammary cancer cells in vivo. *Vet Pathol* **51**, 868-881, doi:10.1177/0300985813505116 (2014).
398 Perou, C. M. *et al.* Molecular portraits of human breast tumours. *Nature* **406**, 747-752, doi:10.1038/35021093 (2000).
399 Cancer Genome Atlas, N. Comprehensive molecular portraits of human breast tumours. *Nature* **490**, 61-70, doi:10.1038/nature11412 (2012).
400 Zhao, W. *et al.* Comparison of RNA-Seq by poly (A) capture, ribosomal RNA depletion, and DNA microarray for expression profiling. *BMC Genomics* **15**, 419, doi:10.1186/1471-2164-15-419 (2014).
401 Hilton, H. N., Clarke, C. L. & Graham, J. D. Estrogen and progesterone signalling in the normal breast and its implications for cancer development. *Mol Cell Endocrinol* **466**, 2-14, doi:10.1016/j.mce.2017.08.011 (2018).
402 Saha Roy, S. & Vadlamudi, R. K. Role of estrogen receptor signaling in breast cancer metastasis. *Int J Breast Cancer* **2012**, 654698, doi:10.1155/2012/654698 (2012).
403 Schroth, W. *et al.* Clinical outcome and global gene expression data support the existence of the estrogen receptor-negative/progesterone receptor-positive invasive breast cancer phenotype. *Breast Cancer Res Treat* **155**, 85-97, doi:10.1007/s10549-015-3651-5 (2016).
404 Kunc, M., Biernat, W. & Senkus-Konefka, E. Estrogen receptor-negative progesterone receptor-positive breast cancer - "Nobody's land" or just an artifact? *Cancer Treat Rev* **67**, 78-87, doi:10.1016/j.ctrv.2018.05.005 (2018).
405 Grimm, S. L., Hartig, S. M. & Edwards, D. P. Progesterone Receptor Signaling Mechanisms. *J Mol Biol* **428**, 3831-3849, doi:10.1016/j.jmb.2016.06.020 (2016).

406 Mohammed, H. *et al.* Progesterone receptor modulates ERalpha action in breast cancer. *Nature* **523**, 313-317, doi:10.1038/nature14583 (2015).
407 Dall, P. *et al.* Trastuzumab without chemotherapy in the adjuvant treatment of breast cancer: subgroup results from a large observational study. *BMC Cancer* **18**, 51, doi:10.1186/s12885-017-3857-5 (2018).
408 Nakashoji, A. *et al.* The updated network meta-analysis of neoadjuvant therapy for HER2-positive breast cancer. *Cancer Treat Rev* **62**, 9-17, doi:10.1016/j.ctrv.2017.10.009 (2018).
409 Harari, D. & Yarden, Y. Molecular mechanisms underlying ErbB2/HER2 action in breast cancer. *Oncogene* **19**, 6102-6114, doi:10.1038/sj.onc.1203973 (2000).
410 Vasconcelos, I. *et al.* The St. Gallen surrogate classification for breast cancer subtypes successfully predicts tumor presenting features, nodal involvement, recurrence patterns and disease free survival. *Breast* **29**, 181-185, doi:10.1016/j.breast.2016.07.016 (2016).
411 Li, Q. & Yan, J. Modulation of BK Channel Function by Auxiliary Beta and Gamma Subunits. *Int Rev Neurobiol* **128**, 51-90, doi:10.1016/bs.irn.2016.03.015 (2016).
412 Williams, R. B., Chan, E. K., Cowley, M. J. & Little, P. F. The influence of genetic variation on gene expression. *Genome Res* **17**, 1707-1716, doi:10.1101/gr.6981507 (2007).
413 Nica, A. C. & Dermitzakis, E. T. Expression quantitative trait loci: present and future. *Philos Trans R Soc Lond B Biol Sci* **368**, 20120362, doi:10.1098/rstb.2012.0362 (2013).
414 Francesconi, M. & Lehner, B. The effects of genetic variation on gene expression dynamics during development. *Nature* **505**, 208-211, doi:10.1038/nature12772 (2014).
415 Weiger, T. M. *et al.* A novel nervous system beta subunit that downregulates human large conductance calcium-dependent potassium channels. *J Neurosci* **20**, 3563-3570 (2000).
416 Lo, W. Y. *et al.* Abstract 2030: The role of genetic variation in calcium-activated potassium channels in breast cancer patients treated with tamoxifen. *Cancer Research*, doi:10.1158/1538-7445.AM2016-2030 (2016).
417 Sausbier, M. *et al.* Elevated blood pressure linked to primary hyperaldosteronism and impaired vasodilation in BK channel-deficient mice. *Circulation* **112**, 60-68, doi:10.1161/01.CIR.0000156448.74296.FE (2005).
418 Ruttiger, L. *et al.* Deletion of the Ca2+-activated potassium (BK) alpha-subunit but not the BKbeta1-subunit leads to progressive hearing loss. *Proc Natl Acad Sci U S A* **101**, 12922-12927, doi:10.1073/pnas.0402660101 (2004).
419 Sausbier, U. *et al.* Osteopenia due to enhanced cathepsin K release by BK channel ablation in osteoclasts. *PLoS One* **6**, e21168, doi:10.1371/journal.pone.0021168 (2011).
420 Nishizuka, M. *et al.* KCNMA1, a pore-forming alpha-subunit of BK channels, regulates insulin signalling in mature adipocytes. *FEBS Lett* **590**, 4372-4380, doi:10.1002/1873-3468.12465 (2016).
421 Lim, I. *et al.* Nitric oxide stimulates a large-conductance Ca-activated K+ channel in human skin fibroblasts through protein kinase G pathway. *Skin Pharmacol Physiol* **18**, 279-287, doi:10.1159/000088013 (2005).
422 Wrzosek, A. Endothelium as target for large-conductance calcium-activated potassium channel openers. *Acta Biochim Pol* **56**, 393-404 (2009).

423 Revermann, M. *et al.* Inhalation of the BK(Ca)-opener NS1619 attenuates right ventricular pressure and improves oxygenation in the rat monocrotaline model of pulmonary hypertension. *PLoS One* **9**, e86636, doi:10.1371/journal.pone.0086636 (2014).

424 Grgic, I. *et al.* Selective blockade of the intermediate-conductance Ca2+-activated K+ channel suppresses proliferation of microvascular and macrovascular endothelial cells and angiogenesis in vivo. *Arterioscler Thromb Vasc Biol* **25**, 704-709, doi:10.1161/01.ATV.0000156399.12787.5c (2005).

425 Garcia, M. L., Shen, D.-M. & Kaczorowski, G. J. High-conductance calcium-activated potassium channels. *Expert Opinion on Therapeutic Patents*, doi:10.1517/13543776.17.7.831 (2007).

426 Nardi, A. & Olesen, S. P. BK channel modulators: a comprehensive overview. *Curr Med Chem* **15**, 1126-1146 (2008).

427 dela Pena, I. & Cheong, J. H. On Benzofuroindole Analogues as SmoothMuscle Relaxants. *Journal of Biomedicine and Biotechnology*, doi:doi:10.1155/2011/389056 (2011).

428 Holdiman, A. J., Fergus, D. J. & England, S. K. 17beta-Estradiol upregulates distinct maxi-K channel transcripts in mouse uterus. *Mol Cell Endocrinol* **192**, 1-6 (2002).

429 Danesh, S. M., Kundu, P., Lu, R., Stefani, E. & Toro, L. Distinct transcriptional regulation of human large conductance voltage- and calcium-activated K+ channel gene (hSlo1) by activated estrogen receptor alpha and c-Src tyrosine kinase. *J Biol Chem* **286**, 31064-31071, doi:10.1074/jbc.M111.235457 (2011).

430 Singh, H., Stefani, E. & Toro, L. Intracellular BK(Ca) (iBK(Ca)) channels. *J Physiol* **590**, 5937-5947, doi:10.1113/jphysiol.2011.215533 (2012).

431 Checchetto, V., Teardo, E., Carraretto, L., Leanza, L. & Szabo, I. Physiology of intracellular potassium channels: A unifying role as mediators of counterion fluxes? *Biochim Biophys Acta* **1857**, 1258-1266, doi:10.1016/j.bbabio.2016.03.011 (2016).

432 Li, B. *et al.* Nuclear BK channels regulate gene expression via the control of nuclear calcium signaling. *Nat Neurosci* **17**, 1055-1063, doi:10.1038/nn.3744 (2014).

433 Htun, H., Holth, L. T., Walker, D., Davie, J. R. & Hager, G. L. Direct visualization of the human estrogen receptor alpha reveals a role for ligand in the nuclear distribution of the receptor. *Mol Biol Cell* **10**, 471-486 (1999).

434 Vrtacnik, P., Ostanek, B., Mencej-Bedrac, S. & Marc, J. The many faces of estrogen signaling. *Biochem Med (Zagreb)* **24**, 329-342, doi:10.11613/BM.2014.035 (2014).

435 Tecalco-Cruz, A. C., Perez-Alvarado, I. A., Ramirez-Jarquin, J. O. & Rocha-Zavaleta, L. Nucleo-cytoplasmic transport of estrogen receptor alpha in breast cancer cells. *Cell Signal* **34**, 121-132, doi:10.1016/j.cellsig.2017.03.011 (2017).

436 Li, L., Haynes, M. P. & Bender, J. R. Plasma membrane localization and function of the estrogen receptor alpha variant (ER46) in human endothelial cells. *Proc Natl Acad Sci U S A* **100**, 4807-4812, doi:10.1073/pnas.0831079100 (2003).

437 Boonyaratanakornkit, V. Scaffolding proteins mediating membrane-initiated extra-nuclear actions of estrogen receptor. *Steroids* **76**, 877-884, doi:10.1016/j.steroids.2011.02.017 (2011).

438 Thomas, P., Pang, Y., Filardo, E. J. & Dong, J. Identity of an estrogen membrane receptor coupled to a G protein in human breast cancer cells. *Endocrinology* **146**, 624-632, doi:10.1210/en.2004-1064 (2005).

439 Pandey, D. P. *et al.* Estrogenic GPR30 signalling induces proliferation and migration of breast cancer cells through CTGF. *EMBO J* **28**, 523-532, doi:10.1038/emboj.2008.304 (2009).

440 Maggiolini, M. & Picard, D. The unfolding stories of GPR30, a new membrane-bound estrogen receptor. *J Endocrinol* **204**, 105-114, doi:10.1677/JOE-09-0242 (2010).

441 Molina, L., Figueroa, C. D., Bhoola, K. D. & Ehrenfeld, P. GPER-1/GPR30 a novel estrogen receptor sited in the cell membrane: therapeutic coupling to breast cancer. *Expert Opin Ther Targets* **21**, 755-766, doi:10.1080/14728222.2017.1350264 (2017).

442 Filardo, E. J. A role for G-protein coupled estrogen receptor (GPER) in estrogen-induced carcinogenesis: Dysregulated glandular homeostasis, survival and metastasis. *J Steroid Biochem Mol Biol* **176**, 38-48, doi:10.1016/j.jsbmb.2017.05.005 (2018).

443 Langer, G. *et al.* A critical review of fundamental controversies in the field of GPR30 research. *Steroids* **75**, 603-610, doi:10.1016/j.steroids.2009.12.006 (2010).

444 Samartzis, E. P. *et al.* The G protein-coupled estrogen receptor (GPER) is expressed in two different subcellular localizations reflecting distinct tumor properties in breast cancer. *PLoS One* **9**, e83296, doi:10.1371/journal.pone.0083296 (2014).

445 Martin, S. G. *et al.* Low expression of G protein-coupled oestrogen receptor 1 (GPER) is associated with adverse survival of breast cancer patients. *Oncotarget* **9**, 25946-25956, doi:10.18632/oncotarget.25408 (2018).

446 Sjostrom, M. *et al.* Lack of G protein-coupled estrogen receptor (GPER) in the plasma membrane is associated with excellent long-term prognosis in breast cancer. *Breast Cancer Res Treat* **145**, 61-71, doi:10.1007/s10549-014-2936-4 (2014).

447 Catalano, S. *et al.* Tamoxifen through GPER upregulates aromatase expression: a novel mechanism sustaining tamoxifen-resistant breast cancer cell growth. *Breast Cancer Res Treat* **146**, 273-285, doi:10.1007/s10549-014-3017-4 (2014).

448 Lappano, R. & Maggiolini, M. GPER is involved in the functional liaison between breast tumor cells and cancer-associated fibroblasts (CAFs). *J Steroid Biochem Mol Biol* **176**, 49-56, doi:10.1016/j.jsbmb.2017.02.019 (2018).

449 Choudhury, N. & Sikdar, S. K. 17beta-estradiol potentiates TREK1 channel activity through G protein-coupled estrogen receptor. *J Steroid Biochem Mol Biol*, doi:10.1016/j.jsbmb.2018.06.001 (2018).

450 Marjon, N. A., Hu, C., Hathaway, H. J. & Prossnitz, E. R. G protein-coupled estrogen receptor regulates mammary tumorigenesis and metastasis. *Mol Cancer Res* **12**, 1644-1654, doi:10.1158/1541-7786.MCR-14-0128-T (2014).

451 Staubach, S. & Hanisch, F. G. Lipid rafts: signaling and sorting platforms of cells and their roles in cancer. *Expert Rev Proteomics* **8**, 263-277, doi:10.1586/epr.11.2 (2011).

452 Harvey, R. D. & Calaghan, S. C. Caveolae create local signalling domains through their distinct protein content, lipid profile and morphology. *J Mol Cell Cardiol* **52**, 366-375, doi:10.1016/j.yjmcc.2011.07.007 (2012).

453 Wang, Z. *et al.* Caveolin-1, a stress-related oncotarget, in drug resistance. *Oncotarget* **6**, 37135-37150, doi:10.18632/oncotarget.5789 (2015).

454 El-Gendi, S. M., Mostafa, M. F. & El-Gendi, A. M. Stromal caveolin-1 expression in breast carcinoma. Correlation with early tumor recurrence and clinical outcome. *Pathol Oncol Res* **18**, 459-469, doi:10.1007/s12253-011-9469-5 (2012).

455 Thomas, N. B. *et al.* Growth of hormone-dependent MCF-7 breast cancer cells is promoted by constitutive caveolin-1 whose expression is lost in an EGF-R-mediated manner during development of tamoxifen resistance. *Breast Cancer Res Treat* **119**, 575-591, doi:10.1007/s10549-009-0355-8 (2010).

456 Ketteler, J. & Klein, D. Caveolin-1, cancer and therapy resistance. *Int J Cancer*, doi:10.1002/ijc.31369 (2018).

457 Clarke, R., van den Berg, H. W. & Murphy, R. F. Reduction of the membrane fluidity of human breast cancer cells by tamoxifen and 17 beta-estradiol. *J Natl Cancer Inst* **82**, 1702-1705 (1990).

458 Wiseman, H., Cannon, M., Arnstein, H. R. & Halliwell, B. Enhancement by tamoxifen of the membrane antioxidant action of the yeast membrane sterol ergosterol: relevance to the antiyeast and anticancer action of tamoxifen. *Biochim Biophys Acta* **1181**, 201-206 (1993).

459 Kazanci, N. & Severcan, F. Concentration dependent different action of tamoxifen on membrane fluidity. *Biosci Rep* **27**, 247-255, doi:10.1007/s10540-007-9050-3 (2007).

460 Wang, X. L. *et al.* Caveolae targeting and regulation of large conductance Ca(2+)-activated K+ channels in vascular endothelial cells. *J Biol Chem* **280**, 11656-11664, doi:10.1074/jbc.M410987200 (2005).

461 Brainard, A. M., Miller, A. J., Martens, J. R. & England, S. K. Maxi-K channels localize to caveolae in human myometrium: a role for an actin-channel-caveolin complex in the regulation of myometrial smooth muscle K+ current. *Am J Physiol Cell Physiol* **289**, C49-57, doi:10.1152/ajpcell.00399.2004 (2005).

462 Baral, E., Nagy, E. & Berczi, I. Modulation of natural killer cell-mediated cytotoxicity by tamoxifen and estradiol. *Cancer* **75**, 591-599 (1995).

463 Watashi, K. *et al.* Anti-hepatitis C virus activity of tamoxifen reveals the functional association of estrogen receptor with viral RNA polymerase NS5B. *J Biol Chem* **282**, 32765-32772, doi:10.1074/jbc.M704418200 (2007).

464 Dolan, K. *et al.* Antifungal activity of tamoxifen: in vitro and in vivo activities and mechanistic characterization. *Antimicrob Agents Chemother* **53**, 3337-3346, doi:10.1128/AAC.01564-08 (2009).

465 Reddel, R. R., Murphy, L. C., Hall, R. E. & Sutherland, R. L. Differential sensitivity of human breast cancer cell lines to the growth-inhibitory effects of tamoxifen. *Cancer Res* **45**, 1525-1531 (1985).

466 Radin, D. P. & Patel, P. Delineating the molecular mechanisms of tamoxifen's oncolytic actions in estrogen receptor-negative cancers. *Eur J Pharmacol* **781**, 173-180, doi:10.1016/j.ejphar.2016.04.017 (2016).

467 Wang, Q. *et al.* Tamoxifen reverses epithelial-mesenchymal transition by demethylating miR-200c in triple-negative breast cancer cells. *BMC Cancer* **17**, 492, doi:10.1186/s12885-017-3457-4 (2017).

468 Medina, D. *et al.* Tamoxifen inhibition of estrogen receptor-alpha-negative mouse mammary tumorigenesis. *Cancer Res* **65**, 3493-3496, doi:10.1158/0008.5472.CAN-04-3869 (2005).

469 Obiorah, I. E. & Jordan, V. C. Differences in the rate of oestrogen-induced apoptosis in breast cancer by oestradiol and the triphenylethylene bisphenol. *Br J Pharmacol* **171**, 4062-4072, doi:10.1111/bph.12762 (2014).

470 Shagufta & Ahmad, I. Tamoxifen a pioneering drug: An update on the therapeutic potential of tamoxifen derivatives. *Eur J Med Chem* **143**, 515-531, doi:10.1016/j.ejmech.2017.11.056 (2018).

471 Schroth, W. *et al.* Association between CYP2D6 polymorphisms and outcomes among women with early stage breast cancer treated with tamoxifen. *JAMA* **302**, 1429-1436, doi:10.1001/jama.2009.1420 (2009).

472 Binkhorst, L. *et al.* Circadian variation in tamoxifen pharmacokinetics in mice and breast cancer patients. *Breast Cancer Res Treat* **152**, 119-128, doi:10.1007/s10549-015-3452-x (2015).

473 Groenland, S. L. *et al.* Therapeutic Drug Monitoring of Oral Anti-Hormonal Drugs in Oncology. *Clin Pharmacokinet*, doi:10.1007/s40262-018-0683-0 (2018).

474 Lien, E. A. *et al.* Serum concentrations of tamoxifen and its metabolites increase with age during steady-state treatment. *Breast Cancer Res Treat* **141**, 243-248, doi:10.1007/s10549-013-2677-9 (2013).

475 Jager, N. G., Rosing, H., Schellens, J. H., Linn, S. C. & Beijnen, J. H. Tamoxifen dose and serum concentrations of tamoxifen and six of its metabolites in routine clinical outpatient care. *Breast Cancer Res Treat* **143**, 477-483, doi:10.1007/s10549-013-2826-1 (2014).

476 Iino, Y. *et al.* Reversible control of oestradiol-stimulated growth of MCF-7 tumours by tamoxifen in the athymic mouse. *Br J Cancer* **64**, 1019-1024 (1991).

477 Kisanga, E. R. *et al.* Tamoxifen and metabolite concentrations in serum and breast cancer tissue during three dose regimens in a randomized preoperative trial. *Clin Cancer Res* **10**, 2336-2343 (2004).

478 Miksys, S. L., Cheung, C., Gonzalez, F. J. & Tyndale, R. F. Human CYP2D6 and mouse CYP2Ds: organ distribution in a humanized mouse model. *Drug Metab Dispos* **33**, 1495-1502, doi:10.1124/dmd.105.005488 (2005).

479 Shishido, S. N., Faulkner, E. B., Beck, A. & Nguyen, T. A. The effect of antineoplastic drugs in a male spontaneous mammary tumor model. *PLoS One* **8**, e64866, doi:10.1371/journal.pone.0064866 (2014).

480 Asghar Butt, S. *et al.* Monitoring mammary tumor progression and effect of tamoxifen treatment in MMTV-PymT using MRI and magnetic resonance spectroscopy with hyperpolarized [1-13C]pyruvate. *Magn Reson Med* **73**, 51-58, doi:10.1002/mrm.25095 (2015).

481 Sacco, M. G. *et al.* Combined effects on tumor growth and metastasis by anti-estrogenic and antiangiogenic therapies in MMTV-neu mice. *Gene Ther* **9**, 1338-1341, doi:10.1038/sj.gt.3301817 (2002).

482 Fuchs-Young, R. *et al.* P53 genotype as a determinant of ER expression and tamoxifen response in the MMTV-Wnt-1 model of mammary carcinogenesis. *Breast Cancer Res Treat* **130**, 399-408, doi:10.1007/s10549-010-1308-y (2011).

483 Nanni, P. *et al.* Prevention of HER-2/neu transgenic mammary carcinoma by tamoxifen plus interleukin 12. *Int J Cancer* **105**, 384-389, doi:10.1002/ijc.11092 (2003).

484 Liu, B. *et al.* Low-dose dietary phytoestrogen abrogates tamoxifen-associated mammary tumor prevention. *Cancer Res* **65**, 879-886 (2005).

485 Sakata, M., Ikeda, T., Imoto, S., Jinno, H. & Kitagawa, Y. Prevention of mammary carcinogenesis in C3H/OuJ mice by green tea and tamoxifen. *Asian Pac J Cancer Prev* **12**, 567-571 (2011).

486 Krishnamurthy, N. *et al.* Induction of quinone reductase by tamoxifen or DPN protects against mammary tumorigenesis. *FASEB J* **26**, 3993-4002, doi:10.1096/fj.12-208330 (2012).

487 Osborne, C. K., Hobbs, K. & Clark, G. M. Effect of estrogens and antiestrogens on growth of human breast cancer cells in athymic nude mice. *Cancer Res* **45**, 584-590 (1985).

488 Jones, L. P. *et al.* Promotion of mammary cancer development by tamoxifen in a mouse model of Brca1-mutation-related breast cancer. *Oncogene* **24**, 3554-3562, doi:10.1038/sj.onc.1208426 (2005).

489 Dabrosin, C., Palmer, K., Muller, W. J. & Gauldie, J. Estradiol promotes growth and angiogenesis in polyoma middle T transgenic mouse mammary tumor explants. *Breast Cancer Res Treat* **78**, 1-6 (2003).

490 Hurtado, A. *et al.* Regulation of ERBB2 by oestrogen receptor-PAX2 determines response to tamoxifen. *Nature* **456**, 663-666, doi:10.1038/nature07483 (2008).

491 Christenson, J. L. *et al.* MMTV-PyMT and Derived Met-1 Mouse Mammary Tumor Cells as Models for Studying the Role of the Androgen Receptor in Triple-Negative Breast Cancer Progression. *Horm Cancer* **8**, 69-77, doi:10.1007/s12672-017-0285-6 (2017).

492 Bai, L. *et al.* An Integrated Genome-Wide Systems Genetics Screen for Breast Cancer Metastasis Susceptibility Genes. *PLoS Genet* **12**, e1005989, doi:10.1371/journal.pgen.1005989 (2016).

493 Bourgier, C. *et al.* Concurrent or sequential letrozole with adjuvant breast radiotherapy: final results of the CO-HO-RT phase II randomized trial. *Ann Oncol* **27**, 474-480, doi:10.1093/annonc/mdv602 (2016).

494 Azria, D. *et al.* Concurrent or sequential adjuvant letrozole and radiotherapy after conservative surgery for early-stage breast cancer (CO-HO-RT): a phase 2 randomised trial. *Lancet Oncol* **11**, 258-265, doi:10.1016/S1470-2045(10)70013-9 (2010).

495 Ishitobi, M. *et al.* Risk of Ipsilateral breast tumor recurrence in patients treated with Tamoxifen or Anastrozole following breast-conserving surgery with or without radiotherapy. *Anticancer Res* **31**, 367-371 (2011).

496 Overgaard, M. *et al.* Postoperative radiotherapy in high-risk postmenopausal breast-cancer patients given adjuvant tamoxifen: Danish Breast Cancer Cooperative Group DBCG 82c randomised trial. *Lancet* **353**, 1641-1648, doi:10.1016/S0140-6736(98)09201-0 (1999).

497 Fyles, A. W. *et al.* Tamoxifen with or without breast irradiation in women 50 years of age or older with early breast cancer. *N Engl J Med* **351**, 963-970, doi:10.1056/NEJMoa040595 (2004).

498 Potter, R. *et al.* Lumpectomy plus tamoxifen or anastrozole with or without whole breast irradiation in women with favorable early breast cancer. *Int J Radiat Oncol Biol Phys* **68**, 334-340, doi:10.1016/j.ijrobp.2006.12.045 (2007).

499 Osborne, C. K., Boldt, D. H., Clark, G. M. & Trent, J. M. Effects of tamoxifen on human breast cancer cell cycle kinetics: accumulation of cells in early G1 phase. *Cancer Res* **43**, 3583-3585 (1983).

500 Cariou, S. *et al.* Down-regulation of p21WAF1/CIP1 or p27Kip1 abrogates antiestrogen-mediated cell cycle arrest in human breast cancer cells. *Proc Natl Acad Sci U S A* **97**, 9042-9046, doi:10.1073/pnas.160016897 (2000).

501 Dong, J. *et al.* Inactivation of DNA-PK by knockdown DNA-PKcs or NU7441 impairs non-homologous end-joining of radiation-induced double strand break repair. *Oncol Rep* **39**, 912-920, doi:10.3892/or.2018.6217 (2018).

502 Wang, M. *et al.* Ionizing radiation, but not ultraviolet radiation, induces mitotic catastrophe in mouse epidermal keratinocytes with aberrant cell cycle checkpoints. *Exp Dermatol*, doi:10.1111/exd.13665 (2018).

503 Wazer, D. E., Tercilla, O. F., Lin, P. S. & Schmidt-Ullrich, R. Modulation in the radiosensitivity of MCF-7 human breast carcinoma cells by 17B-estradiol and tamoxifen. *Br J Radiol* **62**, 1079-1083, doi:10.1259/0007-1285-62-744-1079 (1989).

504 Hoeller, U., Borgmann, K., Feyer, P., Souchon, R. & Organgruppe "Mammakarzinom" der, D. [On the interaction of adjuvant radiotherapy and tamoxifen treatment for

breast cancer]. *Strahlenther Onkol* **183**, 535-544, doi:10.1007/s00066-007-1710-5 (2007).

505 Cecchini, M. J., Yu, E., Potvin, K., D'Souza, D. & Lock, M. Concurrent or Sequential Hormonal and Radiation Therapy in Breast Cancer: A Literature Review. *Cureus* **7**, e364, doi:10.7759/cureus.364 (2015).

506 Zeng, Z. J., Li, J. H., Zhang, Y. J. & Zhao, S. T. Optimal combination of radiotherapy and endocrine drugs in breast cancer treatment. *Cancer Radiother* **17**, 208-214, doi:10.1016/j.canrad.2013.01.014 (2013).

507 Lemon, H. M., Kumar, P. F., Peterson, C., Rodriguez-Sierra, J. F. & Abbo, K. M. Inhibition of radiogenic mammary carcinoma in rats by estriol or tamoxifen. *Cancer* **63**, 1685-1692 (1989).

508 Welsch, C. W. Host factors affecting the growth of carcinogen-induced rat mammary carcinomas: a review and tribute to Charles Brenton Huggins. *Cancer Res* **45**, 3415-3443 (1985).

509 Kantorowitz, D. A., Thompson, H. J. & Furmanski, P. Effect of conjoint administration of tamoxifen and high-dose radiation on the development of mammary carcinoma. *Int J Radiat Oncol Biol Phys* **26**, 89-94 (1993).

510 Kyle, U. G. *et al.* Prevalence of malnutrition in 1760 patients at hospital admission: a controlled population study of body composition. *Clin Nutr* **22**, 473-481 (2003).

511 Sallam, A. A. *et al.* Bioguided discovery and pharmacophore modeling of the mycotoxic indole diterpene alkaloids penitrems as breast cancer proliferation, migration, and invasion inhibitors. *Medchemcomm* **4**, doi:10.1039/C3MD00198A (2013).

512 Ursini-Siegel, J., Schade, B., Cardiff, R. D. & Muller, W. J. Insights from transgenic mouse models of ERBB2-induced breast cancer. *Nat Rev Cancer* **7**, 389-397, doi:10.1038/nrc2127 (2007).

513 Fry, E. A., Taneja, P. & Inoue, K. Oncogenic and tumor-suppressive mouse models for breast cancer engaging HER2/neu. *Int J Cancer* **140**, 495-503, doi:10.1002/ijc.30399 (2017).

514 Guy, C. T. *et al.* Expression of the neu protooncogene in the mammary epithelium of transgenic mice induces metastatic disease. *Proc Natl Acad Sci U S A* **89**, 10578-10582 (1992).

515 Rowse, G. J., Ritland, S. R. & Gendler, S. J. Genetic modulation of neu proto-oncogene-induced mammary tumorigenesis. *Cancer Res* **58**, 2675-2679 (1998).

516 Desai, K. V. *et al.* Initiating oncogenic event determines gene-expression patterns of human breast cancer models. *Proc Natl Acad Sci U S A* **99**, 6967-6972, doi:10.1073/pnas.102172399 (2002).

517 Vargo-Gogola, T. & Rosen, J. M. Modelling breast cancer: one size does not fit all. *Nat Rev Cancer* **7**, 659-672, doi:10.1038/nrc2193 (2007).

518 Hollern, D. P. & Andrechek, E. R. A genomic analysis of mouse models of breast cancer reveals molecular features of mouse models and relationships to human breast cancer. *Breast Cancer Res* **16**, R59, doi:10.1186/bcr3672 (2014).

519 Ghanshani, S. *et al.* Up-regulation of the IKCa1 potassium channel during T-cell activation. Molecular mechanism and functional consequences. *J Biol Chem* **275**, 37137-37149, doi:10.1074/jbc.M003941200 (2000).

520 Nicolaou, S. A., Neumeier, L., Peng, Y., Devor, D. C. & Conforti, L. The Ca(2+)-activated K(+) channel KCa3.1 compartmentalizes in the immunological synapse of human T lymphocytes. *Am J Physiol Cell Physiol* **292**, C1431-1439, doi:10.1152/ajpcell.00376.2006 (2007).

521 Rodriguez-Cortez, V. C. *et al.* Monozygotic twins discordant for common variable immunodeficiency reveal impaired DNA demethylation during naive-to-memory B-cell transition. *Nat Commun* **6**, 7335, doi:10.1038/ncomms8335 (2015).

522 Shao, Z., Makinde, T. O. & Agrawal, D. K. Calcium-activated potassium channel KCa3.1 in lung dendritic cell migration. *Am J Respir Cell Mol Biol* **45**, 962-968, doi:10.1165/rcmb.2010-0514OC (2011).

523 Ferreira, R., Lively, S. & Schlichter, L. C. IL-4 type 1 receptor signaling up-regulates KCNN4 expression, and increases the KCa3.1 current and its contribution to migration of alternative-activated microglia. *Front Cell Neurosci* **8**, 183, doi:10.3389/fncel.2014.00183 (2014).

524 Mark Duffy, S. *et al.* The K+ channel iKCA1 potentiates Ca2+ influx and degranulation in human lung mast cells. *J Allergy Clin Immunol* **114**, 66-72, doi:10.1016/j.jaci.2004.04.005 (2004).

525 Nagarajan, D. & McArdle, S. E. B. Immune Landscape of Breast Cancers. *Biomedicines* **6**, doi:10.3390/biomedicines6010020 (2018).

526 Di, L. *et al.* Inhibition of the K+ channel KCa3.1 ameliorates T cell-mediated colitis. *Proc Natl Acad Sci U S A* **107**, 1541-1546, doi:10.1073/pnas.0910133107 (2010).

527 DeNardo, D. G. *et al.* CD4(+) T cells regulate pulmonary metastasis of mammary carcinomas by enhancing protumor properties of macrophages. *Cancer Cell* **16**, 91-102, doi:10.1016/j.ccr.2009.06.018 (2009).

528 Gross, E. T. *et al.* Immunosurveillance and immunoediting in MMTV-PyMT-induced mammary oncogenesis. *Oncoimmunology* **6**, e1268310, doi:10.1080/2162402X.2016.1268310 (2017).

529 Young, S. & Cowan, D. M. Spontaneous regression of induced mammary tumours in rats. *Br J Cancer* **17**, 85-89 (1963).

530 McLaughlin, A. P., 3rd & Gittes, R. F. Spontaneous tumor regression. Experimental aspects. *Urology* **3**, 544-551 (1974).

531 Tilli, M. T. & Furth, P. A. Conditional mouse models demonstrate oncogene-dependent differences in tumor maintenance and recurrence. *Breast Cancer Res* **5**, 202-205, doi:10.1186/bcr614 (2003).

532 Chimote, A. A. *et al.* A defect in KCa3.1 channel activity limits the ability of CD8(+) T cells from cancer patients to infiltrate an adenosine-rich microenvironment. *Sci Signal* **11**, doi:10.1126/scisignal.aaq1616 (2018).

533 Komohara, Y., Ohnishi, K., Kuratsu, J. & Takeya, M. Possible involvement of the M2 anti-inflammatory macrophage phenotype in growth of human gliomas. *J Pathol* **216**, 15-24, doi:10.1002/path.2370 (2008).

534 Gabrusiewicz, K. *et al.* Characteristics of the alternative phenotype of microglia/macrophages and its modulation in experimental gliomas. *PLoS One* **6**, e23902, doi:10.1371/journal.pone.0023902 (2011).

535 Bai, X. *et al.* Electrophysiological properties of human adipose tissue-derived stem cells. *Am J Physiol Cell Physiol* **293**, C1539-1550, doi:10.1152/ajpcell.00089.2007 (2007).

536 Tarasov, M. V. *et al.* Calcium-gated K(+) channels of the KCa1.1- and KCa3.1-type couple intracellular Ca(2+) signals to membrane hyperpolarization in mesenchymal stromal cells from the human adipose tissue. *Pflugers Arch* **469**, 349-362, doi:10.1007/s00424-016-1932-4 (2017).

537 Bi, D. *et al.* The intermediate conductance calcium-activated potassium channel KCa3.1 regulates vascular smooth muscle cell proliferation via controlling calcium-

dependent signaling. *J Biol Chem* **288**, 15843-15853, doi:10.1074/jbc.M112.427187 (2013).

538 Yang, H. *et al.* Blockade of the intermediate-conductance Ca(2+)-activated K+ channel inhibits the angiogenesis induced by epidermal growth factor in the treatment of corneal alkali burn. *Exp Eye Res* **110**, 76-87, doi:10.1016/j.exer.2013.02.015 (2013).

539 James, S. J., Enger, S. M. & Makinodan, T. DNA strand breaks and DNA repair response in lymphocytes after chronic in vivo exposure to very low doses of ionizing radiation in mice. *Mutat Res* **249**, 255-263 (1991).

540 Liu, S. Z., SuXu, Zhang, Y. C. & Zhao, Y. Signal transduction in lymphocytes after low dose radiation. *Chin Med J (Engl)* **107**, 431-436 (1994).

541 Heise, N. *et al.* Non-selective cation channel-mediated Ca2+-entry and activation of Ca2+/calmodulin-dependent kinase II contribute to G2/M cell cycle arrest and survival of irradiated leukemia cells. *Cell Physiol Biochem* **26**, 597-608, doi:10.1159/000322327 (2010).

542 Herskind, C. *et al.* Biology of high single doses of IORT: RBE, 5 R's, and other biological aspects. *Radiat Oncol* **12**, 24, doi:10.1186/s13014-016-0750-3 (2017).

543 Steel, G. G., McMillan, T. J. & Peacock, J. H. The 5Rs of radiobiology. *Int J Radiat Biol* **56**, 1045-1048 (1989).

544 Good, J. S. & Harrington, K. J. The hallmarks of cancer and the radiation oncologist: updating the 5Rs of radiobiology. *Clin Oncol (R Coll Radiol)* **25**, 569-577, doi:10.1016/j.clon.2013.06.009 (2013).

545 Klumpp, L., Sezgin, E. C., Skardelly, M., Eckert, F. & Huber, S. M. KCa3.1 Channels and Glioblastoma: In Vitro Studies. *Curr Neuropharmacol* **16**, 627-635, doi:10.2174/1570159X15666170808115821 (2018).

546 Huber, S. M. *et al.* Role of ion channels in ionizing radiation-induced cell death. *Biochim Biophys Acta* **1848**, 2657-2664, doi:10.1016/j.bbamem.2014.11.004 (2015).

547 Rufo, P. A. *et al.* The antifungal antibiotic, clotrimazole, inhibits chloride secretion by human intestinal T84 cells via blockade of distinct basolateral K+ conductances. Demonstration of efficacy in intact rabbit colon and in an in vivo mouse model of cholera. *J Clin Invest* **100**, 3111-3120, doi:10.1172/JCI119866 (1997).

548 Bernard, K., Bogliolo, S., Soriani, O. & Ehrenfeld, J. Modulation of calcium-dependent chloride secretion by basolateral SK4-like channels in a human bronchial cell line. *J Membr Biol* **196**, 15-31, doi:10.1007/s00232-003-0621-3 (2003).

549 Matos, J. E. *et al.* Role of cholinergic-activated KCa1.1 (BK), KCa3.1 (SK4) and KV7.1 (KCNQ1) channels in mouse colonic Cl- secretion. *Acta Physiol (Oxf)* **189**, 251-258, doi:10.1111/j.1748-1716.2006.01646.x (2007).

550 Tian, Y. *et al.* Calmodulin-dependent activation of the epithelial calcium-dependent chloride channel TMEM16A. *FASEB J* **25**, 1058-1068, doi:10.1096/fj.10-166884 (2011).

551 Wang, J., Haanes, K. A. & Novak, I. Purinergic regulation of CFTR and Ca(2+)-activated Cl(-) channels and K(+) channels in human pancreatic duct epithelium. *Am J Physiol Cell Physiol* **304**, C673-684, doi:10.1152/ajpcell.00196.2012 (2013).

552 Kucherenko, Y. V., Wagner-Britz, L., Bernhardt, I. & Lang, F. Effect of chloride channel inhibitors on cytosolic Ca2+ levels and Ca2+-activated K+ (Gardos) channel activity in human red blood cells. *J Membr Biol* **246**, 315-326, doi:10.1007/s00232-013-9532-0 (2013).

553 Huang, Q. *et al.* Caspase 3-mediated stimulation of tumor cell repopulation during cancer radiotherapy. *Nat Med* **17**, 860-866, doi:10.1038/nm.2385 (2011).

554 Brugnara, C. *et al.* Therapy with oral clotrimazole induces inhibition of the Gardos channel and reduction of erythrocyte dehydration in patients with sickle cell disease. *J Clin Invest* **97**, 1227-1234, doi:10.1172/JCI118537 (1996).

11. Publications and congress contributions

Publications

Mohr C. J. et al. “Cancer-associated Intermediate Conductance Ca^{2+}-activated K^+ ($K_{Ca}3.1$) Channels” (*Review in preparation*)

Mohr C. J. et al. “Modulation of $K_{Ca}3.1$ channels ameliorates breast cancer outcome and radiotherapy, but not chemotherapy” (*Journal article in preparation*)

Mohr C. J. et al. “BK channels promote breast cancer development and interfere with tamoxifen therapy” (*Journal article in preparation*)

Steudel F. A., Mohr C. J., Stegen B., Nguyen H. Y., Barnert A., Steinle M., Beer-Hammer S., Koch P., Lo W.-Y., Schroth W., Hoppe R., Brauch H., Ruth P., Huber S. M., Lukowski R. “SK4 channels modulate Ca^{2+} signalling and cell cycle progression in murine breast cancer” (*Mol Oncol* **11**, 1172-1188, doi:10.1002/1878-0261.12087, 2017)

Congress contributions

Mohr C. J., Schroth W., Mürdter T. E., Stegen B., Steudel F. A., Lo W.-Y., Hopppe R., Huber S. M., Ruth P., Brauch H., Lukowski R. “Big conductance calcium-activated potassium (BK) channels in hormone-based development and therapy of breast cancer”. *29th Ion Channel Meeting (09/2018) Sète, France (Talk)*.

Awarded for best oral communication

Mohr C. J., Groß D., Steudel F. A., Ruth P., Schroth W., Brauch H., Huber S. M., Lukowski R. “The role of the intermediate conductance calcium-activated potassium channel IK in breast cancer development and therapy”. *17th International Summer School: Inflammation, Immunomodulation, Inspiration (07/2018), Bönigen, Switzerland (Poster)*.

Mohr C. J., Groß D., Steudel F. A., Ruth P., Schroth W., Brauch H., Huber S. M., Lukowski R. “The intermediate conductance calcium-activated potassium channel IK in breast cancer development and therapy”. *Ion Channel Symposium (05/2018), Copenhagen, Denmark (Poster)*.

Mohr C. J., Schroth W., Mürdter T. E., Stegen B., Steudel F. A., Lo W.-Y., Hopppe R., Huber S. M., Ruth P., Brauch H., Lukowski R. “Big conductance calcium-activated potassium (BK) channels in breast cancer”. *33. Deutscher Krebskongress (02/2018), Berlin (Poster)*.

Mohr C. J., Steudel F. A., Lo W.-Y., Stegen B., Huber S. M., Hopppe R., Schroth W., Brauch H., Ruth P., Lukowski R. “The role of the intermediate conductance calcium-activated potassium channel IK in breast cancer”. *2nd German Pharm-Tox Summit (03/2017), Heidelberg (Poster)*.

Mohr C. J., Steudel F. A., Stegen B., Lo W.-Y., Hopppe R., Schroth W., Brauch H., Huber S. M., Ruth P., Lukowski R. “Intermediate conductance calcium-activated potassium channels in breast cancer development and therapy outcome”. *26. Symposium Experimentelle Strahlentherapie und Klinische Strahlenbiologie (02/2017), Tübingen (Poster)*.

Awarded with the OncoRay poster prize

Mohr C. J., Steudel F. A., Lo W.-Y., Stegen B., Huber S. M., Hopppe R., Schroth W., Brauch H., Ruth P., Lukowski R. “Big conductance calcium-activated potassium channels (BK) in murine breast cancer”. *15th International Summer School: Inflammation, Immunomodulation, Inspiration (08/2016), Bönigen, Switzerland (Talk)*.

Steudel F. A., Mohr C. J., Stegen B., Nguyen H. Y., Barnert A., Huber S. M., Ruth P., Lukowski R. “Intermediate conductance calcium-activated potassium channels (IK) in murine breast cancer”. *15th International Summer School: Inflammation, Immunomodulation, Inspiration (08/2016), Bönigen, Switzerland (Talk)*.

Mohr C. J., Steudel F. A., Lo W.-Y., Stegen B., Huber S. M., Hopppe R., Schroth W., Brauch H., Ruth P., Lukowski R. “BK channel in breast cancer”. *Summer-Retreat (07/2016), Abtei Frauenwörth Chiemsee (Talk)*.

Lo W.-Y., Mohr C., Steudel F., Schmidt M., Easton D., Hoppe R., Schroth W., Ruth P., Lukowski R., Brauch H. “The role of genetic variation in calcium-activated potassium channels in breast cancer patients treated with tamoxifen”. *AACR 107th Annual Meeting (04/2016), New Orleans, USA (Poster)*.

Mohr C., Steudel F., Lo W.-Y., Hopppe R., Ruth P., Schroth W., Brauch H., Lukowski R. “Calcium-activated potassium channels in tumour cell proliferation, predications on breast

cancer risk and treatment outcome". *Scientific Retreat: Progress in Clinical Pharmacology (06/2015), Abtei Frauenwörth Chiemsee (Talk)*.

12. Curriculum Vitae

13. Acknowledgements

This thesis was carried out from July 2014 to June 2018 with scientific supervision by Prof. Dr. Robert Lukowski and Prof. Dr. Peter Ruth at the Institute of Pharmacy, University of Tübingen in cooperation with Prof. Dr. Hiltrud Brauch´s research group at the IKP in Stuttgart as part of the ICEPHA graduate programme. The following lines, I want to use to express my sincere gratitude to all people that contributed to the success of this thesis.

First and in particular, I want to thank Prof. Dr. Robert Lukowski to entrust me with this highly interesting translational research topic. His valuable guidance directed this research and he coordinated research cooperations with the IKP in Stuttgart and the Department of Radiation Oncology at the University Hospital in Tübingen as part of the ICEPHA. Besides, I want to thank him for correction and evaluation of my thesis. My thanks also go to Prof. Dr. Peter Ruth for the availability of knockout mouse models, animal house arrangements, his participation in our ICEPHA project and the examination as part of the disputation as well as for many interesting discussions.

Likewise, I want to express many thanks to Prof. Dr. Hiltrud Brauch for the goal-oriented coordination and supervision as part of the ICEPHA graduate programme and the examination of this thesis. For helpful contributions and discussions especially in terms of genetic variant analyses, the K_{Ca} mRNA screen of human breast cancer cell lines as well as supply with CCS, (Z)-TAM, (Z)-endoxifen and human breast cancer cell lines, I also want to thank the members of her research group, namely Dr. Werner Schroth, Dr. Wing-Yee Lo and Dr. Reiner Hoppe. Thanks also to Dr. Thomas Mürdter for fast and reliable HPLC analyses investigating murine tamoxifen plasma levels.

Besides, I want to specially thank Prof. Dr. Stephan M. Huber for the warm welcome and experimental assistance also by Heidrun Faltin and all lab members at the Department of Radiation Oncology, access to the linear accelerator and the possibility to perform parts of the experiments in his cell culture lab. His help with irradiation of our mice together with Efe Cumhur Sezgin and the introduction to patch-clamp analyses are of further note.

In addition, PD Dr. Bertolt Gust´s spontaneous and kind agreement to act as examiner for the disputation is highly acknowledged.

For administrative tasks, I want to thank the secretaries at the Institute of Pharmacy, Mrs. Leitermann and Mrs. Weber, and at the Institute of Clinical Pharmacology, Mrs. Prill and Mrs. Verhagen as well as Mrs. Leicht. Moreover, I want to thank Clément, Isolde, Loni, Michael, Katrin, Sandra and Nadine, who were involved in technical issues, genotyping and

maintenance of the mice. For the supportive and enjoyable time in the lab at the Institute of Pharmacy and for the many activities outside, my thanks go to all former and present scientists and my practical students, especially Lena, Friederike, Dominic, Anne, Rebekka, Christina, Markus, Lucas, Sabrina, Julia I. and Julia S., Sandra, Angelina, Anna, Natalie, Stephanie, Jonas, Malena and Alice.

Finally, I want to thank my family and especially my parents for the great support during the whole process of my scientific education.